

DESIGN AND SYNTHESIS OF SOME NON- CONVENTIONAL CHIRAL DISCOTIC LIQUID CRYSTALS

SHRUTI RANI

*A thesis submitted for the partial fulfillment of
the degree of Doctor of Philosophy*



Department of Chemical Sciences
Indian Institute of Science Education and Research Mohali
Knowledge city, Sector 81, SAS Nagar, Manauli PO, Mohali 140306, Punjab,
India.

May 2023

It's the questions we can't answer that teach us the most.

By Patrick Rothfuss-The Wise Man's Fear

Dedicated to

My beloved parents

Declaration

The work presented in this thesis entitled “*Design and Synthesis of some Non-conventional Chiral Discotic Liquid Crystals*” has been carried out by me under the guidance of **Prof. Santanu Kumar Pal** at the Indian Institute of Science Education and Research Mohali. This work has not been submitted in part or in full for a degree, a diploma, or a fellowship to any other university or institute. Whenever contributions of others are involved, every effort is made to indicate this clearly, with due acknowledgement of collaborative research and discussions. This thesis is a bonafide record of original work done by me and all sources listed within have been detailed in the bibliography.

SHRUTI RANI

In my capacity as the supervisor of the candidate’s thesis work, I certify that the above statements by the candidate are true to the best of my knowledge.

Prof. SANTANU KUMAR PAL

Professor

Department of Chemical Sciences

Indian Institute of Science Education and Research Mohali

Acknowledgements

The doctoral research journey is truly a marathon, filled with experiences and emotions. The researcher would not have been able to complete this journey without the aid and support of countless people who contributed and extended their valuable assistance in one way or another. I would like to convey my heartfelt gratitude, appreciation, and thanks to everyone who has been kind, critiqued, and motivated me to perform better.

First and foremost, with a deep sense of respect and honour, I would like to thank my thesis supervisor, **Prof. Santanu Kumar Pal**, for his patience, support, and encouragement, for giving me rational freedom to design and work on different projects, and his constant help during my research work. Working with him was a delightful journey and provided many learning experiences.

I express my gratitude to the members of the doctorate committee, **Dr Sugumar Venkataramani** and **Dr Sanchita Sengupta**, for their yearly evaluations and insightful comments on my research work. I would like to acknowledge our former directors, Prof. N. Sathyamurthy and Prof. Debi P. Sarkar and our current director Prof. J. Gowrishankar for providing the research and infrastructural facilities. I am thankful to the former HOD, Department of Chemical Sciences, Prof. K. S. Viswanathan and Dr A. S. Arulananda Babu, along with the current HOD, Dr Sanjay Singh, for permitting the use of various departmental facilities. Besides, I am highly grateful to all the faculty members of IISER Mohali for their encouragement and motivation.

I acknowledge IISER Mohali for central NMR, HRMS, SEM, TEM and SAXS/WAXS facility. I would like to thank Department of Chemical Sciences for providing various departmental facilities like UV-vis-NIR, FTIR spectrophotometers, TGA, DSC, Fluorimeter etc. I'd also like to thank Dr Kavita Dorai for training me to operate the NMR instrument in the early years of my PhD. I would like to acknowledge other departments of IISER Mohali and the administration, computer section, accounts, transport, security, canteen, hostel and clinic for their constant support throughout my PhD life. I am also thankful to CSIR for the timely dispersal of the research fellowship and to IISER Mohali for financial aid.

I would like to thank **Dr Santosh Prasad Gupta** (Patna University) for helping with the X-ray diffraction analysis. His simple way of explanation enriches my knowledge of X-ray diffraction. I would like to extend my gratitude to **Prof. C. V. Yelamaggad** of the Centre

for Nano and Soft Matter Sciences (CeNS), Bangalore, and his student Dr Madhu Babu Kanakala for conducting circular dichroism studies and his valuable suggestions in the research problem which helped me to grow as a researcher. **Prof. C. V. Yelamaggad** has consistently been helpful in various discussions, and his enormous knowledge inspires me to perform better every time. I acknowledge **Prof. Subi J. George** (JNCASR, Bangalore) and his student Dr Souvik Sarkar, for conducting the circularly polarized luminescence experiment and helping me understand the related data. I would like to thank **Dr Sanchita Sengupta** and her students, especially **Dr Kavita** and **Sushil**, for helping me with fluorescence-related experiments in their lab. Also, I wanted to thank **Raman Jangra** (Punjab university) for all the DFT related helpful discussion.

I express my deep sense of gratitude to my former and current lab-mates: Dr Monika Gupta, Dr Joydip De, Dr Indu Bala, Dr Ipsita Pani, Dr Supreet Kaur, Dr Vidhika Punjani, Dr Varsha Jain, Yogi, Madhusudan Maity, Tarang Gupta, Shallu Dhingra, Ritobrata De, Anshika Baghla, Soma Sil, Musthafa, Nitya, Abdul, Rahul, Prabhat, Parveen, Ishan, Diksha, Kaveri, Neha and Kavya for providing a comfortable atmosphere for working in the lab and giving me wonderful memories. I would like to thank all the former Post-Doctoral fellows: Dr Golam Mohiuddin, Dr Manisha Devi, Dr Nazma Begum and Dr Rajib Nandi, for sharing their knowledge and enriching discussions. My special thanks to **Yogi** for helping me with discussions and suggestions during my PhD.

I am thankful to all the staff members of stores, purchase office, administrative office, account section, library and computing facility of IISER Mohali for their help and cooperation during the course of time. I also acknowledge Mr. Bahadur, Mr. Mangat, Mr. Prahlad, Mr. Triveni and all the chemistry teaching lab lab assistants for their timely help.

I was lucky to have my friends: **Vedika, Rishika, Shriya, Nisha, Anjali, Rajat, Manu, Arjun**, and **Yogi** for providing me with the best company inside and outside the campus. Special thanks to Vedika for pampering me on my bad days and always being my elder sister, Shriya, for comforting me to share and discuss everything with her. She improved my thinking process towards every relationship in life.

I would like to thank my family-in-law for their support during the last two years of my journey. I acknowledge every second of their motivation, love, sacrifice and patience during this most difficult time of my PhD journey. I appreciate the love and care of my sister-in-law **Bharti** and **Kiran**, my mother-in-law **Mrs. Sudesh**. Above all, my most

profound appreciation for my parents (**Mr. Ved Prakash and Mrs. Roshani Devi**) for providing me everything in my life, my grandparents and my younger brother **Soumya** for unconditional support and endless love. I sincerely express my sincere gratitude to them for their constant motivation and belief in me. Special thanks to my husband (**Mr. Vikram Arya**) for making sure that I always feel heard, comforted and motivated. He is always a good listener during stressful times and makes me feel better. At last, I thank God for everything I have and everything I am today.

Contents

CHAPTER 1: Introduction to discotic liquid crystal and supramolecular chirality

1.1 Overview	1
1.2 Matter and its states.....	2
1.3 Liquid crystals.....	3
1.4 Historical remarks	4
1.5 Classification of LCs.....	6
1.5.1 Lyotropic liquid crystals.....	7
1.5.2 Thermotropic liquid crystals	8
1.5.2.1 Discotic liquid crystals	9
1.5.2.1.1 Nematic phases of discotic mesogens	10
1.5.2.1.2 Smectic phases of discotic mesogens	11
1.5.2.1.3 Columnar phases of discotic mesogens	11
1.6 Characterization of DLCs	13
1.7 Chirality	15
1.8 Supramolecular chirality in liquid crystals	16
1.8.1 Chirality in DLCs	19
1.8.1.1 Chirality induction in discotic nematic (N_D^*) mesophase	20
1.8.1.2 Chirality induction in discotic columnar mesophases	22
1.9 Characterization of supramolecular chirality.....	25
1.9.1 CD spectroscopy	26
1.10 Application of supramolecular assembly	27
1.10.1 Circularly polarized luminescence	28
1.10.1.1 Application of CPL active LCs.....	29
1.11 Outline of thesis	30
<i>References</i>	32

CHAPTER 2: Observation of helical self-assembly in cyclic triphosphazene-based columnar liquid crystals bearing chiral mesogenic units

2.1 Introduction.....	47
2.2 Result and discussions	50
2.2.1 Synthesis, Structural Characterization and Thermal stability	50
2.2.2 Mesomorphic behaviour.....	50
2.2.3 Electron density maps	56

2.2.4 Chiroptical measurements	57
2.2.5 Sensing Property	61
2.3 Conclusions	62
2.4 Experimental section.....	64
2.5 UV-visible and fluorescence measurement.....	73
2.6 Author Contributions	73
2.7 Acknowledgements.....	73
<i>References</i>	73
Appendix I.....	80

CHAPTER 3: Circularly polarized luminescence from pyrrolopyrrole-based discotic columnar liquid crystals

3.1 Introduction.....	101
3.2 Results and discussions	103
3.2.1 Synthesis, Structural Characterization and Thermal stability	103
3.2.2 Mesomorphic behaviour.....	104
3.2.3 Photophysical behavior	106
3.2.4 Circularly polarized luminescence	109
3.3 Conclusion	110
3.4 Experimental section.....	111
3.5 Quantum Yield Measurement	114
3.6 Author Contributions	114
3.7 Acknowledgements.....	115
<i>References</i>	115
Appendix II.....	120

CHAPTER 4: Synthesis of new fluorescent star-shaped liquid crystals derived from thiophene and cholesterol unit

4.1 Introduction.....	131
4.2 Results and discussions	132
4.2.1 Synthesis, Structural Characterization and Thermal stability	132
4.2.2 Mesomorphic behaviour.....	133
4.2.3 Electron density map.....	137
4.2.4 Photophysical behavior	138
4.3 Conclusion	139
4.4 Experimental section.....	141
4.5 Electron density map.....	146

4.6 Quantum Yield Measurement	147
4.7 Author Contributions	147
4.8 Acknowledgements.....	148
<i>References</i>	148
Appendix III.....	154

CHAPTER 5: Color-tunable photoluminescent discotic liquid crystal based on Perylene - Pentaalkynylbenzene triad

5.1 Introduction.....	171
5.2 Result and discussions	173
5.2.1 Synthesis, Structural Characterization and Thermal stability	173
5.2.2 Mesomorphic behaviour.....	173
5.2.3 Electron density maps	175
5.2.4 Photophysical behaviour	177
5.2.5 Electrochemical properties and DFT calculations	180
5.3 Conclusions	180
5.4 Experimental section.....	182
5.5 Electron density map.....	185
5.6 Quantum Yield Measurement	186
5.7 The Lippert-Mataga Plot.....	186
5.8 Author Contributions	186
5.9 Acknowledgements.....	186
<i>References</i>	187
Appendix IV.....	191

CHAPTER 6: Conclusion

6.1 Conclusions	199
List of Publications	205
Conferences and Workshops	207
Originality Reports and Copyrights	209
VITA	217

General Remarks

Chemicals and solvents were all of AR quality and were used without further purification. Column chromatographic separations were performed on silica gel (60-120, 100-200 & 230-400 mesh) and neutral alumina. Thin layer chromatography (TLC) was performed on aluminium sheets precoated with silica gel (Merck, Kieselgel 60, F254). Structural characterization of the synthesized compounds was carried out through a combination of infrared spectroscopy (Perkin Elmer Spectrum AX3), ^1H NMR and ^{13}C NMR (Bruker Biospin Switzerland Avance-iii 400 MHz spectrometer), UV-vis-NIR spectrophotometers (Perkin Elmer Lambda 900 and Agilent Technologies UV-vis-NIR Spectrophotometer), MALDI (Waters synapt G2- S) and elemental analysis (Carlo-Erba 1106 analyser). ^1H NMR spectra were recorded using deuterated chloroform (CDCl_3), dichloromethane (CD_2Cl_2) and dimethylsulphoxide ($\text{DMSO-}d_6$) as solvent and tetramethylsilane (TMS) as an internal standard. The transition temperatures and associated enthalpy values were determined using a differential scanning calorimeter (DSC, Perkin Elmer DSC 8000 coupled to a controlled liquid nitrogen accessory (CLN 2)) which was operated at a scanning rate of $5\text{ }^\circ\text{C min}^{-1}$ or $10\text{ }^\circ\text{C min}^{-1}$ both on heating and cooling. The apparatus was calibrated using indium as a standard. The thermal stability was determined using Thermogravimetric analysis (TGA), which was carried out on a Shimadzu DTG-60 instrument under N_2 atmosphere with a heating rate of $5\text{ }^\circ\text{C min}^{-1}$. Textural observations of the mesophase were performed with Nikon Eclipse LV100POL polarising microscope provided with a Linkam heating stage (LTS 420). All images were captured using a Q-imaging camera. Small-angle/Wide-angle Xray scattering (SAXS/WAXS) studies were carried out on powder samples using $\text{Cu-K}\alpha$ ($\lambda = 1.54\text{ \AA}$) radiation from a source (GeniX 3D, Xenocs) operating at 50 kV and 0.6 mA. The diffraction patterns were collected on a two module Pilatus detector. Fluorescence measurements were performed using a Hitachi F7000 spectrophotometer (Luma 40) from Quantum Northwest. Time resolved lifetime measurements were done on time correlated single photon counter from Horiba Jobin Yvon. For time resolved experiments, excitation was done by 375 nm laser diode. Circular Dichroism (CD) spectra of the samples (thin films) were recorded at $\sim 22\text{ }^\circ\text{C}$ under the nitrogen atmosphere on a J-820 spectropolarimeter (JASCO Ltd., Tokyo, Japan) equipped with a programmable hot stage (Mettler Toledo FP90). Newly procured rectangular quartz plates of dimensions 2 cm x 2 cm and 2 mm thickness were used for the cell fabrication. The requisite sample cells (thin-films) were fabricated by using two clean, regular quartz plates. About 500-

800 μg of the samples, placed individually between the substrates, were heated to their isotropic state, and the top plate was hard-pressed repeatedly to attain the uniform spreading of the analyte over a large area of the cell. This procedure not only expels the air-pockets but also ensures the thin-film formation of the mesogens. The fabrication of such ultra thin-films, using a minute amount of the samples, was essential to circumvent the factual errors associated with experiments and operating limits of the instrument. The samples were then cooled at a faster rate into the LC phase, and the CD spectra were recorded as a function of decreasing temperature. To differentiate the specimens' genuine CD activity from that of the spurious response, the LD spectra were recorded using the instrument's built-in LD data acquisition option. This observation was corroborated using the sample rotation technique, which is very useful and reliable for the thin, evenly spread anisotropic samples. TEM images were recorded using JEOL JEM-F200 at an accelerating voltage of 200 kV. To record the TEM images, drop-casting of isotropic sample on carbon-coated copper TEM grids (TED PELLA, INC. 200 mesh). Thin film Circularly polarized luminescence (CPL) measurements were performed with a Jasco CPL-300 spectrometer. A scanning speed of 50 nm/min, excitation slit width of 4000 μM and emission slit width of 4000 μM , integration time (D.I.T) of 8 sec, and with multiple spectral accumulations were employed.

Cyclic Voltammetry (CV) studies were done using setup by *Princeton Applied Research VersaSTAT 3*. The experimental setup for CV measurements consists of a single compartment cell equipped with Ag/AgNO₃ as reference electrode, platinum wire as counter electrode and glassy carbon as working electrode. 10⁻³ M solutions of all the compounds were used for CV measurements. A 0.1 M solution of tetrabutylammoniumhexafluorophosphate (TBAF) was used as a supporting electrolyte. The half-wave potential of the ferrocene/ferrocenium (Fc/Fc⁺) was calculated as $E_{1/2, \text{Fc}/\text{Fc}^+} = (E_{\text{anodic peak potential}} + E_{\text{cathodic peak potential}})/2$. The LUMO energy levels were obtained by the formula $E_{\text{LUMO}} = -(4.8 - E_{1/2, \text{Fc}, \text{Fc}^+} + E_{\text{red, onset}})$ eV, while the HOMO energy levels by $E_{\text{HOMO}} = -(4.8 - E_{1/2, \text{Fc}, \text{Fc}^+} + E_{\text{ox, onset}})$ eV. DFT calculations were performed with the use of Gaussian 09 suite of packages. A full optimization was carried out using the hybrid functional, Becke's three parameter exchange and the LYP Correlation Functional (B3LYP) at a split valence basis set 6-31G(d,p).

Chapter 1

Introduction to discotic liquid crystal and supramolecular chirality

1.1 Overview

Molecular self-assembly has emerged as a new method for developing soft functional materials with broad implications in materials science and biology. In general, molecular self-assembly is the procedure of arranging molecules into explicit structures via non-covalent and reversible interactions such as π - π stacking, hydrogen bonding, electrostatic, hydrophobic, and van der Waals interactions.^{1,2} The development of microscopic ordering in supramolecular assemblies is significant because molecular architecture plays a crucial role in the optoelectronic properties of the material. It has been the focus of growing areas of chemical research for more than a half-century, involving the design, synthesis, and characterization of novel organic compounds, followed by their application as functional smart materials. Supramolecular assemblies generate by the profound balance between molecule-substrate and intramolecular interactions. In this direction, the molecular engineering of liquid crystals (LCs), particularly discotic liquid crystals (DLCs), has gained expedient space in supramolecular self-assembled systems.⁵⁻⁹

Furthermore, DLCs' molecular architecture, solution processability, self-healing, and self-organizing ability play a vital role in suitable mesophase formation and enhancing optoelectronic scope. One of the key factors in designing DLCs is the molecular shape, terminal groups, and flexible alkyl chains, which all contribute to the molecular organization of these materials. Additionally, it is well known in the literature that small chiral induction in liquid crystalline phases, arising from the doping of chiral molecule or the directly attached chiral molecule, can produce a elicit chiral behaviour in the mesophase. Molecular chirality can also amplify supramolecular chirality in self-assembled liquid-crystalline materials. Supramolecular chirality is generally dynamic property that is sensitive towards external stimuli and the environment. Material scientists find the inclusion of chirality into DLCs fascinating as it not only allows the creation of cholesteric and ferroelectric liquid crystals but also helps understand the overall self-assembly of these molecules.⁵⁻⁹ Liquid crystalline phases that are produced by chiral molecules usually exhibit helical superstructures. The precise control of helicity in DLCs is governed by the shape and size of the central core, peripheral side chain, chiral dopant and donor-acceptor systems. The chirality of the individual molecules

in DLCs reinforces the helical order of discs and side chains and further the arrangement of respective columns. Chiral DLCs with fluorescence characteristics in the solid state are paid much attention to due to their effective integration of intrinsic luminescent ability and molecular self-assembly within a molecule. In this manner, discotic mesogens allow molecular engineering in accordance with the desired property demanded by different device architectures based on OLEDs, organic field-effect transistors (OFETs), OPV solar cells, etc. The assimilation of chirality results in several chirality-related effects such as circularly polarized luminescence (CPL), non-linear optical effect (NLO), ferroelectricity and so on, which can be utilized in novel displays, electro-optical devices, light shutters, polarisation modulators, lasers and other photonic devices, sensors, etc.

The subject of this thesis is the rational design, synthesis and, finally the effect of chirality induction in the DLCs. This thesis aims to investigate the impact of the shape and size of the central core, as well as the side chiral mesogenic unit, on supramolecular self-assembly. The helicoidal columnar self-assembly of chiral DLCs explained via the amplification of molecular chirality to the supramolecular assemblies. Additionally, explained the chirality induced CPL phenomena in DLCs.

1.2 Matter and its states

"Matter is all around you." To date, we have been introduced to matter as something that possesses mass and occupies space. Alternatively, matter is said to be composed of fundamental objects such as atoms, which then combine to make molecules, which in turn make up all known objects in the universe.

Conventionally matter is known to exist in five different states – solid, liquid, gas, plasma and Bose-Einstein (BE) condensates. Intermolecular forces firmly hold molecules together in solids. A highly organised crystalline structure is produced as a result of these intermolecular interactions. In the crystalline state, the molecules are fixed on regular lattice positions possessing only rotational and vibrational freedom.^{3,4} On increasing the temperature, the intermolecular bonding break down and convert to a liquid state, because of thermal energy. Molecules are still close to each other and allowed to rotate, vibrate and translate in all three axes. Still, there is no positional or orientational order in an isotropic liquid state. On further heating, gaseous phase occurs, in which the molecules move apart at high speed with little molecular interaction, and is characterised by the absence of molecular organisation.^{3,4} Materials become ionized as free-floating positively charged ions and negatively charged

electrons at extremely high temperatures, which generally have such a strong attraction that ions and electrons join together (Figure 1.1). This phase of matter defines as the plasma phase.

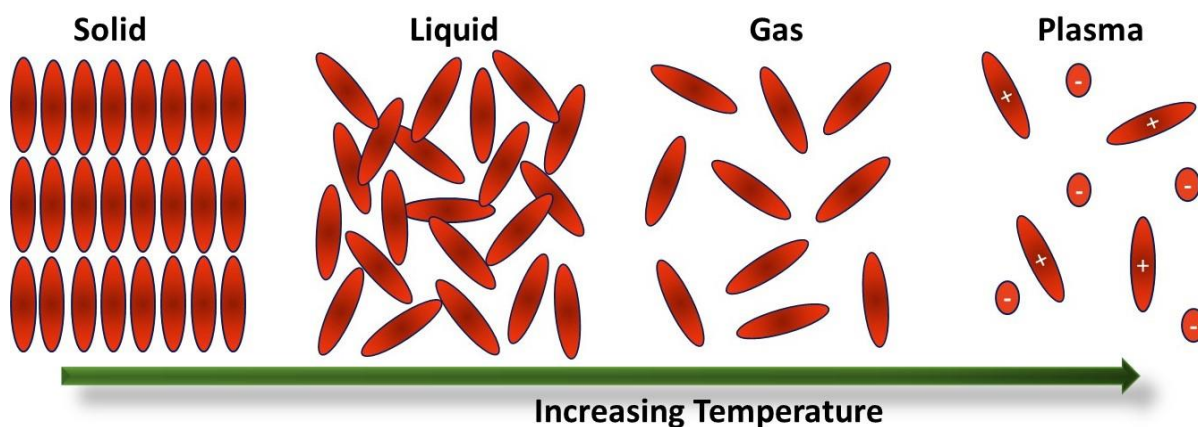


Figure 1.1 Basic phases of matter.

1.3 Liquid crystals

The most common states of matter include solid, liquid and gas. However, in some materials, the transition from solid to liquid does not occur in a single step. It occurs through one or more intermediate phases. These mesophases then fall into two extensive categories: liquid crystals (LCs) and plastic crystals. Plastic crystals are those phases in which molecules retain their positional order within the three-dimensional lattice but lack directional order as they freely rotate. However, liquid crystalline phases possess long-range orientational order and partial positional order. These new phases have optical, mechanical and structural properties between crystalline solid and the corresponding isotropic liquid (Figure 1.2). LCs are one-of-a-kind functional soft materials that integrate order with mobility at the molecular, supramolecular, and macroscopic levels.⁵⁻⁹

As mentioned above, liquid crystal, a unique state of matter between solid and liquid, thereby also called '*mesophases*' uniquely combines the property of order and mobility in this state of matter. The molecules align so that their long axes will tend to orient parallel to each other; hence, the LC molecules are characterized by long-range orientational order and partial positional order. The directional order of LC phases shows that they typically exhibit anisotropic behaviour.¹⁰ This means that various physical properties of the phase are not equivalent if the measure is in different directions. These properties typically include magnetic susceptibility, refractive index, elasticity, dielectric constant etc. Forming a liquid crystalline phase requires a delicate balance of the attractive forces (i.e., dipolar forces between the aromatic cores) and the dispersive forces (i.e., highly dynamic motion of the aliphatic

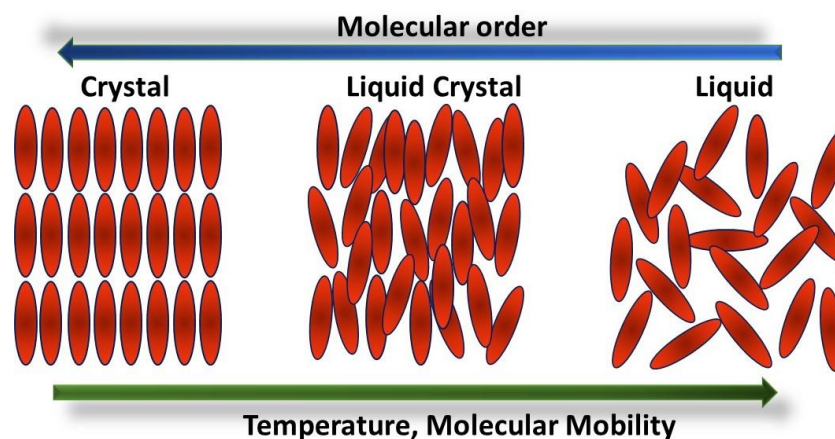


Figure 1.2 Organization of molecules in the crystal, LC, and liquid states of molecules with elongated molecular shape. (Redrawn from reference 6)

side chains) between neighbouring molecules. The fact that LC phases display fluidity and anisotropy makes them useful for device applications such as display technology, temperature sensors, photovoltaic or solar cells, organic field-effect transistors, and organic light-emitting diodes, etc.

This chapter mainly focuses on the basics of LCs, the historical developments in the field of LCs since its discovery in 1888,¹¹ classification of LCs, detailed discussion of discotic liquid crystals (DLCs), chirality in liquid crystals, supramolecular chirality and its application in liquid crystal field.

1.4 Historical remarks

The discovery of LC was a multidisciplinary endeavour and the pinnacle of today's widespread interest among scientists in several domains. Even though researchers in the late 1850s discovered this state of matter, they were unaware of the peculiarities of occurrences. The LC science originated in 1888 when Friedrich Richard Reinitzer, an Austrian botanist and chemist, made critical observations of the coloured phenomena observed in cholesteryl acetate and cholesteryl benzoate, **1** melts.¹¹ He also reported cholesteryl benzoate's "double melting" behaviour, where the crystalline state converted to a cloudy fluid at 145.5 °C. The cloudy fluids clear at a temperature of 178.5 °C (Figure 1.3).

Further, Reinitzer interacted with Otto Lehmann, who worked at the polytechnical school at Aachen. This strange behaviour of double melting was solved by German physicist Otto Lehmann, who first mention them as 'soft crystals'; then 'crystalline fluids' and finally named

as "*Liquid Crystals*" when fully convinced that the opaque phase exhibit property of liquids as well as crystals.¹²

Following this, Lehmann worked extensively on the synthetic LCs and observed that all the LCs were not the same. In 1907 he made the first observation for the exhibition of two liquid crystalline phases in a compound.¹³ After that, in the early twentieth century, chemistry professor Daniel Vorländer at the University of Halle, and his colleagues began a systematic synthetic effort to determine the structure-mesophase link, and by 1935, his laboratory alone had produced around 1100 liquid crystalline substances.¹⁴ He concluded that "*The crystalline-liquid state results from a molecular structure which is as linear as possible,*" implying that molecules with a rod-like or linear molecular shape, generally known as *calamitic LCs*, promote LC behaviour.¹⁵ Later, in 1922, Friedel proposed the classification of calamitics into nematic, smectic and cholesteric solely based on polarized optical microscopy (POM), while the first X-ray experiments were conducted in 1923.^{16,17}

The broad interest in LCs was shown by many researchers around the world, and in 1965, Glenn Brown launched the International Liquid Crystal Conference (ILCC). He organized the first ILCC at Kent state university, Ohio, USA and the application of cholesteric liquid crystals in thermography was described at the conference. The genuine interest was sparked when Heimeier's group presented the first evidence for using LCs in electrooptical display technology at ILCC in 1968. In 1973, George Gray and his co-workers evolved the LC research by introducing the first stable room temperature nematic LC 4'-Pentyl-4-cyanobiphenyl, **2** (5CB) that found applications in LC display technology (Figure 1.3). So now, in the scientific community, the linear rod-like shape of mesogenic molecules has become a generally accepted principle in LC research, which then grew into an interesting field of science.^{18,19}

In 1977, the experimental breakthrough came when one more stunning discovery in the LC field revolutionized the world. In 1977, at Raman Research Institute Bengaluru, Indian scientist S. Chandrashekar and his colleagues reported a new class of LC materials composed of disc-like molecules called *DLCs*. They said the mesomorphic properties in benzene hexa-n-alkanoates, **3** (Figure 1.3).²⁰ After characterizing the phase through POM and XRD, they proposed a model where the disc-shaped molecules stack on top of each other forming columns-like architecture. The development of LCs by disc-shaped molecules also curated a lot of interest among the scientific community worldwide to pursue working in the DLCs domain. Later on, many DLCs were reported by scientists all over the world.

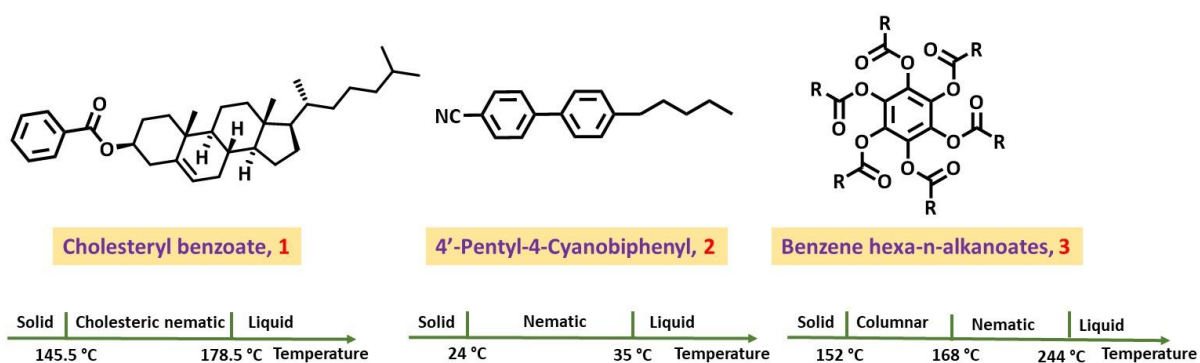


Figure 1.3 Chemical structures of historically important LC molecules.

The most recent advancement in the realm of LCs is banana-shaped or bent-shaped molecules. In 1996, the LC phases formed by banana or bent-shaped molecules were recognized by Niori *et al.* who discovered achiral smectic phases and ferroelectricity.²¹ Although, in 1929, Vorländer synthesized the first bent-shaped LC molecule but did not report the mesomorphic behaviour.²² In the early 1990s, Matsunaga and co-workers also synthesized bent-core mesogens but did not realize the significance of mesophases. An increase in LC research activities was prompted by the finding of ferroelectricity in non-chiral banana-shaped molecules.^{23,24} Additionally, other applications, including flexoelectricity, nonlinear optics, molecular electronics, photoconductivity, and new structural design of the biaxial nematic phase were found for this class of materials.

This final section demonstrates that the applications of LCs have no boundaries and that there are unlimited possibilities for LC applications.

1.5 Classification of LCs

There are several ways to classify LCs, including low molar mass (monomeric and oligomeric) and high molar mass (polymeric) LCs; how LC phases were obtained, such as by varying temperature (thermotropic) or by adding solvent (lyotropic); organic, inorganic, or organometallic based on nature of constituent molecules; the geometrical shape of the molecules (rod-like, disk-like, or banana-like); and the organization of molecules in phase (columnar, smectic, nematic, helical, TGB, etc.) (Figure 1.4). Among the many different types, the most widely recognized and used classification of LCs is into two broad categories:

- (a) Lyotropic LCs (mesophase formation is solvent and concentration-dependent),

(b) Thermotropic LCs (mesophase formation is temperature dependent). If a compound displays both thermotropic and lyotropic crystalline phases, then it is called *amphotropic LC*.²⁵

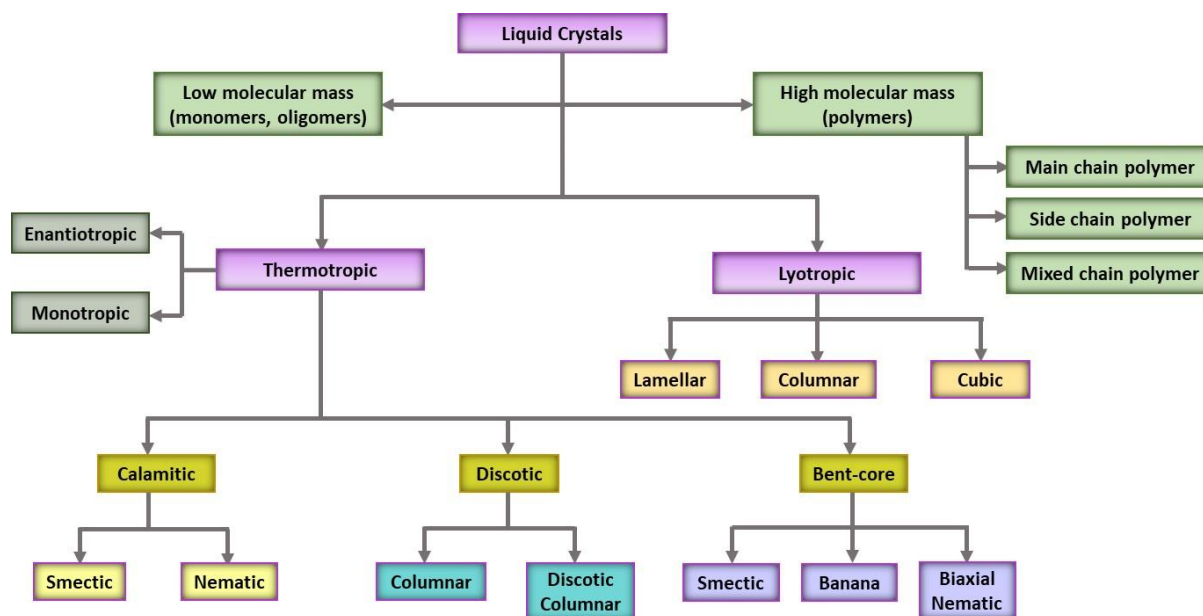


Figure 1.4 Classification of LCs depending on several factors as illustrated in the text.

1.5.1 Lyotropic liquid crystals

Lyotropic LCs, known as anisotropic solutions, are formed by dissolving amphiphilic compounds in suitable solvents under appropriate concentration and temperature conditions. The hydrophilic polar "*head*" and the hydrophobic nonpolar "*tail*" are the two different sections of conflicting character that define amphiphilic substances (Figure 1.5a). When amphiphilic material goes into solution, the hydrophobic tails assemble together and present the hydrophilic polar heads to the solvent, thereby arranging themselves into spheres called *micelles* (Figure 1.5a). The micelles are stable as long as the amphiphilic material is above a *critical micelle concentration* (CMC).²⁵ Concentration or solvent govern the generation of mesophase in lyotropic liquid crystals. Soaps that dissolve in water and phospholipids are two common examples of lyotropic LCs. Lyotropic LC phases can have positional order in one (lamellar), two (columnar), or three (three) dimensions. X-ray diffraction techniques have been used to classify the structures of three main categories of lyotropic liquid crystal phases: lamellar (Figure 1.5b), hexagonal columnar (Figure 1.5c), and cubic phases (Figure 1.5d).

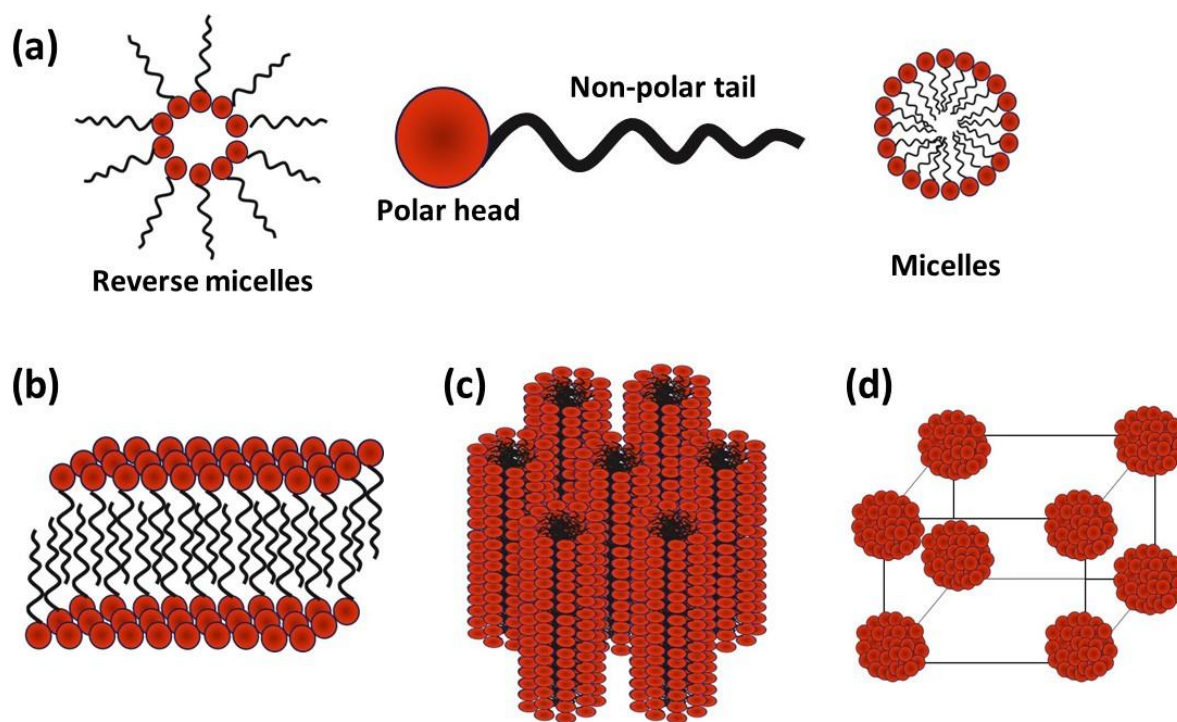


Figure 1.5 Schematic representation of (a) micelles, lyotropic LC organized as (b) Lamellar, (c) Hexagonal columnar, and (d) Cubic phase (Redrawn from reference 23).

1.5.2 Thermotropic liquid crystals

Thermotropic LCs are those LCs where the liquid crystalline phase is formed on varying the temperature of the material. Thermodynamically stable LCs appearing on heating and cooling is called enantiotropic thermotropic LCs. The mesophases that are obtained by temperature variation in the cooling cycle is called monotropic LCs.²⁶ The crystal-to-mesophase transition temperature is defined as the melting point, while the clearing point is the temperature at which a mesophase changes from a mesophase to an isotropic liquid. A molecule must have a central core (typically aromatic) and a flexible peripheral moiety (generally aliphatic chains) in order to be a thermotropic liquid crystal (Figure 1.6). The driving factors for creating mesophases also include interaction anisotropy and micro-segregation, in addition to geometric anisotropy. Thermotropic liquid crystals are divided into three major groupings according to the shape of the mesogenic molecules: (a) calamitic (rod-like); (b) discotic (disc-like), and (c) bent-core (banana-like).

This thesis deals with the DLCs (disk-shaped); therefore, it will be elaborately described in the next section.

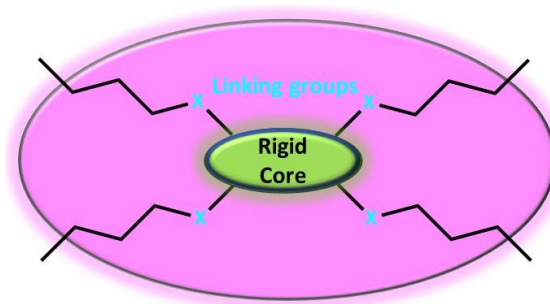


Figure 1.6 General template for liquid crystals.

1.5.2.1 Discotic liquid crystals

The hierarchical self-assembly of disc-shaped molecules leads to the formation of DLCs. The discovery of DLCs in 1977 by S. Chandrasekhar²⁰ and his colleagues showed that the self-organization of disc-shaped molecules, quite different from the conventional rod-shaped LCs (discovered in 1888 by Reinitzer) could also lead to mesomorphism. Since then, sincere efforts have been made to understand the nature of the molecular aspects that can favour the formation of DLCs. It is now well known that the disc-shaped molecules are composed of rigid and highly planar aromatic (π -conjugated) cores decorated with flexible alkyl chains.²⁵ The aromatic cores can be composed of polycyclic aromatic hydrocarbons and hetero-aromatic hydrocarbons. Discotic cores based on the *polycyclic aromatic hydrocarbons* are- perylene, chrysene, anthraquinone, hexabenzocoronene, truxene, graphenes, triphenylene etc., and based on *polycyclic hetero-aromatic hydrocarbons* are hexaazatrinaphthylene, phthalocyanine, heptazine, hexaazatriphenylene, bisphenazine, triazatruxene etc. In addition to discotic molecules, there are other types of mesogens that have a non-disc arrangement which can also be utilized as building blocks for discotic liquid crystals.^{27,32} These include polycatenary mesogens, which are composed of biforked molecules having a rod-like rigid core with two half-disc moieties positioned at each end. Due to their unique molecular structures, polycatenary mesogens can form a columnar mesophase.³³⁻³⁵ Many linkers, such as ether, ester, thioether, amide, alkanoyloxy, alkynyl, and so on, are used to connect the flexible side groups with the central core. The liquid crystallinity in the DLCs mainly results from the nano-segregation between the two parts: crystalline character is prompted by the interaction among rigid π - π conjugated cores, while the melting of flexible alkyl chains is responsible for providing fluidity to the system. These disk-shaped molecules instinctively self-assemble in 1D stacks, which self-organize on distinct 2D lattices; there is no translational order in the third dimension (Figure 1.7). The anisotropic nature of the mesogenic molecules results in various

molecular packing in their respective mesophases. Discotic molecules, in particular, can self-organize into three types of assemblies in a broader way:

- a) Discotic nematic
- b) Discotic smectic, and
- c) Discotic columnar self-assemblies

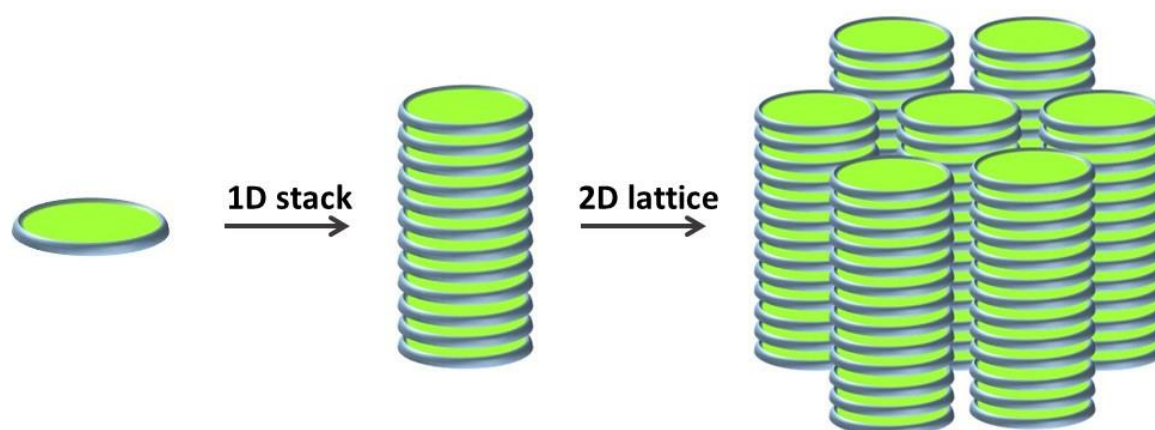


Figure 1.7 Self-assembly of disc shaped molecules in 1D stack, which further organize on 2D lattice.

1.5.2.1.1 Nematic phases of discotic mesogens

Based on the molecular arrangement, the nematic phase of disc-shaped molecules can be divided into four categories (Figure 1.8):

1. Discotic nematic (N_D),
2. Chiral discotic nematic (N_D^*),
3. Columnar nematic (N_{Col}) and
4. Nematic lateral (N_L)

The discotic nematic (N_D) phase is a mesophase that exhibits low order, low viscosity, and high symmetry when compared to other nematic phases. In this phase, the molecules are generally oriented parallel to each other, displaying orientational order but lacking long-range positional order (Figure 1.9a). Typically, the nematic phases formed by disc-shaped molecules and rod-shaped molecules do not mix well. However, the symmetry of the nematic phase resulting from molecules with disc shapes is identical to that of molecules with rod shapes. In the discotic nematic phase, the director is along the short molecular axes of the molecule as the disc normal is arranged orientationally.^{36,37} Additionally, similar to the chiral calamitic nematic or cholesteric phase, a chiral discotic nematic mesophase (N_D^*) also exists, which is characterized by a helical structure. (Figure 1.9b).³⁸ The molecules are stacked in columns during the nematic

columnar phase. These columns exhibit long-range orientational and short-range positional order (Figure 1.9c), but they do not form 2D lattice structures.³⁹

Another nematic phase is reported due to strong lateral contacts, in which disc-shaped molecules cluster into massive superstructures and exhibit a nematic configuration. This is known as the nematic lateral (N_L) mesophase. (Figure 1.9d).⁴⁰

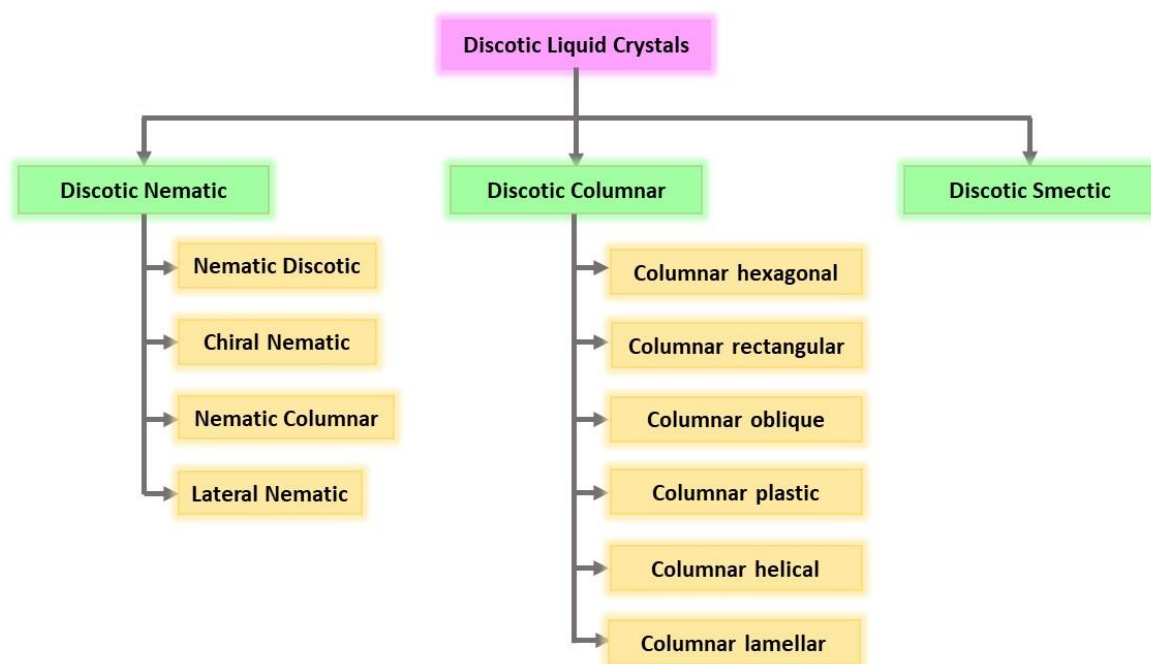


Figure 1.8 Detailed classification of DLCs.

1.5.2.1.2 Smectic phases of discotic mesogens

Similar to calamitic smectic mesophases, the discs in discotic mesophase are stacked and spaced apart by peripheral chain sublayers. Because the layers will constrain molecular rotations at their long molecular axes, they are expected to exhibit biaxial smectic phases.^{41,42} Unlike nematic and columnar, smectic phases are rare in discotic LCs.

1.5.2.1.3 Columnar phases of discotic mesogens

The most common mesophase formed by disc-shaped molecules is the columnar phase. In this phase, molecules stack on top of each other to create columns, and these columns then self-organize into various 2D lattices. Molecules in such a phase have a positional order in two dimensions and are disordered in the third. These molecules can be arranged in an ordered and disordered manner.^{36,43} Columnar phases are prosperous and are normally classified at three levels, according to the symmetry of the 2D array, the orientation of the core with respect to

the column axis, and finally, the degree of order within the column. Based on that, the columnar mesophases are classified into different categories such as:

1. Columnar hexagonal mesophase (Col_h),
2. Columnar rectangle mesophase (Col_r),
3. Columnar oblique phase (Col_{ob}),
4. Columnar plastic phase (Col_p),
5. Columnar helical phase (H), and
6. Columnar lamellar phase (Col_L)

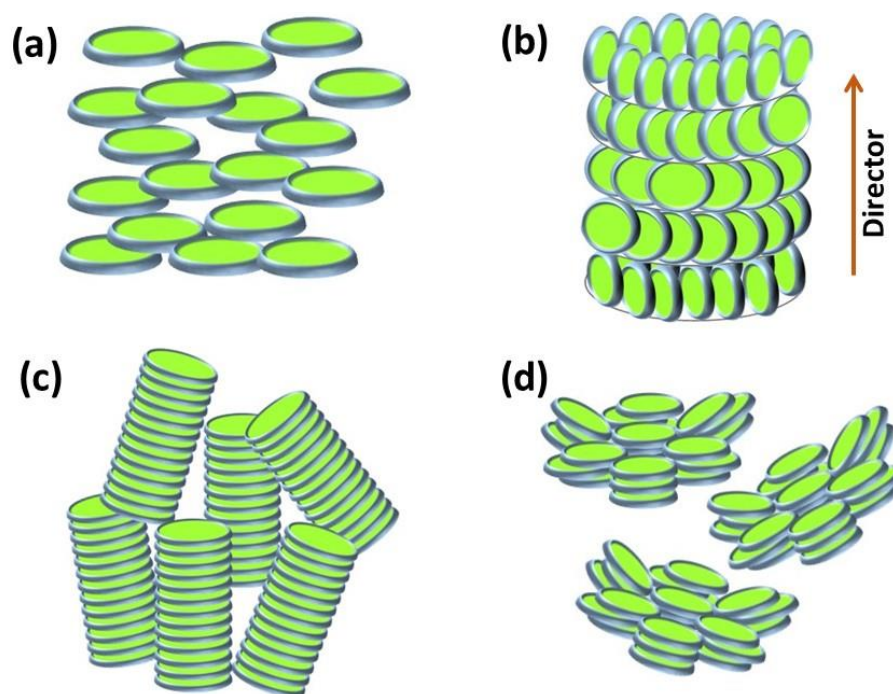


Figure 1.9 Schematic representation of different nematic phases formed by disc shaped molecules (a) Discotic nematic, (b) Chiral discotic nematic, (c) Columnar nematic, and (d) Nematic lateral. (Redrawn from reference 37)

The columnar hexagonal phase refers to a specific arrangement of molecular columns characterized by a hexagonal packing pattern (Figure 1.10a). In Col_h the mesogens are arranged perpendicular to the column axis, while in the Col_r the molecules are tilted with respect to the column axis (Figure 1.10b).⁴³ Another variation, Col_{ob} , features an oblique unit cell arrangement of the columns (Figure 1.10c). Col_p has 3D crystal-like organization in a hexagonal lattice, and the discs within the column can rotate about the column axis. (Figure 1.10d).⁴⁴ Despite some structural abnormalities that can occur in the hexagonal phase, such as

longitudinal and lateral displacements, non-parallel disc arrangement, and rotation around the columnar axis, the discs still experience restricted motional freedom within the plastic phase. Another phase, the columnar helical phase, is characterized by the formation of helical columns that interdigitate in groups of three columnar stacks. (Figure 1.10e).^{45,46} A layered structure, i.e., Col_L, exists for mesophases of certain discotic mesogens (Figure 1.10f).⁴⁷

Columnar mesophases formed by disc-shaped molecules are fascinating because of their importance in functional materials. They have found applications in the field of 1D conductors, photoconductors, photo voltaic solar cells, organic light emitting diodes (OLEDs), organic field effect transistors (OFETs), etc.

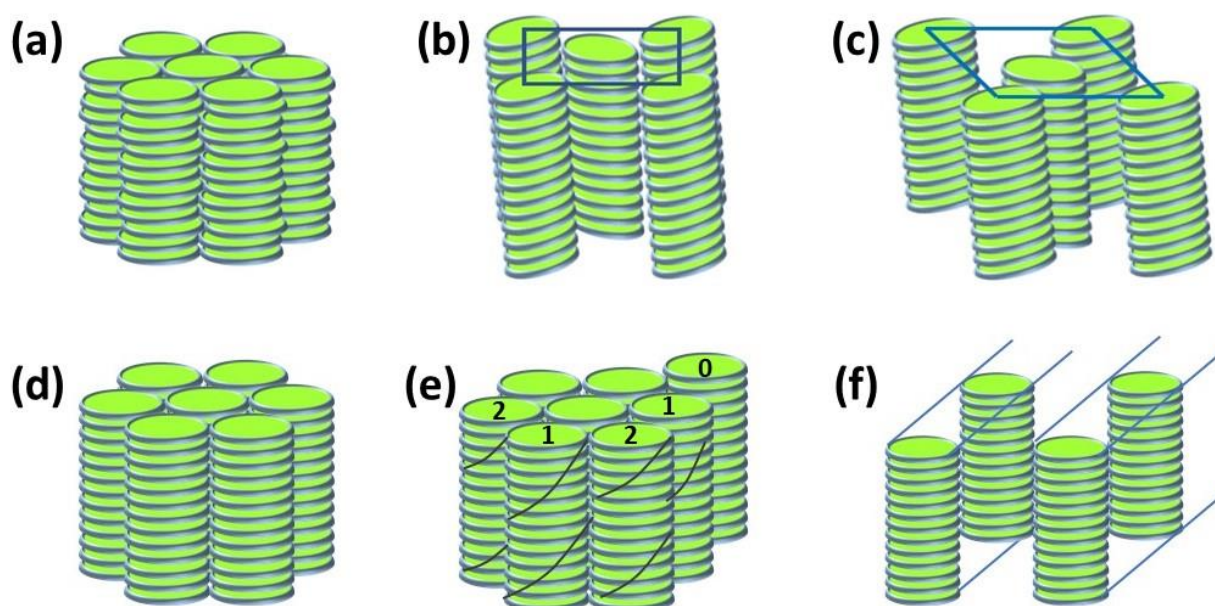


Figure 1.10 Schematic representation of different columnar phases (a) Hexagonal columnar phase, (b) Rectangular columnar phase, (c) Columnar oblique phase, (d) Columnar plastic phase, (e) Columnar helical phase, and (f) Columnar lamellar phase. (Redrawn from refence 43)

1.6 Characterization of DLCs

LC mesophases are generally characterized by using a combination of techniques such as Polarized Optical Microscopy (POM), Differential Scanning Calorimetry (DSC) and Small/Wide Angle X-ray Diffraction (SAXS/WAXS). POM is used for textural observation, which is observed due to its anisotropic nature, as shown in the Figure 1.11. The exact phase transition temperatures can be obtained by DSC (Figure 1.12). The molecular packing in

different lattices can be determined using the SAXS/WAXS study (Figure 1.13). The first step to detect the existence of the LC phase is the presence of shearable birefringent textures under

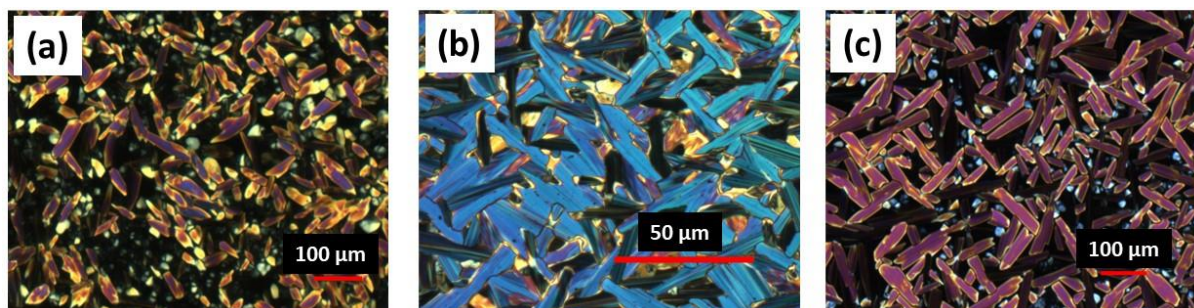


Figure 1.11 POM textures of discotic columnar compound, (a) Col_h phase at 280 °C, (b) Col_{ob} phase at 150.9 °C, (c) Col_r phase at 225 °C.¹⁰⁰

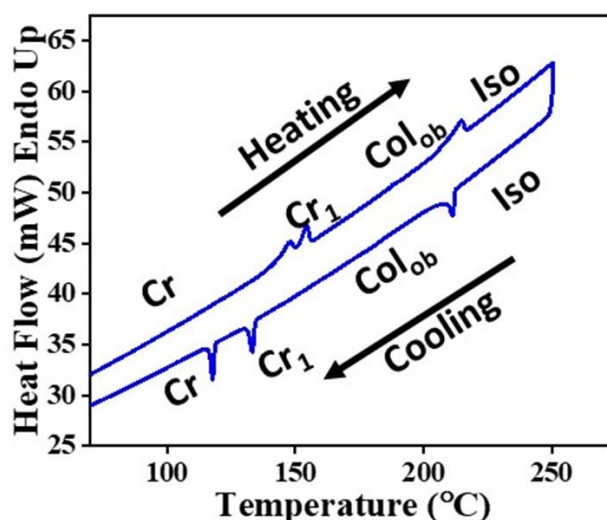
POM. A polarizing optical microscope consists of a pair of crossed polarizers, and a thin film of the compound under investigation is placed below it. Crossed polarizers typically don't emit any light since the light coming from the first polarizer is entirely absorbed by the second polarizer. In LCs, the director normally points in various directions at various places in the sample. Areas with the director parallel or perpendicular to the polarizer axis seem dark, whereas areas having an angle with the polarizer axis other than 0° and 90° appear bright. In addition, the LC phases show shearability due to the rotational motion of molecules.

The exact phase transition temperatures and their associated enthalpies are estimated from the corresponding peaks observed in the DSC thermogram (Figure 1.12). DSC determines how much heat a substance absorbs or releases as a function of temperature or time (isothermally). The enthalpy value is an indication of the order present in the mesophase. The less-ordered nematic phases are usually associated with lower enthalpies than the columnar phases.

The X-ray analysis provides direct information about the positional order in a liquid crystal, which aids in determining the structure of a specific phase. The small-angle region indicates the type of columnar lattice, while the wide-angle region provides the intracolumnar information. The basic principle of XRD is Bragg's law which states that x-rays reflected from adjacent atomic planes separated by distance d of a crystal interfere constructively when the path difference between them is an integer multiple of wavelength λ ,

$$2d\sin\theta = n\lambda$$

where n is an integer that gives the order of reflection. The reflected rays make an angle of 2θ with the direction of the incident beam.



DSC transition temperatures

Heating: Cr 147.6 °C Cr₁ 154.5 °C Col_{ob} 214.7 °C Iso
 Cooling: Iso 211.3 °C Col_{ob} 133.2 °C Cr₁ 117.7 °C Cr

Figure 1.12 A DSC thermogram displaying the phase transitions in Col_{ob} mesophase.¹⁰⁰

Another useful information about molecular self-organization in the mesophases can be obtained from the electron density maps (EDM). EDM provides electron density variation; for instance, high electron density regions correspond to the rigid aromatic cores, while the low electron density regimes represent the alkyl chains. The obtained electron density contrast clearly visualizes the molecular arrangement in the columnar 2D lattice. The EDM is usually calculated by taking into account the intensity of intense diffraction peaks observed in XRD pattern.

1.7 Chirality

"Chirality is a basic characteristic of living matter and nature." Chirality is a property that describes an object's inability to be superimposed on its mirror image. To determine if a molecule is chiral, it is preferable to identify an asymmetric carbon atom in the molecule. An asymmetric carbon is defined as a sp^3 carbon atom that is linked to four different types of atoms or groups of atoms.⁴⁸ However, a molecule may also be defined as chiral even if there is no asymmetric carbon atom, such as when it has two non-coplanar rings that are dissymmetrically connected and cannot rotate around their connecting bond, or if it contains an axis on which a group of substituents is arranged in a manner that cannot be superimposed on its mirror image.^{49,50} This type of chirality can be referred to as planar or axial chirality. As a result, there are three types of molecule chirality: point, plane, and axis chirality.⁵¹

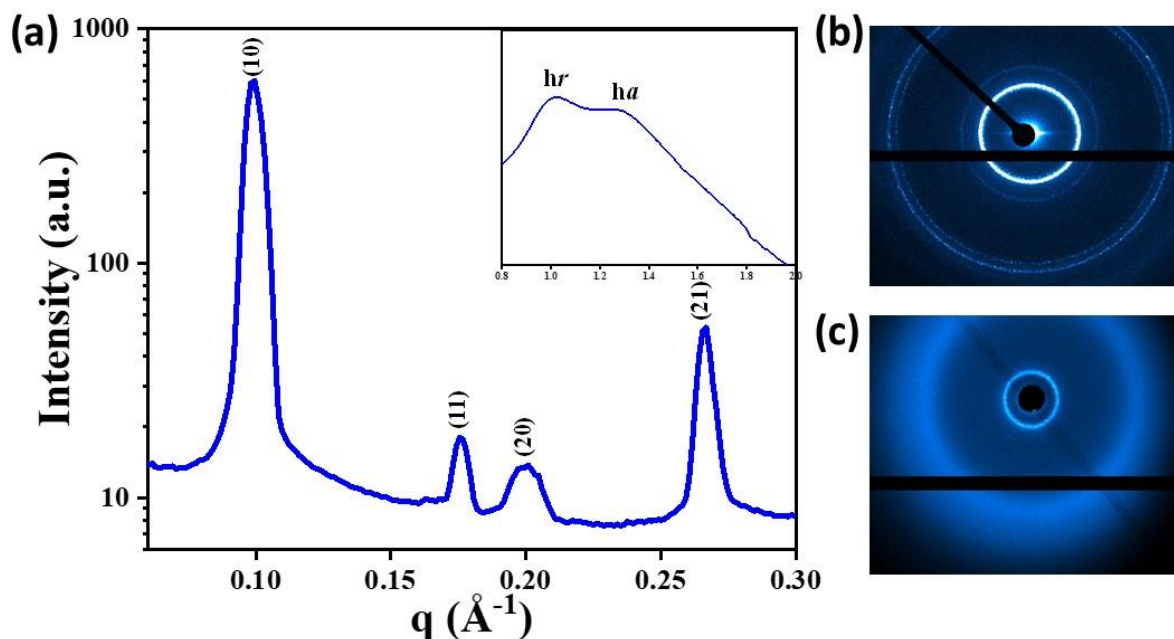


Figure 1.13 (a) Small- and wide-angle (inset) X-ray diffraction patterns of the Col_h phase formed by compound upon cooling (hr, cholesterol–cholesterol correlation; ha, alkyl chain–chain correlation;), (b) 2D SAXS, and (c) 2D WAXS, diffraction patterns for the compound.¹⁰⁰

Chirality plays a fundamental role in guiding the assembly of constituent building blocks into self-assembled helical structures.^{52,55} The resulting chiral structure is highly ordered, leading to the hierarchical self-assembly of molecules with different interactions. The properties and design of building blocks are essential for hierarchical self-assembly into chiral nanostructures.⁵⁶ Introducing a chiral element to molecules or units is generally what determines the final supramolecular chirality, while the balance between different interactions directs the hierarchical self-assembly. Introducing a chiral element to molecules is generally determines the final supramolecular chirality and the balance between different interactions promotes the hierarchical self-assembly. Both of these factors are equally significant for chiral annotation on different scales and the corresponding functions of the resulting structures.

1.8 Supramolecular chirality in liquid crystals

The history of LC started with chiral molecules, the ester of cholesterol, and since then, several new chiral molecules have been extensively explored.¹¹ These compounds have asymmetric molecular structures and, therefore, promotes optical activity and chirality in the system. This finding by Lehmann and Reinitzer had two effects: it launched research into the new field of liquid crystals. It marked a new era of interest in organized systems' optical activity and chirality. This modest demonstration of the first liquid crystal highlights two essential

symmetry elements in complicated fluids. First, the molecular structures of the constituent molecules of the phase have no mirror symmetry and hence have the feature of being handed. As a result, the molecules are both optically active and chiral. Second, the assembly of these molecules in the cholesteric phase, fluid forms a helical liquid crystal that is also optically active and chiral.

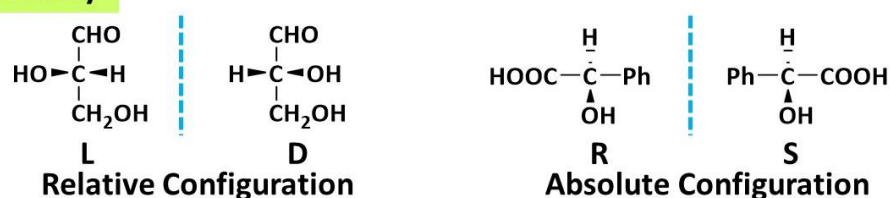
Chirality plays an important role in the design of liquid crystal-based supramolecular materials. It is widely recognized that even a small chiral perturbation in liquid crystalline phases, which can arise from either a chiral dopant or from the mesogen itself, can induce a highly cooperative chiral response in the mesophase. For instance, the design and synthesis of materials can produce molecular chirality, and the resulting molecular chirality can then be used to modulate the chirality of the liquid-crystalline mesophase. Supramolecular chirality in liquid crystal systems can arise from chiral molecules, a combination of chiral and achiral molecules, or exclusively achiral molecules. The way in which the LC mesogens assemble plays a crucial role in determining supramolecular chirality, but the chirality of the LC mesogens is also important in determining this assembly in supramolecular systems.⁵¹ In combined systems of chiral and achiral molecules, the interaction between these molecules can induce achiral molecules to form chiral assemblies. In exclusively achiral systems, supramolecular chirality arises from the formation of supramolecular structures.⁵⁷ For example, the ability to control the pitch and handedness of the helical structure of the chiral phase in liquid crystals is highly dependent on the molecular geometry of the constituent molecules. This knowledge has been applied to the design of chiral liquid crystal mixtures for the development of low-cost liquid crystalline thermometers and thermochromic paints and coatings used in surface thermography. By carefully controlling the molecular design of the constituent molecules, it is possible to achieve highly tunable and responsive chiral LCs, and opening up new opportunities for the development of advanced functional materials.^{58,59}

The chirality of a supramolecular structure is often determined by the chirality of its constituent molecules, which may possess point chirality or axial chirality. The molecular chirality can also affect the way the molecules assemble into supramolecular structures, leading to different types of helical, spiral, or sheet-like architectures with supramolecular chirality. Supramolecular chirality is often dynamic and can be influenced by external factors such as temperature, pressure, and solvents, leading to changes in the molecular packing and the overall supramolecular chirality, which makes it a useful property for a wide range of applications (Figure 1.14).^{57,60}

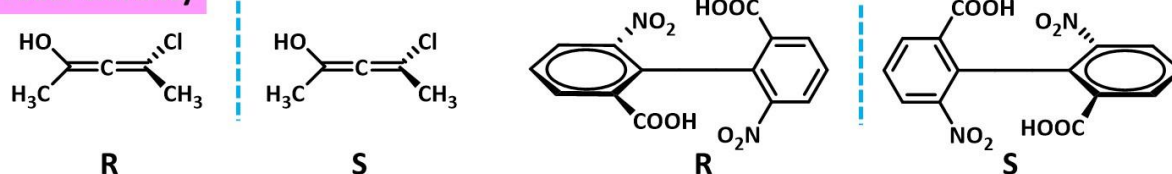
Helicity is a type of axial chirality, which refers to a molecule or entity with an axis that holds a group of substituents in a spatial arrangement that cannot be superimposed on its mirror image. When noncovalent bonds connect these substituents along the axis, supramolecular assemblies can exhibit helical chirality. This type of chirality is quite prevalent in supramolecular systems, and can be classified as either *P* or *M* helicity. (Figure 1.14).⁵⁷⁻⁶¹ When a molecule or supermolecule is rotated clockwise or anticlockwise, the system has *P* and *M* helicity, respectively, when seen from either end along the helical axis.

Liquid crystalline phases that are composed of chiral molecules usually have helical macrostructures. Generally, the molecules' orientational ordering twists and produces a helical configuration. In liquid crystalline phases, the molecules have two primary helical configurations. One forms a single-twist structure when the orientational ordering of the molecules occurs in one preferred direction. The helix forms in more than one favoured direction in the alternative scenario, resulting in a three-dimensional helical network.⁶² Just like other molecules, the introduction of chirality to the system dramatically impacts the properties. Several phases exhibit helical superstructures, for example, the chiral nematic or cholesteric phase, where the director describes a spiral along the axis.

Point chirality



Axial chirality



Helical chirality

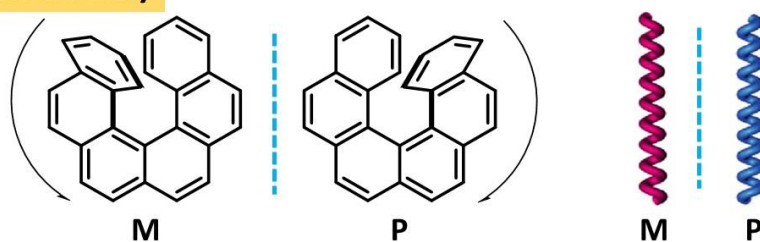


Figure 1.14 Some typical chiral molecules showing different ways of chirality and corresponding naming convention. (Redrawn from reference 51)

This results in the reflection of circularly polarised light, which can be employed in various applications.⁶³ The formation of helix in the chiral smectic phase is linked to the development of spontaneous polarisation and ferroelectricity.⁶⁴ Chiral LCs also exhibit frustrated phases, including blue phases and twist grain boundary phases. Additionally, these phases exhibit various chirality-related effects, which can be utilized in the development of novel displays, photonic devices, light shutters, polarisation modulators, lasers, sensors, and other similar applications.

The foundation of this thesis is based on chirality in discotic liquid crystals, which is explored in detail in the next section.

1.8.1 Chirality in DLCs

The inclusion of chirality into DLCs is an intriguing and crucial element for LC community, not only because it allows for the creation of cholesteric and ferroelectric liquid crystals but also as a tool for understanding the overall self-assembly of these molecules. The chiral discotic-columnar phases are of particular interest because the chirality of the individual molecules can be improved first within the respective columns and then by the arrangement of the columns (Figure 1.15).⁶⁵ The initial reinforcing effect is thought to be caused by the helical order of discs or their side chains, while the helical order of columns leads to the second reinforcing effect. In essence, molecular chirality controls supramolecular chirality.

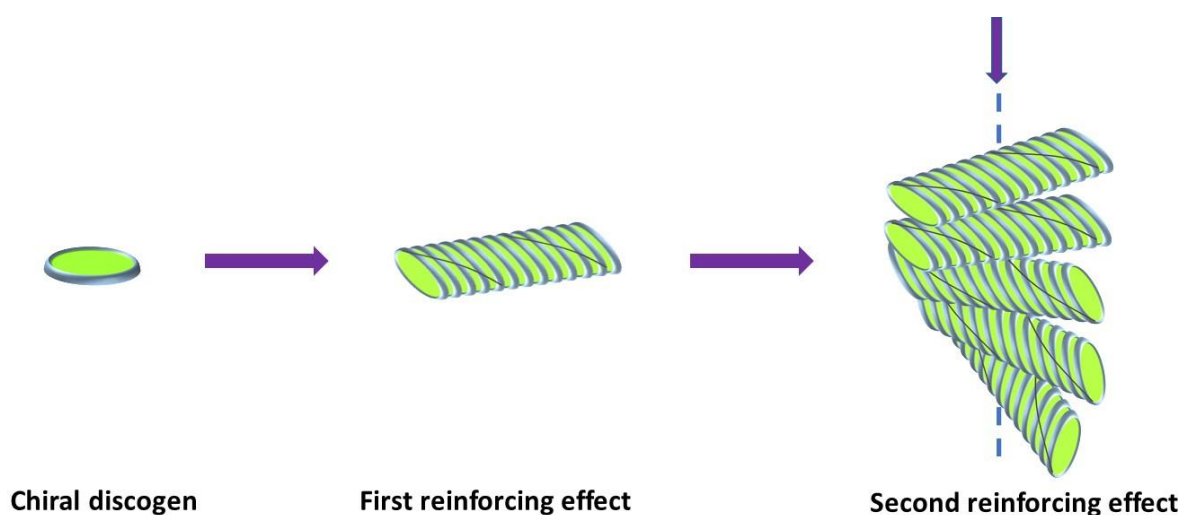
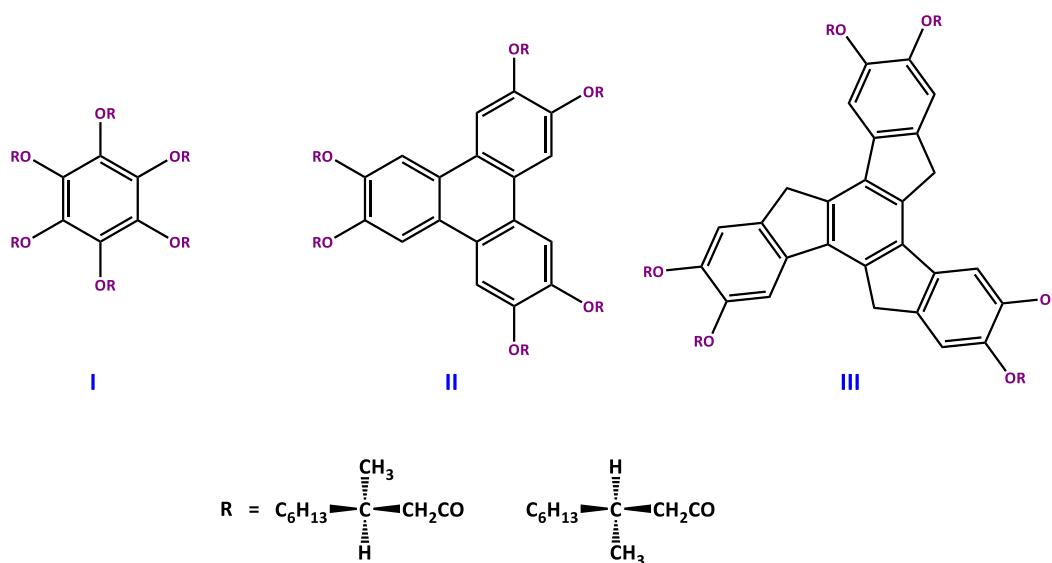


Figure 1.15 Induced helicity in chiral discotic liquid crystals. (Redrawn from reference 65)

1.8.1.1 Chirality induction in discotic nematic (N_D^*) mesophase

After discovering DLCs in 1977, efforts were made to prepare optically active discotic LCs to observe the effect of molecular chirality on mesophase formation and their physical properties. The approach by which molecular chirality transitioned to supramolecular chirality is the attention of numerous groups worldwide. In 1980, Destradre and co-workers tried to induce chirality to the discotic nematic mesophase using chiral benzene, triphenylenes, and truxenes esters (compound I, II and III) as mesogenic units.⁶⁶ Although these compounds exhibited columnar mesomorphism, no mesoscopic signs of chirality existed. After mixing these esters with 2,3,6,10,11-hexa-*n*-heptyloxybenzoate of triphenylene (IV), the cholesteric textures were shown. The chiral compounds successfully twisted the nematic mesophase (N_D) of IV into a chiral phase. This resulting mesophase is called chiral nematic discotic mesophase (N_D^*), molecular arrangements shown in Figure 1.9b.



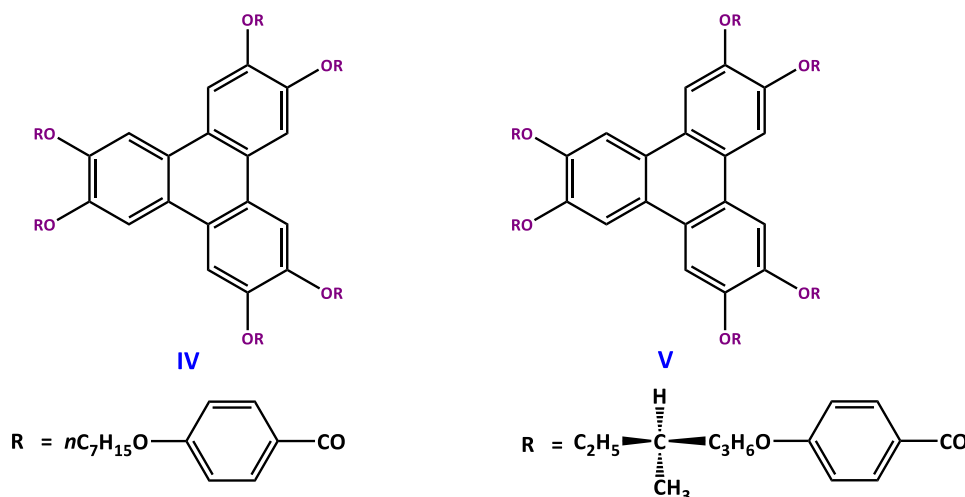
In the extension of this work, the same group synthesized chiral triphenylene derivative V, and this was the first discotic molecule to show a (N_D^*) mesophase. The chiral side chains induce a twist in the N_D phase. Although several related derivatives failed to display the same properties, cholesteric properties highly depended on the chiral chain structure. After observing that the nematic phase of IV was twisted by adding a small amount of II and finding a chiral nematic phase for V, the authors carefully re-examined the two columnar mesophases they had previously observed for II.⁶⁷ They observed some spirallization in the mesophase textures,

which is an indication of twisting. The spiralling structure is observed with the director twisting around an axis perpendicular to the long molecular axis. The chiral N_D^* phase formed by compound V is completely miscible with the N_D phase of no-chiral molecules, indicating the structural similarities between the two mesophases. In addition, it was observed that the chiral mesophase could be oriented in a magnetic field. N_D^* phase consists of a spatial arrangement of molecules that spontaneously rotate with a constant angle along the helical axis direction (Figure 1.9b). The helical sense of the director is correlated with the configuration of the chiral group present in the molecule. The helical pitch (p) is the distance over which liquid crystalline molecules rotate by an angle of 180° . This periodic arrangement of the LC molecules is responsible for the selective Bragg's reflection of light. Hence, the reflection of light can be controlled by changing the helical pitch via some modification in the molecules. Bragg's reflection can be defined as:

$$\lambda = n \times p^{127}$$

where $n = (n_o + n_e)/2$, n is the average of ordinary refractive index (n_o) and extraordinary refractive index (n_e) and p is the helical pitch.

On passing the unpolarized light through the helical macrostructure, circularly polarized light of the same handedness is reflected, whereas the rest 50 % is transmitted. The wavelength of the circularly polarized light reflected is dependent on the helical pitch. Therefore, helical pitch



(p) and the orientation of the helix play an important role in determining the wavelength of the light reflected from the helix. The ability of the chiral dopant to induce twist deformation in the nematic LC is known as helical twisting power (HTP, β), represented as:

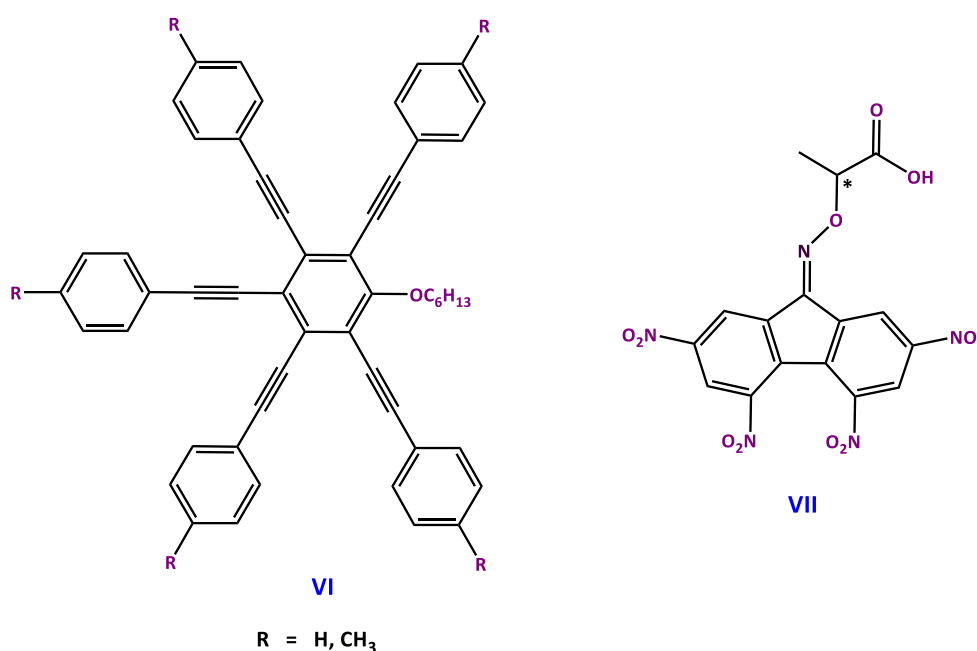
$$\beta = 1/(p \times e.e. \times c)$$

where p , is the helical pitch, e.e. is the enantiomeric excess of the chiral dopant, and c is the concentration of the chiral dopant.

In 1993, Praefcke and co-workers showed that the chirality can be induced in N_D phases by π - π stacking ability of molecules and their different charge transfer properties. The binary mixture of electron-rich mesogenic unit VI and the chiral electron-deficient molecule VII displayed a twist in the mesophase.⁶⁸ The same group published structurally comparable chiral pentaynes in 1995, demonstrating that a variation in lateral substituents could induce a small helical pitch or a temperature-induced helix inversion.⁶⁹ The temperature of the helix inversion was unaffected by the addition of a nonchiral nematic discotic, showing that a molecular characteristic of the chiral molecule alone predominantly caused the effect.

1.8.1.2 Chirality induction in discotic columnar mesophases

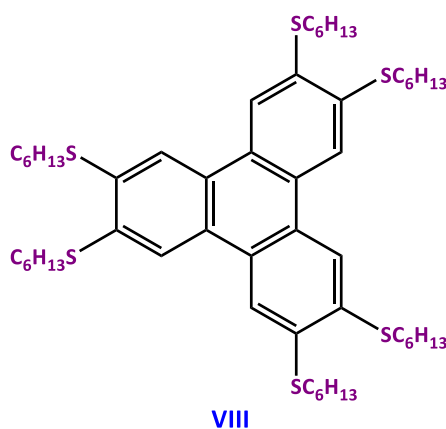
The most well-known example of helical order in the column can be found in nature, in deoxyribonucleic acid (DNA). Helicoidal columns are not formed by most chiral and achiral discotic molecules. The chirality of chiral DLCs is typically found in the side chains, with the flat core being achiral.



The self-assembled columns are not helical because of the lack of substantial interactions between the chiral side chains. On the other hand, helical columns are formed if the core has an intrinsic shape, steric hindrance, or presence of some polar group that give rise to stacking with a preferred rotation. Chirality presented in the side chain and the central core works hand-in-hand for the helical order in the columnar mesophase.

Heiney and colleagues were the first to report the presence of helical order in a discotic columnar mesophase in hexa-hexylthiotriphenylene (VIII).^{70,71} This compound displayed a Col_{hd} mesophase at high temperatures and a Col_{ho} organization at low temperatures. At low-temperature, a triangular array of columns with a periodic, positional, and uneven helical intracolumn arrangement was observed. The helicity amid the columns of VIII was attributed to the steric bulk provided by the sulphur atoms connecting the tails to the core. Triphenylenes with sulphur atoms, unlike their oxygen analogues, cannot stack neatly on top of one other due to the sulphur atom's relatively large Vander Waals radius. (1.85 Å). Hence, discs are arranged with a preferred rotation that preserves the arene-arene interaction, and this hindered stacking leads to helical arrangements.

In 1997, Meijer and co-workers reported a series of compounds with propeller-like geometry and extended core planarization via intramolecular hydrogen bonding.⁷² They observed quadruplet split signals in the XRD and explained that these signals appeared due to the twist prompted into the column by the non-perpendicular arrangement of the propeller-like aromatic core concerning the columnar axis. Intermolecular hydrogen bonding, in addition to the propeller-like organization of the molecules, plays a significant role in the helical order of columns.



However, these compounds are achiral but possess supramolecular helicity. The significance of side alkyl chains was similarly addressed by replacing aliphatic chains with glycolic chains,

and no change in helical organization was seen.⁷³ Following that, various groups reported the columnar helical order in propeller-shaped discogens and hydrogen-bonded LCs.⁷⁴⁻⁷⁸

In 1998, Nuckolls and Katz used a different approach to produce the helical columnar liquid crystal. They used helicene as a central core, a helix on its own. These DLCs successfully develop a helical column in the aggregated state because of the intrinsic shape effect of helicenes.⁷⁹ These chiral discotic LCs have been proven to be interesting materials for second-order non-linear optics because of high amplification of chirality. The above discussion showed that steric factor, propeller-like structure and hydrogen bonding play an important role in the chirality induction in columnar mesophase.

Spiess and co-workers have shown that triphenylene with a chiral side chain gives rise to the helical columnar arrangement arises because of ester's out-of-plane conformation.⁸⁰ This is also observed in phthalocyanines, where the presence of chiral centers in the side chain induces chirality in the mesoscopic system, despite the formation of nonhelical columns by the phthalocyanines themselves. In 1993, Van Nostrum and colleagues were the first to report a confirmation of a chiral superstructure in the discotic mesophase of chiral phthalocyanines.⁸¹⁻⁸³ Apart from phthalocyanine, Müllen and co-workers in 2001 induced chiral side chains in hexabenzocoronene and results explained that the molecule successfully exhibits helical columnar arrangement.⁸⁴ Hereafter, researchers tried various methods to produce helicity in the columnar mesophase, one of which was by inserting distinct polar units into the central core. In this series, Praecke *et al.* and Boden *et al.* displayed triphenylene-based DLCs where the halogen atom is directly attached to the core.^{85,86} These derivatives become helical, but no expression of the helicity is observed at the mesoscopic level. A recent example of inducing helicity in DLCs with a polar group linked to the core is observed in tetraphenylbenzene-based LCs by applying an electric field. The helical twist that appeared in columns from the electric field is because of a polar fluorobenzene ring that directs the propeller-like conformation to the molecule.⁸⁷ On the other hand, chiral nature of carbohydrate-based core and shape give rise to intrinsically chiral DLCs. The helical arrangement of these systems was very sensitive towards the changes in alkyl chains, and even slight modifications destroy the helicity.

In this thesis, chiral side chain mesogenic units and the propeller-like shape of the core are employed to induce helicity in the columnar organization. The chiral side chain moiety used in this thesis is cholesterol, consisting of 8 chiral centres. The structure of cholesterol, along with eight chiral centres, is presented in Figure 1.16.

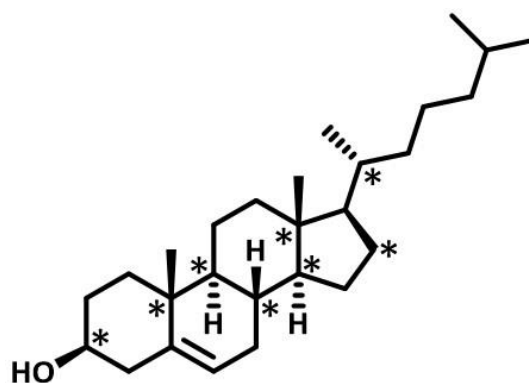


Figure 1.16 Molecular structure of cholesterol representing eight chiral centres.

1.9 Characterization of supramolecular chirality

An important step is the characterization of the supramolecular chirality. Although there are many ways to characterize, generally, two classes of characterization of supramolecular chirality are applied. One is morphological observation, and the other class includes spectroscopic characterization. Although chiral molecules' absolute configuration can be determined via X-ray structural analysis, but this method requires crystallised samples. Self-assembled systems, on the other hand, are typically not crystalline and are not suitable for x-ray crystallography.

The techniques used for morphological observation of supramolecular assembly are scanning tunnelling microscopy (STM), atomic force microscopy (AFM), scanning electron microscopy (SEM) and transmission electron microscopy (TEM). AFM is a technique that relies on the measurement of the force exerted by a sharp tip against the surface of a sample. In most cases, the sample is deposited on an extremely flat surface made of silica or mica. As the sample moves beneath the tip, the force between the tip and the surface is measured, resulting in an AFM image. This process forms the basis of AFM imaging.⁶¹

STM is a quantum tunnelling-based technology. When a conducting tip is brought very close to a conductive surface and a bias voltage is supplied, a tunnelling current develops between two. The resulting tunnelling current depends on the distance between the tip and the surface.⁸⁸ The STM technique is capable of directly distinguishing the absolute configuration of chiral molecules, which makes it a valuable tool for chiral analysis.⁸⁹ Furthermore, it can also be used for the observation of supramolecular chirality at surfaces.⁹⁰

In contrast, the SEM is the most commonly used electron microscopy technique for morphology investigations. When electrons interact with atoms in the sample, they generate

various signals, such as scattered electrons and X-rays, that can be detected and utilized for imaging.⁹¹ While in the case of TEM, a beam of electrons is propagated through an ultra-thin specimen, interacting with it as it passes through. A TEM image has a high resolution (0.1 nm) and is produced by the interaction of electrons that have been transmitted through an extremely thin specimen (<200 nm).⁹² Moreover, TEM can be used to obtain a diffraction pattern.

Along with morphological observations, spectroscopic methods such as circular dichroism (CD), vibrational CD (VCD), and Raman optical activity (ROA) are used to describe supramolecular chirality. These methods make it possible to observe the dynamic properties of supramolecular chirality and reveal the self-assembly procedure. This thesis uses CD spectroscopy, one of these methods to characterise chirality.

1.9.1 CD spectroscopy

CD spectroscopy is a powerful analytical tool used in the field of chemistry and biochemistry. This type of light absorption spectroscopy is designed to measure the difference in absorbance of right and left-circularly polarized light by a substance.^{93,95} The resulting CD spectrum provides a visual representation of circular dichroism as a function of wavelength. In order to obtain an accurate CD spectrum, the sample being analyzed must contain chromophores, and the absorption must occur within the wavelength range.⁹⁶ Isotropic sample measurements are typically preferred for CD spectroscopy, as anisotropic chiral nanostructures, turbidity, birefringence, and other factors can significantly impact the accuracy of data collection and interpretation. Linear dichroism (LD) can also interfere with CD spectroscopy results. As a result, simultaneous measurement of the LD and CD spectra may convey unequivocal warnings about the precision of the CD spectra.⁹⁷ Overall, CD spectroscopy is an important tool for analyzing the structure and properties of chiral molecules, and can provide valuable insights into the behavior of complex supramolecular systems. CD is measured either as ellipticity θ (in mdeg) or as differential absorption ΔA in absorption units, the two values being correlated as

$$\Delta A = \theta/32980$$

Observation of a peak in the CD spectrum is referred to as the Cotton effect, which is the characteristic change in circular dichroism in the vicinity of an absorption band of a substance. The Cotton effect is an important concept in CD spectroscopy, and is used to assign the sign of the CD spectrum based on the direction of its change with respect to wavelength. When the CD first increases as the wavelength decreases, the Cotton effect is said to be positive, while if

the CD decreases first, it is negative (Figure 1.17).^{98,99} Another type of CD spectrum, known as the exciton type CD spectrum (Figure 1.17, dashed line), is characterized by the presence of two bands with opposite signs. This bisignate band is obtained when two or more strongly absorbing units are aligned chirally with respect to each other. The zero value of CD between the valley and peak is referred to as the crossover, which typically occurs at the location of the UV-vis absorption maximum. In supramolecular systems, the exciton CD spectrum is commonly found, and the two bands typically do not have the same intensity due to the presence of aggregated or cooperatively interacting chromophores. The scattering effect may also impact the shape of the CD spectra. In liquid crystalline systems, temperature-dependent CD spectra are often used to describe the helicity. The helical organization is characterized by a gradual increase in the intensity of the CD peak as the temperature decreases.¹⁰⁰

1.10 Application of supramolecular assembly

The introduction of chirality gives rise to interesting physical properties and the potential application of liquid crystals for chiral recognition, thermochromism, chemosensors, temperature sensors, ferroelectricity etc. In addition, circularly polarized luminescence (CPL) is also one of the interesting features of the supramolecular helical assemblies of π -conjugated molecules such as liquid crystals, small molecules, polymers etc, because such assemblies could enhance the CPL emission intensity as a result of the helical arrangement of the luminophores.

The creation of functional devices is one of the primary goals of supramolecular assembly. Several characteristics of the supramolecular organisation are directly relevant to chiral optics and electrical devices.

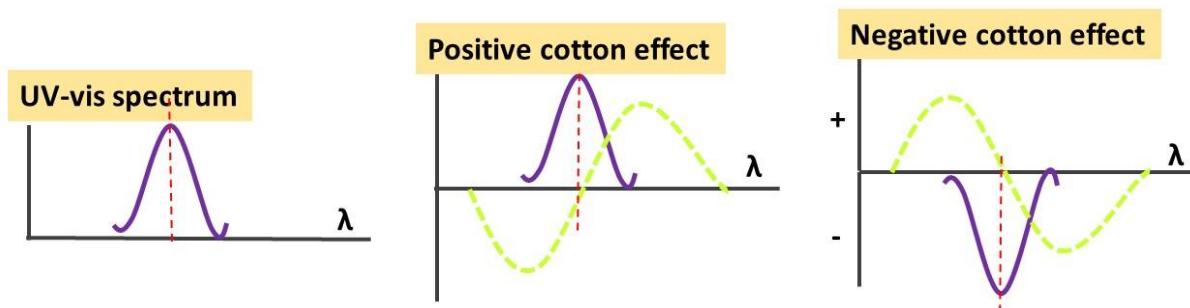


Figure 1.17 General template for different CD spectra in supramolecular systems. (Redrawn from reference 49)

For example, when molecules are subjected to a chiral system with different handedness, the electrical conductivity changes.^{101,102} Also, in the literature, it is reported that the second-order NLO susceptibility of the chiral assemblies can be 30 times higher than that of the racemic material with the same chemical structure.¹⁰³

The supramolecular chirality was also found to play an essential role in the semiconductor properties of supramolecular assemblies. Mullen *et al.* reported that DLC formed from the assembly of coronene shows an increase in charge carrier mobility of the device when there is a certain twisting angle within the self-assembly of DLCs.¹⁰⁴ Not only this, if only achiral molecules can be found in supramolecular assemblies, CPL can be created in the system by adding supramolecular chirality with controlled handedness.

1.10.1 Circularly polarized luminescence

Polarized light can be classified into various types, including linearly, circularly, elliptically, and partially polarized light, based on their polarization characteristics.¹⁰⁵⁻¹⁰⁸ Circularly polarized light has gained significant attention due to its potential applications in optical sensors, 3D displays, and optical information storage, as well as its benefits for eye health.^{109,110} In the past, circularly polarized light was generated through an indirect physical process in which emitted unpolarized light was first turned into linearly polarized light by the linear polarizer, which was then decomposed into right or left-circularly polarized light by the quarter-wave plate (Figure 1.18a). However, this process resulted in a loss of 50% of energy,^{114,116} making it crucial to develop novel luminescent materials that can directly generate circularly polarized light. Such materials would eliminate the need for the indirect conversion process and lead to more efficient circularly polarized light generation. Overall, the development of materials that can directly generate circularly polarized light has the potential to revolutionize a wide range of fields, from biomedicine to telecommunications. CPL measures the difference in the emission of left and right-circularly polarized light in a system. CPL is the ideal approach to directly generate the circularly polarized light with simplified device structure and improved efficiency (Figure 1.18b), in which the energy loss instigated by the circularly polarized filters can be diminished. The arrangement of the luminescent chromophores must be chiral in order to produce CPL from chiral supramolecular assemblies. When luminophores are in a dissymmetric environment during the photo-excited state, CPL is produced. The CPL strength can be estimated by using the luminescence dissymmetry factor defined as $g_{lum} = 2(I_L - I_R)/(I_L + I_R)$, where I_L and I_R represent the luminescence intensities of

left and right CP light, respectively. The highest $|g_{lum}|$ of 2 represents entirely left or right-CPL, while $g_{lum} = 0$ corresponds to unpolarized luminescence. The higher $|g_{lum}|$ indicates, the better polarization degree of the emitted light, which refers to the lower energy loss.

When it comes to designing circularly polarized luminescent (CPL) active materials for liquid crystals (LCs), there are mainly three approaches: (a) self-assembly of chiral luminescent LCs, (b) self-assembly of achiral luminescent LCs with chiral doping, and (c) symmetry breaking of achiral luminescent LCs. Among these approaches, the assembly of chiral luminescent LCs has shown beneficial interest. However, self-assembly can often lead to fluorescence quenching in the solid state due to the dissipation of excited state energy by non-radiative transition pathways, even though it can amplify the $|g_{lum}|$ values. To overcome this challenge, it is very important to develop aggregation-induced emission (AIE) chiral LCs. These AIE systems offer an approach for achieving both high $|g_{lum}|$ and high efficiency, making them ideal for promoting aggregation-induced CPL phenomena.^{117,118} Following this, various AIE systems have been used to produce the aggregation-induced CPL phenomena, such as cyanostilbene derivatives,¹¹⁷ tetraphenylethylene derivatives,^{120,121} silole derivatives^{122,123} and Schiff base groups.¹²⁴ In this thesis, several AIE DLCs have been studied for CPL phenomena.

1.10.1.1 Application of CPL active LCs

Luminescent LCs combine photophysical properties with anisotropic behaviour and provide promising applications in display and imaging technology.¹²⁵ The attention has been focused on the field of chiroptical materials with CPL due to their exciting applications in 3D imaging,¹²⁶ chemical sensors,¹²⁷ CPL lasers,¹²⁸ optoelectronic devices,^{129,130} optical data storage,¹³¹ and chirality switching.¹³² OLED devices are another prominent application of CPL-active LCs, and a detailed discussion is given below.

In OLEDs, circular polarizers are commonly used to reduce the reflectivity of the surrounding environment and produce high contrast images. However, this results in a significant loss of brightness and energy efficiency as only half of the emitted light reaches the eyes. To address this, circularly polarized OLEDs (CP-OLEDs) have emerged as a promising technology for achieving high brightness and energy efficiency in display devices. By emitting circularly polarized light with the same handedness as the circular polarizer, CP-OLEDs can significantly reduce energy loss and power usage.^{116,133} The first CP-OLEDs were reported in 1997, and following this various CP-OLEDs have been developed.¹³⁴ However, obtaining CP-OLEDs with high $|g_{lum}|$ and external quantum efficiency (EQE) is still a challenge. To improve the EQE

of CP-OLEDs, researchers have explored the use of thermally activated delayed fluorescence (TADF) materials. TADF materials have the ability to convert triplets to singlets through the reversed intersystem crossing, resulting in 100% internal quantum efficiency.¹³⁵ Wu *et al.* reported that TADF materials exhibit high photoluminescence quantum yield (92%), mirror symmetric CD signals, and intense CPL activities with a high $|g_{lum}|$ value and high EQE of 32.6%.¹³⁶ Thus, the use of TADF materials in CP-OLEDs is a promising strategy to improve their performance and reduce energy consumption.

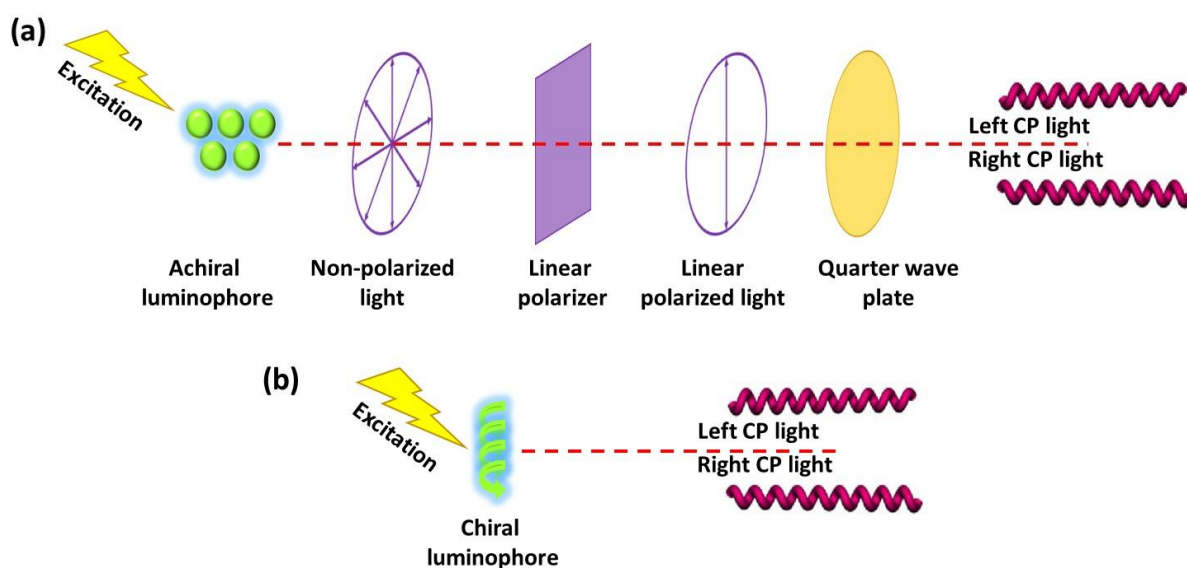


Figure 1.18 Typical method for generating CP light (a) Physical method, (b) CPL. (Redrawn from reference 133)

1.11 Outline of thesis

This thesis describes the different approaches to designing and synthesizing highly ordered chiral DLCs. It is very important to carefully design and understand the building blocks' properties. The small chiral perturbation in LCs is the prime step in determining the materials' final supramolecular chirality and chiroptical properties. Furthermore, the balance between different interactions plays a crucial role in directing the hierarchical self-assembly process. The chiroptical properties and stimuli-responsive nature of chiral LCs and the helical structure of the column give rise to unique physical and optical properties such as CD, CPL, NLO etc. and making it a promising area of research for various applications, including optoelectronic devices, sensing applications, asymmetric catalysis and so on. A different strategy has been used to synthesize the self-assembled luminescent chiral LCs. A brief overview of subsequent chapters is given below:

Chapter 2 illustrates the design, synthesis and characterization of cyclotriphosphazene and cholesterol-based chiral columnar LCs. To understand the structure-property correlation, the length and parity of the spacer of the cholesterol-based dimeric units have been varied, and detailed investigations reveal the influence of the spacer's length on the packing of the columns on a 2D lattice. The helicity of the columnar LCs has been confirmed by temperature-dependent chiroptical measurements where the intensity of peak in circular dichroism (CD) spectra increases with a decrease in temperature, implying the core-core correlation within the columns and, thus, the proximity of the chromophores varies with the temperature. Additionally, these molecules exhibit fluorescent "turn-on" characteristics in their solid state upon exposure to hydrochloric acid (HCl) that can be visualized by the naked eye instantly.

Keeping in mind the exclusive advantage of luminescent chiral materials in the field of optoelectronics, we are interested in designing the helically organized luminescent DLCs. **Chapter 3** demonstrates the new approach towards achieving luminescent chiral DLCs for exciting chiroptical properties. Herein this chapter, we report the design and synthesis of a non-doped, highly adequate CPL material with columnar self-assembly, derived from thermotropic chiral luminescent liquid crystal using tetraarylpyrrolo[3,2-b]pyrrole (TAP) as a luminescent unit and cholesterol as the side chiral mesogenic unit. These chiral DLCs exhibit a fluorescent property in both solution and thin-film states. The supramolecular self-assembly stabilizes the mesophase in columnar centered rectangular mesophase and freeze to glassy state at room temperature. The emission behaviour of TAP-n shows interesting solvent-dependent behaviour, such as the ability to entirely lose fluorescence when dispersed in a high polarity solvent. Furthermore, the fluorescence emission exhibited a strong hypsochromic shift in non-polar solvents. To the best of our knowledge, this is the first report of chiral columnar self-assembly of TAP-based materials, leading to fascinating chiroptical and CPL properties in the aggregate state.

Chapter 4 describes the supramolecular self-assembly of thiophene-induced cholesterol-decorated liquid crystal derivatives by varying the spacer alkyl chain lengths. The supramolecular self-assembly of all the products stabilized the lamellar arrangement that sustains over a significant temperature range and freezes to a glassy state at room temperature. Here, the motivation is to lower the isotropic temperature and solid-state luminescence behaviour. Photophysical studies showed that all three derivatives display blue-emission in solution and thin-film states, exhibiting notable fluorescence quantum yield. Furthermore, these compounds stabilized in a glassy state at room temperature, which revealed their potential

application for many exciting applications. Also, the bulky cholesterol broadens the material range for chiroptical characteristics.

Chapter 5 presents the conventional synthetic methodology to achieve the columnar organization of perylene and pentaalkynylbenzene-based discotic liquid crystal triad, in which perylene is sandwiched between two pentaalkynylbenzene units. This strategy of combining two mesogenic units with different structural organizations inspired us to gain a complete structural understanding of the packing of the molecule in the phase arrangement. As a result, this strategy accelerates the supramolecular self-assembly of the hybrid triad in an oblique columnar arrangement that sustains over a significant temperature range. The photophysical studies showed that the material shows the solution state luminescent properties. A detailed experiment of the photophysical behaviour of the compound in various solvents of varying polarity has been performed. The compound shows positive solvatochromism with a significant increase in Stoke's shift. The compound shows high fluorescence quantum yield in non-polar solvents and the lowest in polar solvents. This luminescent triad with positive solvatochromism will reveal its potential application in fluorescence imaging and optoelectronic organic materials.

Chapter 6 summarizes the work described in this thesis and discusses the scope of the studies. We have also discussed the prospects and the importance of the work explained for the functional smart materials.

The structural analysis is also provided in the Appendix at the end of each chapter.

References

1. Whitesides, G. M.; Boncheva, M. Beyond molecules: Self-assembly of mesoscopic and macroscopic components. *Proc. Natl. Acad. Sci. USA* **2002**, *99*, 4769–4774.
2. Menger, F. M. Supramolecular chemistry and self-assembly. *Proc. Natl. Acad. Sci. USA* **2002**, *99*, 4818–4822.
3. Demus, D.; Goodby, J.; Gray, G. W.; Spiess, H. W.; Vill, V. *Handbook of Liquid Crystals*; Wiley, **1998**.
4. Collings, P. J.; Hird, M. *Introduction to Liquid Crystals: Chemistry and Physics*; Taylor & Francis: London, **1997**.
5. Collings, P. J.; Goodby, J. W. *Introduction to Liquid crystals: Physics and Chemistry*, 2nd ed.; CRC Press: Boca Raton, FL, **2020**.

6. Bisoyi, H. K.; Li, Q. *Liquid Crystals. Kirk-Othmer Encyclopedia of Chemical Technology*; **2014**.
7. Chandrasekhar, S. *Liquid Crystals*; Cambridge University Press: Cambridge, U.K., **1992**.
8. Collings, P. J. *Liquid Crystals: Natures Delicate Phase of Matter*; Princeton University Press: Princeton, NJ, **2002**.
9. Kumar, S. Liquid Crystals: Experimental Study of Physical Properties and Phase Transitions. *Molecules*, **2001**, *6*, 1055-1056.
10. Gray, G. W. *Thermotropic Liquid Crystals*; Wiley, New York, **1987**.
11. Reinitzer, F. Beiträge zur Kenntnis des Cholesterins, *Monatsch. Chem.* **1888**, *9*, 421-441; for an English translation see Reinitzer, F. Contributions to the knowledge of cholesterol, *Liq. Cryst.* **1989**, *5*, 7-18.
12. Lehmann, O. Über fließende Krystalle. *Zeitschrift für Physikalische Chemie.* **1889**, *4*, 462.
13. Vorländer, D.; Meyer, F. Aromatische Diazoniumsalze und ammoniakalische Kupferoxydullösung. *Justus Liebigs Annalen der Chemie.* **1902**, *320*, 122-144.
14. Vorländer D. *Kristallinisch-flüssige Substanzen. Enke.* **1908**.
15. Vorländer, D. Einfluss der molekularen Gestalt auf den kristallinisch-flüssigen Zustand. *Ber Dtsch Chem Ges.* **1907**, *40*, 1970-1972.
16. Friedal, G. Les états mésomorphes de la matière. *Ann. Phys.* **1922**, *9*, 18, 273-474.
17. Vorländer, D. Chemische Kristallographie der Flüssigkeiten: kurze Anleitung zur Synthese und Untersuchung polymorpher und kristallinflüssiger Substanzen. *Akademische Verlagsgesellschaft* **1924**.
18. Gray, G.W.; Harrison, K.J.; Nash, J.A. New family of nematic liquid crystals for displays. *Electron. Lett.* **1973**, *9*, 130-131.
19. Gray, G. W.; Harrison, K.J.; Nash, J.A.; Constant, J.; Hulme, J.S.; Kirton, J.; Raynes, E.P. Liquid Crystals and Ordered Fluids. *Plenum Press, New York* **1973**, *2*, 617.
20. Chandrasekhar, S.; Sadashiva, B. K.; Suresh, K. A. Liquid Crystals of disc-like molecules. *Pramana* **1977**, *9*, 471-480.

21. Niori, T; Sekine, T.; Watanabe, J.; Furukawa, T.; Takezoe, H. J. Distinct ferroelectric smectic liquid crystals consisting of banana shaped achiral molecules. *Mater. Chem.* **1996**, *6*, 1231-1233
22. Vorländer, D.; Fuchs, K.; Katscher, E. E. Über die Einwirkung von Chlorsulfonsäure auf Aldehyde. *Ber. Dtsch. Chem. Ges.* **1929**, *62*, 2381-2386.
23. Matsunaga, Y.; Miyamoto, S. Mesomorphic Behavior of 2,4-Bis-(4-alkoxybenzylidene)cyclopentanones and Related Compounds. *Mol. Cryst. Liq. Cryst.* **1993**, *237*, 311-317.
24. Matsuzaki, H.; Matsunaga, Y. New mesogenic compounds with unconventional molecular structures 1,2-Phenylene and 2,3-naphthylene bis[4-(4-alkoxyphenyliminomethyl)benzoates] and related compounds. *Liq. Cryst.* **1993**, *14*, 105-120.
25. Kumar, S. *Chemistry of Discotic Liquid Crystals*; CRC Press, Taylor and Francis Group, LLC, 2011.
26. Kleinert, H.; Maki, K. Lattice Textures in Cholesteric Liquid Crystals. *Fortschritte der Physik* **1981**, *29*, 219–259.
27. Sarkar, M.; Spielberg, N.; Praefcke, K.; Zimmermann, H. Further X-ray studies of mesophase structure of Hexakis(Alkylsulfo)benzene (HASBn) and Tribenzocyclononene (II-n) homologues. *Mol. Cryst. Liq. Cryst.* **1991**, *203*, 159–169.
28. Poupko, R.; Luz, Z.; Spielberg, N.; Zimmermann, H. Structure and dynamics of pyramidal liquid crystals by deuterium NMR and x-ray diffraction. *J. Am. Chem. Soc.* **1989**, *111*, 6094-6105.
29. Zimmermann, H.; Poupko, R.; Luz, Z.; Billard, J. Tetrabenzocyclododecatetraene a new core for mesogens exhibiting columnar mesophase. *Liq. Cryst.* **1988**, *3*, 759–770.
30. Percec, V.; Cho, C. G.; Pugh, C. Alkyloxy-substituted CTTV derivatives that exhibit columnar mesophases. *J. Mater. Chem.* **1991**, *1*, 217–222.
31. Morris, N. L.; Zimmermann, R. G.; Jameson, G. B.; Dalziel, A. W.; Reuss, P. M.; Weiss, R. G. Chiral discotic columnar mesophases from the α and β anomers of penta-*O*-*n*-alkanoylglucopyranoses. *J. Am. Chem. Soc.* **1988**, *110*, 2177-2185.

32. Lehn, J. M.; Malthête, J.; Levelut, A. M. Tubular mesophases: liquid crystals consisting of macrocyclic molecules. *J. Chem. Soc. Chem. Commun.* **1985**, 1794–1796.
33. Tuffin, R. P.; Toyne, K. J.; Goodby, J. W. Phasmidic phases in macrocyclic liquid crystals. *J. Mater. Chem.* **1996**, *6*, 1271–1282.
34. Hoag, B. P.; Gin, D. L. Fluorescent phasmidic liquid crystals. *Adv. Mater.* **1998**, *10*, 1546–1551.
35. Yasuda, T.; Kishimoto, K.; Kato, T. Columnar liquid crystalline pi-conjugated oligothiophenes. *Chem. Commun.* **2006**, 3399–3401.
36. Wöhrle, T.; Wurzbach, I.; Kirres, J.; Kostidou, A.; Kapernaum, N.; Litterscheidt, J.; Haenle, J. C.; Staffeld, P.; Baro, A.; Giesselmann, F.; Laschat, S. Discotic Liquid Crystals. *Chem. Rev.* **2016**, *116*, 1139–1241.
37. Bisoyi, H. K.; Kumar, S. Discotic nematic liquid crystals: science and technology. *Chem. Soc. Rev.* **2010**, *39*, 264–285.
38. Yelamagad, C.V.; Prasad, V.; Manickam, M.; Kumar, S. New Chiral Discotic Liquid Crystals. *Mol. Cryst. Liq. Cryst.* **1998**, *325*, 33–41.
39. Bala, I.; Gupta, S. P.; De, J.; Pal, S. K. Room-Temperature Columnar Nematic and Soft Crystalline Columnar Assemblies of a New Series of Perylene-Centred Disc Tetramers. *Chem. Eur. J.* **2017**, *23*, 12767–12778.
40. Kouwer, P. H. J.; Jager, W. F.; Mijs, W. J.; Picken, S. J. The Nematic Lateral Phase: A Novel Phase in Discotic Supramolecular Assemblies. *Macromolecules* **2001**, *34*, 7582–7584.
41. Bruce, D. W.; Dunmur, D. A.; Santa, L. S.; Wali, M. A. Mesomorphic metalloporphyrins showing calamitic mesophases. *J. Mater. Chem.* **1992**, *2*, 363–364.
42. Alameddine, B.; Aebischer, O. F.; Amrein, W.; Donnio, B.; Deschenaux, R.; Guillon, D.; Savary, C.; Scanu, D.; Schidegger, O.; Jenny, T. A. Mesomorphic Hexabenzocoronenes Bearing Perfluorinated Chains. *Chem. Mater.* **2005**, *17*, 4798–4807.
43. Kumar, S. Self-organization of disc-like molecules: chemical aspects. *Chem. Soc. Rev.* **2006**, *35*, 83–109.

-
44. Glösen, B.; Heitz, W.; Kettner, A.; Wendorff, J. H. A plastic columnar discotic phase DP. *Liq. Cryst.* **1996**, *20*, 627-633.
45. Malthete, J.; Jacques, J.; Tinh, N. H.; Destrade, C. Macroscopic Evidence of Molecular Chirality in Columnar Mesophases. *Nature* **1982**, *298*, 46-48.
46. Fontes, E.; Heiney, P. A.; de Jeu, W. H. Liquid-Crystalline and Helical Order in a Discotic Mesophase. *Phys. Rev. Lett.* **1988**, *61*, 1202-1205.
47. Ong, C. W.; Chan, Y. C.; Yeh, M. C.; Lin, H. Y.; Hsu, H. F. Lamellar Organization of Discotic Dimer Enforced by Steric Manipulation. *RSC Adv.* **2013**, *3*, 8657-8659.
48. Bentley, R. Chiral: A Confusing Etymology. *Chirality* **2010**, *22*, 1-2.
49. Hegstrom, R. A.; Kondepudi, D. K. The Handedness of the Universe. *Sci. Am.* **1990**, *262*, 108-115.
50. Bai, C.; Liu, M. From Chemistry to Nanoscience: Not Just a Matter of Size. *Angew. Chem. Int. Ed.* **2013**, *52*, 2678-2683.
51. Liu, M.; Zhang, L.; Wang, T. Supramolecular Chirality in Self-Assembled Systems, *Chem. Rev.* **2015**, *115*, 7304-7397.
52. Pieraccini, S.; Masiero, S.; Ferrarini, S.; Spada, G. P. Chirality transfer across length-scales in nematic liquid crystals: fundamentals and applications. *Chem. Soc. Rev.* **2011**, *40*, 258-271.
53. Aida, T.; Meijer E. W.; Stupp, S. I. Functional Supramolecular Polymers. *Science*, **2012**, *335*, 813-817.
54. Duan, P.; Cao, H.; Zhang, L.; Liu, M. Gelation induced supramolecular chirality: chirality transfer, amplification and application. *Soft Matter* **2014**, *10*, 5428-5448.
55. Yashima, E.; Ousaka, N.; Taura, D.; Shimomura, K.; Ikai, T.; Maeda, K. Supramolecular Helical Systems: Helical Assemblies of Small Molecules, Foldamers, and Polymers with Chiral Amplification and Their Functions. *Chem. Rev.* **2016**, *116*, 13752-13990.
56. Morrow, S. M.; Bisette, A. J.; Fletcher, S. P. Transmission of chirality through space and across length scales. *Nature Nanotech* **2017**, *12*, 410-419.

-
57. Joseph, G. Stereochemical Vocabulary for Structures that are Chiral but not Asymmetric: History, Analysis, and Proposal for a Rational Terminology. *Chirality* **2011**, *23*, 647-659.
58. Grabmaier, J. G. *Applications of Liquid Crystals*, ed. Meier, G.; Sackmann, E.; Grabmaier, J. G. Springer-Verlag, Berlin-New York, **1975**, 83-160.
59. Kelker, H.; Hatz, R. *Handbook of Liquid Crystals*, Verlag Chemie, Basel, **1980**, and references therein
60. Moss, G. P. Basic Terminology of Stereochemistry. *Pure Appl. Chem.* **1996**, *68*, 2193-2222.
61. Jiang, J.; Wang, T.; Liu, M. Creating Chirality in The Inner Walls of Silica Nanotubes Through a Hydrogel Template: Chiral Transcription and Chiroptical Switch. *Chem. Commun.* **2010**, *46*, 7178–7180.
62. Goodby, J. W. Chirality in Liquid Crystals. *J. Mater. Chem.* **1991**, *3*, 307-318.
63. De Vries, H. Rotatory power and other optical properties of certain liquid crystals. *Acta Cryst.* **1951**, *4*, 219–226.
64. Martinot-Lagarde, P.H. Flexo and ferroelectricity observation of ferroelectrical monodomains in the chiral smectic C liquid crystals. *J. Phys.* **1976**, *37*, 129–132.
65. Green, M. M.; Ringsdorf, H.; Wagner, J.; Wiistefeld, R. Induction and Variation of Chirality in Discotic Liquid Crystalline Polymers. *Angew. Chem. Int. Ed. Engl.* **1990**, *29*, 12.
66. Destrade, C.; Tinh, N. H.; Malthete, J.; Jacques, ON A “CHOLESTERIC” PHASE IN DISC-LIKE MESOGENS. *J. Phys. Lett.* **1980**, *79A*, 189–192.
67. Malthete, J.; Jacques, J.; Tinh, N. H.; Destrade, C. Macroscopic evidence of molecular chirality in columnar mesophases. *Nature* **1982**, *298*, 46–48.
68. Praefcke, K.; Singer, D.; Eckert, A. Induction of nematic cholesteric (N*) phases by charge transfer complexation of disc-shaped multiynes. *Liq. Crystallogr.* **1994**, *16*, 53–65.
69. Langner, M.; Praefcke, K.; Krüerke, D.; Heppke, G. Chiral radial pentaynes exhibiting cholesteric discotic phases. *J. Mater. Chem.* **1995**, *5*, 693–699.

-
70. Fontes, E.; Heiney, P. A.; de Jeu, W. H. Liquid-Crystalline and Helical Order in a Discotic Mesophase. *Phys. Rev. Lett.* **1988**, *61*, 1202–1205.
71. Heiney, P. A.; Fontes, E.; de Jeu, W. H.; Riera, A.; Carroll, P.; Smith, A. B. Frustration and helicity in the ordered phases of a discotic compound. *J. Phys. France* **1989**, *50*, 461–483.
72. Palmans, A. R. A.; Vekemans, J. A. J. M.; Fischer, H.; Hikmet, R. A.; Meijer, E. W. Extended-Core Discotic Liquid Crystals Based on the Intramolecular H-Bonding in N-Acylated 2,2'-Bipyridine-3,3'-diamine Moieties. *Chem. Eur. J.* **1997**, *3*, 300–307.
73. Brunsveld, L.; Zhang, H.; Glasbeek, M.; Vekemans, J. A. J. M.; Meijer, E. W. Hierarchical Growth of Chiral Self-Assembled Structures in Protic Media. *J. Am. Chem. Soc.* **2000**, *122*, 6175–6182.
74. Lightfoot, M. P.; Mair, F. S.; Pritchard, R. G.; Warren, J. E. New supramolecular packing motifs: π -stacked rods encased in triply-helical hydrogen bonded amide strands. *Chem. Commun.* **1999**, 1945–1946.
75. Brunsveld, L.; Schenning, A. P. H. J.; Broeren, M. A. C.; Janssen, H. M.; Vekemans, J. A. J. M.; Meijer, E. W. Chiral Amplification in Columns of Self-Assembled N,N',N''-Tris((S)-3,7-dimethyloctyl)benzene-1,3,5-tricarboxamide in Dilute Solution. *Chem. Lett.* **2000**, 292–293.
76. Trzaska, S. T.; Hsu, H.-F.; Swager, T. M. Cooperative Chirality in Columnar Liquid Crystals: Studies of Fluxional Octahedral Metallomesogens. *J. Am. Chem. Soc.* **1999**, *121*, 4518–4519.
77. Serrano, J. L.; Sierra, T. Switchable Columnar Metallomesogens. *Chem. Eur. J.* **2000**, *6*, 759–766.
78. Barberá, J.; Iglesias, R.; Serrano, J. L.; Sierra, T.; de la Fuente, M. R.; Palacios, B.; Pérez-Jubindo, M. A.; Vázquez, J. T. Switchable Columnar Metallomesogens. New Helical Self-Assembling Systems. *J. Am. Chem. Soc.* **1998**, *120*, 2908–2918.
79. Nuckolls, C.; Katz, T. J. Synthesis, Structure, and Properties of a Helical Columnar Liquid Crystal. *J. Am. Chem. Soc.* **1998**, *120*, 9541–9544.
80. Werth, M.; Vallerien, S. U.; Spiess, H. W. *Liq. Crystallogr.* **1991**, *10*, 759–770.

-
81. Cho, I.; Lim, Y. Synthesis and Morphology of New Discogenic Phthalocyanine Derivatives. *Mol. Crystallogr. Liq. Crystallogr.* **1988**, *154*, 9–26.
82. van Nostrum, C. F.; Bosman, A. W.; Gelinck, G. H.; Picken, S. J.; Schouten, P. G.; Warman, J. M.; Schouten, A.-J.; Nolte, R. J. M. Evidence of a chiral superstructure in the discotic mesophase of an optically active phthalocyanine. *Chem. Commun.* **1993**, 1120–1122.
83. van Nostrum, C. F.; Bosman, A. W.; Gelinck, G. H.; Schouten, P. G.; Warman, J. M.; Kentgens, A. P. M.; Devillers, M. A. C.; Meijerink, A.; Picken, S. J.; Sohling, U.; Schouten, A. J.; Nolte, R. J. M. Supramolecular Structure, Physical Properties, and Langmuir-Blodgett Film Formation of an Optically Active Liquid-Crystalline Phthalocyanine. *Chem. Eur. J.* **1995**, *1*, 171–182.
84. Fechtenkötter, A.; Tchegotareva, N.; Watson, M.; Müllen, K. Discotic liquid crystalline hexabenzocoronenes carrying chiral and racemic branched alkyl chains: supramolecular engineering and improved synthetic methods. *Tetrahedron* **2001**, *57*, 3769–3783.
85. Praefcke, K.; Eckert, A.; Blunk, D. Core-halogenated, helical-chiral triphenylene-based columnar liquid crystals. *Liq. Crystallogr.* **1997**, *22*, 113–119.
86. Boden, N.; Bushby, R. J.; Cammidge, A. N.; Duckworth, S.; Headdock, G. α -Halogenation of triphenylene-based discotic liquid crystals: towards a chiral nucleus. *J. Mater. Chem.* **1997**, *7*, 601–605.
87. Concellón, A.; Lu, R. Q.; Yoshinaga, K.; Hsu, H. F.; Swager, T. M. Electric-Field-Induced Chirality in Columnar Liquid Crystals. *J. Am. Chem. Soc.* **2021**, *143*, 9260–9266.
88. Chen, J. C. *Introduction to Scanning Tunneling Microscopy*; Oxford University Press: New York, **1993**.
89. Xu, Q.; Wang, D.; Wan, L.; Wang, C.; Bai, C.; Feng, G.; Wang, M. Discriminating Chiral Molecules of (R)-PPA and (S)-PPA in Aqueous Solution by ECSTM. *Angew. Chem. Int. Ed.* **2002**, *41*, 3408–3411
90. De Feyter, S.; De Schryver, F. C. Two-Dimensional Supramolecular Self-Assembly Probed by Scanning Tunneling Microscopy. *Chem. Soc. Rev.* **2003**, *32*, 139–150

-
91. Rong, Y.; Chen, P.; Liu, M. Self-Assembly of Water-Soluble TPPS in Organic Solvents: From Nanofibers to Mirror Imaged Chiral Nanorods. *Chem. Commun.* **2013**, *49*, 10498-10500.
92. Duan, P.; Zhu, X.; Liu, M. Isomeric Effect in the Self-Assembly of Pyridine-Containing L-Glutamic Lipid: Substituent Position Controlled Morphology and Supramolecular Chirality. *Chem. Commun.* **2011**, *47*, 5569–5571.
93. Berova, N.; Nakanishi, K.; Woody R. W. *Circular dichroism: principles and applications*, 2nd ed. New York: Wiley-VCH; **2000**.
94. Mason, S. F. *Molecular optical activity and the chiral discriminations*. Cambridge: Cambridge University Press; **1982**.
95. Grosjean, M.; Legrand, M. Polarimétrie-appareil de mesure du dichroïsme circulaire dans le visible et l'ultraviolet, *Comptes Rendus* **1960**, *251*, 2150-2152.
96. Harada, N.; Nakanishi, K. *Circular dichroic spectroscopy: exciton coupling in organic stereochemistry*. Sausalito: University Science Books; **1983**.
97. Arteaga, O.; Canillas, A.; Purrello, R.; Ribó, J. M. Evidence of Induced Chirality in Stirred Solutions of Supramolecular Nanofibers. *Opt. Lett.* **2009**, *34*, 2177–2179.
98. Fischer, P.; Hache, F. Nonlinear Optical Spectroscopy of Chiral Molecules. *Chirality* **2005**, *17*, 421–437.
99. Taniguchi, T.; Usuki, T. *Circular Dichroism Spectroscopy. Supramolecular Chemistry: From Molecules to Nanomaterials*. John Wiley & Sons, Ltd.: New York, **2012**.
100. Rani, S.; Punjani, V.; Gupta, S. P.; Kanakala, M. B.; Yelamaggad C. V.; Pal, S. K. Observation of helical self-assembly in cyclic triphosphazene-based columnar liquid crystals bearing chiral mesogenic units. *J. Mater. Chem. C* **2023**, *11*, 1067-1075.
101. Zou, W.; Yan, Y.; Fang, J.; Yang, Y.; Liang, J.; Deng, K.; Yao, J.; Wei, Z. Biomimetic Superhelical Conducting Microfibers with Homochirality for Enantioselective Sensing. *J. Am. Chem. Soc.* **2013**, *136*, 578–581.
102. Yang, Y.; Zhang, Y.; Wei, Z. Supramolecular Helices: Chirality Transfer from Conjugated Molecules to Structures. *Adv. Mater.* **2013**, *25*, 6039–6049.

-
103. Verbiest, T.; Elshocht, S. V.; Kauranen, M.; Hellemans, L.; Snauwaert, J.; Nuckolls, C.; Katz, T. J.; Persoons, A. Strong Enhancement of Nonlinear Optical Properties through Supramolecular Chirality. *Science* **1998**, *282*, 913–915.
104. Feng, X.; Marcon, V.; Pisula, W.; Hansen, M. R.; Kirkpatrick, J.; Grozema, F.; Andrienko, D.; Kremer, K.; Müllen, K. Towards High Charge-Carrier Mobilities by Rational Design of The Shape and Periphery of Discotics. *Nat. Mater.* **2009**, *8*, 421–426.
105. Ding, Y. T.; Pau, S. Circularly and elliptically polarized light under water and the Umov effect. *Light: Sci. Appl.* **2019**, *8*, 32.
106. Ögüt, E.; Şendur, K. Circularly and elliptically polarized near-field radiation from nanoscale subwavelength apertures. *Appl. Phys. Lett.* **2010**, *96*, 141104.
107. Nikolova, L.; Todorov, T.; Ivanov, M.; Andruzzi, F.; Hvilsted, S.; Ramanujam, P. S. Polarization holographic gratings in side-chain azobenzene polyesters with linear and circular photoanisotropy. *Appl. Opt.* **1996**, *35*, 3835–3840.
108. Zhang, H.; Hi, Y.; Yan, C.; Zhang, J. Three-dimensional polarization ray tracing calculus for partially polarized light. *Opt. Express* **2017**, *25*, 26973–26986.
109. Yang, Y.; da Costa, R. C.; Fuchter M. J.; Campell, A. J. Circularly polarized light detection by a chiral organic semiconductor transistor. *Nat. Photonics* **2013**, *7*, 634–638.
110. Lee, C. T.; Lin, H. Y.; Tsai, C. H. Designs of broadband and wide-view patterned polarizers for stereoscopic 3D displays. *Opt. Express* **2010**, *18*, 27079–27094.
111. Hao, C.; Xu, L.; Sun, M.; Zhang, H.; Kuang H.; Xu, C. Circularly polarized light triggers biosensing based on chiral assemblies. *Chemistry* **2019**, *25*, 12235–12240.
112. Farshchi, R.; Ramsteiner, M.; Herfort, J.; Tahraoui, A.; Grahn, H. T. Optical communication of spin information between light emitting diodes. *Appl. Phys. Lett.* **2011**, *98*, 162508-162510.
113. Stanciu, C. D.; Hansteen, F.; Kimel, A. V.; Kirilyuk, A.; Tsukamoto, A.; Itoh A.; Rasing, T. All-optical magnetic recording with circularly polarized light. *Phys. Rev. Lett.* **2007**, *99*, 047601-047605.
114. Xu, L.; Feng, Y.; Yu, D.; Zheng, Z.; Chen, X.; Hong, W. Recoverable photolithographic patterning for polarized display and encryption. *Adv. Mater. Technol.* **2020**, *5*, 2000373.

-
115. Basiri, A.; Chen, X.; Bai, J.; Amrollahi, P.; Carpenter, J.; Holman, Z.; Wang C.; Yao, Y. Nature-inspired chiral metasurfaces for circular polarization detection and full-stokes polarimetric measurements. *Light: Sci. Appl.* **2019**, *8*, 78-89.
116. Baek, K.; Lee, D. M.; Lee, Y. J.; Choi, H.; Seo, J.; Kang, I.; Yu, C. J.; Kim, J. H. Simultaneous emission of orthogonal handedness in circular polarization from a single luminophore. *Light: Sci. Appl.* **2019**, *8*, 120-128.
117. Song, F.; Zhao, Z.; Liu, Z.; Lam J. W. Y.; Tang, B. Z. Circularly polarized luminescence from AIEgens. *J. Mater. Chem. C* **2020**, *8*, 3284–3301.
118. Li, H. K.; Li, B. S.; Tang, B. Z. Molecular design, circularly polarized luminescence, and helical self-assembly of chiral aggregation-induced emission molecules. *Chemistry* **2019**, *14*, 674–688.
119. Shang, H.; Ding, Z.; Shen, Y.; Yang, B.; Liu, M.; Jiang, S. Multi-color tunable circularly polarized luminescence in one single AIE system. *Chem. Sci.* **2020**, *11*, 2169–2174.
120. Zhang, S.; Fan, J.; Wang, Y.; Li, D.; Jia, X.; Yuan, Y.; Cheng, Y. Tunable aggregation-induced circularly polarized luminescence of chiral AIEgens via the regulation of mono-/di-substituents of molecules or nanostructures of self-assemblies. *Mater. Chem. Front.* **2019**, *3*, 2066–2071.
121. Li, H.; Cheng, J.; Zhao, Y.; Lam, J. W. Y.; Wong, K. S.; Wu, H.; Li, B. S.; Tang, B. Z. L-valine methyl ester-containing tetraphenylethene: aggregation-induced emission, aggregation-induced circular dichroism, circularly polarized luminescence, and helical self-assembly. *Mater. Horiz.* **2014**, *1*, 518–521.
122. Liu, J.; Su, H.; Meng, L.; Zhao, Y.; Deng, C.; Ng, J. C. Y.; Lu, P.; Faisal, M.; Lam, J. W. Y.; Huang, X.; Wu, H.; Wong, K. S.; Tang, B. Z. What makes efficient circularly polarised luminescence in the condensed phase: aggregation-induced circular dichroism and light emission. *Chem. Sci.* **2012**, *3*, 2737–2747.
123. Ng, J. C. Y.; Li, H.; Yuan, Q.; Liu, J.; Liu, C.; Fan, X.; Li, B. S.; Tang, B. Z. Valine-containing silole: synthesis, aggregation-induced chirality, luminescence enhancement, chiral-polarized luminescence and self-assembled structures. *J. Mater. Chem. C* **2014**, *2*, 4615–4621.

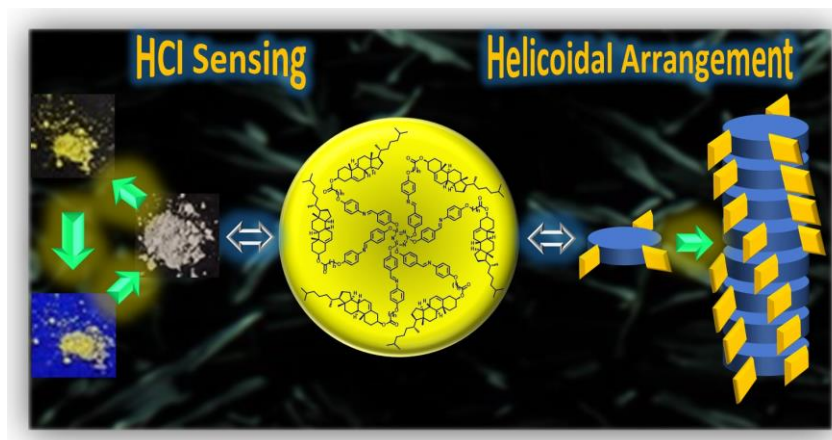
-
124. Huang, G.; Wen, R.; Wang, Z.; Li, B. S.; Tang, B. Z. Novel chiral aggregation induced emission molecules: self-assembly, circularly polarized luminescence and copper(II) ion detection. *Mater. Chem. Front.* **2018**, *2*, 1884–1892.
125. Yang, X.; Jin, X.; Zhao, T.; and Duan, P. Circularly polarized luminescence in chiral nematic liquid crystals: generation and amplification, *Mater. Chem. Front.* **2021**, *5*, 4821-4832.
126. Schadt, M. Liquid Crystal Materials and Liquid Crystal Displays, *Annu. Rev. Mater. Sci.* **1997**, *27*, 305-379.
127. Emeis, C. A.; Oosterhoff, L. J. Emission of Circularly Polarised Radiation by Optically-Active Compounds. *Chem. Phys. Lett.* **1967**, *1*, 129-132.
128. Zinna, F.; Giovanella, U.; Bari, L. D. Highly Circularly Polarized Electroluminescence from a Chiral Europium Complex. *Adv. Mater.* **2015**, *27*, 1791-1795.
129. Jiménez, J.; Cerdán, L.; Moreno, F.; Maroto, B. L., Moreno, I. G.; Lunkley, J. L.; Muller, G.; de la Moya, S. Chiral Organic Dyes Endowed with Circularly Polarized Laser Emission. *J. Phys. Chem. C* **2017**, *121*, 527-5292.
130. Maeda, H.; ando, Y.; Shimomura, K.; Yamada, I.; Naito, M.; Nobusawa, K.; Tsumatori, H.; Kawai, T. Chemical Stimuli-Controllable Circularly Polarized Luminescence from Anion-Responsive p-Conjugate Molecules. *J. Am. Chem. Soc.* **2011**, *133*, 9266-9269.
131. Grell, M.; Oda, M.; Whitehead, K. S.; Asimakis, A.; Neher, D.; Bradley, D. D. C. A Compact Device for the Efficient, Electrically Driven Generation of Highly Circularly Polarized Light. *Adv. Mater.* **2001**, *13*, 577-580.
132. Yan, J.; Ota, F.; San Jose, B. A.; Akagi, K. Chiroptical Resolution and Thermal Switching of Chirality in Conjugated Polymer Luminescence via Selective Reflection using a Double-Layered Cell of Chiral Nematic Liquid Crystal. *Adv. Funct. Mater.* **2017**, *27*, 1604529-1604539.
133. Zhang, D. W.; Li, M.; Chen, C. F. Recent advances in circularly polarized electroluminescence based on organic light-emitting diodes. *Chem. Soc. Rev.* **2020**, *49*, 1331-1343.

134. Peeters, E.; Christiaans, M. P. T.; Janssen, R. A. J.; Schoo, H. F. M.; Dekkers, H. P. J. M.; Meijer, E. W. Circularly polarized electroluminescence from a polymer light-emitting diode. *J. Am. Chem. Soc.* **1997**, *119*, 9909-9910.
135. Deng, Y.; Wang, M.; Zhuang, Y.; Liu, S.; Huang, W.; Zhao, Q. Circularly polarized luminescence from organic micro-/nano-structures. *Light Sci Appl* **2021**, *10*, 76-94.
136. Wu, Z. G.; Han, H. G.; Yan, Z. P.; Luo, X. F.; Wang, Y.; Zheng, Y. X.; Zuo, J. L.; Pan, Y. Chiral octahydro-binaphthol compound-based thermally activated delayed fluorescence materials for circularly polarized electroluminescence with superior EQE of 32.6% and extremely low efficiency roll off. *Adv. Mater.* **2019**, *31*, 1900524-1900533.

Chapter 2

Observation of helical self-assembly in cyclic triphosphazene-based columnar liquid crystals bearing chiral mesogenic units

Nowadays, intensive research has focused on the design and synthesis of function-integrated smart materials resulting from the spontaneous self-assembly of the predestined functional molecules. Working in this direction, we have synthesized a new series of non-conventional, chiral columnar liquid crystals (Col LCs), where the cyclotriphosphazene core is surrounded by cholesterol-based Schiff base dimeric units. Cholesterol, which is covalently bound to the two-ring Schiff base core via a flexible spacer of varying length and parity, has been premeditatedly incorporated to induce handedness in Col fluid macrostructure. The investigations using a number of complementary techniques clearly reveal the influence of the length of the spacer, rather than the parity, on the symmetries of 2D lattices resulting from the intrinsic columnar assemblies of the synthesized compounds. The different columnar assemblies were further confirmed through detailed electron density mapping and small-angle/wide-angle X-ray scattering (SAXS/WAXS) studies. As conceived, the bulky cholesterol, rendering molecular chirality, directs the molecular assemblies in a helical manner in individual columns. The handedness (helicity) of the Col LCs has been confirmed by temperature-dependent chiroptical measurements where the intensity of peak in circular dichroism (CD) spectra increases with a decrease in temperature, implying that the core-core correlation within the columns and, thus, the proximity of the chromophores varies with the temperature. The helicity of the mesophases was also supported by transmission electron microscopy (TEM) technique. Notably, these novel materials exhibit fluorescent “turn-on” characteristics in their solid (as synthesized) state upon exposure to hydrochloric acid (HCl) that can be visualized by naked eye instantly where the color change occurs with a low detection limit of 5.6 μM .



Reproduced/Adapted from (Rani, S.; Punjani, V.; Gupta, S. P.; Kanakala, M. B.; Yelamagad, C. V.; Pal, S. K. Observation of helical self-assembly in cyclic triphosphazene-based columnar liquid crystals bearing chiral mesogenic units. *J. Mater. Chem. C*, **2023**, *11*, 1067-1075; <https://doi.org/10.1039/D2TC03847A>) with permission from The Royal Society of Chemistry

2.1 Introduction

Phosphazenes are a fascinating class of organophosphorus materials.¹⁻⁶ They have received significant attention over the past years due to their ease in functionalization and high thermal stability. The phosphazene molecule can be a ring (cyclotriphosphazene, cyclotetraphosphazene) (Figure 2.1) or could be a linear chain (polyphosphazene) consisting of a backbone of phosphorus and nitrogen with halide atoms connected to the phosphorus center.⁷

In recent years, cyclophosphazenes (CPs) have been incorporated as a functional core in dendrimers to accomplish novel materials capable of exhibiting a range of physical and chemical properties.⁸⁻¹⁷ It is shown that the structure of the CP dendrimers can be well diversified by increasing the number of substituents/end-groups.⁸ Owing to their unique structure, they enable the formation of internal cavities closer to the core, and also lead to the generation of spherical structures.⁸ In fact, various exciting applications of CP-based dendrimers have been proposed in the field of medicinal chemistry,^{9,10} catalysis,¹¹ and material science.¹²⁻¹⁴ Additionally, these CP derivatives, occurring in the form of ligands/thermally stable macromolecules, have found applications in the field of liquid crystals (LCs), low-temperature elastomers, solid-state fuel cells, electro-optical polymers^{7,15} including flame retardants.¹⁵⁻¹⁷ Most of these applications are related to the nature of the side arms connected to the central core. Among all the explorations mentioned above, their incorporation in the soft material's design, especially LCs, is noteworthy.

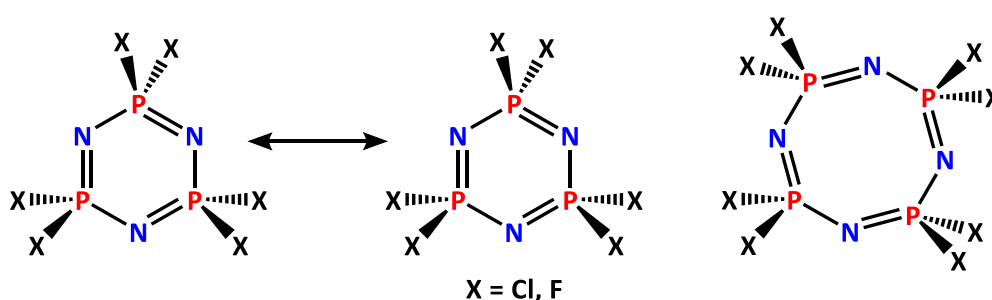


Figure 2.1 The molecular structures of the six- and eight-membered cyclic phosphazenes that are frequently employed as building blocks for the construction of various functional materials.

For instance, the phosphazene backbone has been extensively explored for realizing liquid crystal-based smart materials.¹⁸⁻²⁹ The calamitic phases have been attained by constituting the rod-like mesogens incorporating the CP unit as a central core in the molecular architecture;¹⁸⁻

²⁹ the occurrence of the calamitic mesophases has been explained using a model where the side arms are arranged perpendicular to the central moiety.³⁰

On the other hand, the self-organization of the disc-like mesogens (discotics) into columnar self-assembly has attracted growing interest in material science.^{31,32} These materials have received immense attention due to their unique features such as self-healing of organizational defects and one-dimensional (1D) charge migration resulting in wide range of exciting applications. For example, they can be employed as an active media in photovoltaic devices, thin-film transistors, organic light-emitting diodes and so on.^{33,34} Furthermore, the induction of molecular chirality enables the discotic LCs to self-organize into highly ordered macroscopic structure characterized by handedness - the chirality. The mesogens in such a helicoidal arrangement, having either macromolecular or supramolecular order, are of great interest in designing responsive materials, chirality sensors, and chiroptical devices.³⁴ As expected, the CP core has been employed to realized Col LCs.

The first occurrence of columnar hexagonal (Col_h) phase in a CP-based dendrimer was reported in 2005.³⁵ The microphase segregation of the rigid and flexible parts of the structure along with the space-filling requirements enabled their organization into Col LC structure.³⁵ Since then, many researchers have been working towards realizing Col phases in phosphazene-based systems. However, a few reports describe Col mesomorphism in discotic LCs (DLCs) derived from CP core.^{36,37} However, to our knowledge, the chiral Col LC phases derived from CP core have not been reported hitherto. Herein, we report the first examples of CP-based non-conventional LCs self-assembling into helicoidal columns. Precisely, we describe molecular design, synthesis, and characterization of a new series of hexa-substituted CP-based chiral columnar LCs. With the prime objective of accomplishing chiral LC phases persisting over an extended thermal width, we incorporated cholesterol-based dimeric Schiff bases in the molecular architecture; the mesogenic Schiff base units have been inserted purposely as they possess various properties including chemical sensing.^{15,53} To understand the structure-property correlation, the length and parity of the spacer of the cholesterol-based dimeric units have been varied. The general molecular structure of the Col LCs synthesized is shown in Figure 2.2; for convenience this series of mesogens will be here after referred to as **P-n** series where **n** signifies the number of methylene units in the spacer. As described in succeeding sections, the detailed investigations clearly reveal the influence of the spacer's length on the packing of the columns on a 2D lattice. For example, mesogens **P-6**, **P-7**, and **P-11** show the

columnar centered rectangular (Col_r) phase, whereas the LCs **P-8** and **P-10** exhibit Col oblique (Col_{ob}) phase. On the other hand, the compound **P-5** display Col hexagonal (Col_h) phase, which is notably fascinating in terms of its structure.

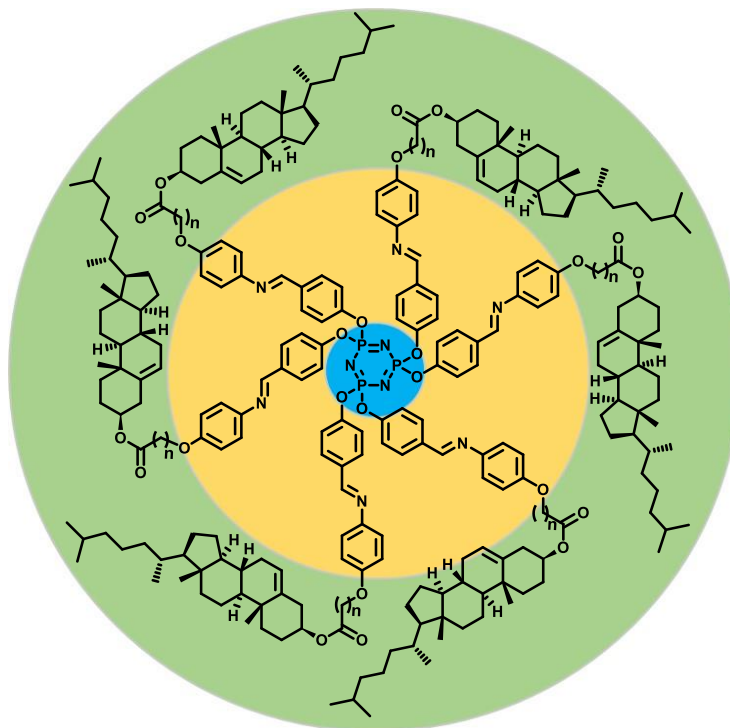


Figure 2.2 Schematic representation of the general molecular structure of a series of chiral Col LCs synthesized and investigated in this study (**P-n**, $n = 5, 6, 7, 8, 10$ and 11).

The structural assignment of the newly synthesized Col LCs and their key precursors has been performed systematically with the help of standard characterization techniques. The phase transitional behaviour of all the target materials has been ascertained by polarising optical microscopy (POM), differential scanning calorimetry (DSC), and small-angle/wide-angle X-ray scattering (SAXS/WAXS) measurements. Temperature-dependent circular dichroism (CD) measurements have been used to prove the helicity of all the mesophases. The data derived from the transmission electron microscopy (TEM) technique have been used to substantiate the results of CD experiments. The intrinsic fluorescence behaviour of all the compounds has been demonstrated to be useful in sensing HCl vapours, which is likely to be originating from the Schiff-base units of the LC materials.³⁸⁻⁴⁵

2.2 Result and discussions

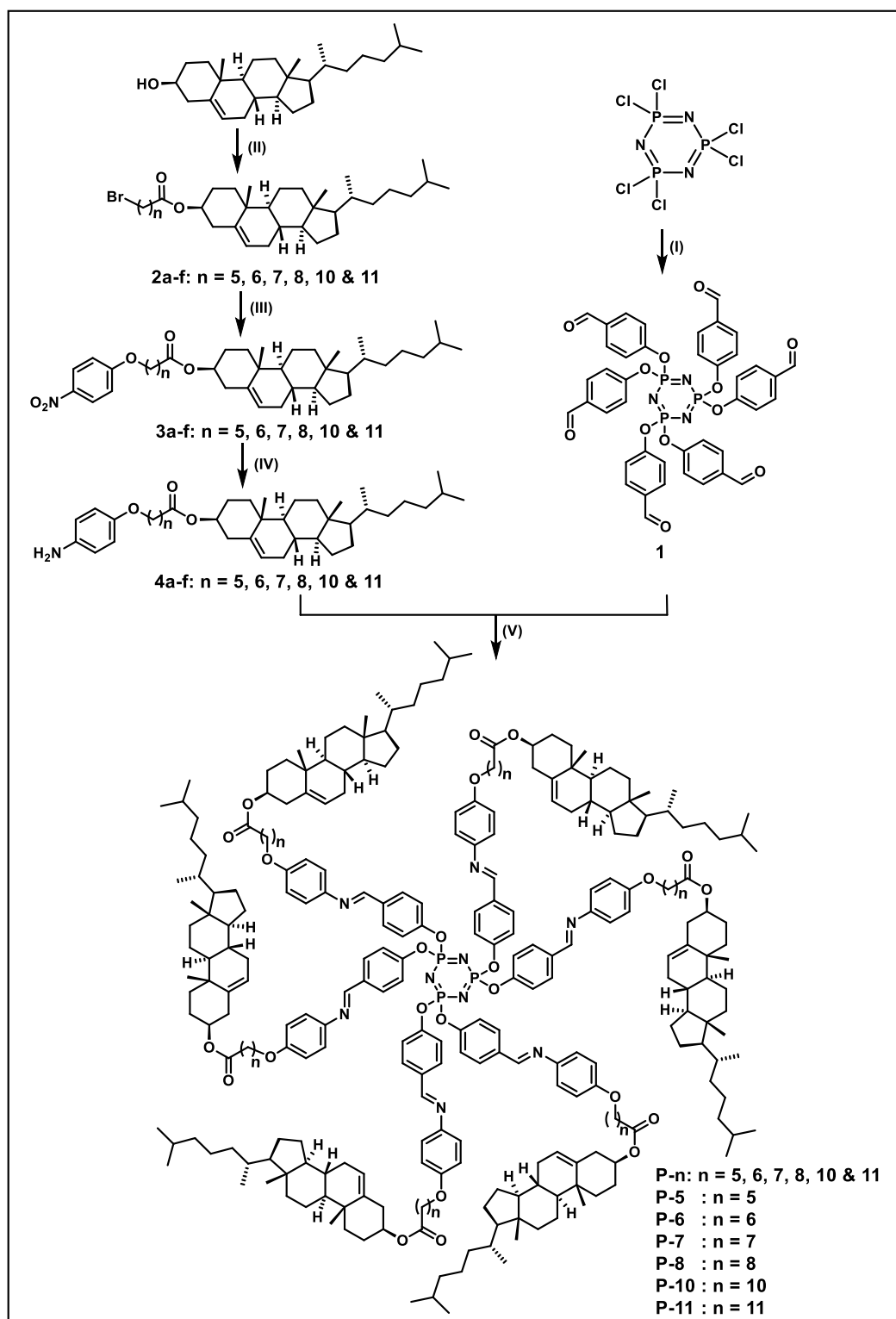
2.2.1 Synthesis, Structural Characterization and Thermal stability

The detailed synthetic steps employed for the synthesis of target mesogenic materials (**P-n**) are described in Scheme 2.1. The target materials synthesized by treating compound 1 with cholesteryl ω -(4-aminophenoxy) alkanoates (4a-f). ^1H NMR and ^{13}C NMR spectra, and the microanalytical data have been respectively presented in appendix (Figure A1-A15 and Table A1) and experimental section. The thermal stability of all the synthesized materials was determined using thermogravimetric analysis (TGA) (Figure A16 and Table 2.1); apparently, all the compounds are stable up to 300 °C - 350 °C.

2.2.2 Mesomorphic behaviour

Table 2.1 portrays the phase transition temperatures and related transition enthalpy changes seen in the DSC thermograms (Figure 2.3). The transition temperatures were found to be consistent with the POM data. For all the samples, three consecutive heating - cooling cycles were performed to record the DSC thermograph (Figure 2.3). All the members of the series showed thermodynamically stable Col mesomorphism. The fluidity of the LC phases was evidenced by the shearing test of the samples during both heating and cooling cycles. All the mesogens, as expected, have elevated clearing temperatures varying between 215 °C - 310 °C, according to spacer length; precisely, the isotropization temperature decreases with increasing spacer length. Notably, as can be seen in Table 2.1, the length of the central spacer greatly influences the structure (symmetry) of the Col phase.

The first member, **P-5**, of the series displayed an enantiotropic columnar mesophase. It showed the typical broken fan-shaped pattern along with homeotropic domains under crossed polarisers³² (Figure 2.4a). In the DSC trace obtained during heating, the endothermic peak at ~ 160.8 °C ($\Delta H = 15 \text{ kJ mol}^{-1}$) was attributed to crystal to Col phase transition, and the peak at ~ 303.5 °C ($\Delta H = 43.6 \text{ kJ mol}^{-1}$) corresponded to columnar to isotropic transition. On cooling, the exothermic peaks appeared at ~ 286.9 °C ($\Delta H = 14.5 \text{ kJ mol}^{-1}$) and 142.8 °C ($\Delta H = 3.9 \text{ kJ mol}^{-1}$) are due to the transition from isotropic liquid to Col phase and mesophase to crystallization, respectively (Figure 2.3a). During cooling, the enthalpy change of the liquid to mesophase transition was quite low as compared to the heating cycle because of the supercooling effect. This LC phase was assigned to be a hexagonal columnar phase based on X-ray diffraction (XRD) measurements. The XRD patterns recorded at various chosen



Scheme 2.1 Synthesis of the target compounds (**P-n**), Reagents and conditions: (I) 4-Hydroxybenzaldehyde, K₂CO₃, THF, 70 °C, 48 h, 60 %; (II) DCC, DMAP, dry DCM, 60 °C, 12 h, (Yield = 75 - 78 %); (III) 4-nitrophenol, K₂CO₃, butanone, KI, 90 °C, 24 h, (Yield = 85 - 90%); (IV) H₂, 10 % Pd/C, THF, RT, 48 h, (quantitative yield); (V) dry THF, 60 °C, 24 h (Yield = 35 - 40%).

temperatures for the mesophase possessed the characteristic features of the Col_h phase in agreement with POM observations. In small-angle region, the occurrence of multiple peaks with *d*-spacing in the ratio $\frac{1}{1} : \frac{1}{\sqrt{3}} : \frac{1}{\sqrt{4}} : \frac{1}{\sqrt{7}}$, corresponded to the strong reflection from (10) plane and three weak reflections from (11), (20), and (21) planes, respectively of the hexagonal structure. Besides, two broad peaks in the wide-angle region, *h_r* with spacing 6.3 Å, appeared due to cholesterol-cholesterol correlation and *h_a* with spacing 5.1 Å, attributed to the fluid alkyl chain-chain correlation, were seen. The calculated value of the lattice parameter is equal to *a* = 72.7 Å (Figure 2.5a, Table A2). The structure remained columnar hexagonal in the mesophase temperature regime. The 2D diffractograms of compound **P-5** (Figure 2.5d, 3.5g) in the SAXS, as well as WAXS region, also suggested the formation of Col_h mesophase.

Table 2.1. Thermotropic phase transitional behaviour of the cyclotriphosphazenes (**P-n**).

Compound	Phase Transition ^a (°C)	<i>T</i> _{5%} ^b (°C)
P-5	Heating: Cr 160.8 Col _h 303.5 Iso Cooling: Iso 286.9 Col _h 142.8 Cr	330.0
P-6	Heating: Cr 108.0 Col _r 231.0 Iso Cooling: Iso 222.0 Col _r 84.9 Cr	346.0
P-7	Heating: Cr 144.0 Col _r 265.0 Iso Cooling: Iso 258.8 Col _r 129.0 Cr	325.3
P-8	Heating: Cr 121.2 Cr ₁ 163.7 Col _{ob} 210.0 Iso Cooling: Iso 203.2 Col _{ob} 95.6 Cr	351.0
P-10	Heating: Cr 147.6 Cr ₁ 154.5 Col _{ob} 214.7 Iso Cooling: Iso 211.3 Col _{ob} 133.2 Cr ₁ 117.7 Cr	306.3
P-11	Heating: Cr 123.6 Cr ₁ 154.0 Col _r 220.1 Iso Cooling: Iso 216.7 Col _r 152.5 Cr ₁ 85.9 Cr	342.0
^a Temperatures of phase transitions (peak, in °C) obtained from DSC analysis. Abbreviations: Col _h = Columnar hexagonal, Col _r = Columnar centered rectangular, Col _{ob} = Columnar oblique, Iso = Isotropic liquid. ^b Decomposition temperature corresponding to a weight loss of 5 % as measured by TGA.		

The next two homologues (**P-6**, **P-7**) showed the enantiotropic columnar centered rectangular (Col_r) phase over a wide temperature range. The heating DSC trace of **P-6** displayed one peak at ~108 °C ($\Delta H = 10.6 \text{ kJ mol}^{-1}$) corresponding to crystal to Col_r transition and second peak for Col_r to isotropic transition at 231 °C ($\Delta H = 8.5 \text{ kJ mol}^{-1}$). Upon cooling, the mesophase appeared at 222 °C ($\Delta H = 9.1 \text{ kJ mol}^{-1}$) and remained stable up to 84.9 °C ($\Delta H = 4.5 \text{ kJ mol}^{-1}$) (Figure 2.3b). The growth of *pseudo*-focal-conic textures under POM supported the

arrangement of discs in columnar fashion³² (Fig. 2.4b). The other compound, **P-7**, also showed the two-phase transition both in the heating and cooling cycle (Figure 2.3c). The mesophase

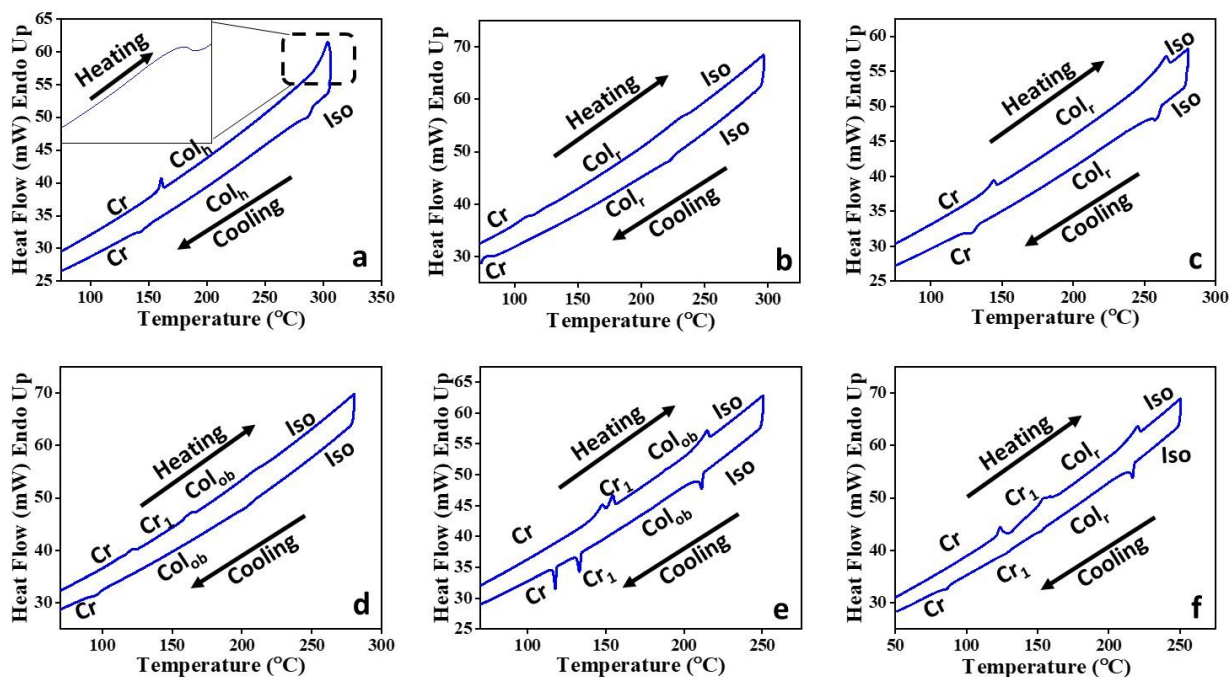


Figure 2.3 DSC thermograms of compounds (a) **P-5**, (b) **P-6**, (c) **P-7**, (d) **P-8**, (e) **P-10**, (f) **P-11**, recorded at a rate of 10 °C/min.

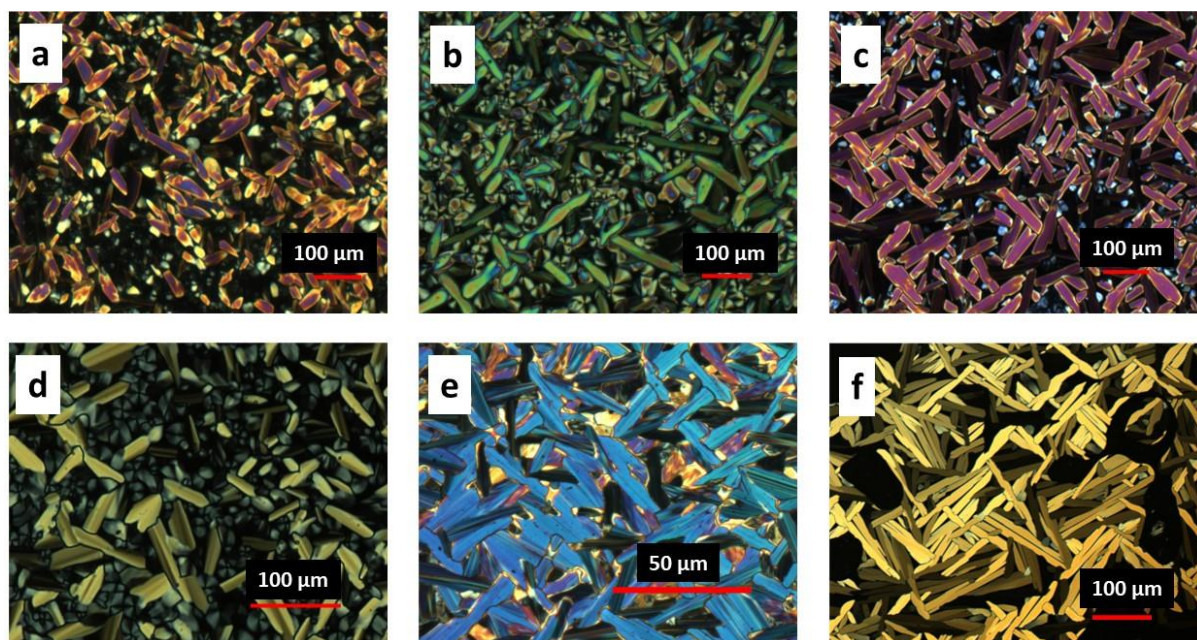


Figure 2.4 POM microphotographs of the optical texture of Col phases formed by (a) **P-5** at 280 °C, (b) **P-6** at 230 °C, (c) **P-7** at 225 °C, (d) **P-8** at 190.7 °C, (e) **P-10** at 150.9 °C and (f) **P-11** at 214.9 °C.

assignment was done purely based on XRD analysis, and the pattern could be indexed to a 2D centred rectangular lattice. The XRD pattern of compound **P-6** at temperature 190 °C is shown in Figure A17a (Table A3). It exhibited four narrow peaks in the small-angle region at the d -spacings 66.1 Å, 48.1 Å, 24.2 Å, and 22.9 Å.

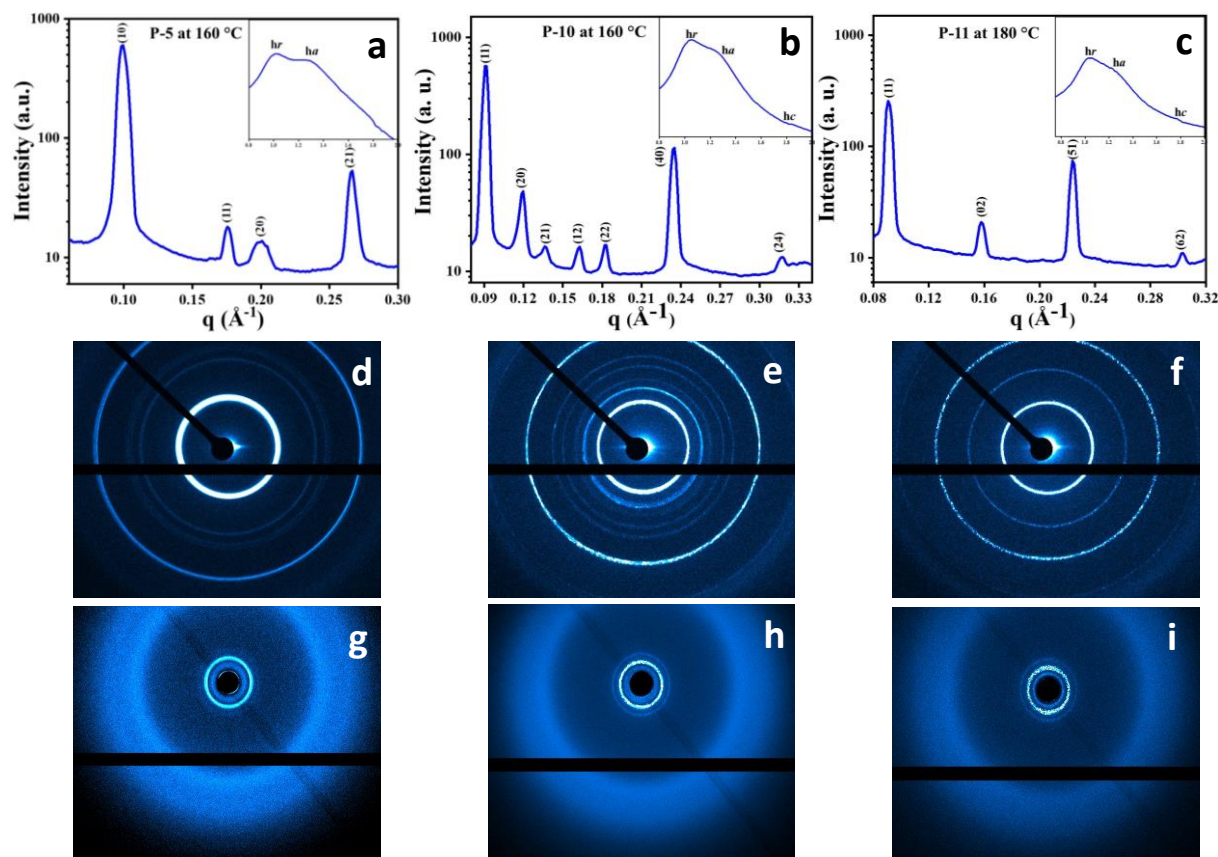


Figure 2.5 Small and wide-angle (inset) X-ray diffraction patterns of the Col phases formed by compounds (a) **P-5** at 160 °C (Col_h), (b) **P-10** at 160 °C (Col_{ob}) and (c) **P-11** at 180 °C (Col_l) upon cooling, h_r - cholesterol-cholesterol correlation, h_a - alkyl chain-chain correlation, h_c - disc-disc correlations. The lower panel shows the respective 2D diffraction patterns of SAXS (d, e, f) and WAXS (g, h, i).

These peaks corresponded to the diffractions from (11), (20), (40), and (04) planes of the centred rectangular lattice. The lattice parameters were found to be $a = 96.1$ Å, $b = 91.1$ Å. In the wide-angle region, there are three peaks, h_r , h_a , and h_c . The h_c peak of d -spacing 3.57 Å reflected the disc-disc correlation and confirmed the columnar structure of the mesophase. The compound **P-7** also exhibited 2D columnar centred rectangular phase in the entire mesophase temperature range (Figure 2.4c, Figure A17b, Table A4). The 2D diffractograms of compound

P-6 (Figure A17d, A17g) and **P-7** (Figure A17e, A17h) in the SAXS as well as WAXS region also suggested the formation of Col_r mesophase.

As shown in Table 1, the mesogens **P-8** and **P-10** also stabilize thermodynamically stable Col phase over a wide temperature range. The heating DSC profiles revealed three phase transitions in both materials (Figure 2.3d and 2.3e). They showed crystal-to-crystal, crystal-to-columnar, and columnar-to-liquid phase transitions. The corresponding cooling cycle traces possessed the signatures due to the transition from the isotropic liquid state to Col phase and the transformation from Col state to crystallization. The POM photomicrographs of the compounds **P-8** (Figure 2.4d) and **P-10** (Figure 2.4e) comprised of homeotropic domains as well as long fan-shaped patterns. These textures are characteristic of the columnar mesophase.³² As shown in Figure A17c (Table A5), the XRD pattern of the compound **P-8** recorded at 160 °C suggested the occurrence of the Col_{ob} phase; it consisted of narrow peaks in the small-angle region and two broad peaks, h_r and h_a , in the wide-angle regime. The lattice parameters were found to be $a = 105.2 \text{ \AA}$, $b = 73.7 \text{ \AA}$ and $\alpha = 69.3^\circ$. Likewise, the XRD profile of the mesogen **P-10** evidenced the existence of Col_{ob} phase (Figure 2.5b, Table A6). The 2D diffractograms of mesogens **P-8** (Figure A17f, A17i) and **P-10** (Figure 2.5e, 2.5h) in the SAXS, as well as WAXS region, also suggested the formation of Col_{ob} mesophase.

The last member of the series, **P-11**, also exhibited columnar mesomorphism over a wide thermal width. It showed three phase transitions in the heating and cooling cycle, as evidenced by DSC traces (Figure 2.3f) and the POM (Figure 2.4f) study. The XRD profile obtained in the mesophase at 180 °C exhibited four sharp peaks in small-angle region which corresponds to

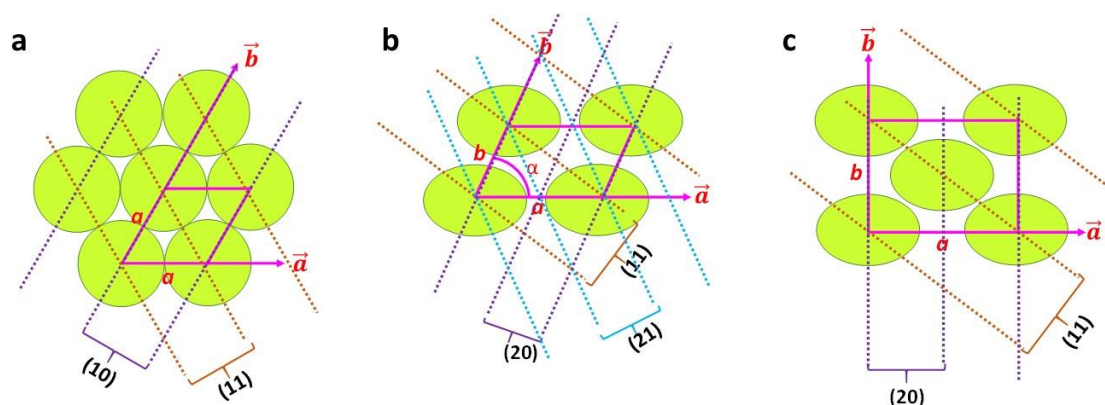


Figure 2.6 2-D projection model of (a) columnar hexagonal (Col_h) (b) columnar oblique (Col_{ob}) and (c) columnar centered rectangular (Col_r) phases; along with various representative reflecting planes, where a , b , α are the lattice parameters.

reflection from the (11), (02), (51), and (62) planes, respectively of the Col_r phase. Only these kinds of reflections are present because, the corresponding lattice for this phase is centered rectangular which allow only the reflection having $h+k = \text{even}$, where h, k are the Miller indices. Moreover, there are three peaks, h_r , h_a , and h_c , in the wide-angle regime, and they appeared for the same reason as explained before. The calculated values of the lattice parameters are $a = 148.2 \text{ \AA}$ and $b = 79.9 \text{ \AA}$ (Figure 2.5c, Table A7). The 2D patterns (Figure 2.5f, 2.5i) in the SAXS as well as the WAXS region also suggested the formation of Col_r mesophase.

2.2.3 Electron density maps

To figure out the arrangement of these mesogens on the various 2D lattices, the electron density maps⁴⁶ were constructed by using the information derived from the peak, indexes, and intensities of the XRD pattern and the 2D projection model (Figure 2.6) of all the columnar arrangements is also displayed. The electron density maps for the compounds **P-5**, **P-6**, **P-7**, **P-8**, **P-10** and **P-11** are shown in Figure 2.7a-2.7f, respectively. From electron density maps, it is clear that the individual mesogenic molecule appears, more or less, as a circular disc in the columnar hexagonal phase.

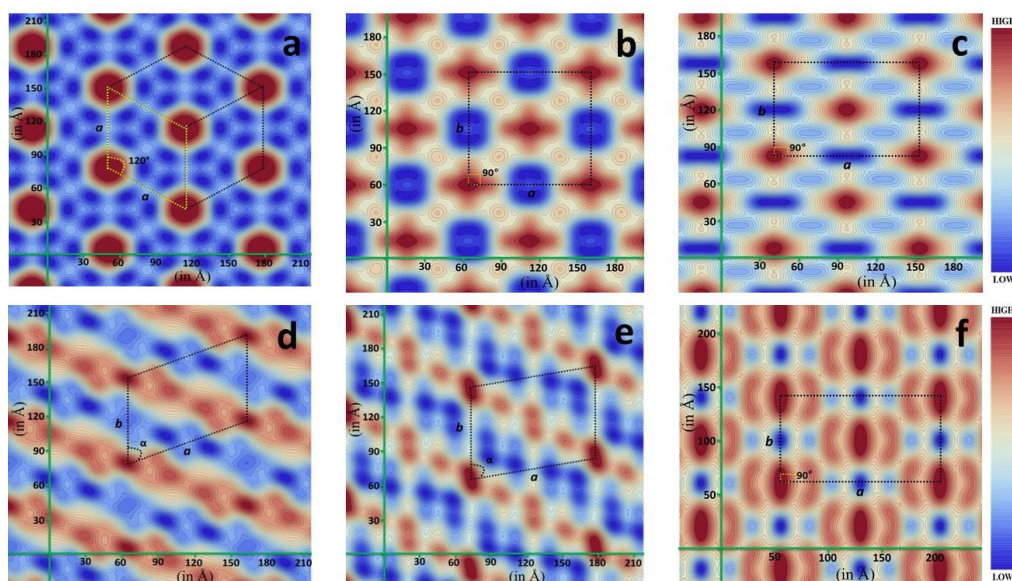


Figure 2.7 Electron density map of compound (a) **P-5** in Col_h phase, (b) **P-6** in Col_r phase, (c) **P-7** in Col_r phase, (d) **P-8** in Col_{ob} phase (e) **P-10** in Col_{ob} phase and (f) **P-11** in Col_r phase; where a, b, α are the lattice parameters.

The 2D projection model (Figure 2.6a, 2.6b, 2.6c), explained the reflecting planes of Col_h, Col_{ob} and Col_r, respectively, along with the unit cells of the different phases, represented by

2D closed region of pink colour. The shape seems to change to elliptical when the columnar centred rectangular phase is formed. Further, the shape of the molecules in the columnar oblique phase is dumbbell type (Figure 2.7d, 2.7e).

2.2.4 Chiroptical measurements

The newly synthesised chiral mesogens bearing accessible chromophores were probed for their chiroptical property in their mesomorphic (columnar) and isotropic liquid states by means of the circular dichroism (CD) spectroscopy, which essentially reveals the differential absorption of left and right circularly polarised waves by the light-absorbing groups (chromophores) surrounded by chiral medium. This absorption spectroscopic study has been carried out mainly to determine if the peripherally located bulky chiral (cholesterol) segments accounting for the molecular chirality have enabled the molecular organization in the Col phase in a helical manner where the constituent, intrinsically dissymmetric (chiral) mesogens within the columns follow a helical array. An organization of mesogens yielding a helical superstructure displays an exciton-split effect related to a through-space interaction among two or more chromophores exhibiting the allowed π - π^* absorption bands.⁴⁷ CD spectrum of the anisotropic media are generally accompanied by artefacts such as linear birefringence (LB) and linear dichroism (LD). However, the presence of small anisotropic (mesophase) domains in abundance are known to rescind such artefacts.⁴⁸ Four mesogens viz., **P-5**, **P-6**, **P-10**, and **P-11** were chosen for the chiroptical investigation. The isotropic liquid thin films of the aforesaid samples (except **P-5**) were subjected to CD spectral measurement.

The requisite sample cells (thin-films) were fabricated by using two clean, regular quartz plates. About 500-800 μg of the samples, **P-6**, **P-10** and **P-11**, placed individually between the substrates, were heated to their isotropic state, and the top plate was hard-pressed repeatedly to attain the uniform spreading of the analyte over a large area of the cell. This procedure not only expels the air-pockets but also ensures the thin-film formation of the mesogens. Although an analyte cell was fabricated for the study using a tiny amount ($\sim 600 \mu\text{g}$) of mesogen **P-5**, the aforesaid protocol could not be adopted due to its high isotropization temperature. The fabrication of such ultra thin-films, using a minute amount of the samples, was essential to circumvent the factual errors associated with experiments and operating limits of the instrument. The samples were then cooled at a faster rate into the LC phase, and the CD spectra were recorded as a function of decreasing temperature. Tables A8, A9, A10 and A11 respectively portray the CD data, presented in terms of ellipticity (θ , in millidegrees, mdeg) as

a function of wavelength, derived from the temperature-dependent CD profiles of the mesogens **P-5** (Figure A18b), **P-6** (Figure 2.8a) **P-10** (Figure 2.8b), and **P-11** (Figure 2.8c). As can be seen in Figure 2.8d, 2.8e, and 2.8f that the CD response of the isotropic liquid state remains totally absent, implying that the chromophores are not affected by the chirality stemming from the stereogenic centres of the peripheral cholesterol segments.

As noted earlier, CD spectra are often affected by the LD artifacts resulting from the macroscopic optical anisotropies of the analyte. Thus, to differentiate the specimens' genuine CD activity from that of the spurious response, the LD spectra were recorded using the instrument's built-in LD data acquisition option. This observation was corroborated using the sample rotation technique, which is very useful and reliable for the thin, evenly spread anisotropic samples. The CD spectra were recorded at six different positions attained by step-wise 60° rotation of the cell in the observing plane, i.e., in the direction perpendicular to the measuring beam. As expected, the CD profiles recorded for different cells' orientations largely resembled each other implying the absence of the LD. The spectra recorded did not show any signatures due to LD activity (Figure A18a and Figure 2.9), as contemplated.

The rapid cooling of the samples from their isotropic phase to LC phase generally helps in realising small domains.⁴⁹ The CD spectrum recorded in the Col phase as a function of temperature, from well below the isotropization temperature of the material **P-5**, is shown in Figure A18b. Similarly, the other three mesogens showed CD signals in the entire temperature width of the Col phase, meaning that the macroscopic structure, the fluid anisotropic medium, is optically active. The spectra recorded did not show any signatures due to LD activity (Figures 2.9a, 2.9b and 2.9c), as contemplated. The LD spectra have been recorded for the Col phase appearing just below the isotropization temperature.

The CD spectrum recorded as a function of temperature in the Col phase of mesogen **P-5** possessed a strong band with a negative maximum at ~390 nm, a wavelength closer to the electronic absorption maximum (~350 nm) of the solution spectra of the sample. The intensity (magnitude) of the CD peak increases progressively with the decrease in temperature (Figure A18b, Table A8), implying the core-core correlation within the columns and, thus, the proximity of the chromophores varies with the temperature. However, the CD curve position (and the sign) remained unaffected, demonstrating that the mesophase absorbs either left or right circularly polarised light in preference to scattering where the wavelength of the band changes as a function of temperature.⁵⁰ The CD profiles of the compound **P-6** recorded in the

higher temperature range (140 °C - 220 °C) revealed a relatively weak circular dichroism in the 310 - 430 nm spectral region. The spectrum was characterised by two negative peaks with maxima at 350 and 400 nm. Interestingly, in the corresponding low-temperature CD spectrum (55 °C - 130 °C) recorded, these two peaks appeared at 297 and 360 nm with a significant increase in the band intensities (Figure 2.8a, Table A9). Such a blue shift of the absorption maximum of the circular dichroism along with the enhanced band intensity suggests a considerable variation in the face-to-face parallel organisation of chromophores surrounded by the chiral environment. Figure 2.8b illustrates the results of temperature-dependent CD measurement carried out in the Col phase of oligomer **P-10**.

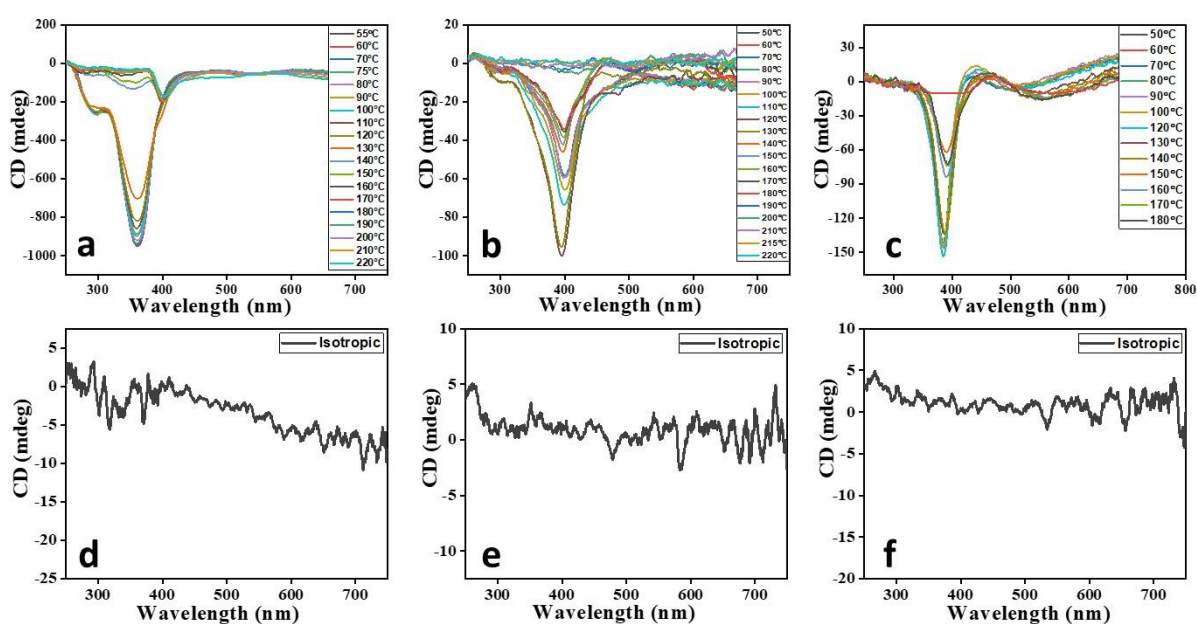


Figure 2.8 The optical response of the isotropic state and Col LC phase of mesogens **P-6** (a and d), **P-10** (b and e), and **P-11** (c and f). Profiles a, b & c: CD spectra recorded as a function of temperature in the Col phase of the mesogens. Profiles d, e & f: CD spectra of isotropic liquid phase. Notice that the CD intensity increases with the decrease in temperature of the Col phase.

The spectrum comprised a well-defined (strong) negative band centred at 395 nm, the magnitude of which decreases continually with the increase in the temperature (Figure 2.8b); besides, the marginal blue shift occurs in the peak position when the temperature of the sample decreases (Table A10). On the other hand, the spectrum recorded as a function of temperature in the Col phase of material **P-11** showed the bisignate CD curve with 1st positive Cotton effect at the longer wavelength (~440 nm) and negative 2nd Cotton effect at the relatively shorter wavelength (~385 nm) with the crossover point closer to the chromophore absorption maximum (Figure 2.8c). The CD curve shifts towards a shorter wavelength upon decreasing

the temperature, which is also seen in the other three compounds measured (Figure 2.8c, Table A11). The appearance of bisignate CD signal essentially implies the chiral excitonic coupling originating due to the aggregation of chromophores with their transition dipoles organized in a helical manner.⁵¹

Thus, the CD measurements as a function of the temperature of the Col phase belonging to four compounds reveal intense curves in the CD spectra, demonstrating significant chiral correlations in the molecular organization within the columns. In other words, the intrinsic CD activity of the mesophase evidenced the occurrence of a helix within the columns resulting from the closer packing of mesogens adopting a helical arrangement and this arrangement remains in crystallization stage as well. As reported earlier, scanning electron microscopy (SEM) and transmission electron microscopy (TEM) techniques were used to examine the solid morphologies of the helical assembly at different THF/H₂O ratio.⁵² Inspired from this earlier work, we also tried to examine the helical self-assembly for the compound **P-11** at room

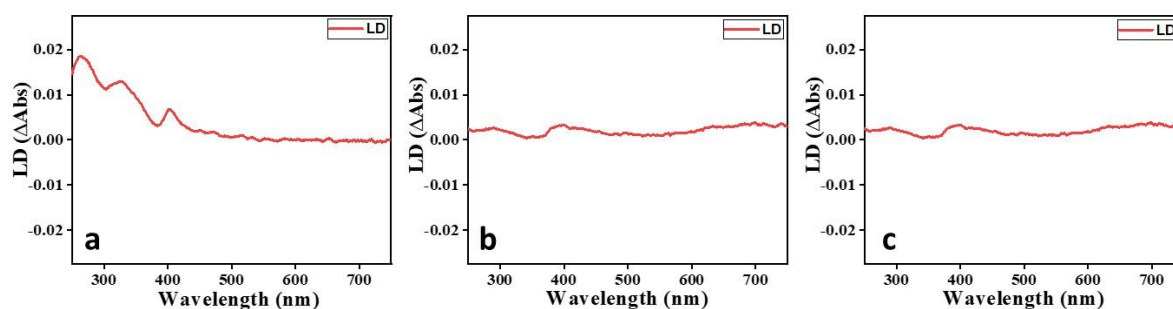


Figure 2.9 The LD spectra of compound (a) **P-6**, (b) **P-10**, and (c) **P-11**, in the fluid Col phase.

temperature via TEM. As shown in Figure 2.10, we observed well-defined twisting, corresponding to helical self-assembly of mesogens. To record TEM images, the samples in their isotropic liquid state were drop casted on carbon coated copper TEM grids (TED PELLA, INC. 200 mesh) and cooled down to room temperature. The TEM images of the compound are recorded in crystalline state, which interpret that the molecules remain in helical arrangement at room temperature. The schematic representation of the helicoidal columns in Col_h, Col_r and Col_{ob} are demonstrated in Figure 2.11.

2.2.5 Sensing Property

The design and development of novel sensors capable of showing the change in colour, which is recognizable by the naked eye, is highly desirable. Over the years, it has been well demonstrated that the imine (-CH=N-) bond of Schiff-base (electron-rich) core can be easily

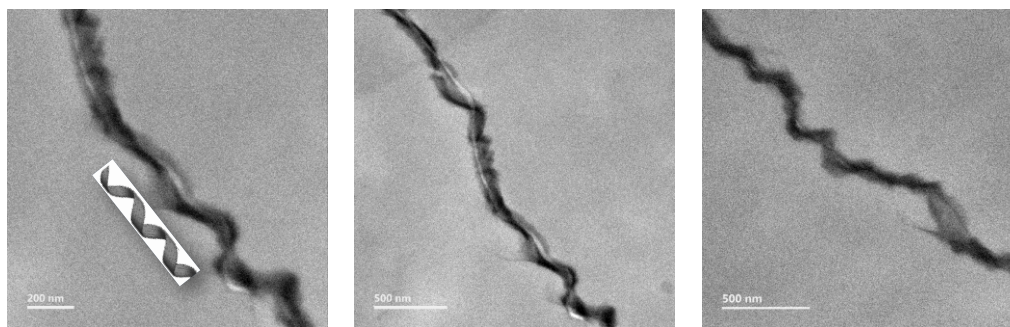


Figure 2.10 TEM images of compound **P-11**, image was recorded after heating to isotropic phase followed by cooling to room temperature.

protonated and hence can be used to sense the proton donors such as acids.⁵³ The π -conjugated electrons and a pair of electrons on the nitrogen atom are responsible for this behaviour of an imine group. Thus, these Schiff base mesogens featuring six imine bonds should be able to sense the acid traces, especially HCl vapours.⁵³ Working in this direction, we first investigated the photophysical behaviour of the new synthesized mesogens by UV-vis (Figure A19) and fluorescence spectroscopy (Figure A20).

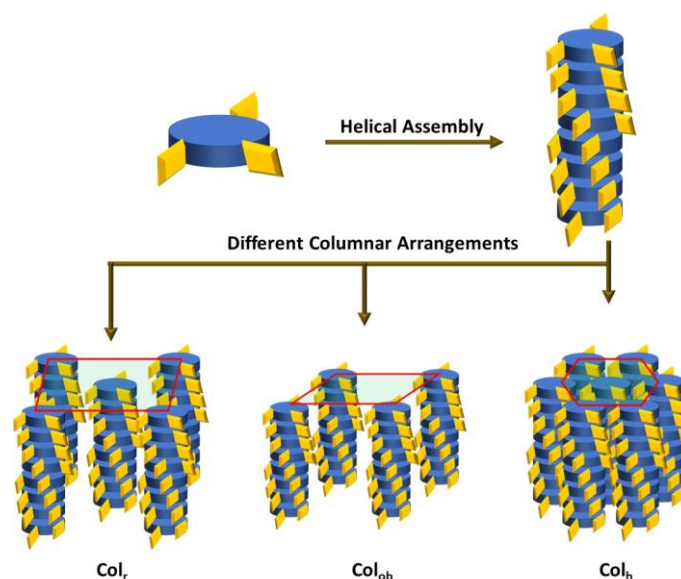


Figure 2.11 Schematic representation of helicoidal column arranged in different columnar organization.

The fluorescence experiments were carried out to examine the ability of mesogen **P-11** in sensing the presence of HCl, as an illustrative case. Precisely, the measurements were performed in solution as well as in solid-state of the chosen mesogen. For the sensing experiments, stock solutions of compound **P-11** and HCl were prepared. In particular, 10^{-5} M solution of compound **P-11** in THF and 10^{-2} M HCl solution in ACN were prepared. Titration

experiments were performed by adding HCl solution at a gradual interval of 10 μL to the stock solution of compound **P-11**, where the excitation wavelength is 338 nm. The fluorescence spectra were recorded accordingly with excitation and emission slit widths of 5.0 nm. As depicted in Figure 2.12a, the solid compound **P-11** upon exposure to acid vapours shows a broad fluorescence emission band (red-trace), unlike the pristine (un-exposed) solid sample (blue-trace) or the former specimen after exposing to ammonia vapours for neutralization or recovery (black-trace). Figure 2.12b illustrates the emission profiles recorded, at the excitation wavelength of 338 nm, for the pristine sample in THF (10^{-5} M) solution (black-trace) and its interactions with 10^{-2} M HCl solution (in acetonitrile) of varying concentrations. Apparently, the magnitude of fluorescence emission intensity increases progressively with the increase in the concentration of acid. Such a turn-on fluorescence enhancement is likely to be attributed to the protonation for imine nitrogen, which changes molecular planarity.⁵³ Similarly, the sensing behaviour of **P-11** was also probed with other acids and the selectivity experiments were carried out by adding 50 μL of 0.1 M stock solution of various acids in 600 μL stock solution of compound **P-11**. The detection limit (LOD) was also calculated using the formula $3\sigma/\rho$, where σ is the standard deviation of blank measurements of compound **P-11** and ρ is the slope of the calibration curve plotted between fluorescence intensity and HCl concentration. However, this material showed high selectivity towards HCl (Figure 2.12c), and the detection limit for HCl was found to be 5.6 μM (Figure 2.12d). The colour of compound **P-11** in solid-state changed from off white to bright yellow in normal light (Figure 2.12e) and also showed fluorescent turn-on phenomena when it was placed in HCl atmosphere under a UV lamp (Figure 2.12f), and this enables the naked eye detection of HCl gas. The other homologues of the series (**P-5**, **P-6**, **P-7**, **P-8**, and **P-10**) displayed a similar behaviour towards HCl vapour as shown in Figure A21 to Figure A25, respectively.

2.3 Conclusions

The first examples of chiral Col LCs derived from cyclic triphosphazene core, which is peripherally substituted with cholesterol-based Schiff-base dimeric segments, have been synthesized and characterized systematically. The length and parity of the spacer of the dimeric units that covalently bind cholesterol and two-ring Schiff base core have been varied to examine the structure-property correlations. As clearly revealed by the XRD measurement coupled with electron density mapping, the length of the spacer critically dictates the 2D periodic order characteristic of the Col LC phases formed by the spontaneous self-assembly of triphosphazene mesogens. The effect of the parity seems to have not been reflected. The

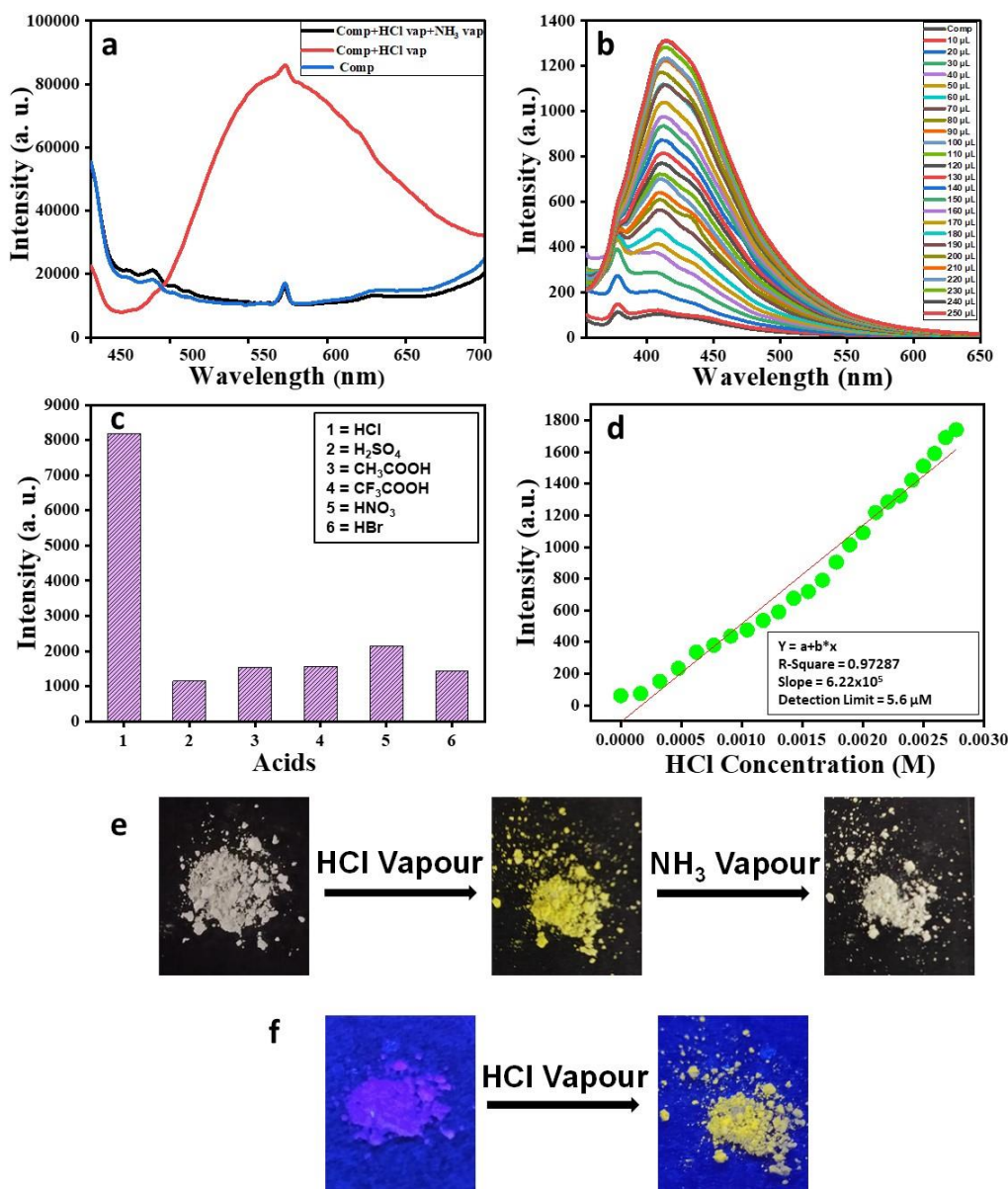


Figure 2.12 (a) Fluorescence spectra of mesogen **P-11** in a solid state when exposed to HCl vapour and NH₃ vapour (338 nm). (b) Fluorescence spectra of **P-11** (10^{-5} M in THF) recorded before and after its exposure to different concentrations of HCl solution (10^{-2} M in acetonitrile). (c) The fluorescence intensity of compound **P-11** after addition of 50 μ L of 10^{-2} M solution of various acids in the stock solution. (d) Calibration curve of the fluorescence intensity versus HCl concentration. Optical photographs of **P-11** upon exposure to HCl vapour and ammonia vapour under normal light (e), and upon exposure to HCl vapour under UV light (f).

mesogens, depending upon the length of the spacer, yield mesophases such as Col_h, Col_r, and Col_{ob} phases. The temperature-dependent chiroptical studies revealed the helical self-assembly in columnar arrangements. Notably, these Col LCs, being Schiff bases, show sensing characteristics due to their facile protonation. Particularly, the HCl sensing in solid and

solutions has been demonstrated with the help of fluorescent emission measurements. Notably, the fluorescent “turn-on” phenomena were observed. The detection limit for HCl was found to be 5.6 μM .

2.4 Experimental section

2.4.1 General procedure for the synthesis of compound 1:

Hexachlorocyclotriphosphazene (600 mg, 1 equiv.) and potassium carbonate (3 g, 12 equiv.) was dissolved in dry THF (50 mL) under a nitrogen atmosphere with continuous vigorous stirring. After vigorously stirring this suspension for 15 min, 4-hydroxy-benzaldehyde (1.7 g, 8 equiv.) dissolved in dry THF (10 mL) was added. The resultant reaction mixture was heated to reflux for 48 h. The reaction mixture was concentrated in vacuum, and the residue obtained was purified by column chromatography using silica gel with an eluent made of mixing hexane and ethyl acetate (v/v 100/50). Yield = 60 %. HRMS (Figure A3) m/z : (M + H)⁺ calculated for $\text{C}_{42}\text{H}_{31}\text{N}_3\text{O}_{12}\text{P}_3$ 862.1120. Found 862.1093. The ^1H , ^{13}C (Figure A1 and A2) are given in Appendix I.

Characterization details of compound 1:

^1H NMR (400 MHz, CDCl_3 , δ in ppm) 9.93 (s, 6H), 7.73 (d, $J = 8.5$ Hz, 12H), 7.14 (d, $J = 8.5$ Hz, 12H).

^{13}C NMR (100 MHz, CDCl_3 , δ in ppm) 190.44, 154.48, 133.77, 131.42, 121.25, 121.23.

FTIR (cm^{-1}) 1703.9, 1598.1, 1500.4, 1421.6, 1390.3, 1299.9, 1274.1, 1207.2, 1177.4, 1155.2, 1101.4, 1012.2, 952.7, 887.8, 839.5, 761.5, 707.7, 609.2, 557.2, 514.5.

2.4.2 General procedure for the synthesis of compounds 2(a - f):

Cholesterol (1.2 equiv.) was added to the stirred solution of bromoalkanoic acid (2 g, 1 equiv.) in dry DCM (40 mL). The resulting mixture was stirred under a nitrogen atmosphere, and DMAP (catalytic amount) was added to the solution. A solution of DCC (1.25 equiv.) in DCM was further added to the reaction mixture, and the mixture was stirred at 60 $^\circ\text{C}$ for 12 h. The reaction mixture was filtered, and the filtrate obtained was concentrated in a vacuum. The crude product was then purified by column chromatography using silica gel with a mixture of hexane/ethyl acetate (v/v, 100/1) as an eluent. The white solid obtained was air-dried and stored in a clean sample vial. Yield = 75 – 78 %.

Characterization details of 2(a - f):

2a: Yield = 76 %, ^1H NMR (400 MHz, CDCl_3 , δ in ppm) 5.37 (d, $J = 5.5$ Hz, 1H), 4.65 – 4.59 (m, 1H), 3.41 (t, $J = 6.8$ Hz, 2H), 2.35 – 2.25 (m, 4H), 1.99 (s, 2H), 1.92 – 1.79 (m, 5H), 1.69 – 1.62 (m, 2H), 1.59 – 1.44 (m, 8H), 1.39 – 1.25 (m, 4H), 1.20 – 1.04 (m, 8H), 1.02 (s, 4H), 0.97 (d, $J = 11.0$ Hz, 2H), 0.91 (d, $J = 6.5$ Hz, 3H), 0.86 (dd, $J = 6.6, 1.9$ Hz, 6H), 0.68 (s, 3H).

^{13}C NMR (100 MHz, CDCl_3 , δ in ppm) 172.89, 139.66, 122.67, 73.89, 56.69, 56.14, 50.03, 42.32, 39.73, 39.53, 38.16, 37.00, 36.60, 36.19, 35.80, 34.43, 33.52, 32.42, 31.91, 31.87, 28.24, 28.03, 27.82, 27.63, 24.29, 24.18, 23.84, 22.84, 22.58, 21.04, 19.33, 18.73, 11.87.

FTIR (cm^{-1}) 2949, 2888, 2867, 2850, 1733, 1467, 1434, 1373, 1324, 1255, 1190, 1174.

2b: Yield = 75 %, ^1H NMR (400 MHz, CDCl_3 , δ in ppm) 5.37 (d, $J = 5.0$ Hz, 1H), 4.62 – 4.58 (m, 1H), 3.44 – 3.38 (m, 2H), 2.29 (q, $J = 7.5$ Hz, 4H), 2.04 – 1.93 (m, 2H), 1.90 – 1.80 (m, 5H), 1.67 – 1.52 (m, 7H), 1.46 (ddd, $J = 14.2, 7.5, 4.5$ Hz, 6H), 1.35 (h, $J = 6.2, 5.3$ Hz, 5H), 1.25 (d, $J = 4.4$ Hz, 1H), 1.13 (ddd, $J = 19.4, 13.0, 7.4$ Hz, 6H), 1.02 (s, 4H), 0.98 (d, $J = 4.9$ Hz, 1H), 0.91 (d, $J = 6.5$ Hz, 3H), 0.86 (dd, $J = 6.6, 1.9$ Hz, 6H), 0.68 (s, 3H).

^{13}C NMR (100 MHz, CDCl_3 , δ in ppm) 173.09, 139.67, 122.66, 73.81, 56.69, 56.13, 50.02, 42.32, 39.73, 39.53, 38.17, 37.00, 36.61, 36.19, 35.81, 34.53, 33.82, 32.56, 31.92, 31.86, 28.25, 28.22, 28.03, 27.82, 24.82, 24.30, 23.84, 22.85, 22.59, 21.04, 19.35, 18.73, 11.87.

FTIR (cm^{-1}) 2946, 2888, 2868, 2848, 1732, 1465, 1435, 1376, 1324, 1247, 1187, 1172.

2c: Yield = 78 %, ^1H NMR (400 MHz, CDCl_3 , δ in ppm) 5.37 (d, $J = 5.4$ Hz, 1H), 4.67 – 4.57 (m, 1H), 3.40 (t, $J = 6.8$ Hz, 2H), 2.34 – 2.24 (m, 4H), 2.04 – 1.93 (m, 2H), 1.89 – 1.78 (m, 5H), 1.65 – 1.53 (m, 7H), 1.52 – 1.39 (m, 6H), 1.33 (p, $J = 3.7$ Hz, 7H), 1.28 – 1.21 (m, 1H), 1.13 (ddd, $J = 19.3, 9.7, 5.8$ Hz, 6H), 1.02 (s, 4H), 0.96 (t, $J = 5.8$ Hz, 1H), 0.91 (d, $J = 6.5$ Hz, 3H), 0.86 (dd, $J = 6.6, 1.9$ Hz, 6H), 0.68 (s, 3H).

^{13}C NMR (100 MHz, CDCl_3 , δ in ppm) 173.18, 139.69, 122.63, 73.76, 56.69, 56.14, 50.03, 42.32, 39.74, 39.53, 38.17, 37.01, 36.60, 36.19, 35.81, 34.61, 33.89, 32.72, 31.91, 31.87, 28.90, 28.42, 28.25, 28.03, 27.99, 27.83, 24.91, 24.30, 23.84, 22.84, 22.58, 21.04, 19.34, 18.73, 11.87.

FTIR (cm^{-1}) 2945, 2888, 2869, 1733, 1559, 1543, 1468, 1440, 1367, 1242, 1184, 1173.

2d: Yield = 75 %, ^1H NMR (400 MHz, CDCl_3 , δ in ppm) 5.37 (d, $J = 5.0$ Hz, 1H), 4.66 – 4.57 (m, 1H), 3.40 (t, $J = 6.8$ Hz, 2H), 2.33 – 2.24 (m, 4H), 2.04 – 1.92 (m, 2H), 1.89 – 1.78 (m, 5H), 1.65 – 1.52 (m, 6H), 1.52 – 1.48 (m, 2H), 1.45 – 1.39 (m, 3H), 1.32 (d, $J = 5.0$ Hz, 10H), 1.13 (ddd, $J = 19.6, 13.5, 5.7$ Hz, 7H), 1.02 (s, 5H), 0.97 (d, $J = 11.0$ Hz, 1H), 0.91 (d, $J = 6.4$ Hz, 3H), 0.86 (dd, $J = 6.6, 1.9$ Hz, 6H), 0.68 (s, 3H).

^{13}C NMR (100 MHz, CDCl_3 , δ in ppm) 173.25, 139.70, 122.62, 73.73, 56.69, 56.13, 50.02, 42.31, 39.73, 39.53, 38.17, 37.01, 36.60, 36.19, 35.81, 34.67, 34.00, 32.79, 31.92, 31.86, 29.08, 28.99, 28.59, 28.25, 28.11, 28.03, 27.83, 24.99, 24.30, 23.84, 22.85, 22.59, 21.04, 19.35, 18.73, 11.87.

FTIR (cm^{-1}) 2942, 2889, 2866, 2852, 1736, 1466, 1435, 1375, 1263, 1228, 1172.

2e: Yield = 77 %, ^1H NMR (400 MHz, CDCl_3 , δ in ppm) 5.37 (d, $J = 5.0$ Hz, 1H), 4.67 – 4.54 (m, 1H), 3.40 (t, $J = 6.9$ Hz, 2H), 2.34 - 2.22 (m, 4H), 2.03 - 1.93 (m, 2H), 1.90 - 1.79 (m, 5H), 1.66 - 1.47 (m, 8H), 1.46 - 1.39 (m, 5H), 1.28 (s, 12H), 1.16 - 1.10 (m, 7H), 1.01 (s, 6H), 0.91 (d, $J = 6.5$ Hz, 3H), 0.86 (dd, $J = 6.7, 1.9$ Hz, 6H), 0.67 (s, 3H).

^{13}C NMR (100 MHz, CDCl_3 , δ in ppm) 173.33, 139.72, 122.62, 73.70, 56.69, 56.13, 50.02, 42.32, 39.73, 39.53, 38.17, 37.01, 36.61, 36.19, 35.81, 34.72, 34.08, 32.84, 31.92, 31.86, 29.37, 29.34, 29.22, 29.09, 28.75, 28.25, 28.18, 28.03, 27.83, 25.05, 24.30, 23.84, 22.85, 22.59, 21.04, 19.35, 18.73, 11.87.

FTIR (cm^{-1}) 2941, 2889, 2868, 2852, 1736, 1599, 1577, 1467, 1438, 1380, 1364, 1168.

2f: Yield = 76 %, ^1H NMR (400 MHz, CDCl_3 , δ in ppm) 5.37 (d, $J = 5.0$ Hz, 1H), 4.63 – 4.57 (m, 1H), 3.40 (td, $J = 6.9, 1.9$ Hz, 2H), 2.33 – 2.23 (m, 4H), 1.98 (t, $J = 15.5$ Hz, 2H), 1.84 (p, $J = 6.3, 5.7$ Hz, 5H), 1.60 – 1.52 (m, 4H), 1.49 (q, $J = 8.9, 7.5$ Hz, 3H), 1.41 (t, $J = 7.5$ Hz, 3H), 1.30 (d, $J = 18.9$ Hz, 18H), 1.12 (ddd, $J = 20.1, 13.1, 6.9$ Hz, 6H), 1.01 (s, 5H), 0.96 (d, $J = 11.1$ Hz, 1H), 0.91 (d, $J = 6.4$ Hz, 3H), 0.86 (d, $J = 6.6$ Hz, 6H), 0.67 (s, 3H).

^{13}C NMR (100 MHz, CDCl_3 , δ in ppm) 173.34, 139.72, 122.61, 73.70, 56.69, 56.13, 50.03, 42.32, 39.74, 39.53, 38.17, 37.01, 36.61, 36.19, 35.81, 34.72, 34.06, 32.85, 31.92, 31.87, 29.46, 29.41, 29.25, 29.11, 28.77, 28.25, 28.19, 28.03, 27.83, 25.06, 24.30, 23.84, 22.84, 22.58, 21.04, 19.34, 18.73, 11.87.

FTIR (cm^{-1}) 2944, 2886, 2869, 2851, 1737, 1649, 1554, 1467, 1461, 1381, 1365, 1172.

2.4.3 General procedure for the synthesis of compounds 3(a - f):

Potassium carbonate (5 equiv.) was added to the solution of 4-nitrophenol (1.5 equiv.) in *n*-butanone. The above suspension was stirred for 15 min, and then compound **2** (3.5 g, 1 equiv.) was added, followed by the addition of potassium iodide (KI) in a catalytic amount. The reaction mixture was refluxed and continuously stirred for 24 h. The crude product was poured into ice-cold water and extracted with DCM. The organic phase dried over Na₂SO₄ was concentrated in vacuum. The crude product obtained was purified by column chromatography using silica gel with a mixture of hexane/ethyl acetate (v/v 100/2.5) as eluent. Yield = 85 – 90 %.

Characterization details of 3(a - f):

3a: Yield = 87 %, ¹H NMR (400 MHz, CDCl₃, δ in ppm) 8.19 (d, J = 9.2 Hz, 2H), 6.93 (d, J = 9.3 Hz, 2H), 5.37 (d, J = 5.8 Hz, 1H), 4.67 - 4.57 (m, 1H), 4.05 (t, J = 6.4 Hz, 2H), 2.36 - 2.25 (m, 4H), 2.04 - 1.93 (m, 2H), 1.89 - 1.79 (m, 5H), 1.70 (q, J = 7.6 Hz, 2H), 1.60 (s, 3H), 1.57 - 1.40 (m, 8H), 1.37 - 1.27 (m, 3H), 1.16 - 1.07 (m, 7H), 1.01 (s, 5H), 0.91 (d, J = 6.5 Hz, 3H), 0.86 (dd, J = 6.6, 1.9 Hz, 6H), 0.67 (s, 3H).

¹³C NMR (100 MHz, CDCl₃, δ in ppm) 172.94, 164.12, 141.37, 139.61, 125.93, 122.71, 114.39, 73.90, 68.52, 56.69, 56.13, 50.02, 42.32, 39.73, 39.52, 38.17, 36.98, 36.60, 36.19, 35.80, 34.48, 31.91, 31.86, 28.68, 28.24, 28.02, 27.82, 25.48, 24.68, 24.29, 23.84, 22.84, 22.58, 21.04, 19.32, 18.73, 11.87.

FTIR (cm⁻¹) 2962, 2946, 2904, 2888, 2868, 1731, 1594, 1517, 1468, 1342, 1267, 1174, 1110, 1031, 845, 750.

3b: Yield = 85 %, ¹H NMR (400 MHz, CDCl₃, δ in ppm) 8.19 (d, J = 9.2 Hz, 2H), 6.93 (d, J = 9.2 Hz, 2H), 5.35 (d, J = 5.1 Hz, 1H), 4.66 - 4.57 (m, 1H), 4.04 (t, J = 6.4 Hz, 2H), 2.32 - 2.26 (m, 4H), 2.03 - 1.93 (m, 2H), 1.83 (m, 6H), 1.65 (q, J = 7.4 Hz, 3H), 1.49 (q, J = 7.6, 7.1 Hz, 6H), 1.43 - 1.37 (m, 3H), 1.36 - 1.31 (m, 3H), 1.25 (d, J = 3.7 Hz, 1H), 1.12 (ddd, J = 19.0, 13.4, 6.8 Hz, 8H), 1.01 (s, 4H), 0.96 (d, J = 11.7 Hz, 1H), 0.91 (d, J = 6.5 Hz, 3H), 0.86 (dd, J = 6.6, 1.9 Hz, 6H), 0.67 (s, 3H).

¹³C NMR (100 MHz, CDCl₃, δ in ppm) 173.11, 164.18, 141.34, 139.62, 125.94, 122.69, 114.39, 73.82, 68.6, 56.68, 56.12, 50.01, 42.31, 39.72, 39.52, 38.17, 36.98, 36.60, 36.18, 35.80,

34.53, 31.90, 31.85, 28.78, 28.73, 28.24, 28.03, 27.82, 25.62, 24.88, 24.29, 23.83, 22.84, 22.58, 21.03, 19.33, 18.72, 11.86.

FTIR (cm^{-1}) 2954, 2941, 2898, 2887, 2869, 1734, 1593, 1510, 1471, 1342, 1271, 1176, 1110, 1027, 1005, 848, 748.

3c: Yield = 89 %, ^1H NMR (400 MHz, CDCl_3 , δ in ppm) 8.19 (d, $J = 8.7$ Hz, 2H), 6.93 (d, $J = 8.7$ Hz, 2H), 5.36 (d, $J = 5.0$ Hz, 1H), 4.60 (m, 1H), 4.03 (t, $J = 6.5$ Hz, 2H), 2.32 – 2.25 (m, 4H), 1.98 (t, $J = 16.1$ Hz, 2H), 1.88 – 1.77 (m, 5H), 1.65 – 1.53 (m, 6H), 1.51 – 1.42 (m, 6H), 1.39 – 1.32 (m, 6H), 1.25 (d, $J = 6.8$ Hz, 2H), 1.12 (ddd, $J = 19.7, 13.3, 6.7$ Hz, 7H), 1.01 (s, 4H), 0.96 (d, $J = 11.4$ Hz, 1H), 0.91 (d, $J = 6.4$ Hz, 3H), 0.86 (d, $J = 6.7$ Hz, 6H), 0.67 (s, 3H).

^{13}C NMR (100 MHz, CDCl_3 , δ in ppm) 173.20, 164.21, 141.32, 139.66, 125.93, 122.66, 114.39, 73.78, 68.79, 56.68, 56.13, 50.02, 42.31, 39.73, 39.52, 38.18, 37.00, 36.60, 36.19, 35.80, 34.61, 31.91, 31.86, 28.96, 28.94, 28.90, 28.24, 28.03, 27.83, 25.74, 24.91, 24.29, 23.84, 22.84, 22.58, 21.04, 19.33, 18.73, 11.87.

FTIR (cm^{-1}) 2941, 2931, 2887, 2870, 2847, 1736, 1592, 1516, 1467, 1343, 1265, 1172, 1112, 1031, 1007, 845, 753.

3d: Yield = 90 %, ^1H NMR (400 MHz, CDCl_3 , δ in ppm) 8.20 (d, $J = 9.2$ Hz, 2H), 6.94 (d, $J = 9.2$ Hz, 2H), 5.36 (d, $J = 5$ Hz, 1H), 4.64 – 4.60 (m, 1H), 4.04 (t, $J = 6.5$ Hz, 2H), 2.33 – 2.26 (m, 4H), 2.03 – 1.94 (m, 2H), 1.87 – 1.79 (m, 5H), 1.61 (d, $J = 7.4$ Hz, 2H), 1.54 – 1.42 (m, 8H), 1.39 – 1.30 (m, 10H), 1.25 (d, $J = 4.3$ Hz, 1H), 1.13 (td, $J = 11.2, 10.1, 5.1$ Hz, 7H), 1.01 (s, 5H), 0.99 – 0.96 (m, 1H), 0.91 (d, $J = 6.5$ Hz, 3H), 0.86 (dd, $J = 6.6, 1.9$ Hz, 6H), 0.67 (s, 3H).

^{13}C NMR (100 MHz, CDCl_3 , δ in ppm) 173.2, 164.24, 141.31, 139.68, 125.94, 122.66, 114.40, 73.75, 68.84, 56.68, 56.12, 50.01, 42.31, 39.72, 39.53, 38.18, 37.00, 36.61, 36.19, 35.81, 34.66, 31.91, 31.86, 29.14, 29.10, 28.98, 28.95, 28.25, 28.03, 27.83, 25.85, 24.99, 24.29, 23.84, 22.85, 22.58, 21.04, 19.34, 18.73, 11.87.

FTIR (cm^{-1}) 2963, 2948, 2900, 2885, 2869, 1735, 1593, 1507, 1471, 1339, 1268, 1176, 1112, 1019, 849, 751.

3e: Yield = 85 %, ^1H NMR (400 MHz, CDCl_3 , δ in ppm) 8.20 (d, $J = 9.2$ Hz, 2H), 6.94 (d, $J = 9.3$ Hz, 2H), 5.37 (d, $J = 5.0$ Hz, 1H), 4.65 - 4.57 (m, 1H), 4.04 (t, $J = 6.5$ Hz, 2H), 2.32 - 2.25

(m, 4H), 2.03 - 1.93 (m, 2H), 1.87 - 1.78 (m, 5H), 1.60 (s, 4H), 1.53 - 1.43 (m, 6H), 1.36 - 1.25 (m, 15H), 1.20 - 1.06 (m, 8H), 1.02 (s, 4H), 0.99 - 0.96 (m, 1H), 0.91 (d, $J = 6.5$ Hz, 3H), 0.86 (dd, $J = 6.6, 1.9$ Hz, 6H), 0.67 (s, 3H).

^{13}C NMR (100 MHz, CDCl_3 , δ in ppm) 173.31, 164.25, 141.30, 139.70, 125.92, 122.62, 114.39, 73.71, 68.88, 56.68, 56.12, 50.01, 42.31, 39.72, 39.52, 38.17, 37.00, 36.60, 36.18, 35.80, 34.70, 31.91, 31.86, 29.44, 29.33, 29.27, 29.22, 29.08, 28.97, 28.24, 28.03, 27.82, 25.91, 25.03, 24.29, 23.83, 22.84, 22.58, 21.03, 19.34, 18.72, 11.86.

FTIR (cm^{-1}) 2946, 2939, 2886, 2869, 2852, 1734, 1594, 1517, 1470, 1340, 1266, 1172, 1112, 1010, 848, 753.

3f: Yield = 87 %, ^1H NMR (400 MHz, CDCl_3 , δ in ppm) 8.19 (d, $J = 7.3$ Hz, 2H), 6.93 (d, $J = 8.7$ Hz, 2H), 5.36 (d, $J = 5.0$ Hz, 1H), 4.62 - 4.59 (m, 1H), 4.04 (t, $J = 6.6$ Hz, 2H), 2.31 - 2.24 (m, 4H), 2.05 - 1.93 (m, 3H), 1.82 (q, $J = 9.9, 7.4$ Hz, 6H), 1.57 (dd, $J = 20.1, 9.6$ Hz, 6H), 1.46 (q, $J = 9.1, 7.9$ Hz, 6H), 1.28 (s, 12H), 1.16 - 1.09 (m, 8H), 1.01 (s, 4H), 0.97 (s, 1H), 0.94 (d, $J = 5.7$ Hz, 1H), 0.91 (d, $J = 6.4$ Hz, 3H), 0.87 (s, 6H), 0.67 (s, 3H).

^{13}C NMR (100 MHz, CDCl_3 , δ in ppm) 173.33, 16.26, 141.31, 139.71, 125.93, 122.62, 114.40, 73.71, 68.89, 56.69, 56.13, 50.02, 42.31, 39.73, 39.53, 38.18, 37.01, 36.61, 36.19, 35.81, 34.71, 31.91, 31.86, 29.72, 29.49, 29.41, 29.31, 29.25, 29.10, 28.98, 28.24, 28.03, 27.83, 25.92, 25.05, 24.29, 23.84, 22.72, 22.84, 22.58, 21.04, 19.34, 18.72, 11.86.

FTIR (cm^{-1}) 2936, 2886, 2870, 2853, 1736, 1595, 1519, 1469, 1341, 1262, 1173, 1113, 1020, 848, 751.

2.4.4 General procedure for the synthesis of compounds 4(a - f):

The procedure for the synthesis of compound 4(a - f) is similar, as reported in the literature.⁵⁴ Compound 3 (2 g, 1 equiv.) was dissolved in a minimum amount of dry THF. To the above solution, 10 % Pd/C was added, and the mixture was stirred under H_2 atmosphere. The reaction was monitored with the help of TLC; the reaction was found to be completed after 48 h of stirring. After completion of the reaction, the mixture was filtered through a celite/silica gel bed and the product obtained after the evaporation of the solvent under vacuum was directly used for the next step without any purification.

2.4.5 General procedure for the synthesis of compounds P-n:

The final Schiff base compounds were synthesized by refluxing a mixture of compounds **4** (467 mg, 7 equiv.) and **1** (100 mg, 1 equiv.) in dry THF for 24 h. The crude product was obtained by evaporating the solvent in vacuum. The residue obtained was purified by recrystallization technique using a mixture of DCM and methanol (1:9). Yield = 35 - 40 %. The ^1H , ^{13}C spectra (Figure A4-A15) and elemental analysis (Table A1) of final compounds are given in Appendix I.

Characterization details of final compounds:

P-5: Yield = 39 %, UV-vis (absorbance in nm): 273, 338, Fluorescence: 377, 407, 431. ^1H NMR (400 MHz, CDCl_3 , δ in ppm) 8.37 (s, 6H), 7.72 (d, $J = 8.6$ Hz, 12H), 7.10 (dd, $J = 26.4$, 8.6 Hz, 24H), 6.82 (d, $J = 8.9$ Hz, 12H), 5.37 (d, $J = 5.0$ Hz, 6H), 4.66 – 4.58 (m, 6H), 3.96 (t, $J = 6.4$ Hz, 12H), 2.33 (dd, $J = 9.0$, 6.3 Hz, 24H), 2.02 – 1.93 (m, 12H), 1.83 (q, $J = 8.9$, 8.1 Hz, 36H), 1.72 (p, $J = 7.6$ Hz, 18H), 1.57 – 1.45 (m, 54H), 1.34 (d, $J = 8.0$ Hz, 18H), 1.25 (d, $J = 6.7$ Hz, 6H), 1.12 (dt, $J = 14.2$, 10.6 Hz, 42H), 1.01 (s, 24H), 0.91 (d, $J = 6.5$ Hz, 18H), 0.86 (dd, $J = 6.6$, 1.9 Hz, 36H), 0.67 (s, 18H).

^{13}C NMR (100 MHz, CDCl_3 , δ in ppm) 173.04, 157.82, 156.57, 152.22, 144.34, 139.67, 133.70, 129.93, 122.66, 122.29, 121.24, 121.21, 114.92, 73.84, 67.87, 56.69, 56.13, 50.02, 42.31, 39.73, 39.53, 38.18, 37.01, 36.60, 36.20, 35.82, 34.59, 31.92, 31.86, 29.06, 28.26, 28.03, 27.84, 25.68, 24.85, 24.30, 23.85, 22.86, 22.60, 21.05, 19.35, 18.74, 11.88.

FTIR (cm^{-1}) 2936.1, 2866.6, 2851.4, 1732.8, 1626.5, 1602.5, 1574.1, 1506.6, 1467.5, 1378.15, 1258.5, 1208.5, 1173.6, 1106.1, 1014.6, 958.3, 883.7, 844.1, 746.9, 603.9, 569.7, 542.1.

P-6: Yield = 35 %, UV-vis (absorbance in nm): 273, 338, Fluorescence: 377, 407, 431. ^1H NMR (400 MHz, CDCl_3 , δ in ppm) 8.37 (s, 6H), 7.71 (d, $J = 8.5$ Hz, 12H), 7.10 (dd, $J = 27.3$, 8.6 Hz, 24H), 6.83 (d, $J = 8.9$ Hz, 12H), 5.37 (d, $J = 8.0$ Hz, 6H), 4.64 - 4.59 (m, 6H), 3.95 (t, $J = 6.5$ Hz, 12H), 2.31 (d, $J = 7.8$ Hz, 24H), 2.01 - 1.94 (m, 12H), 1.86 - 1.78 (m, 36H), 1.67 (t, $J = 7.6$ Hz, 12H), 1.57 - 1.47 (m, 48H), 1.44 - 1.41 (m, 12H), 1.36 - 1.32 (m, 18H), 1.26 - 1.23 (m, 6H), 1.16 - 1.07 (m, 48H), 1.01 (s, 24H), 0.98 (s, 6H), 0.91 (d, $J = 6.6$ Hz, 18H), 0.86 (dd, $J = 6.6$, 1.9 Hz, 36H), 0.67 (s, 18H).

^{13}C NMR (100 MHz, CDCl_3 , δ in ppm) 173.17, 157.88, 156.53, 152.28, 144.31, 139.84, 139.68, 131.45, 129.93, 122.65, 122.30, 121.22, 116.43, 115.64, 114.93, 73.78, 68.04, 56.69, 56.13, 50.02, 42.31, 39.73, 39.53, 38.18, 37.00, 36.60, 36.19, 35.82, 34.63, 31.92, 31.86, 29.20, 28.25, 28.04, 27.84, 25.82, 24.99, 24.30, 23.85, 22.86, 22.59, 21.04, 19.35, 18.73, 11.88.

FTIR (cm^{-1}) 2935.7, 2867.8, 2853.7, 1732.7, 1624.9, 1603.9, 1576.6, 1507.4, 1465.6, 1376.9, 1249.6, 1210.7, 1173.8, 1108.6, 1013.5, 965.7, 883.1, 794.8, 734.9, 607.9, 570.9, 546.3.

P-7: Yield = 37 %, UV-vis (absorbance in nm): 273, 338, Fluorescence: 377, 407, 431. ^1H NMR (400 MHz, CDCl_3 , δ in ppm) 8.37 (s, 6H), 7.71 (d, $J = 8.5$ Hz, 12H), 7.10 (dd, $J = 26.3$, 8.6 Hz, 24H), 6.83 (d, $J = 8.9$ Hz, 12H), 5.37 (d, $J = 8.0$ Hz, 6H), 4.65 – 4.59 (m, 6H), 3.95 (t, $J = 6.6$ Hz, 12H), 2.32 – 2.27 (m, 24H), 2.02 – 1.93 (m, 12H), 1.83 (ddd, $J = 24.2$, 12.6, 5.1 Hz, 36H), 1.64 (t, $J = 7.2$ Hz, 18H), 1.52 – 1.44 (m, 36H), 1.43 (d, $J = 4.8$ Hz, 6H), 1.40 – 1.31 (m, 48H), 1.25 (d, $J = 9.8$ Hz, 6H), 1.17 – 1.04 (m, 48H), 1.01 (s, 24H), 0.91 (d, $J = 6.6$ Hz, 18H), 0.86 (dd, $J = 6.6$, 1.9 Hz, 36H), 0.67 (s, 18H).

^{13}C NMR (100 MHz, CDCl_3 , δ in ppm) 173.20, 157.91, 139.71, 129.91, 122.62, 122.27, 121.22, 114.95, 73.74, 68.15, 56.70, 56.15, 50.04, 42.32, 39.74, 39.53, 38.19, 37.02, 36.61, 36.20, 35.81, 34.67, 31.87, 29.32, 29.08, 28.24, 28.02, 27.84, 25.95, 25.00, 24.29, 23.85, 22.83, 22.58, 21.05, 19.34, 18.73, 11.87.

FTIR (cm^{-1}) 2934.8, 2866.4, 2852.2, 1732.5, 1625.1, 1604.6, 1577.8, 1507.6, 1467.9, 1377.2, 1249.9, 1207.5, 1173.8, 1107, 1012.7, 960.5, 881.5, 841.8, 796.9, 764.1, 749.7, 607, 545.5.

P-8: Yield = 40 %, UV-vis (absorbance in nm): 273, 338, Fluorescence: 377, 407, 431. ^1H NMR (400 MHz, CDCl_3 , δ in ppm) 8.37 (s, 6H), 7.71 (d, $J = 8.4$ Hz, 12H), 7.10 (dd, $J = 26.9$, 8.6 Hz, 24H), 6.83 (d, $J = 8.9$ Hz, 12H), 5.37 (d, $J = 8.0$ Hz, 6H), 4.63 – 4.59 (m, 6H), 3.95 (t, $J = 6.5$ Hz, 12H), 2.29 (q, $J = 6.8$, 5.3 Hz, 24H), 2.02 – 1.95 (m, 12H), 1.84 (ddd, $J = 18.5$, 11.0, 5.3 Hz, 36H), 1.65 – 1.59 (m, 18H), 1.56 (d, $J = 3.2$ Hz, 6H), 1.53 (d, $J = 3.0$ Hz, 6H), 1.52 – 1.45 (m, 36H), 1.43 (d, $J = 4.5$ Hz, 6H), 1.37 – 1.32 (m, 54H), 1.27 – 1.23 (m, 6H), 1.16 – 1.07 (m, 42H), 1.02 (s, 24H), 0.91 (d, $J = 6.4$ Hz, 18H), 0.87 – 0.85 (m, 36H), 0.67 (d, $J = 1.9$ Hz, 18H).

^{13}C NMR (100 MHz, CDCl_3 , δ in ppm) 173.28, 157.93, 156.50, 144.26, 139.70, 133.72, 131.45, 129.93, 122.63, 122.29, 121.23, 116.44, 115.64, 115.00, 114.93, 73.73, 68.63, 68.19, 56.69, 56.26, 56.13, 50.02, 42.32, 39.73, 39.53, 38.18, 37.01, 36.61, 36.19, 35.82, 34.71, 31.92,

31.86, 29.37, 29.31, 29.26, 29.22, 29.10, 28.26, 28.04, 27.84, 26.07, 25.06, 24.31, 23.85, 22.86, 22.60, 21.05, 19.35, 18.74, 11.88.

FTIR (cm^{-1}) 2933, 2867.6, 2852.5, 1733.8, 1624.6, 1603.9, 1578.1, 1507, 1467.2, 1377.3, 1275.3, 1259.7, 1211.3, 1175, 1109.2, 1101.2, 964.4, 881.5, 841.2, 794.5, 750.3, 609.4, 546.9.

P-10: Yield = 36 %, UV-vis (absorbance in nm): 273, 338, Fluorescence: 377, 407, 431. ^1H NMR (400 MHz, CDCl_3 , δ in ppm) 8.37 (s, 6H), 7.71 (d, $J = 8.6$ Hz, 12H), 7.09 (dd, $J = 25.9$, 8.6 Hz, 24H), 6.83 (d, $J = 8.9$ Hz, 12H), 5.37 (d, $J = 5.0$ Hz, 6H), 4.64 - 4.58 (m, 6H), 3.95 (t, $J = 6.6$ Hz, 12H), 2.32 - 2.25 (m, 24H), 2.02 - 1.94 (m, 12H), 1.88 - 1.75 (m, 36H), 1.62 - 1.60 (m, 12H), 1.57 - 1.53 (m, 12H), 1.50 - 1.42 (m, 42H), 1.31 (d, $J = 2.9$ Hz, 78H), 1.25 (d, $J = 7.6$ Hz, 6H), 1.16 - 1.07 (m, 36H), 1.02 (s, 24H), 0.96 (dd, $J = 13.5$, 3.6 Hz, 12H), 0.91 (d, $J = 6.5$ Hz, 18H), 0.86 (dd, $J = 6.6$, 1.9 Hz, 36H), 0.67 (s, 18H).

^{13}C NMR (100 MHz, CDCl_3 , δ in ppm) 173.33, 157.94, 156.51, 152.22, 144.26, 139.72, 133.72, 129.92, 122.62, 122.29, 121.23, 116.43, 115.00, 114.93, 73.70, 68.24, 56.69, 56.13, 50.01, 42.31, 39.73, 39.53, 38.18, 37.01, 36.61, 36.19, 35.82, 34.73, 31.92, 31.86, 29.57, 29.46, 29.41, 29.31, 29.16, 28.25, 28.04, 27.83, 26.13, 25.08, 24.30, 23.85, 22.86, 22.59, 21.04, 19.35, 18.73, 11.88.

FTIR (cm^{-1}) 2932.2, 2869.4, 2852.4, 1733.3, 1625.6, 1604.4, 1577.1, 1507.3, 1467.1, 1376.37, 1275, 1260.3, 1207.5, 1173.6, 1108.1, 1015.7, 964.5, 880.6, 842, 765.1, 749.4, 605.4, 547.1.

P-11: Yield = 36 %, UV-vis (absorbance in nm): 273, 338, Fluorescence: 377, 407, 431. ^1H NMR (400 MHz, CDCl_3 , δ in ppm) 8.37 (s, 6H), 7.71 (d, $J = 8.7$ Hz, 12H), 7.09 (dd, $J = 25.5$, 8.6 Hz, 24H), 6.82 (d, $J = 8.9$ Hz, 12H), 5.37 (d, $J = 5.0$ Hz, 6H), 4.62 - 4.58 (m, 6H), 3.94 (t, $J = 6.7$ Hz, 12H), 2.32 - 2.25 (m, 24H), 2.02 - 1.94 (m, 12H), 1.86 - 1.76 (m, 36H), 1.61 (s, 12H), 1.56 (t, $J = 2.4$ Hz, 6H), 1.51 - 1.42 (m, 42H), 1.30 (d, $J = 3.8$ Hz, 90H), 1.17 - 1.06 (m, 48H), 1.01 (s, 24H), 0.98 - 0.96 (m, 6H), 0.94 (d, $J = 5.5$ Hz, 6H), 0.91 (d, $J = 6.6$ Hz, 18H), 0.86 (dd, $J = 6.6$, 1.9 Hz, 36H), 0.67 (s, 18H).

^{13}C NMR (100 MHz, CDCl_3 , δ in ppm) 173.35, 157.95, 139.72, 129.93, 122.61, 122.29, 121.21, 116.43, 115.65, 115.00, 114.93, 73.70, 68.24, 56.69, 56.13, 50.02, 42.31, 39.73, 39.53, 38.18, 37.01, 36.61, 36.19, 35.82, 34.74, 31.92, 31.86, 29.61, 29.51, 29.32, 29.16, 28.25, 28.04, 27.83, 25.09, 24.30, 23.85, 22.85, 22.59, 21.04, 19.35, 18.73, 11.87.

FTIR (cm⁻¹) 2930.2, 2867.4, 2851.2, 1732.7, 1624.7, 1603.6, 1576.5, 1507.4, 1466.8, 1376.71, 1250.9, 1172.2, 1033.8, 1016.4, 969.6, 883.6, 842.1, 795.6, 749.3, 606.6, 570.4, 546.5.

2.5 UV-visible and fluorescence measurement

The photophysical behaviour of phosphazene based mesogens has been investigated by UV-vis spectroscopy. The absorption spectra have been recorded in the 10⁻⁵ M THF solution for all the compounds at room temperature as shown in Figure A19(a-f). All the compounds show a strong absorption band around 273 nm, which corresponds to π - π^* transition due to phosphazene and benzene, and a lower peak around 338 nm, which indicates the n- π^* transition due to nitrogen and oxygen atoms of the molecule.⁵⁵ The fluorescence spectra have also been recorded in the 10⁻⁵ M THF ($\lambda_{\text{max}} = 338$ nm) solution for all the compounds at room temperature, as shown in Figure A20(a-f).

2.6 Author Contributions

SR and SKP conceptualised the project. SR performed all the experiments and analysed the data. VP helped in the SAXS/WAXS experiments and SPG analysed the SAXS/WAXS data. CVY and MBK performed and analysed the chiro-optical measurements. SKP, CVY did the overall project administration, reviewed, edited, and finalized the chapter. All authors have given approval to the final version of the chapter.

2.7 Acknowledgements

SR and VP thank CSIR for fellowship with file no (09/947(0091)/2017-EMR-I) and (09/947(0253)/2020-EMR-I), respectively. SKP acknowledges project file no. CRG/2019/000901/OC from DST-SERB project. We are thankful to IISER Mohali for central and departmental facilities.

References

1. Allcock, H. R. *Phosphorus-Nitrogen Compounds*, Academic Press, New York, **1972**.
2. Allcock, H. R. Recent Advances in Phosphazene (Phosphonitrilic) Chemistry. *Chem. Rev.* **1972**, 72, 315-356.
3. Allen, C. W. Regio- and Stereochemical control in Substitution Reactions of Cyclophosphazenes. *Chem. Rev.* **1991**, 91, 119–135.

4. Uslu, A.; Yeşilot, S. Chiral configuration in cyclophosphazene chemistry. *Coord. Chem. Rev.* **2015**, *291*, 28-67.
5. Yeşilot, S.; Uslu, A. Stereochemical Aspects of Polyphosphazenes. *Polym. Rev.* **2017**, *57*, 213-247.
6. Bowers, D. J.; Wright, B. D.; Scionti, V.; Schultz, A.; Panzner, M. J.; Twum, E. B.; Li, L. L.; Katzenmeyer, B. C.; Thome, B. S.; Rinaldi, P. L.; Wesdemiotis, C.; Youngs, W. J.; Tessier, C. A. Structure and Conformation of the Medium-Sized Chlorophosphazene Rings. *Inorg. Chem.* **2014**, *53*, 8874-8886.
7. Uslu, A.; Yeşilot, S. Recent advances in the supramolecular assembly of cyclophosphazene derivatives. *Dalton Trans.* **2021**, *50*, 2324-2341.
8. (a) Karpus, A.; Mignani, S.; Zablocka, M.; Majoral, J. P. Crown Macromolecular Derivatives: Stepwise Design of New Types of Polyfunctionalized Phosphorus Dendrimers. *J. Org. Chem.* **2022**, *87*, 3433-3441; (b) Jiménez, J.; Laguna, A.; Gascón, E.; Sanz, J. A.; Serrano, J. L.; Barberá, J.; Oriol, L. New Liquid Crystalline Materials Based on Two Generations of Dendronised Cyclophosphazenes. *Chem. Eur. J.* **2012**, *18*, 16801-16814.
9. Schneider, R.; Köllner, C.; Weber, I.; Togni, A. Dendrimers based on cyclophosphazene units and containing chiral ferrocenyl ligands for asymmetric catalysis. *Chem. Commun.* **1999**, 2415-2416.
10. Caminade, A. M.; Turrin, C. O.; Majoral, J. P. Biological properties of phosphorus dendrimers. *New J. Chem.* **2010**, *34*, 1512-1524.
11. Milowska, K.; Gabryelak, T.; Bryszewska, M.; Caminade, A. M.; Majoral, J. P. Phosphorus-containing dendrimers against α -synuclein fibril formation. *International Journal of Biological Macromolecules* **2012**, *50*, 1138-1143.
12. Marmillon, C.; Gauffre, F.; Krzywicki, T. G.; Loup, C.; Caminade, A. M.; Majoral, J. P.; Vors, J. P.; Rump, E. Organophosphorus Dendrimers as New Gelators for Hydrogels. *Angew. Chem.* **2001**, *40*, 2696-2699.
13. Caminade, A. M.; Majoral, J. P. Nanomaterials Based on Phosphorus Dendrimers. *Acc. Chem. Res.* **2004**, *37*, 6, 341-348.

14. Ciepluch, K.; Katir, N.; Kadib, A. E.; Weber, M.; Caminade, A. M.; Bousmina, M.; Majoral, J. P.; Bryszewska, M. Photo-physical and structural interactions between viologen phosphorus-based dendrimers and human serum albumin. *Journal of Luminescence* **2012**, *132*, 1553-1563.
15. Usri, S. N. K.; Jamain, Z.; Makmud, M. Z. H.; A Review on Synthesis, Structural, Flame Retardancy and Dielectric Properties of Hexasubstituted Cyclotriphosphazene. *Polymers* **2021**, *13*, 2916.
16. Zhao, B.; Liang, W. J.; Wang, J. S.; Li, F.; Liu, Y. Q. Synthesis of a novel bridged-cyclotriphosphazene flame retardant and its application in epoxy resin. *Polym. Degrad. Stab.* **2016**, *133*, 162-173.
17. Levchik, G. F.; Grigoriev, Y. V.; Balabanovich, A. I.; Levchik, S. V.; Klatt, M. Phosphorus–nitrogen containing fire retardants for poly(butylene terephthalate). *Polym. Int.* **2000**, *49*, 1095-1100.
18. Moriya, K.; Suzuki, T.; Kawanishi, Y.; Masuda, T.; Mizusaki, H.; Nakagawa, S.; Ikematsu, H.; Mizuno, K.; Yano, S.; Kajiwara, M. Liquid-Crystalline Phase Transition in Organophosphazenes. *Appl. Organomet. Chem.* **1998**, *12*, 771-779.
19. Moriya, K.; Yano, S.; Kajiwara, M. Liquid Crystalline State in Hexakis[4-(4-cyano)biphenoxy]- and Hexakis[4-(phenylazo)phenoxy]cyclotriphosphazenes. *Chem. Lett.* **1990**, *19*, 1039-1042.
20. Moriya, K.; Mizusaki, H.; Kato, M.; Yano, Y.; Kajiwara, M. Liquid crystalline phase transitions in hexakis(4-(4'-heptyloxy)biphenoxy)cyclotriphosphazene. *Liq. Cryst.* **1995**, *18*, 795-800.
21. Levelut, A. M.; Moriya, K.; Structure of the liquid crystalline state in hexakis (4-(4'-alkyloxy)biphenoxy)cyclotriphosphazenes. *Liq. Cryst.* **1996**, *20*, 119-124.
22. Moriya, K.; Suzuki, T.; Mizusaki, H.; Yano, S.; Kajiwara, M. Liquid Crystalline Phase Transition in Organophosphazenes with 4-Octyloxybiphenyl Mesogenic Groups. *Chem. Lett.* **1997**, *26*, 1001-1002.
23. Moriya, K.; Mizusaki, H.; Kato, M.; Suzuki, T.; Yano, S.; Kajiwara, M.; Tashiro, K. Thermal and Structural Study on Liquid-Crystalline Phase Transition in Hexakis(4-(4'-alkyloxy)biphenoxy)cyclotriphosphazene. *Chem. Mater.* **1997**, *9*, 255-263.

-
24. Moriya, K.; Suzuki, T.; Yano, Y.; Kajiwara, M. Liquid crystalline phase transitions in cyclotriphosphazenes with different mesogenic moieties in the side chains. *Liq. Cryst.* **1995**, *19*, 711-713.
25. Moriya, K.; Nakagawa, S.; Yano, S.; Kajiwara, M. Ferroelectric liquid crystalline phase transition of (S)-hexakis(4-(4'-(6-methyloctyloxy)biphenoxy) cyclotriphosphazene. *Liq. Cryst.* **1995**, *18*, 919-921.
26. Moriya, K.; Kawanishi, Y.; Yano, S.; Kajiwara, M. Mesomorphic phase transition of a cyclotetraphosphazene containing Schiff base moieties: comparison with the corresponding cyclotriphosphazene. *Chem. Commun.* **2000**, *13*, 1111-1112.
27. Moriya, K.; Ikematsu, H.; Nakagawa, S.; Yano, S.; Negita, K. Dielectric Properties of Ferroelectric Liquid Crystal Hexakis(4-(4'-(s)-6-methyloctyloxy)cyclophosphazene. *Jpn. J. Appl. Phys.* **2001**, *40*, 340-342.
28. Moriya, K.; Yamane, T.; Suzuki, T.; Masuda, T.; Mizusaki, H.; Yano, S.; Kajiwara, M. Mesogenicity of Organophosphazenes: The Effect of Phosphazene Rings and Side Groups on the Phase Transition. *Relat. Elem.* **2010**, *177*, 1427-1432.
29. Moriya, K.; Masuda, T.; Suzuki, T.; Yano, S.; Kajiwara, M. Liquid Crystalline Phase Transition in Hexakis(4-(N-(41-alkoxyphenyl)iminomethyl)phenoxy)cyclotriphosphazene. *Mol. Cryst. Liq. Cryst.* **2006**, *318*, 267-277.
30. Jiménez, J.; Callizo, L.; Serrano, J. L.; Barbera, J.; Oriol, L. Mixed-Substituent Cyclophosphazenes with Calamitic and Polycatenar Mesogens. *Inorg. Chem.* **2017**, *56*, 7907-7921.
31. De, J.; Gupta, S. P.; Bala, I.; Kumar, S.; Pal, S. K. Phase Behavior of a New Class of Anthraquinone-Based Discotic Liquid Crystals. *Langmuir* **2017**, *33*, 13849-13860.
32. Bala, I.; Singh, N.; Yadav, R. A. K.; De, J.; Gupta, S. P.; Singh, D. P.; Dubey, D. K.; Jou, J. H.; Douali, R.; Pal, S. K. Room temperature perylene based columnar liquid crystals as solid-state fluorescent emitters in solution-processable organic light-emitting diodes. *J. Mater. Chem. C* **2020**, *8*, 12485-12494.

33. Bala, I.; De, J.; Gupta, S. P.; Singh, H.; Pandey, U. K.; Pal, S. K. High hole mobility in room temperature discotic liquid crystalline tetrathienoanthracenes. *Chem. Commun.* **2020**, *56*, 5629-5632.
34. (a) De, J.; Bala, I.; Gupta, S. P.; Pandey, U. K.; Pal, S. K. High Hole Mobility and Efficient Ambipolar Charge Transport in Heterocoronene-Based Ordered Columnar Discotics. *J. Am. Chem. Soc.* **2019**, *141*, 18799-18805; (b) Metzroth, T.; Hoffmann, A.; Martín-Rapún, R.; Smulders, M. M.; Pieterse, K.; Palmans, A. R. A.; Vekemans, J. A. J. M.; Meijer, E. W.; Spiess, H. W.; Gauss, J. Unravelling the fine structure of stacked bipyridine diamine-derived C3-discotics as determined by X-ray diffraction, quantum-chemical calculations, Fast-MAS NMR and CD spectroscopy. *Chem. Sci.* **2011**, *2*, 69-76.
35. (a) Barberà, J.; Bardají, M.; Jiménez, J.; Laguna, A.; Martínez, M. P.; Oriol, L.; Serrano, J. L.; Zaragoza, I.; Columnar Mesomorphic Organizations in Cyclotriphosphazenes. *J. Am. Chem. Soc.* **2005**, *127*, 8994-9002; (b) Barberà, J.; Jiménez, J.; Laguna, A.; Oriol, L.; Pérez, S.; Serrano, J. L. Cyclotriphosphazene as a Dendritic Core for the Preparation of Columnar Supermolecular Liquid Crystals. *Chem. Mater.* **2006**, *18*, 5437-5445.
36. Jimnez, J.; Laguna, A.; Molter, A. M.; Serrano, J. L.; Barber, J.; Oriol, L. Supermolecular Liquid Crystals with a Six-Armed Cyclotriphosphazene Core: From Columnar to Cubic Phases. *Chem. Eur. J.* **2011**, *17*, 1029-1039.
37. Hincapié, C. A.; Sebastián, R. M.; Barberá, J.; Serrano, J. L.; Sierra, T.; Majoral, J. P.; Caminade, A. M. Supermolecular Columnar Liquid-Crystalline Phosphorus Dendrimers Decorated with Sulfonamide Derivatives. *Chem. Euro. J.* **2015**, *20*, 17047-17058.
38. Li, L.; Sun, J.; Zhang, L. L.; Yao, R.; Yan, C. G. Crystal structure and fluorescence sensing properties of tetramethoxyresorcinarene functionalized Schiff bases. *J. Mol. Struct.* **2015**, *1081*, 355-361.
39. Özdemir, Ö. Novel symmetric diimine-Schiff bases and asymmetric triimine-Schiff bases as chemosensors for the detection of various metal ions. *J. Mol. Struct.* **2016**, *1125*, 260-271.
40. Reena, V.; Suganya, S.; Velmathi, S. Synthesis and anion binding studies of azo-Schiff bases: Selective colorimetric fluoride and acetate ion sensors. *J. Fluorine Chem.* **2013**, *153*, 89-95.

-
41. Xiea, Y. Z.; Shana, G. G.; Zhoua, Z. Y.; Sua, Z. M. Schiff-base as highly sensitive and reversible chemosensors for HCl gas. *Sensors and Actuators B* **2013**, *177*, 41-49.
42. Li, X. C.; Wang, C. Y.; Wan, Y.; Lai, W. Y.; Zhao, L.; Yin, M. F.; Huang, W. A T-shaped triazatruxene probe for the naked-eye detection of HCl gas with high sensitivity and selectivity. *Chem. Commun.* **2016**, *52*, 2748-2751.
43. Li, X.; Shao, T.; Shi, Q.; Hu, M. A diaryl Schiff base as a photo- and pH-responsive bifunctional molecule. *RSC Adv.* **2013**, *3*, 22877-22881.
44. Xu, N.; Wang, R. L.; Li, D. P.; Zhou, Z. Y.; Zhang, T.; Xie, Y. Z.; Su, Z. M. Continuous detection of HCl and NH₃ gases with a high-performance fluorescent polymer sensor. *New J. Chem.* **2018**, *42*, 13367-13374.
45. Cui, F. Z.; Xie, J. J.; Jiang, S. Y.; Gan, S. X.; Ma, D. L.; Liang, R. R.; Jiang, G. F.; Zhao, X. A gaseous hydrogen chloride chemosensor based on a 2D covalent organic framework. *Chem. Commun.* **2019**, *55*, 4550-4553.
46. Gupta, S. P.; Gupta, M.; Pal, S. K. Highly Resolved Morphology of Room-Temperature Columnar Liquid Crystals Derived from Triphenylene and Multialkynylbenzene Using Reconstructed Electron Density Maps. *Chemistry Select* **2017**, *2*, 6070-6077.
47. (a) Serrano, J. L.; Sierra, T. Switchable Columnar Metallomesogens. *Chem. Eur. J.* **2000**, *6*, 759-766; (b) L. Álvarez, J. Barbera', L. Puig, P. Romero, J. L. Serrano and T. Sierra, Supramolecular chirality of columnar mesophases consisting of H-bonded complexes of melamine and polycatenar benzoic acids. *J Mater. Chem.* **2006**, *16*, 3768-3773; (c) Yelamaggad, C. V.; Achalkumar, A. S.; Rao, D. S. S.; Prasad, S. K. The first examples of optically active tris(N-salicylideneaniline)s: manifestation of chirality from molecules to fluid columnar phases. *J. Mater. Chem.* **2007**, *17*, 4521-4529.
48. Gottarelli, G.; Lena, S.; Masiero, S.; Pieraccini, S.; Spada, G. P. The use of circular dichroism spectroscopy for studying the chiral molecular self-assembly: An overview. *Chirality* **2008**, *20*, 471-485; (b) Otani, T.; Araoka, F.; Ishikawa, K.; Takezoe, H. Enhanced Optical Activity by Achiral Rod-Like Molecules Nanosegregated in the B4 Structure of Achiral Bent-Core Molecules. *J. Am. Chem. Soc.* **2009**, *131*, 12368-12372; (c) Cseh, L.; Mang, X.; Zeng, X.; Liu, F.; Mehl, G. H.; Ungar, G.; Siligardi, G. Helically Twisted Chiral Arrays of Gold Nanoparticles Coated with a Cholesterol Mesogen. *J. Am. Chem. Soc.* **2015**, *137*, 12736-12739; (d) Yu, H.; Welch, C.; Qu, W.; Schubert, C. J.; Liu, F.; Siligardi, G.;

- Mehl, G. H. Chirality enhancement in macro-chiral liquid crystal nanoparticles. *Mater. Horiz.* **2020**, *7*, 3021-3027.
49. Trzaska, S. T.; Hsu, H. F.; Swager, T. M. Cooperative Chirality in Columnar Liquid Crystals: Studies of Fluxional Octahedral Metallomesogens. *J. Am. Chem. Soc.* **1999**, *121*, 4518-4519.
50. Spector, M. S.; Prasad, S. K.; Weslowski, B. T.; Kamien, R. D.; Selinger, J. V.; Ratna, B. R.; Shashidhar, R. Chiral twisting of a smectic-A liquid crystal. *Phys. Rev. E* **2000**, *61*, 3977-3983.
51. (a) Albano, G.; Pescitelli, G.; Bari, L. D. Chiroptical Properties in Thin Films of π -Conjugated Systems. *Chem. Rev.* **2020**, *18*, 10145-10243; (b) Pescitelli, G.; Gabriel, S.; Wang, Y.; Fleischhauer, J.; Woody, R. W.; Berova, N. Theoretical Analysis of the Porphyrin–Porphyrin Exciton Interaction in Circular Dichroism Spectra of Dimeric Tetraarylporphyrins. *J. Am. Chem. Soc.* **2003**, *125*, 7613-7628; (c) Hoeben, F. J. M.; Wolfs, M.; Zhang, J.; Feyter, S. D.; Leclère, P.; Schenning, A. P. H. J.; Meijer, E. W. Influence of Supramolecular Organization on Energy Transfer Properties in Chiral Oligo(p-phenylene vinylene) Porphyrin Assemblies. *J. Am. Chem. Soc.* **2007**, *129*, 9819-9828; (d) Harada, N.; Nakanishi, K. *Circular dichroic spectroscopy: exciton coupling in organic stereochemistry*, University Science Books: Mill Valley, CA, **1983**.
52. Wagalgave, S. M.; Padghan, S. D.; Burud, M. D.; Kobaisi, M. A.; La, D. D.; Bhosale, R. S.; Bhosale, S. V.; Bhosale, S. V. Supramolecular super-helix formation via self-assembly of naphthalene diimide functionalised with bile acid derivatives. *Scientific Reports* **2019**, *9*, 12825-12834.
53. Nailwal, Y.; Wonanke, A. D. D.; Addicoat, M. A.; Pal, S. K. A Dual-Function Highly Crystalline Covalent Organic Framework for HCl Sensing and Visible-Light Heterogeneous Photocatalysis. *Macromolecules* **2021**, *54*, 6595-6604.
54. Bhat, S. A.; Rao, D. S. S.; Prasad, S. K.; Yelamggad, C. V. Chiral plasmonic liquid crystal gold nanoparticles: self-assembly into a circular dichroism responsive helical lamellar superstructure. *Nanoscale Adv.* **2021**, *3*, 2269–2279.
55. Örum, S. M.; Demircioğlu, Y. S. Crosslinked Polyphosphazene Nanospheres with Anticancer Quercetin: Synthesis, Spectroscopic, Thermal Properties, and Controlled Drug Release. *Macromol. Res.* **2018**, *26*, 671-679.

Appendix I

Table A1. The observed C H N % for the final compounds.

Compound	Molecular Weight	Molecular Formula	Elemental Analysis (%)		
			Found (Theoretical)		
			C	H	N
P-5	4305.07	C ₂₇₆ H ₃₈₄ N ₉ O ₂₄ P ₃	76.54 (77)	9.3 (8.9)	3.2 (2.9)
P-6	4389.23	C ₂₈₂ H ₃₉₆ N ₉ O ₂₄ P ₃	77.1 (77.2)	9.6 (9.1)	2.8 (2.9)
P-7	4473.39	C ₂₈₈ H ₄₀₈ N ₉ O ₂₄ P ₃	76.9 (77.3)	9.5 (9.2)	2.8 (2.8)
P-8	4557.55	C ₂₉₄ H ₄₂₀ N ₉ O ₂₄ P ₃	77.3 (77.5)	9.5 (9.3)	2.8 (2.8)
P-10	4725.88	C ₃₀₆ H ₄₄₄ N ₉ O ₂₄ P ₃	77.3 (77.8)	9.7 (9.5)	2.6 (2.7)
P-11	4810.04	C ₃₁₂ H ₄₅₆ N ₉ O ₂₄ P ₃	77.5 (77.9)	9.7 (9.6)	2.7 (2.6)

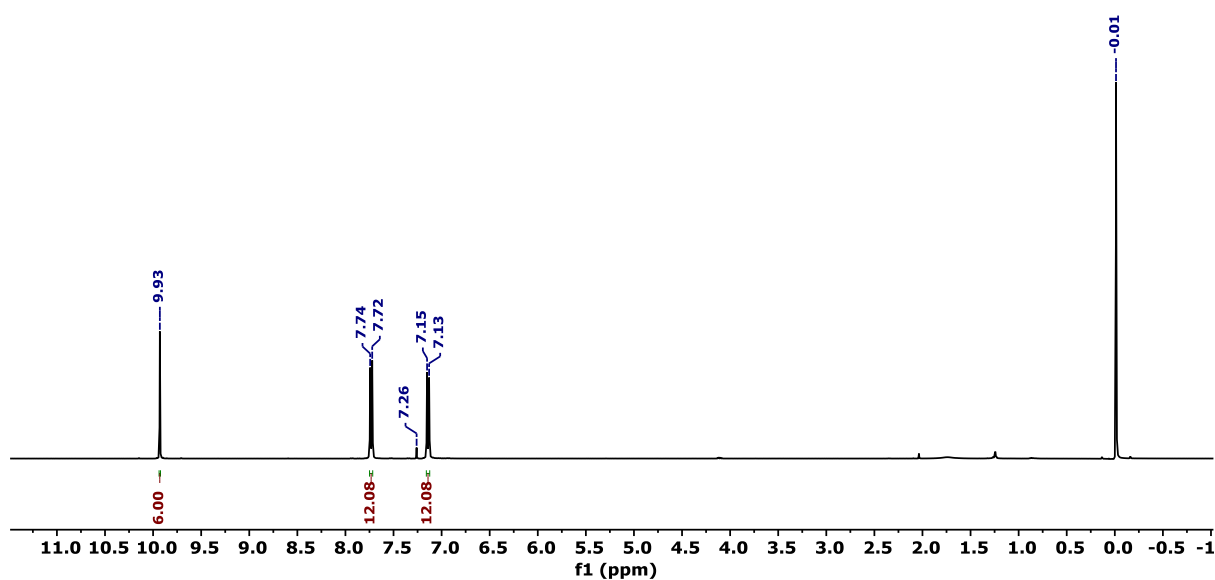


Figure A1 ¹H NMR spectrum of compound **1** in CDCl₃.

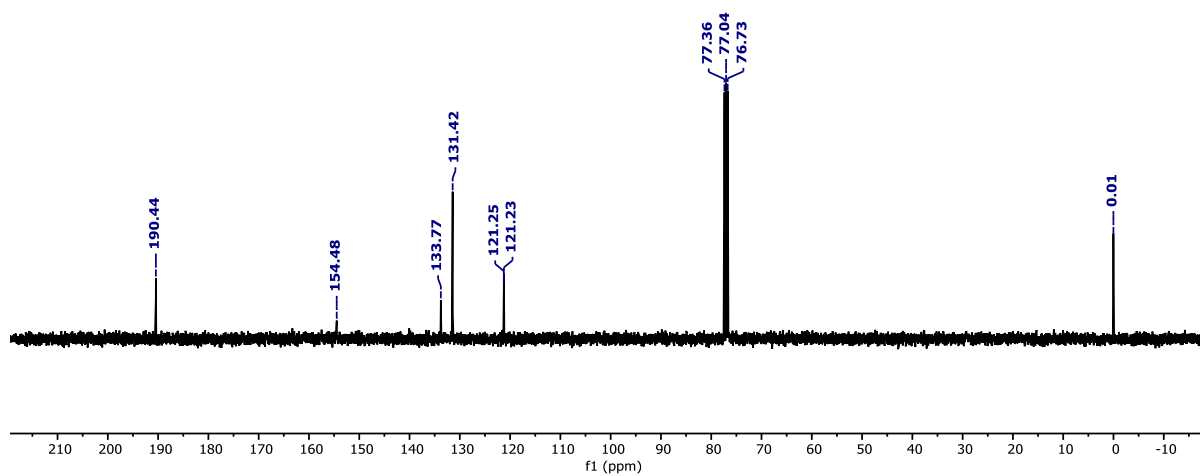
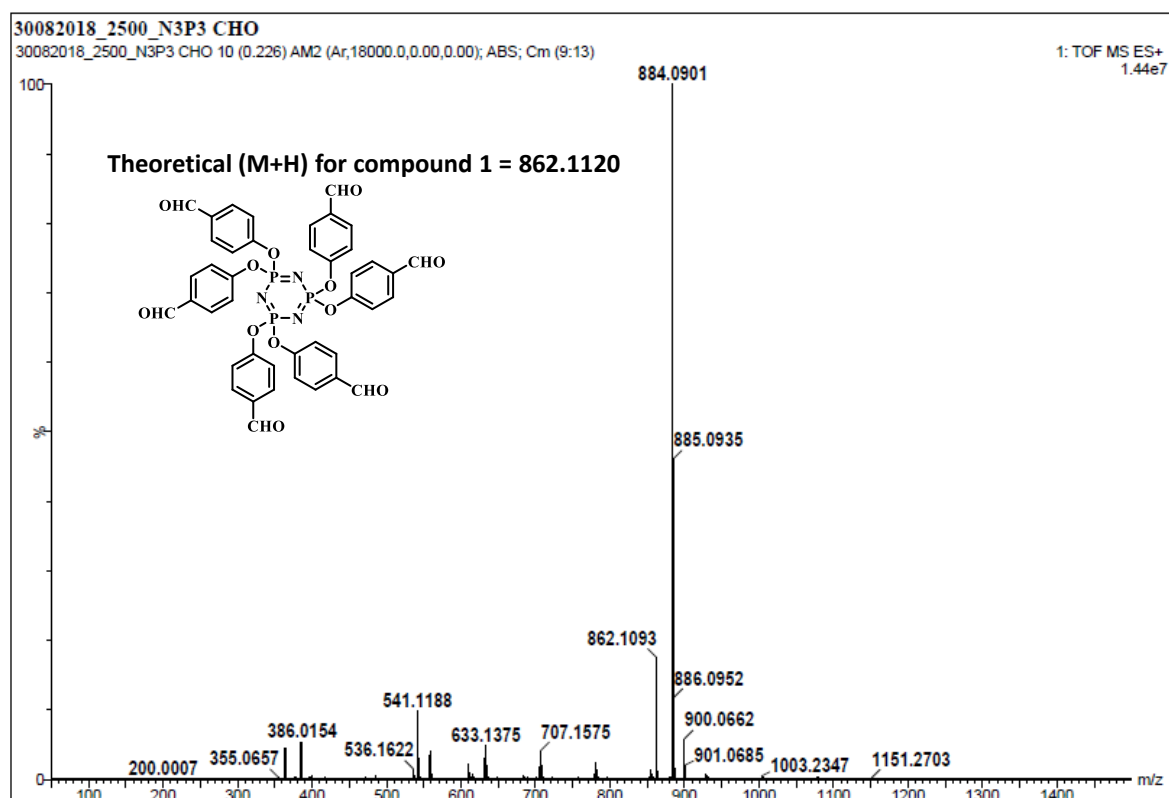
Figure A2 ^{13}C NMR spectrum of compound 1 in CDCl_3 .

Figure A3 HRMS spectrum of compound 1.

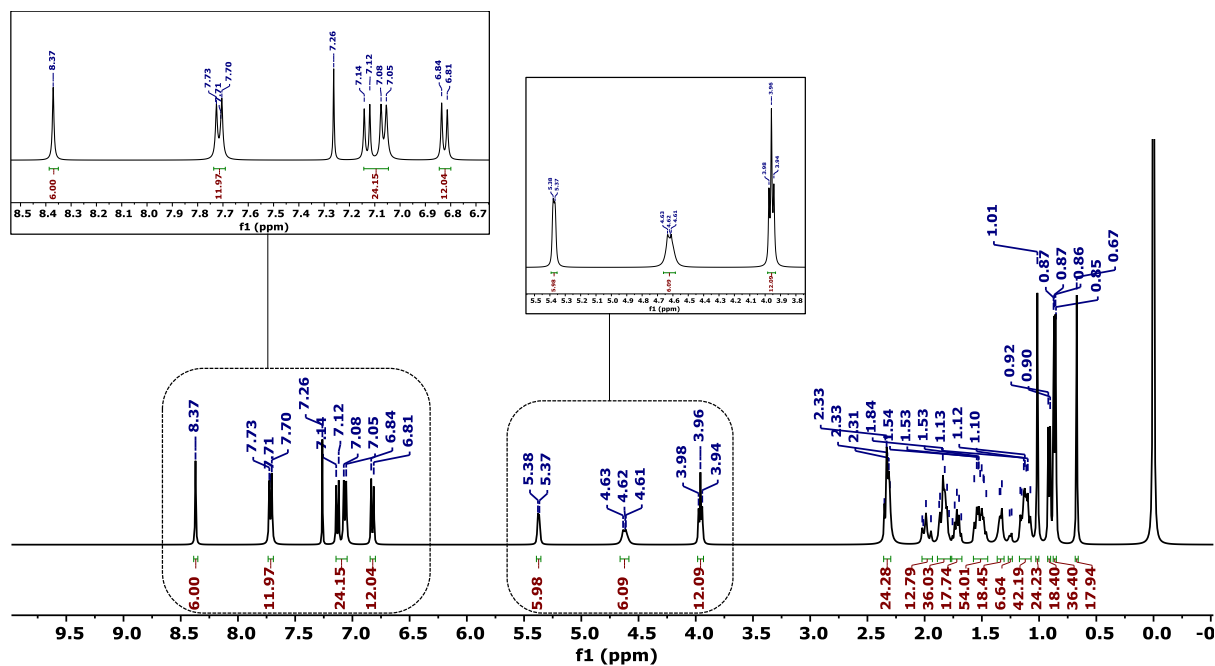


Figure A4 ^1H NMR spectrum of compound **P-5** in CDCl_3 .

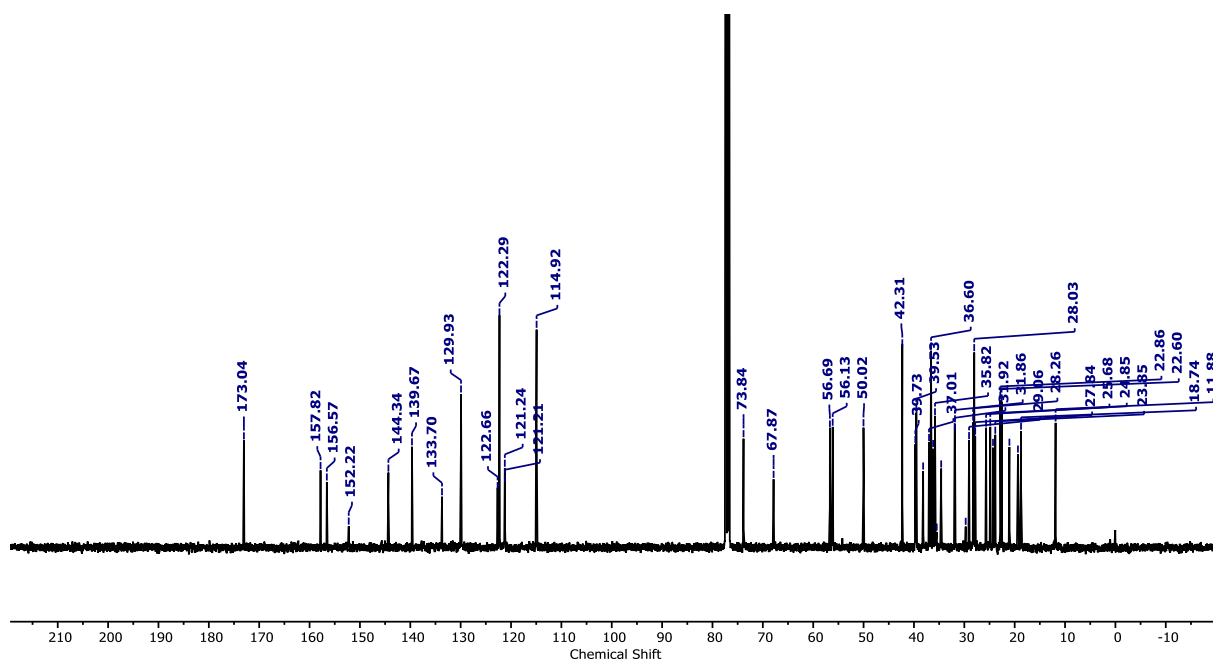
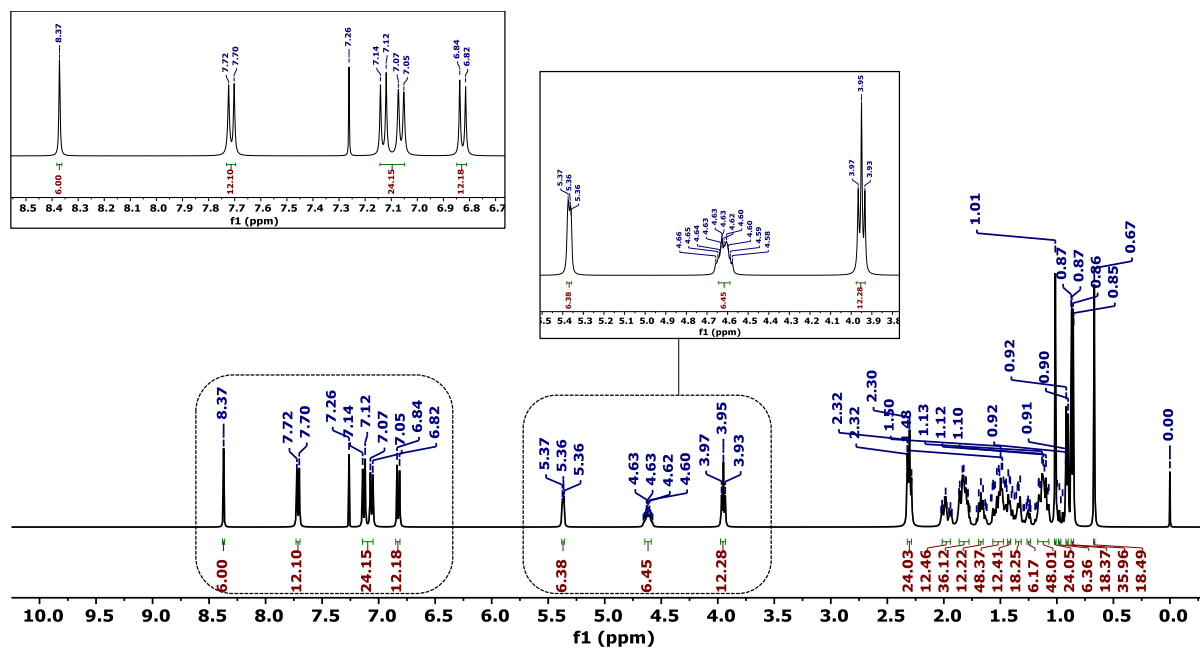
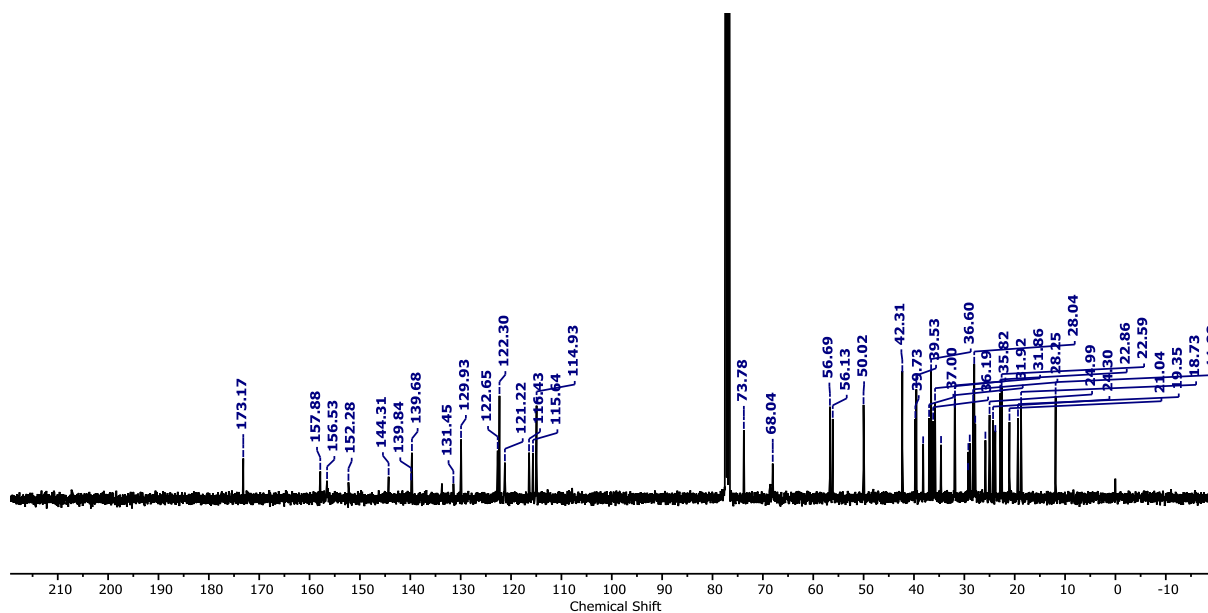


Figure A5 ^{13}C NMR spectrum of compound **P-5** in CDCl_3 .

Figure A6 ^1H NMR spectrum of compound P-6 in CDCl_3 .Figure A7 ^{13}C NMR spectrum of compound P-6 in CDCl_3 .

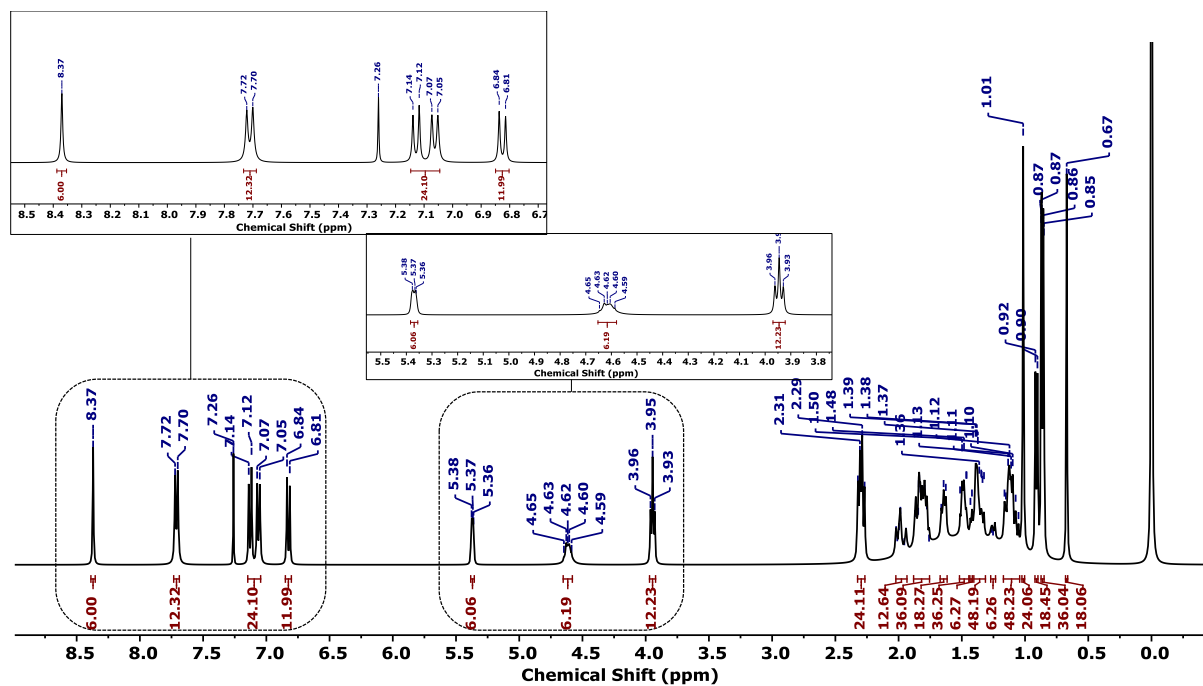


Figure A8 ^1H NMR spectrum of compound **P-7** in CDCl_3 .

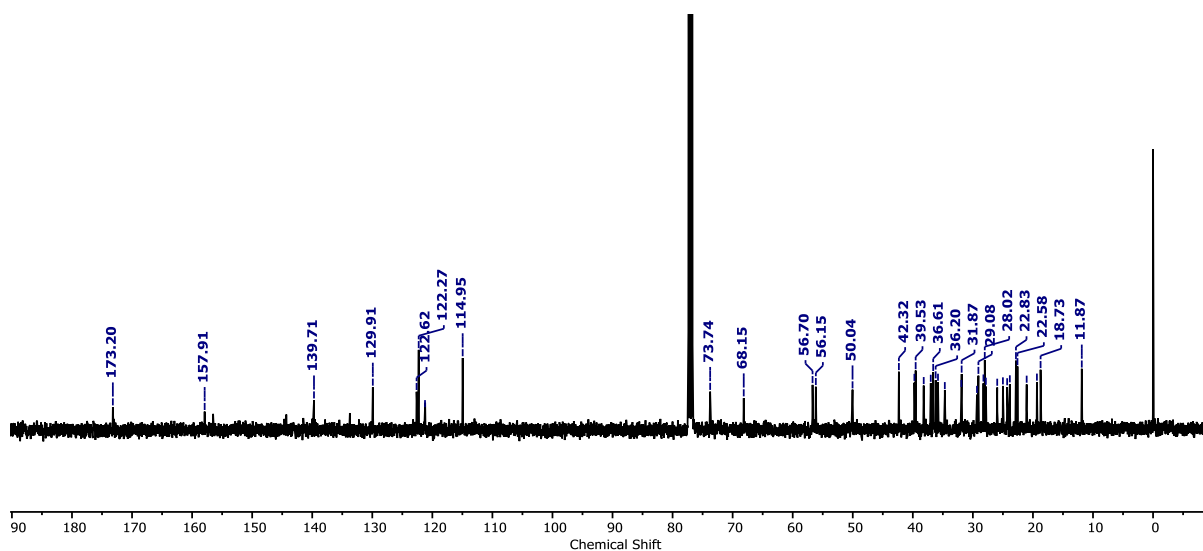


Figure A9 ^{13}C NMR spectrum of compound **P-7** in CDCl_3 .

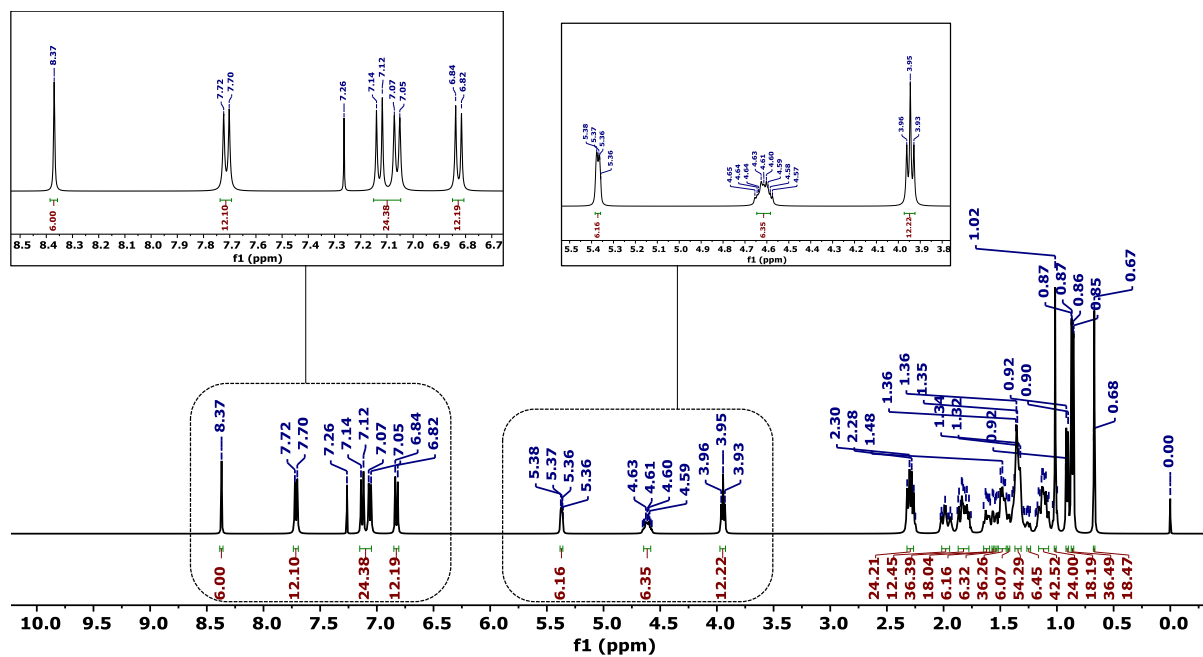


Figure A10 ^1H NMR spectrum of compound **P-8** in CDCl_3 .

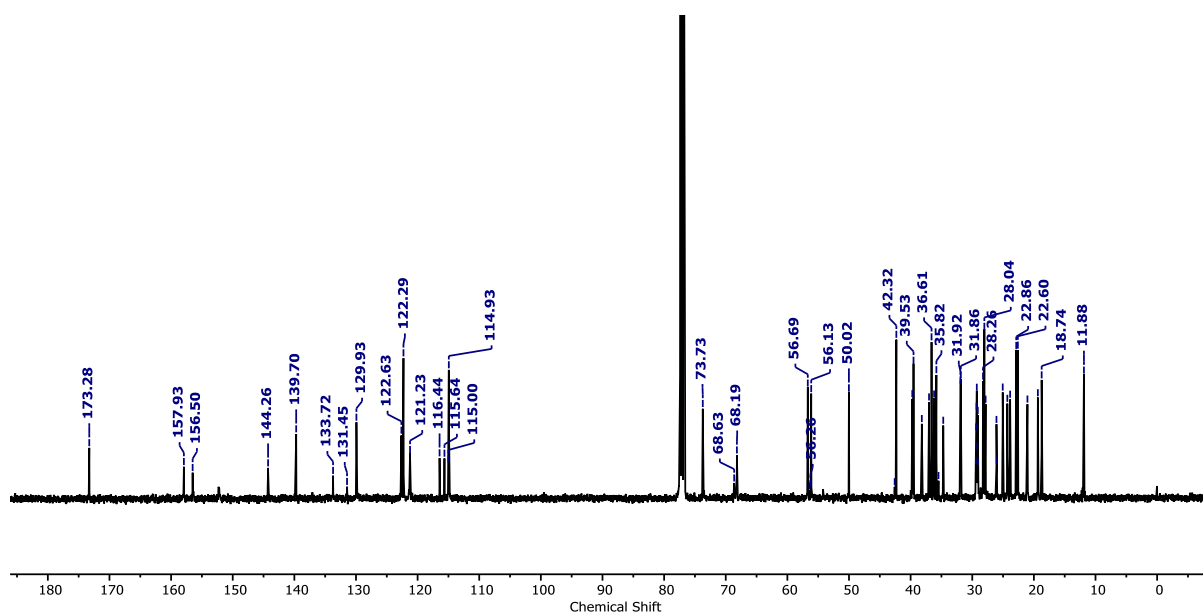


Figure A11 ^{13}C NMR spectrum of compound **P-8** in CDCl_3 .

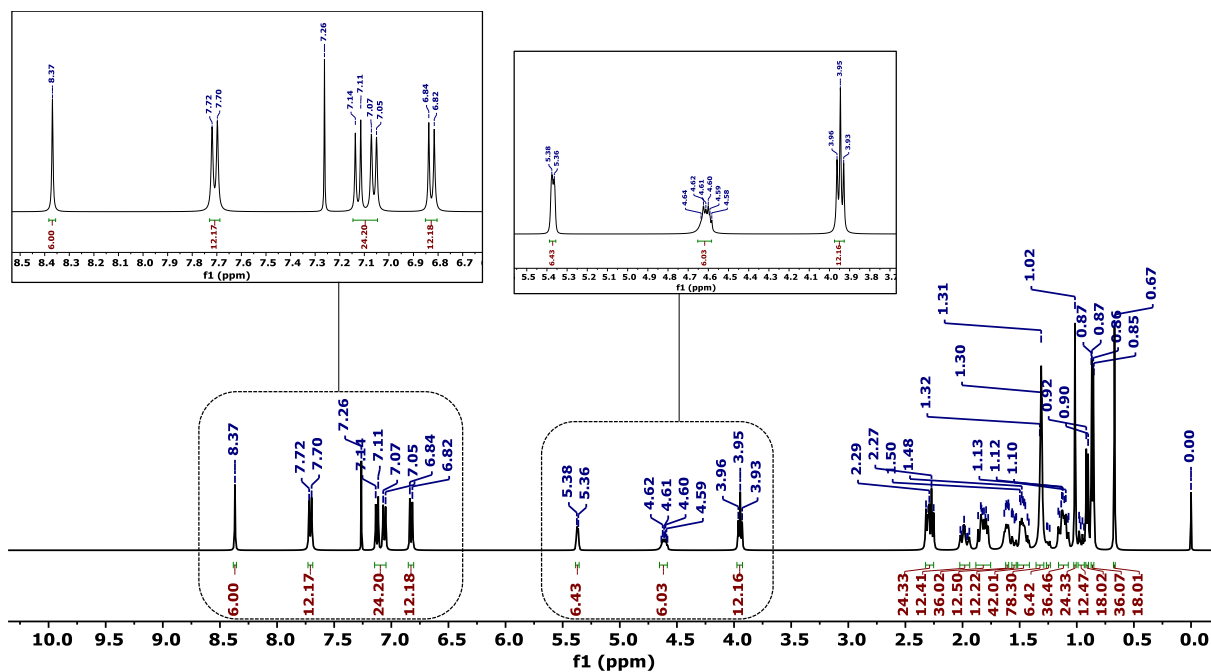


Figure A12 ^1H NMR spectrum of compound **P-10** in CDCl_3 .

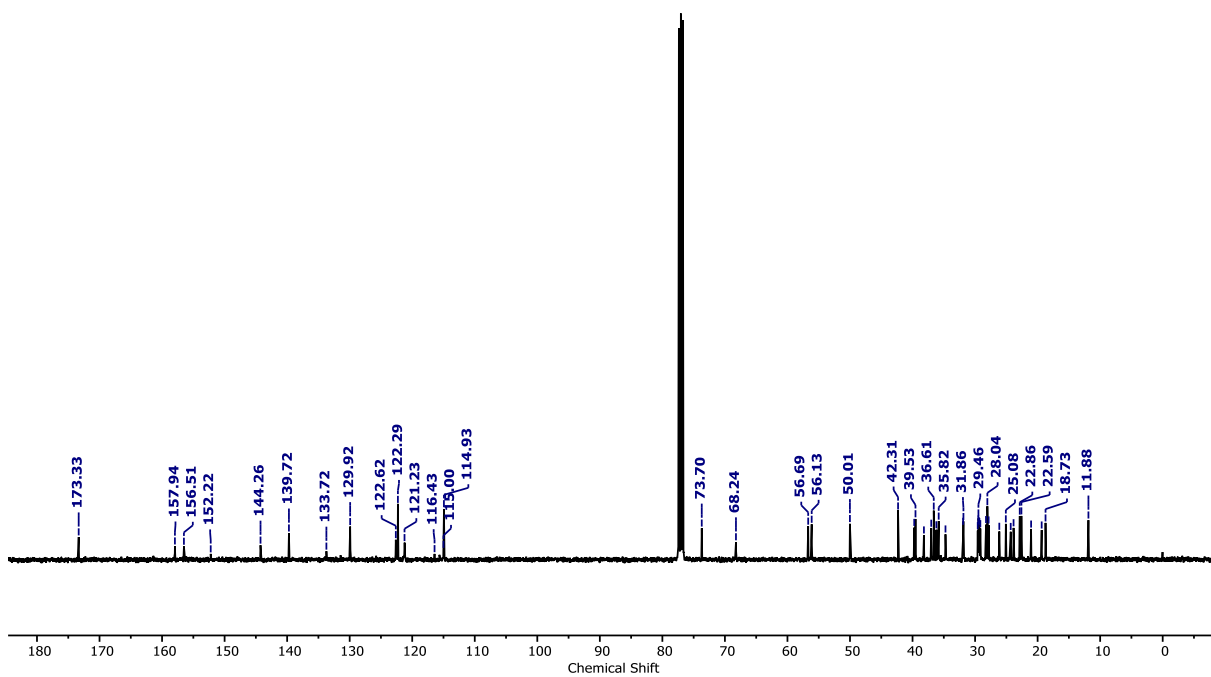


Figure A13 ^{13}C NMR spectrum of compound **P-10** in CDCl_3 .

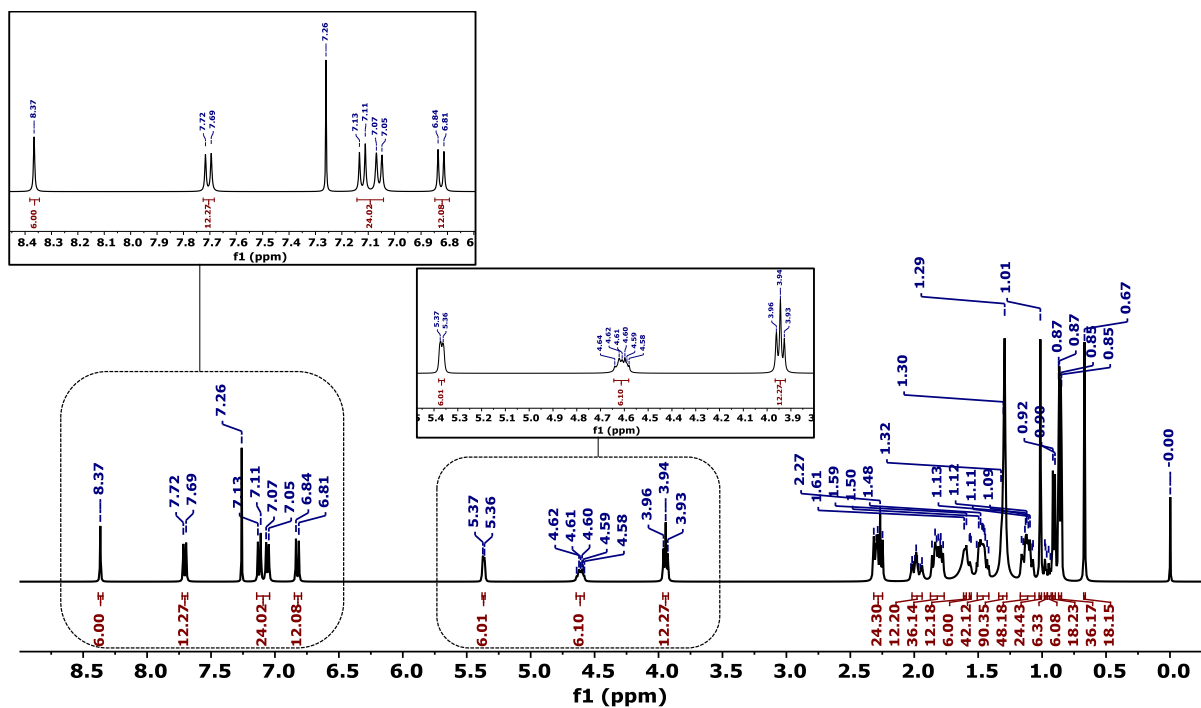


Figure A14 ^1H NMR spectrum of compound **P-11** in CDCl_3 .

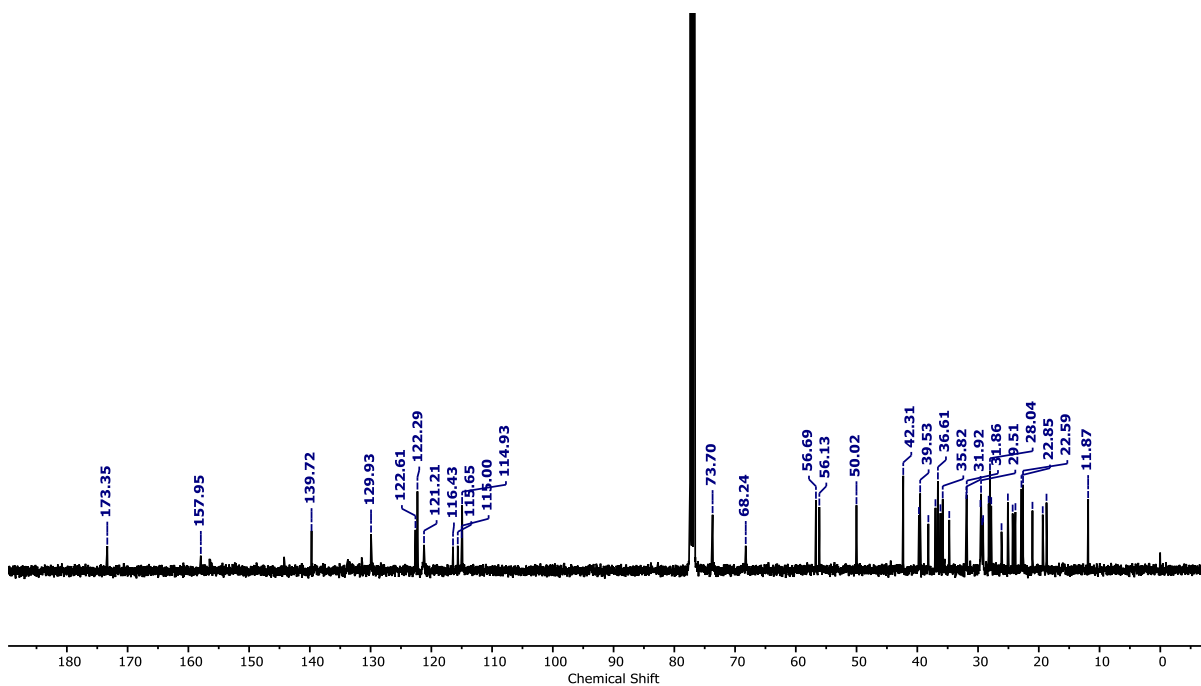


Figure A15 ^{13}C NMR spectrum of compound **P-11** in CDCl_3 .

TGA Curves:

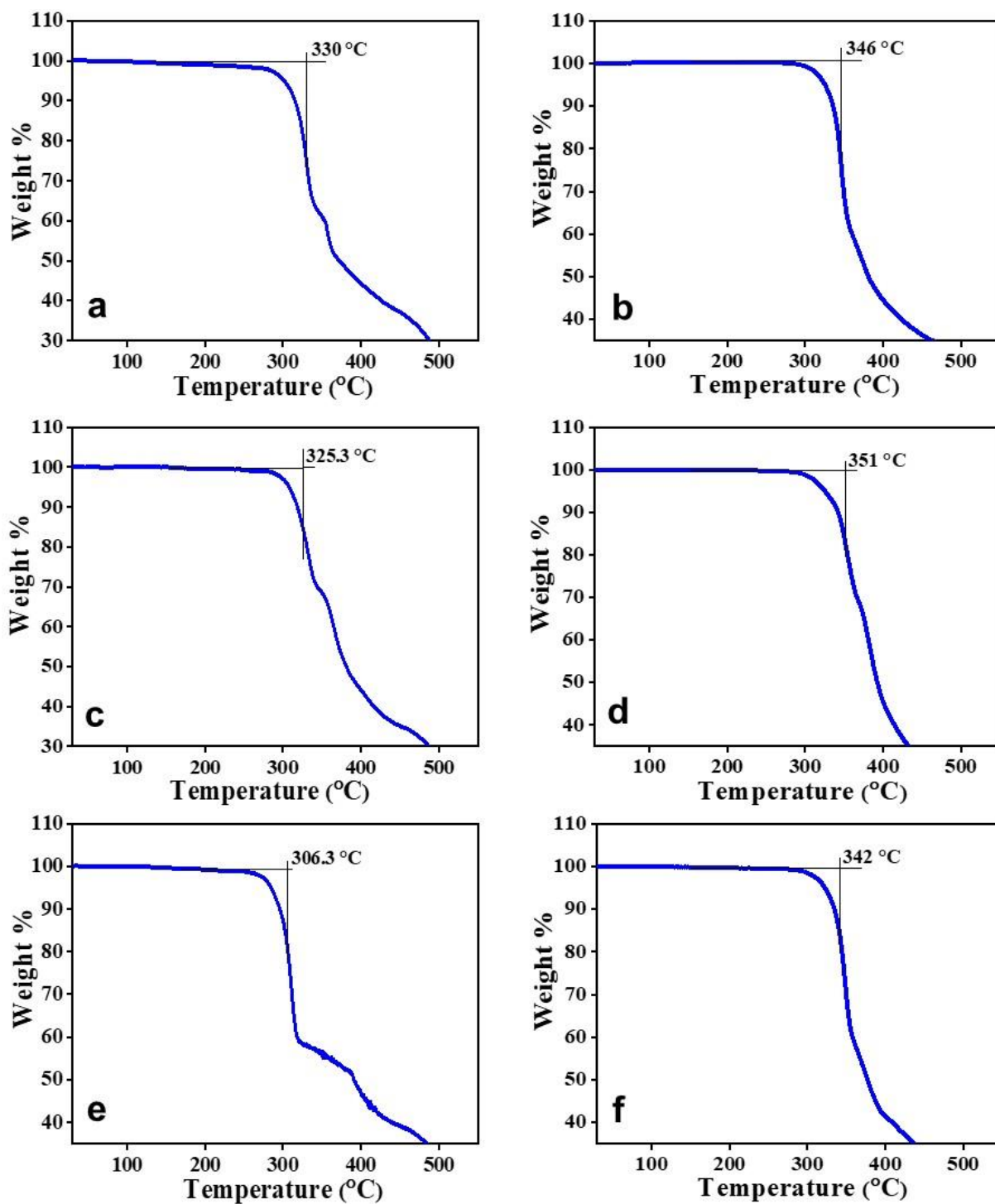


Figure A16 TGA thermographs of compounds (a) P-5, (b) P-6, (c) P-7, (d) P-8, (e) P-10, (f) P-11, obtained at a rate of 5 °C/min.

X-Ray Diffraction Studies:

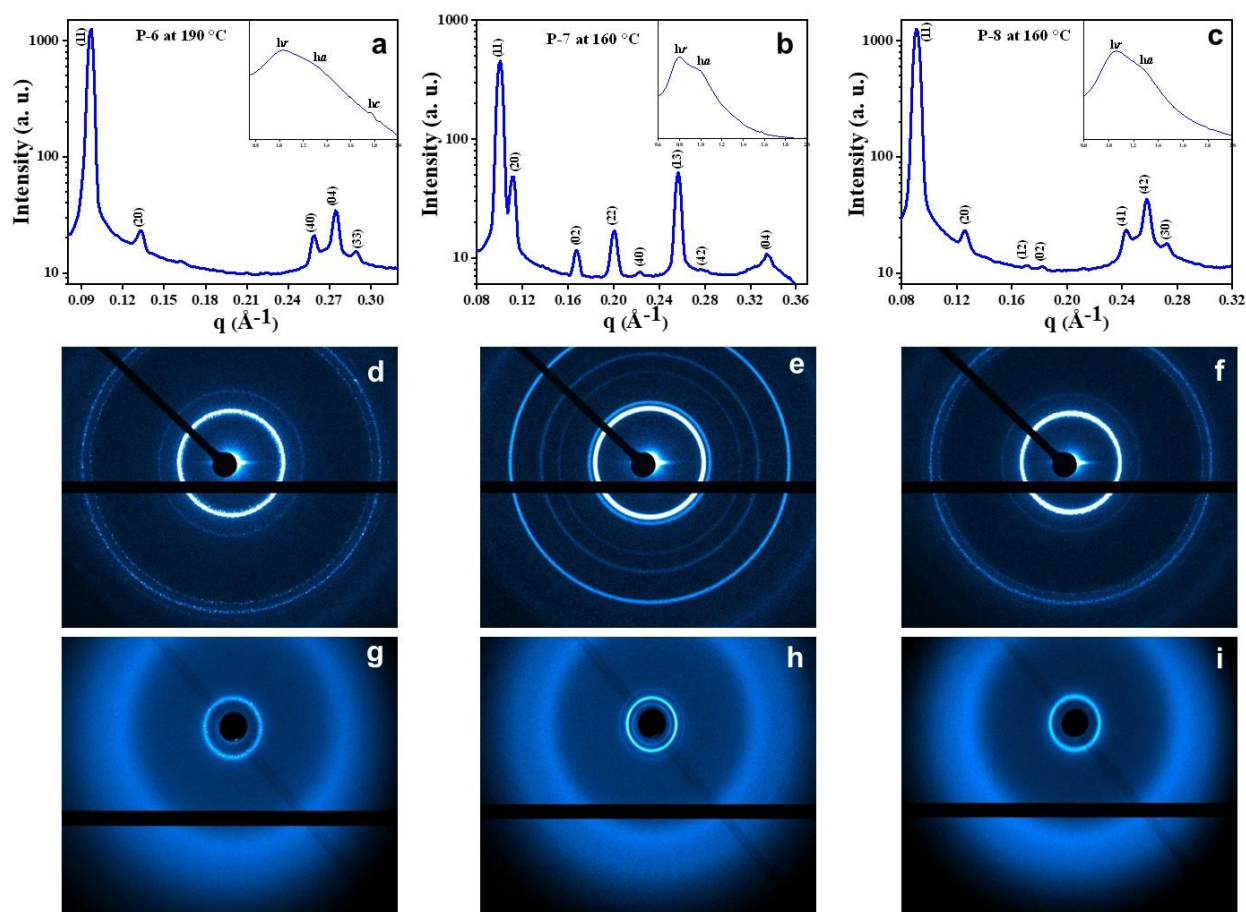


Figure A17 Small and wide angle (inset) X-ray diffraction patterns of compound (a) **P-6** at 190 °C (Col_r), (b) **P-7** at 160 °C (Col_r) and (c) **P-8** at 160 °C (Col_{ob}) upon cooling, h_r - cholesterol-cholesterol correlation, h_a - alkyl chain-chain correlation. The lower panel shows the respective 2D diffraction patterns of SAXS (d, e, f) and WAXS (g, h, i).

Table A2. The indices observed and calculated d -spacings and planes of the diffraction peaks of the hexagonal lattice observed at 160 °C for compound **P-5**. The lattice parameter is $a = 72.7 \text{ \AA}$. h_r - cholesterol-cholesterol correlation, h_a - alkyl chain-chain correlation. ^aMI: Miller indices. ^b d_{obs} : experimental d -spacing. ^c d_{cal} : calculated d -spacing by using the relation $\frac{1}{d_{cal}^2} =$

$\frac{4}{3} \left[\frac{h^2 + hk + k^2}{a^2} \right]$; ^dRI: Relative Intensity. ^eM: Multiplicity.

^a MI (hk)	^b d_{obs} (\AA)	^c d_{cal} (\AA)	^d RI (hk)	^e M	Phase Φ (hk)
10	62.9	62.9	100	6	0
11	36.1	36.4	3	6	0
20	31.7	31.5	2	6	0
21	23.7	23.8	8.5	12	π
h_r	6.3				
h_a	5.1				

Table A3. The indices observed and calculated d -spacings and planes of the diffraction peaks of the rectangular lattice observed at 190 °C for compound **P-6**. The lattice parameters are $a = 96.1 \text{ \AA}$, $b = 91.1 \text{ \AA}$. h_r - cholesterol-cholesterol correlation, h_a - alkyl chain-chain correlation, h_c - disc-disc correlations. ^aMI: Miller indices. ^b d_{obs} : experimental d -spacing. ^c d_{cal} : calculated d -spacing by using the relation: $\frac{1}{d_{cal}^2} = [\frac{h^2}{a^2} + \frac{k^2}{a^2}]$ ^dRI: Relative Intensity. ^eM: Multiplicity.

^a MI (hk)	^b d_{obs} (\AA)	^c d_{cal} (\AA)	^d RI (hk)	^e M	Phase Φ (hk)
11	66.1	66.1	100	4	0
20	48.1	48.1	1.8	2	π
40	24.2	24	1.7	2	0
04	22.9	22.8	2.8	2	0
33	21.8	22.1	1.3	4	π
h_r	6.1				
h_a	5.1				
h_c	3.6				

Table A4. The indices observed and calculated d -spacings and planes of the diffraction peaks of the rectangular lattice observed at 160 °C for compound **P-7**. The lattice parameters are $a = 112 \text{ \AA}$, $b = 75.1 \text{ \AA}$. h_r - cholesterol-cholesterol correlation, h_a - alkyl chain-chain correlation. ^aMI: Miller indices. ^b d_{obs} : experimental d -spacing. ^c d_{cal} : calculated d -spacing by using the relation: $\frac{1}{d_{cal}^2} = [\frac{h^2}{a^2} + \frac{k^2}{a^2}]$ ^dRI: Relative Intensity. ^eM: Multiplicity.

^a MI (hk)	^b d_{obs} (\AA)	^c d_{cal} (\AA)	^d RI (hk)	^e M	Phase Φ (hk)
11	62.3	62.3	100	4	0
20	56	60	10.6	2	0
02	37.4	37.5	2.6	2	0
22	31.3	31.2	3.8	4	π
40	28.1	28	1.7	2	0
13	24.5	24.4	11.5	4	0
42	22.5	22.4			//
04	18.8	18.8	2.4	2	π
h_r	6.1				
h_a	5				

Table A5. The indices observed and calculated d -spacings and planes of the diffraction peaks of the oblique lattice observed at 160 °C for compound **P-8**. The lattice parameters are $a = 105.2 \text{ \AA}$, $b = 73.7 \text{ \AA}$ and $\alpha = 69.3^\circ$. h_r - cholesterol-cholesterol correlation, h_a - alkyl chain-chain correlation. ^aMI: Miller indices. ^b d_{obs} : experimental d -spacing. ^c d_{cal} : calculated d -

spacing by using the relation: $\frac{1}{d_{cal}^2} = \frac{1}{\sin^2 \alpha} \left[\frac{h^2}{a^2} + \frac{k^2}{b^2} - \frac{2 h k \cos \alpha}{a b} \right]$; d RI: Relative Intensity. e M:

Multiplicity.

a MI (hk)	$^b d_{obs}$ (Å)	$^c d_{cal}$ (Å)	d RI (hk)	e M	Phase Φ (hk)
11	69.2	69.1	100	2	0
20	49.5	49.2	1.8	2	π
12	36.9	36.9	0.9	2	0
02	34.5	34.5	0.9	2	0
41	26	26.3	1.9	2	0
42	24.6	24.6	3.4	2	0
03	23.1	22.9	1.4	2	0
h_r	6.1				
h_a	4.9				

Table A6. The indices observed and calculated d -spacings and planes of the diffraction peaks of the oblique lattice observed at 160 °C for compound **P-10**. The lattice parameters are $a = 106.7$ Å, $b = 78.5$ Å and $\alpha = 79.6^\circ$. h_r - cholesterol-cholesterol correlation, h_a - alkyl chain-chain correlation. a MI: Miller indices. $^b d_{obs}$: experimental d -spacing. $^c d_{cal}$: calculated d -spacing by using the relation: $\frac{1}{d_{cal}^2} = \frac{1}{\sin^2 \alpha} \left[\frac{h^2}{a^2} + \frac{k^2}{b^2} - \frac{2 h k \cos \alpha}{a b} \right]$; d RI: Relative Intensity. e M:

Multiplicity.

a MI (hk)	$^b d_{obs}$ (Å)	$^c d_{cal}$ (Å)	d RI (hk)	e M	Phase Φ (hk)
11	68.4	68.4	100	2	0
20	52.4	52.5	8.2	2	0
21	47.5	47.6	2.8	2	0
12	38.6	38.6	3	2	0
22	34.6	34.2	3	2	0
40	26.5	26.2	19.5	2	0
24	19.6	19.3	2.3	2	π
h_r	6.1				
h_a	4.9				

Table A7. The indices observed and calculated d -spacings and planes of the diffraction peaks of the rectangular lattice observed at 180 °C for compound **P-11**. The lattice parameters are $a = 148.2$ Å, $b = 79.9$ Å. h_r - cholesterol-cholesterol correlation, h_a - alkyl chain-chain correlation,

h_c - disc-disc correlations. ${}^a\text{MI}$: Miller indices. ${}^b d_{\text{obs}}$: experimental d -spacing. ${}^c d_{\text{cal}}$: calculated d -spacing by using the relation: $\frac{1}{d_{\text{cal}}^2} = \left[\frac{h^2}{a^2} + \frac{k^2}{a^2} \right]$; ${}^d\text{RI}$: Relative Intensity. ${}^e\text{M}$: Multiplicity.

${}^a\text{MI}$ (hk)	${}^b d_{\text{obs}}$ (Å)	${}^c d_{\text{cal}}$ (Å)	${}^d\text{RI}$ (hk)	${}^e\text{M}$	Phase Φ (hk)
11	70.3	70.3	100	4	Π
02	40	39.9	8.2	2	Π
51	27.9	27.8	28.9	4	Π
62	20.8	21	4.3	4	Π
h_r	6.1				
h_a	5.2				
h_c	3.6				

Circular Dichroism (CD) Spectroscopy:

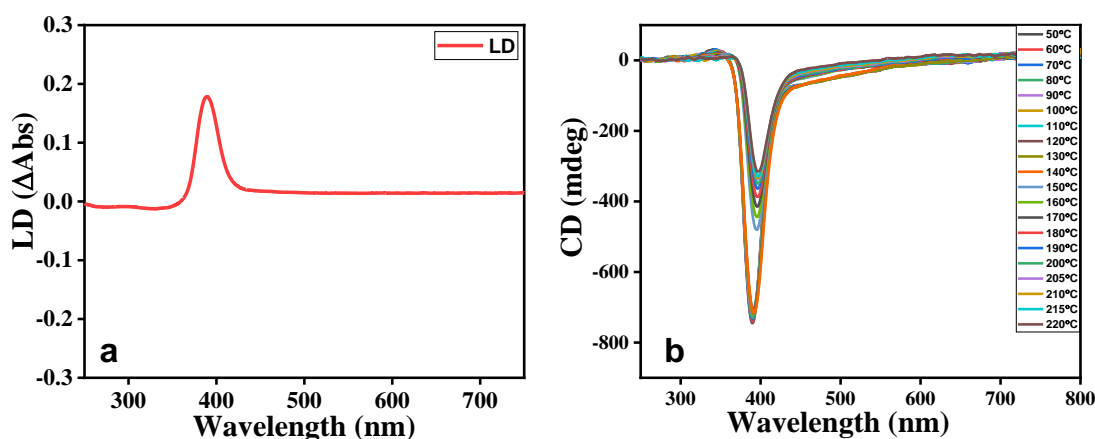


Figure A18 (a) The LD spectrum of the fluid Col phase of compound **P-5**, (b) CD spectra were obtained as a function of temperature for the Col phase of compound **P-5**. It may be noted here that the CD intensity increases with the decrease in temperature of the Col phase.

Table A8. CD spectral data of the Col phase exhibited by the compound **P-5**.

Temperature (°C)	CD	
	λ_{max} / nm	CD (mdeg)
50	390	-744
60	390	-742
70	390	-740
75	390	-738
80	390	-736
90	390	-734
100	390	-732
110	390	-730
120	390	-728

130	390	-726
140	390	-725
150	390	-479
160	393	-436
170	393	-409
180	393	-375
190	395	-357
200	395	-339
210	395	-332
215	395	-324
220	396	-313

Table A9. CD spectral data of the Col phase exhibited by the compound **P-6**.

Temperature (°C)	CD	
	λ_{\max} / nm	CD (mdeg)
55	360, 297	-947, -270
60	360, 297	-942, -270
70	360, 297	-940, -269
75	360, 297	-938, -269
80	360, 297	-913, -264
90	360, 297	-880, -259
100	360, 297	-875, -254
110	360, 297	-853, 249
120	360, 297	-819, -245
130	360, 297	-700, -231
140	400, 350	-198, -134
150	400, 350	-197, -90
160	400, 350	-194, 58
170	400, 350	-188, -35
180	400, 350	-175, -25
190	400	-170
200	400	-168
210	400	-168
220	400	-167

Table A10. CD spectral data of the Col phase exhibited by the compound **P-10**.

Temperature (°C)	CD	
	λ_{\max} / nm	CD (mdeg)
70	393	-100
80	393	-95
90	398	-73
100	399	-65
110	398	-58
120	398	-57
130	397	-56

140	397	-56
150	398	-55
160	398	-45
170	398	-40
180	398	-37
190	399	-34
200	399	-33

Table A11. CD spectral data of the Col phase exhibited by the compound **P-11**.

Temperature (°C)	CD	
	λ_{\max} / nm	CD (mdeg)
90	385	-153
100	385	-144
110	385	-143
120	385	-140
130	387	-132
140	387	-130
150	388	-82
160	388	-74
170	388	-71
180	390	-61

UV-visible and fluorescence data:

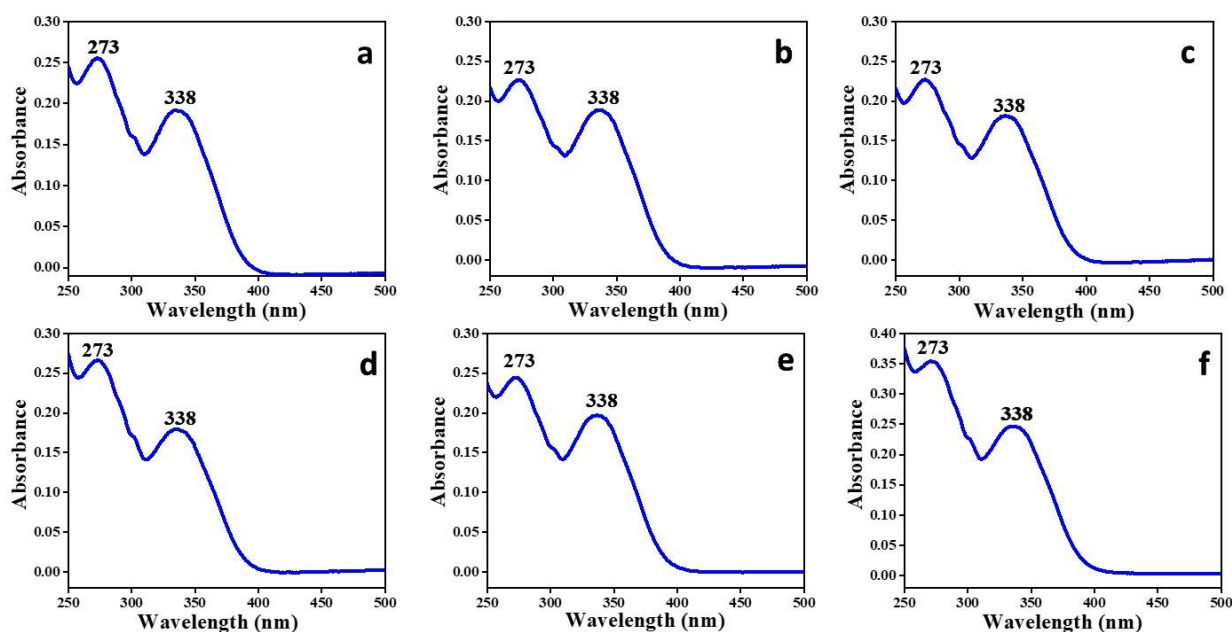


Figure A19 Absorption spectra of compounds (a) **P-5**, (b) **P-6**, (c) **P-7**, (d) **P-8**, (e) **P-10**, (f) **P-11**, in 10^{-5} M THF solution.

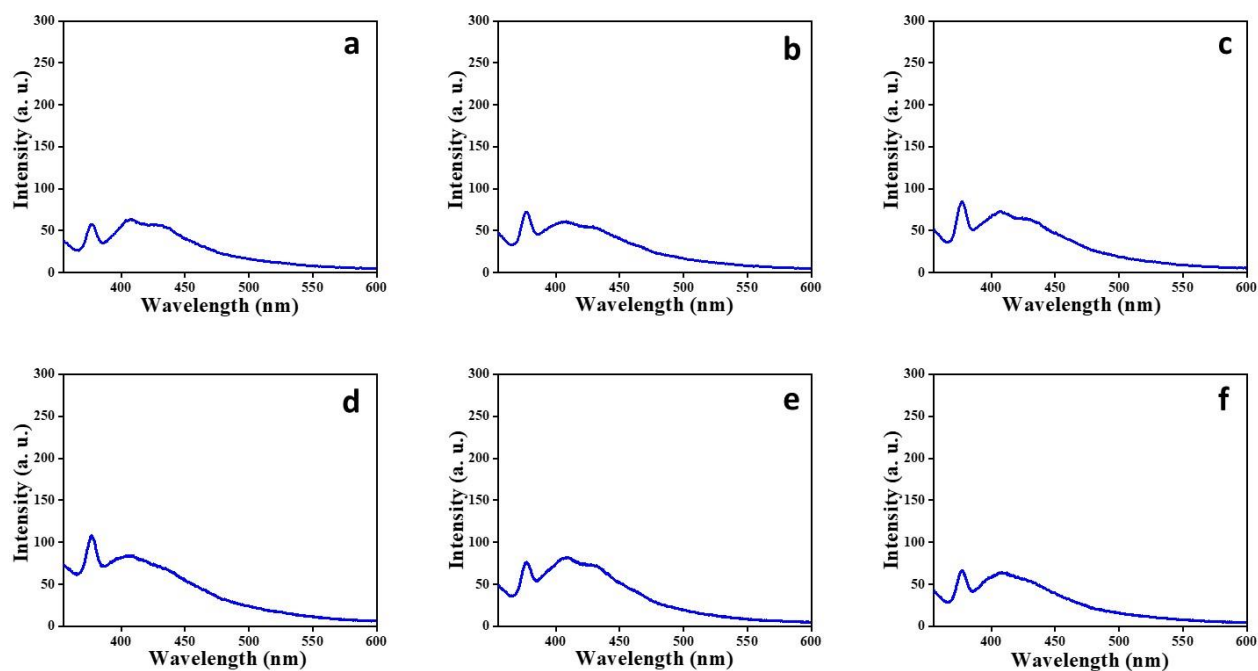


Figure A20 Emission spectra of compounds (a) **P-5**, (b) **P-6**, (c) **P-7**, (d) **P-8**, (e) **P-10**, (f) **P-11**, in 10^{-5} M THF solution, where the excitation wavelength is 338 nm.

HCl Sensing:

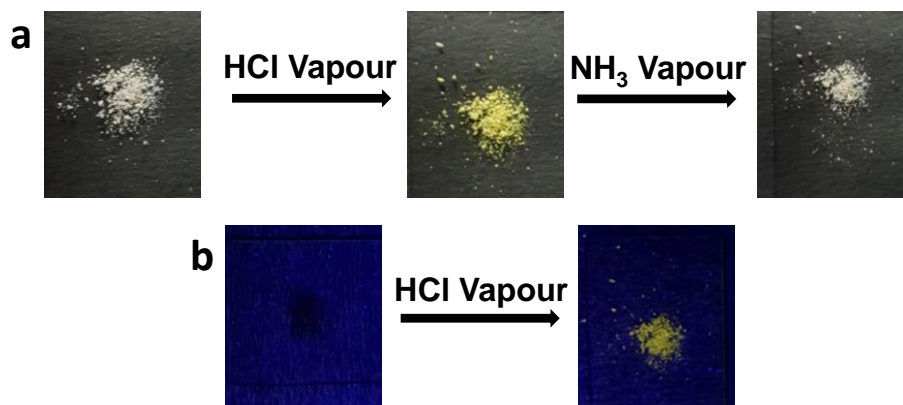


Figure A21 Optical photographs of **P-5**, (a) upon exposure to HCl vapor and ammonia vapor under normal light, and (b) upon exposure to HCl vapor under UV light.

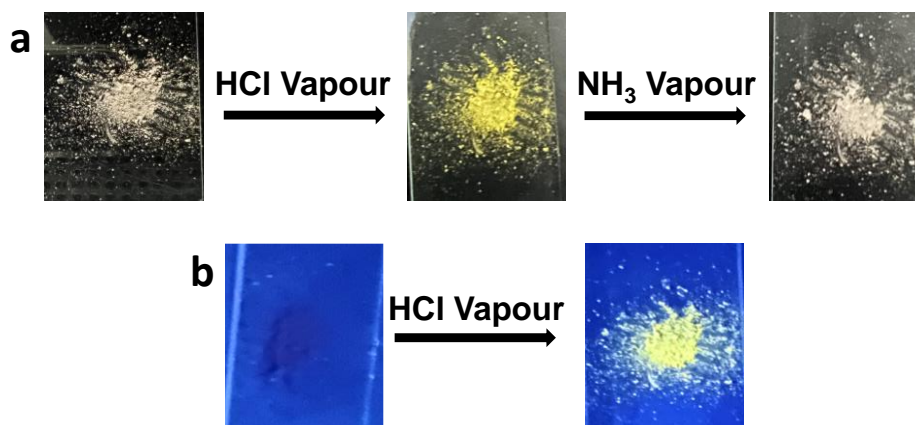


Figure A22 Optical photographs of **P-6**, (a) upon exposure to HCl vapor and ammonia vapor under normal light, and (b) upon exposure to HCl vapor under UV light.

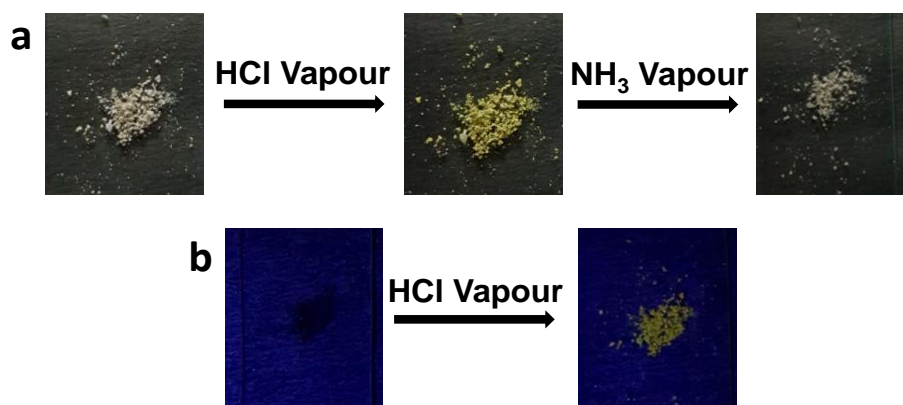


Figure A23 Optical photographs of **P-7**, (a) upon exposure to HCl vapor and ammonia vapor under normal light, and (b) upon exposure to HCl vapor under UV light.

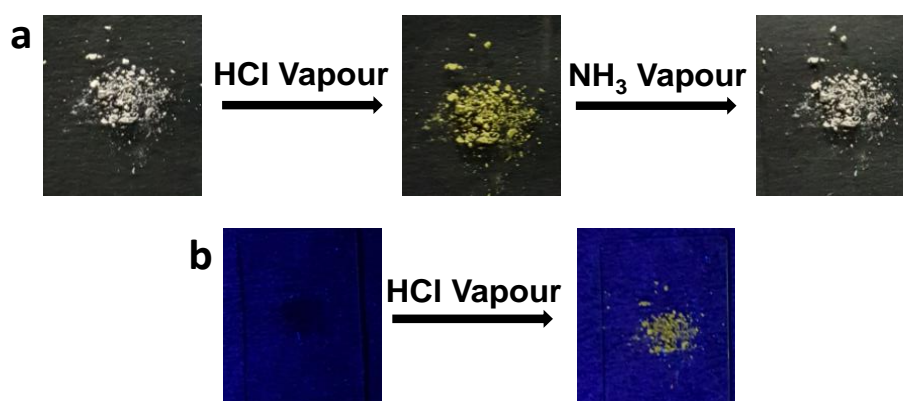


Figure A24 Optical photographs of **P-8**, (a) upon exposure to HCl vapor and ammonia vapor under normal light, and (b) upon exposure to HCl vapor under UV light.

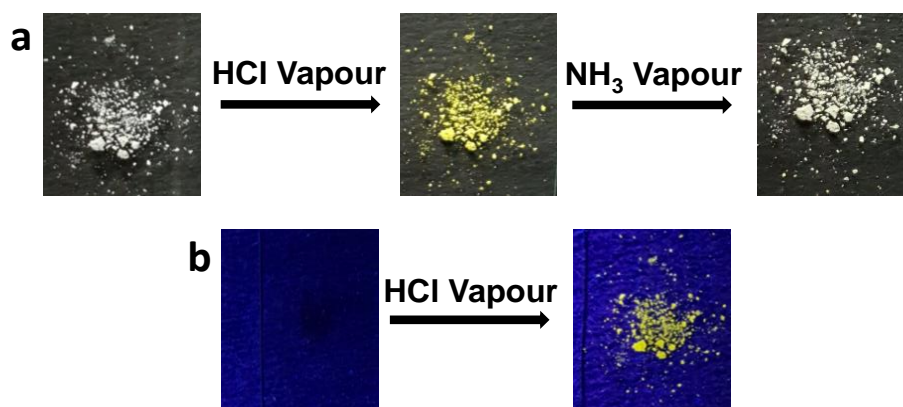
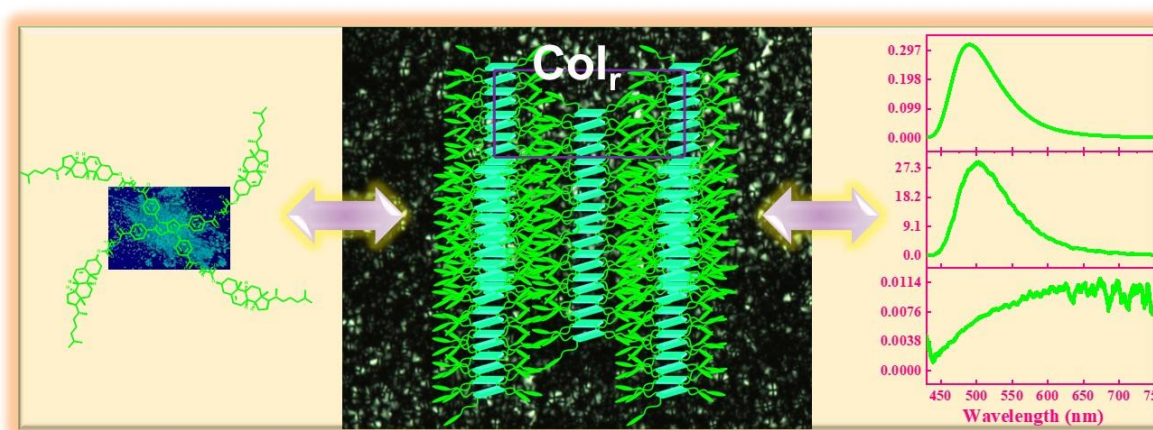


Figure A25 Optical photographs of **P-10**, (a) upon exposure to HCl vapor and ammonia vapor under normal light, and (b) upon exposure to HCl vapor under UV light.

Chapter 3

Circularly polarized luminescence from pyrrolopyrrole-based discotic columnar liquid crystals

Molecular functional materials with helical supramolecular organization and chiroptical properties are in high demand for their utilization in organic optoelectronics. Herein this chapter, we presented the design, synthesis and characterization of novel luminescent tetrarylpyrrolopyrrole (TAP) based chiral columnar discotic liquid crystal. Cholesterol was used as a side mesogenic unit to amplify the supramolecular chirality. Enantiomeric mesomorphic behaviour over a significant temperature range with columnar centred rectangular organization, freezes to glassy state at room temperature, was observed for all the derivatives. The photophysical studies in different solvents of varying polarity showed a decrease in quantum yield from non-polar to polar solvents. These chiral luminescent discotic liquid crystals emit circularly polarized luminescence (CPL) with a $|g_{lum}|$ of around 6.39×10^{-3} . This chapter describes the first TAP-based CPL active DLCs, which are expected to have potential applications in optoelectronics and photonics.



3.1 Introduction

Circularly polarized luminescence (CPL) is a spectroscopic technique that examines the different emissions of left- and right-circularly polarized light in chiral emitters (luminogens), and it offers a viable approach for directly producing circularly polarized light with better efficiency and simplified device structure. In recent decades, organic materials with CPL activity in aggregated state have attracted substantial recognition due to their fascinating photophysical properties and potential applications in optical sensing,¹ high-security systems,²⁻⁴ 3-D displays,⁵ data storage,⁶ 3-D imaging,^{7,8} CPL lasers,⁹⁻¹¹ colour- image projection,^{12,13} electro-optic displays,^{14, 15} OLEDs^{16, 17} and so-on. The CPL activity of a molecular system is measured in terms of luminescence dissymmetry factor (degree of circular polarization), g_{lum} , where $g_{\text{lum}} = 2(I_{\text{L}} - I_{\text{R}})/(I_{\text{L}} + I_{\text{R}})$. I_{L} and I_{R} represent the emission intensity of left and right circularly polarized light, respectively.¹⁸⁻²⁰ The typical strategy for developing a CPL active material is synthesizing a chromophore with a chiral configuration. The CPL activity demonstrates the chirality of materials in the excited state, is dependent on the mesoscopic architecture of molecular assemblies in an aggregated state in addition to chiral functions at the molecular level since molecular aggregates have variable physiochemical behaviour in the excited and ground states.²¹ In principle, helical self-assembled supramolecular structure formed by specific intermolecular interactions usually contribute to the effective transfer or amplify the CPL behavior of chiral materials.²²⁻²⁵

Liquid crystalline materials are very well known for their orderly self-assembly behaviour in the aggregated state; chiral liquid crystals are having a periodic self-assembly structure and helical stacking ability. Therefore, it is worth mentioning that emissive chiral liquid crystals are considered to be perfect candidates for CPL-active materials because of their significant chiral amplification effect.^{21,11,26} Different techniques have been used to prepare emissive chiral liquid crystals wherein CPL is involved. The first method involved doping, i.e., dope luminescent dye to the chiral liquid crystal matrix or chiral material to the luminescent liquid crystal.²⁷⁻³¹ The other involved the covalent bonding between the chiral unit and the luminescent material.^{25,32-34}

Many efforts have recently been dedicated to developing a CPL active liquid crystalline system due to their high emission efficiency in the condensed phase.³⁵⁻³⁸ At the macroscopic level, the CPL performance of chiral luminogens in the condensed matter state may significantly affect high-performance CPL-based devices. However, the problem is that most of the conventional

luminogens cannot show the emission behaviour in the aggregated state, which is why many reported chiral liquid crystalline materials could not generate the CPL properties.

Here in this article, we report the design and synthesis of a non-doped, highly adequate CPL material with columnar self-assembly, derived from thermotropic chiral luminescent liquid crystal using tetraarylpyrrolo[[3,2-b]pyrrole (TAP) as a luminescent unit and cholesterol as the side chiral mesogenic unit. TAP unit is composed of two large planar rigid conjugated pyrrole units and has 10- π electrons, which makes it have a strong electron-donating ability for a donor-acceptor pair.³⁹ TAP have many sites for structural modification, which is very useful for synthesizing various smart materials.⁴⁰ The properties of its derivatives can be altered, such as better thermal stability, morphological stability, hole transport properties and aggregation-induced emission (AIE) properties etc. The excellent optical properties, like AIE and high fluorescence quantum yields, make the TAP unit a perfect choice for application in various areas of photonics. The chiral unit cholesterol is used successfully for producing a chiral phase in a liquid crystalline system.⁴¹

To date, researchers have been focused on developing TAP-based LCs, all the derivatives with two peripheral mesogenic units self-assemble to smectic and lamellar assembly.^{42, 43} The propeller shape of the TAP unit endowed TAP with typical AIE properties. In this work, the TAP core is linked with four peripherals chiral mesogenic substituents, which were self-assembled to columnar architecture. The chirality induction enables the LCs to self-assemble into a highly ordered helical structure. The presence of an electron-withdrawing group at the phenyl ring makes it a donor-acceptor system, which also gives it interesting luminescence properties due to the intramolecular charge transfer process. The emission behaviour of TAP shows interesting solvent-dependent behaviour, such as the ability to entirely lose fluorescence when dispersed in a high polarity solvent. Furthermore, the fluorescence emission exhibited a hypsochromic shift in non-polar solvents.

To understand the structure-property relationship, two molecules with different spacers, i. e. **TAP-n** (n = 9,10) have been synthesized. All the intermediate derivatives and **TAP-n** molecules were characterized by ¹H NMR, ¹³C NMR, FTIR spectroscopy and MALDI-MS to confirm their structures. The mesophase behaviour of all the target compounds has been approved by polarising optical microscopy (POM), differential scanning calorimetry (DSC), and small-angle/wide-angle X-ray scattering (SAXS/WASX) experiments. The chiroptical properties of the molecules have been proved by temperature-dependent circular dichroism

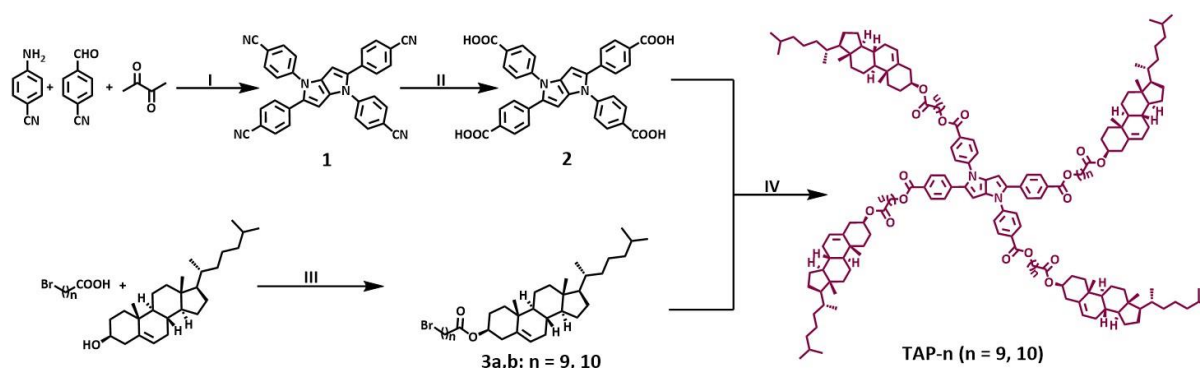
(CD) and CPL spectroscopy. To the best of our knowledge, this is the first report of chiral columnar self-assembly of TAP-based materials, leading to fascinating chiroptical and CPL properties in the aggregate state.

3.2 Results and discussions

3.2.1 Synthesis, Structural Characterization and Thermal stability

The synthesis of propeller-shaped, **TAP-n** derivatives and all the intermediates involved is represented in Scheme 3.1. The synthetic procedure started with the synthesis of compound **1**. The first step is the formation of Schiff base, and the second step involves a Mannich reaction and cyclo-condensations, followed by oxidation with air. The cyano-decorated compound **1** was then subjected to hydrolysis to give the corresponding acid-functionalized compound **2**. On the other hand, cholesterol-based intermediates were synthesized by an esterification reaction between cholesterol and bromoalkanoic acid, yielding the ester derivatives compound **3(a,b)**. The ester derivatives underwent phase transfer catalysis reaction with compound **2** in refluxing aq. KOH in the presence of TOAB to give the desired targeted compounds **TAP-n** (yield: 39 % and 37 % for **TAP-9** and **TAP-10**, respectively)

The purity and identity of all the derivatives and intermediate compounds have been analyzed by standard analytical techniques such as ^1H NMR, ^{13}C NMR, FTIR and mass spectroscopy (Figure A1-A13). All characterization results were well in accordance with the proposed molecular structure of the final synthesized compounds. The thermal stability of all the targeted compounds was explored using thermogravimetric analysis (TGA) (Figure A13 and Table 3.1); apparently, all the compounds presented good thermal stability, with a decomposition temperature above 330 °C.



Scheme 3.1 (I) $\text{Fe}(\text{ClO}_4)_3 \cdot x\text{H}_2\text{O}$, Toluene, AcOH, 60 °C, 12 h, Yield = 45 % (II) KOH, Ethanol+Water, 100 °C, 24 h, Yield = 68 % (III) DCC, DMAP, Dry DCM, 60 °C, 16 h, Yield = 75-78 % (IV) Aq. KOH, TOAB, 85 °C, 12 h, Yield = 35-40 %.

3.2.2 Mesomorphic behaviour

TAP-n derivatives were investigated under POM, DSC and X-ray diffraction studies for their liquid crystalline behaviour. The mesomorphic behaviour of the compounds was first observed under POM and evidenced by the anisotropic nature of the birefringent sample showing good shearability and fluidity in both the heating/cooling cycle. The compound shows the pseudo-focal-conic textures (Figure 3.1a-b) and dramatic intensity changes when we shear the sample in a different direction. The textures show the characteristics of columnar arrangement. Additionally, this columnar organization is readily frozen to a glassy state at room temperature. The exact LC phase temperature transitions and corresponding enthalpy changes of both compounds were determined using DSC (Figure 3.1c-d and Table 3.1).

Table 3.1 Thermal behaviour of **TAP-n** derivatives.^a

C	Heating cycle	Cooling cycle	T_d^b (°C)
TAP-9	G 52 Col _r 116.44 [26.45] Iso	Iso 93.96 [8.50] Col _r 63.8 [4.00] G	335
TAP-10	G 57.62 G ₁ 71.55 [7.64] Col _r 102.79 [13.18] Iso	Iso 90.03 [15.11] Col _r 60.34 [1.88] G	332

^aEnthalpy values in parentheses in kJ mol⁻¹ and temperature in °C. ^bDecomposition temperature corresponding to 5 % weight loss. Abbreviations: C = compound; G and G₁ = glassy state; Col_r = columnar centred rectangular; Iso = isotropic.

In DSC, during heating **TAP-9** showed two transitions; the first at 52 °C corresponds to the glassy state to mesophase transition and the second at 116.44 °C ($\Delta H = 26.45$ kJ mol⁻¹), represents the mesophase to isotropic transition; while **TAP-10** displayed three transitions. The first transition at 57.62 °C appeared due to glassy-to-glassy state reorganization, the second at 71.55 °C ($\Delta H = 7.64$ kJ mol⁻¹) corresponds to glassy-to-mesophase and the third at 102.79 °C ($\Delta H = 13.18$ kJ mol⁻¹), represents the mesophase to the isotropic phase transition. During cooling, both **TAP-9** (Figure 3.1c, Table 3.1) and **TAP-10** (Figure 3.1d, Table 3.1) displayed the two transitions, one for isotropic to mesophase and other appeared due to mesophase to glassy state. Furthermore, the phase transitions observed from POM and DSC measurements were consistent across numerous heating and cooling cycles, supporting the thermal stability of the columnar organization.

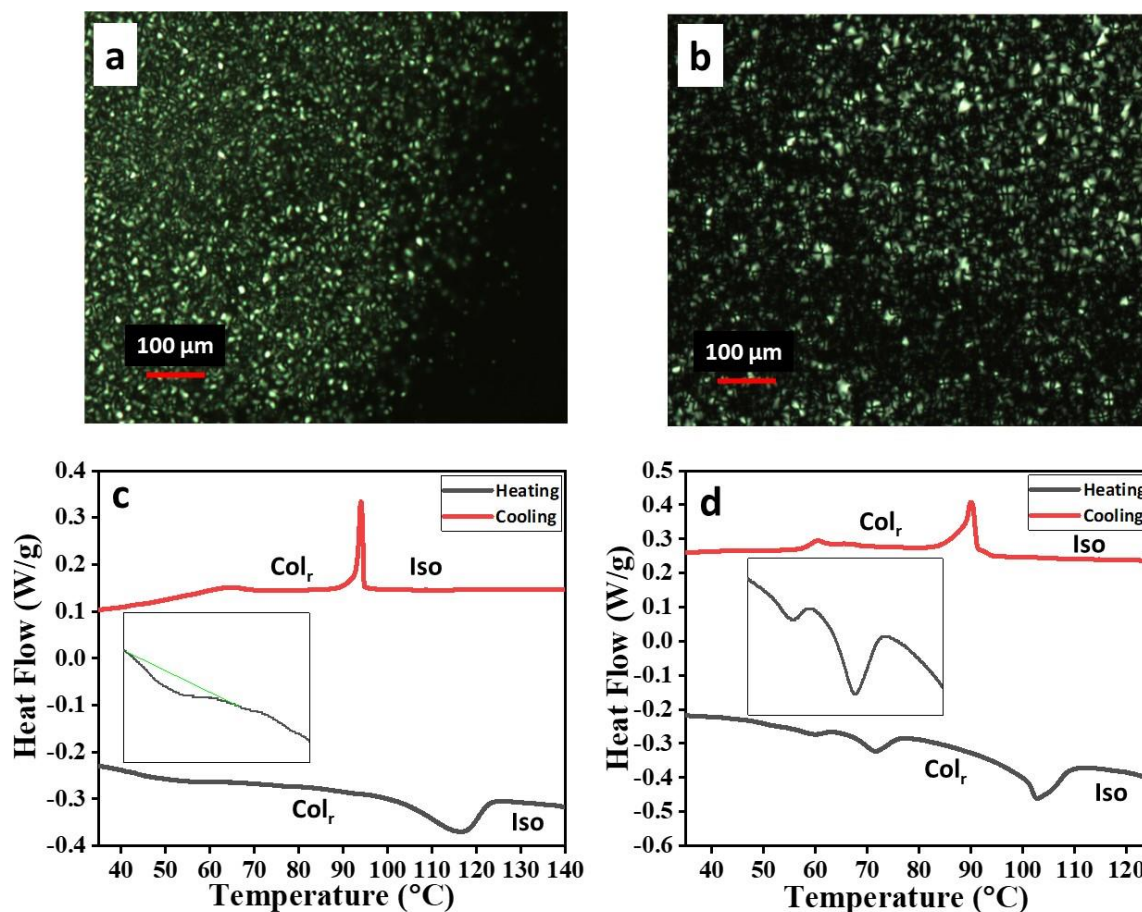


Figure 3.1 POM microphotographs of the optical texture of columnar centered rectangular phase formed by (a) **TAP-9** at 90 °C, (b) **TAP-10** at 80 °C observed during the cooling cycle, and DSC thermograms of compound (c) **TAP-9**, (d) **Tap-10** recorded at a rate of 5 °C/min.

The detailed structural assembly of compounds can be further identified by the XRD. The XRD pattern of compound **TAP-9** exhibits many reflections in the small angle and the wide-angle regime. These peaks could be indexed on a two-dimensional centred rectangular lattice (Figure 3.2a, Table A1). The calculated lattice parameters at 80 °C are found to be $a = 46.65 \text{ \AA}$ and $b = 44.92 \text{ \AA}$. Further, the X-ray diffraction pattern of the compound shows one non-Bragg's reflection, namely, h_{cl} in the wide-angle regime with d-spacing 5.82 Å. The h_{cl} peak appears due to the fluid cholesterol - cholesterol chain correlations. Moreover, there is a peak with a d-spacing 3.51 Å corresponding to disc-to-disc separation and indicative of columnar structure. Therefore, the molecules self-assemble in columnar centred rectangular phase, denoted by Col_r .

Similarly, the compound **TAP-10** exhibit columnar centred rectangular phase (Figure A15, Table A1). The calculated lattice parameters at 85 °C are found to be $a = 64.51 \text{ \AA}$ and $b = 41.98 \text{ \AA}$. The schematic representation of Col_r self-assembly of compound shows in Figure 3.2b.

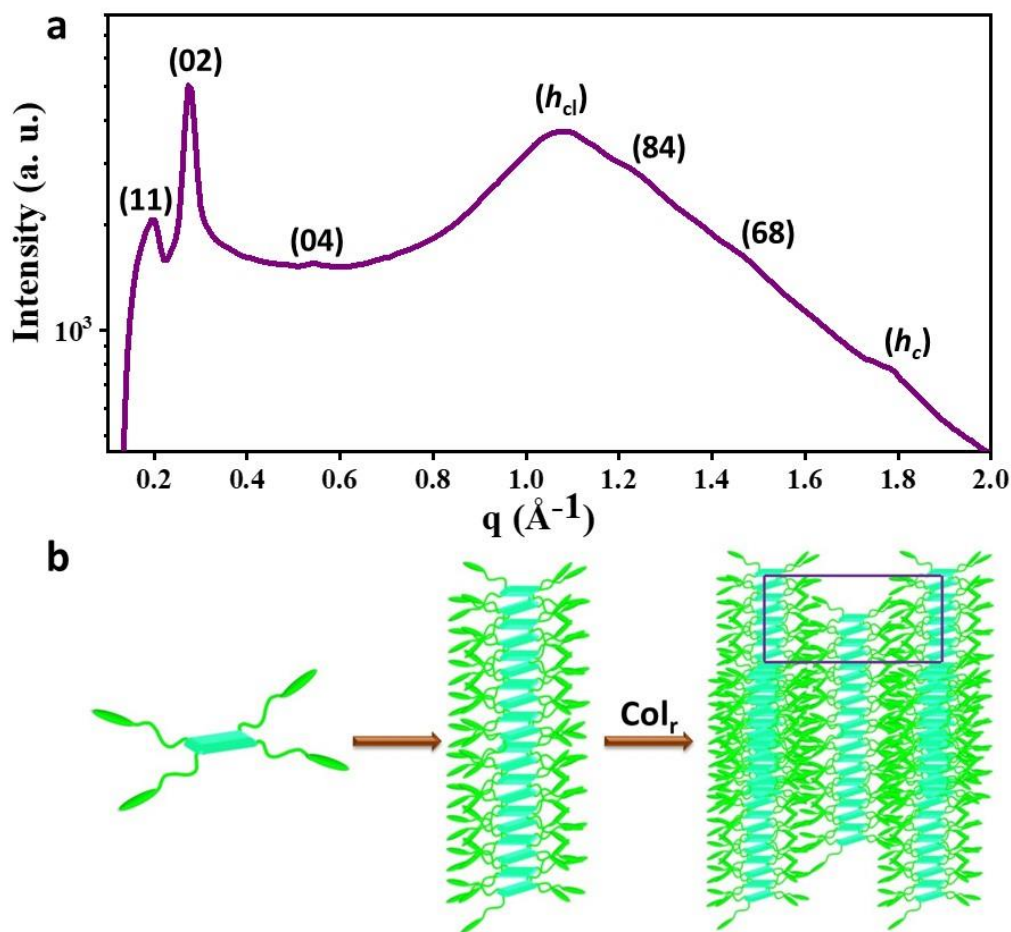


Figure 3.2 (a) Wide angle X-ray diffraction of **TAP-9**, representing the Col_r phase at 85 °C, h_{cl} – due to cholesterol - cholesterol chain correlations and h_c – due to disc-to-disc separation; (b) Schematic showing the self-assembly in Col_r organization.

3.2.3 Photophysical behavior

TAP-n derivatives exhibit excellent absorption and emission properties. The absorption spectra of **TAP-n** derivatives were measured in THF (10^{-5} M) solution at room temperature (Figure 3.3a-b). Both the derivatives show similar absorption peaks. The 288 nm and 330 nm peaks are described as π - π^* transition of the benzene rings and conjugated molecules, respectively.⁴² The longer absorption at 395 nm is ascribed to the intramolecular charge transfer (ICT) from the pyrrolopyrrole core (donor) to the electron-withdrawing ester group on the phenyl rings (acceptor).⁴³ The emission spectra of **TAP-n** derivatives in THF ($\lambda_{max} = 395$ nm) also shows a similar emission peak at 455 nm (Figure 3.3c-d), which suggests that the alkyl chain has no significant effect on the absorption and emission properties. **TAP-n** also displays good absorption and emission behaviour in the aggregated state, presented in the Figure A16. The absorption peaks in the thin-film state were observed to be around the same as those in the solution state, where the emission maxima appeared at 474 nm. In addition, in comparison to

the solution state, the emission peak becomes broader and red-shifted (Figure A16); due to the increased intermolecular interactions.

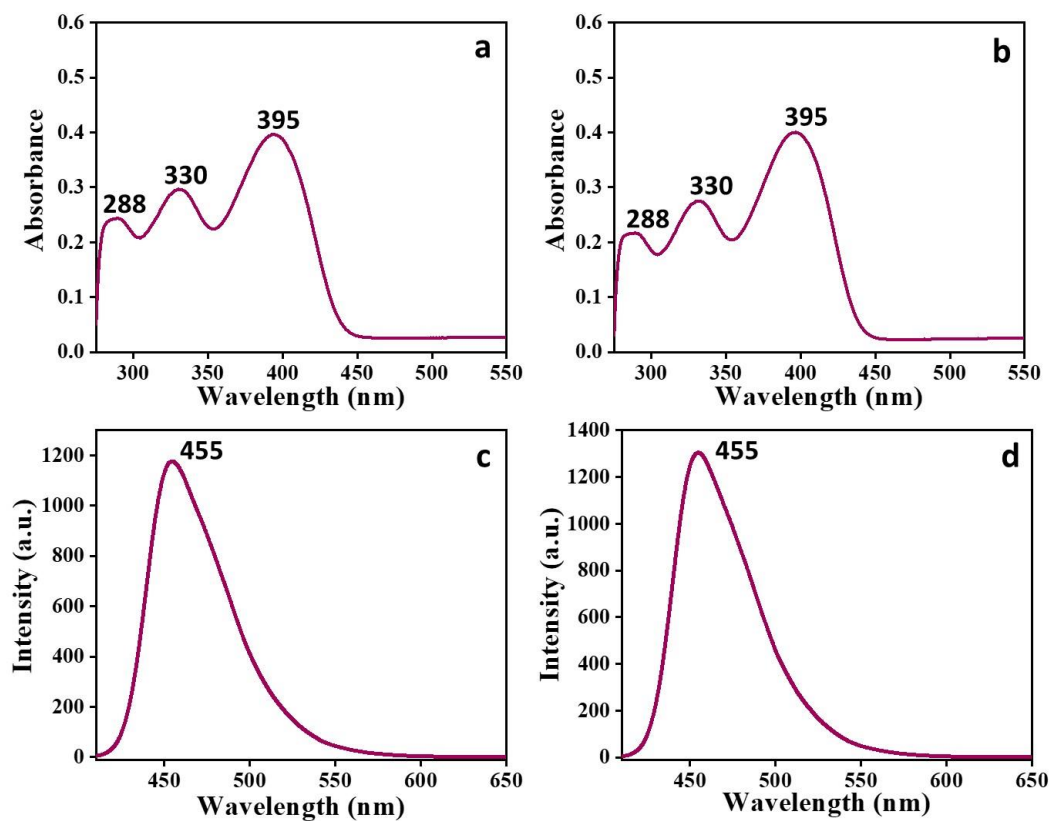


Figure 3.3 Absorption spectra (a, b) and emission spectrum (c, d) of compounds **TAP-9** and **TAP-10**, respectively, recorded in 10^{-5} M THF solution.

To study the electronic communication across the skeleton of **TAP-n** derivatives, the emission behaviour of these compounds was studied in different solvents (10^{-5} M). The fluorescence spectra showed a strong dependence on the solvent polarities, as shown in the Figure 3.4. The emission band exhibits a red shift and dramatic decrease in intensity from non-polar to polar solvents. The emission spectra of **TAP-n** in solvents with low (Hexane) and medium (THF) polarity were normalized to compare the fluorescence wavelength (Figure 3.4 inset), and a bathochromic shift of 18 nm is clearly observed from n-hexane to THF, which was in accordance with the ICT.⁴⁴ In the same solvents, the relative luminescence quantum yield was also calculated. **TAP-n** derivatives displayed a high fluorescence quantum yield in non-polar solvents, specifically in toluene and very low in polar solvents (Table 3.2).

To elucidate the effect of electronic transitions on the photophysical properties of **TAP-n**, density functional theory (DFT) calculations were performed at the B3LYP/631g (d,p) basis set (Figure A17). The electron cloud distribution in the highest occupied molecular orbital

(HOMO) of **TAP-10** was localized on the pyrrolopyrrole core, while the distribution of the lowest unoccupied molecular orbitals was affected by substituents and localized over the whole TAP unit. There is less clear spatial isolation of HOMO and LUMO, showing substandard ICT behaviour.

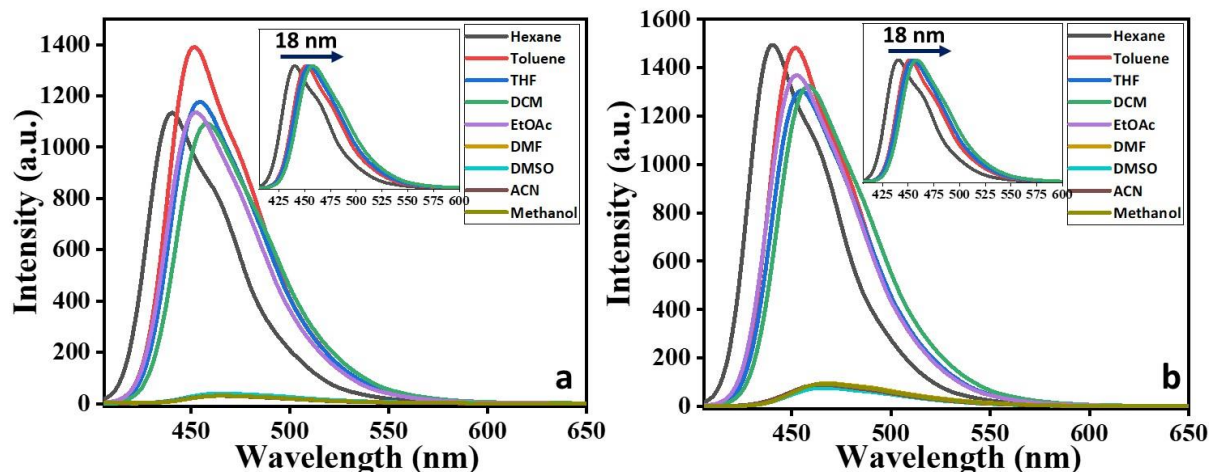


Figure 3.4 Solvent-dependent emission spectra of compounds (a) **TAP-9** and (b) **TAP-10**; inset showing the normalized spectra of compounds in non-polar to medium polarity solvents.

Table 3.2 Photophysical properties of target compound **TAP-n**.

Solvents	η^a	ϕ_F^b (TAP-9)	ϕ_F^b (TAP-10)
Hexane	1.37	0.74	0.88
Toluene	1.50	0.92	0.96
THF	1.41	0.73	0.78
DCM	1.42	0.68	0.75
Ethyl Acetate	1.37	0.69	0.80
DMF	1.43	0.03	0.09
DMSO	1.48	0.04	0.09
ACN	1.34	0.02	0.07
Methanol	1.33	0.02	0.05

^aRefractive Index; ^bFluorescence Quantum Yield. Quantum yield was measured by using Quinine sulphate in 0.1 M sulphuric acid as a standard.

As explained earlier, TAP's aggregation-induced emission (AIE) behaviour is influenced by the electron-withdrawing group attached with the central core and the length of the peripheral alkyl chains.⁴²⁻⁴⁴ Although both **TAP-9** and **TAP-10** showed good greenish-blue luminescence in the aggregated state (Figure A16 inset), but in the THF-H₂O experiment, **TAP-9** first showed

a decreasing luminescence intensity up to 80 %, and after that, there is a slight increase in intensity with increasing water ratio (Figure 3.5a) visible in optical photograph (Figure 3.5c); while the **TAP-10** fluorescence exhibited a rising tendency in THF and a declined trend in with increasing water ratio (Figure 3.5b). From the THF-H₂O experiment, we can say that molecules' AIE properties depend on the alkyl spacers.

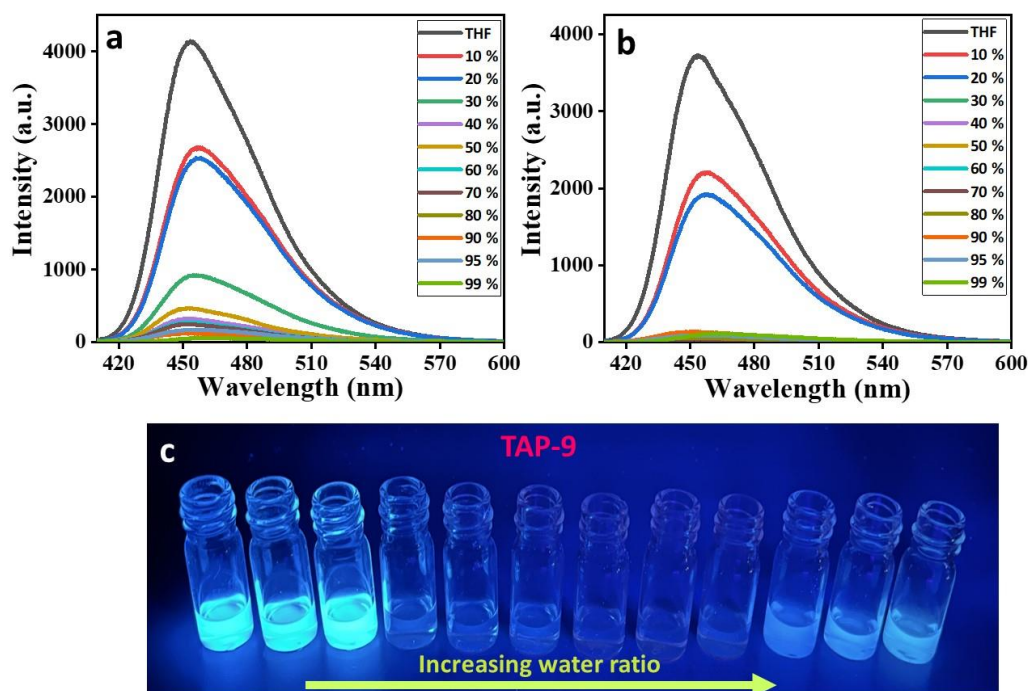


Figure 3.5 Emission spectra of compounds (a) **TAP-9**, (b) **TAP-10**, in different THF-water ratio, and (c) optical photograph of **TAP-9** under UV light.

3.2.4 Circularly polarized luminescence

In order to fully understand the fluorescent behaviour of helical self-assembly, we performed CPL experiment. To perform the CPL experiments, we will make a thin film of the samples using a regular quartz plate, which will be heated to an isotropic temperature and then cooled to room temperature. CPL behaviour of **TAP-9**, as an illustrative case in a thin-film state, was explored. As shown in Figure 3.6, the **TAP-9** exhibit an excellent mirror image CPL signal at about 490 nm, which coincides well with the fluorescence emission peak. The linear dichroism (LD) contribution was ruled out by the rotation-dependent ($\phi = 0^\circ, 90^\circ$ with respect to the direction of excitation light) spectroscopic measurements, which show similar results.⁴⁵ Further, the CPL efficiency could be evaluated by luminescence dissymmetry factor (g_{lum}), with a $|g_{lum}|$ of around 6.39×10^{-3} .

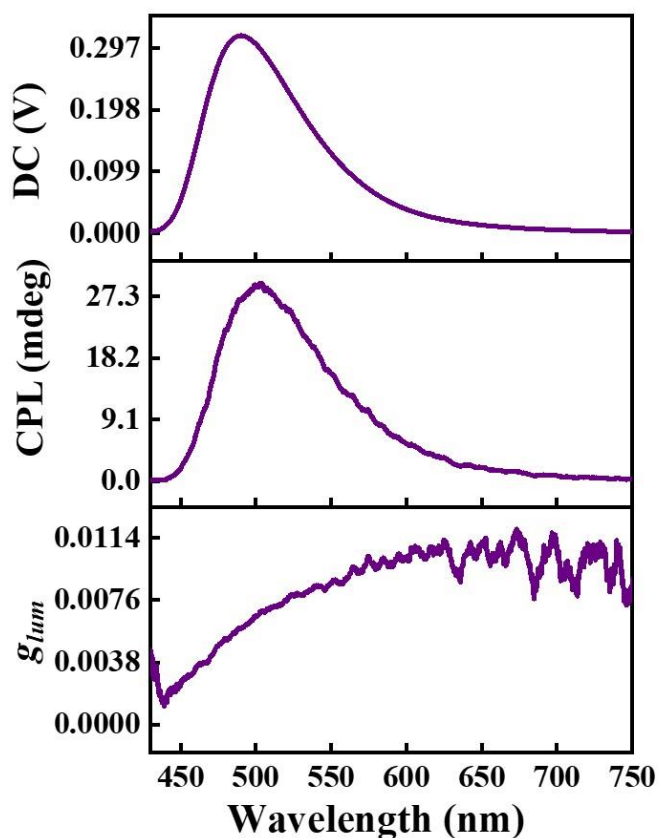


Figure 3.6 Plot of dissymmetry versus wavelength, CPL and direct current (DC) spectrum of **TAP-9**.

3.3 Conclusion

In summary, tetrarylpyrrolopyrrole (TAP) and cholesterol were used as a building block for developing highly fluorescent CPL active DLCs. Both **TAP-n** derivatives were self-assembled in a Col_r mesophase organization over a significant temperature range and freeze to a glassy state at ambient temperature. Photophysical studies showed that the compound exhibits highly fluorescent behavior in solution and thin-film states. Furthermore, changing the solvents from non-polar to polar caused a red shift, decreased emission spectra intensity, and a loss in fluorescence quantum yield. Due to excellent luminescence properties in a thin-film state, THF-H₂O experiments have been performed, which reflect the effect of the alkyl spacer. Additionally, the CPL activity of compound **TAP-9** was investigated, and the effectiveness was assessed using the luminescence dissymmetry factor (g_{lum}), with a $|g_{lum}|$ value of around 6.39×10^{-3} . This work presented here, revealed a straight forward way for producing CPL active materials, which have promising applications in optical devices and photonics.

3.4 Experimental section

3.4.1 General procedure for the synthesis of 4,4',4'',4'''-(pyrrolo[3,2-b]pyrrole-1,2,4,5-tetrayl)tetrabenzonitrile (compound 1):

Toluene (8 mL), Glacial acetic acid (8 mL), 4-Cyanoenzaldehyde (7.6 mmol, 1 equiv.) and 4-Cyanoaniline (7.6 mmol, 1 equiv.) were placed in a round bottom flask. The mixture was stirred at 50 °C for one hour. After one hour, Iron(III) perchlorate hydrate (90 mg) was added, followed by 2,3-butadione (0.35 mL). The resulting mixture was stirred at 60 °C for 12 h in an open flask under air. The precipitate was filtered off with cold ACN and dried under a vacuum. Yield = 45 %. The ¹H (Figure A1) spectrum of compound provided in Appendix II.

Characterization details of compound 1:

¹H NMR (400 MHz, DMSO-*d*₆, δ in ppm) 7.96 (d, *J* = 8.1 Hz, 4H), 7.78 (d, *J* = 8.0 Hz, 4H), 7.49 (d, *J* = 8.4 Hz, 4H), 7.40 (d, *J* = 8.0 Hz, 4H), 6.93 (s, 2H).

FTIR (cm⁻¹) 2226, 1602, 1524, 1473, 1451, 1414, 1375, 1275, 1177, 1137.

3.4.2 General procedure for the synthesis of 4,4',4'',4'''-(pyrrolo[3,2-b]pyrrole-1,2,4,5-tetrayl)tetrabenzoic acid (compound 2):

A mixture of compound 1 (500 mg, 0.9 mmol), an aqueous solution of KOH (20 M, 30 mL) and ethanol (30 mL) was heated to reflux in a round bottom flask for 24 h. Upon cooling to room temperature, the mixture was acidified with HCl to pH = 1. The product was collected by vacuum filtration and washed with water and ethanol several times; obtained solid was dried under vacuum. Yield = 68 %. The ¹H (Figure A2) and ¹³C NMR (Figure A3) spectrum are given in Appendix II.

Characterization details of compound 2:

¹H NMR (400 MHz, DMSO-*d*₆, δ in ppm) 12.99 (s, 4H), 8.01 (d, *J* = 8.6 Hz, 4H), 7.84 (d, *J* = 8.5 Hz, 4H), 7.40 (d, *J* = 8.6 Hz, 4H), 7.34 (d, *J* = 8.4 Hz, 4H), 6.80 (s, 2H).

¹³C NMR (100 MHz, DMSO-*d*₆, δ in ppm) 167.48, 167.17, 143.11, 137.16, 135.59, 132.70, 131.26, 129.97, 128.89, 128.61, 127.96, 125.08.

FTIR (cm⁻¹) 2925, 2849, 1735, 1505, 1472, 1456, 1276, 1264, 1098.

3.4.3 General procedure for the synthesis of compound 3a-b:

Compound 3 was prepared by the previously reported procedure.⁴¹ "Cholesterol (1.2 equiv.) was added to the stirred solution of bromoalkanoic acid (2 g, 1 equiv.) in dry DCM (40 mL). The resulting mixture was stirred under a nitrogen atmosphere, and DMAP (catalytic amount) was added to the solution. A solution of DCC (1.25 equiv.) in DCM was further added to the reaction mixture, and the mixture was stirred at 60 °C for 12 h. The reaction mixture was filtered, and the filtrate thus obtained was concentrated in a vacuum. The crude product was then purified by column chromatography using silica gel with a mixture of hexane/ethyl acetate (v/v, 100/1) as an eluent. The white solid obtained was air dried and stored in a clean sample vial." Yield range = 75 – 78 %. The ¹H (Figure A4, A6) and ¹³C NMR (Figure A5, A7) spectrum are given in Appendix II.

Characterization details of compound 3a-b:

3a: Yield = 75 %, ¹H NMR (400 MHz, CDCl₃, δ in ppm) 5.37 (d, *J* = 4.9 Hz, 1H), 4.66 – 4.56 (m, 1H), 3.40 (t, *J* = 6.9 Hz, 2H), 2.33 – 2.23 (m, 4H), 1.98 (tt, *J* = 20.0, 16.6, 4.4 Hz, 2H), 1.89 – 1.80 (m, 5H), 1.60 - 1.56 (m, 6H), 1.51 – 1.45 (m, 3H), 1.43 – 1.40 (m, 3H), 1.34 (t, *J* = 2.5 Hz, 2H), 1.29 (s, 10H), 1.16 - 1.10 (m, 6H), 1.02 (s, 4H), 1.00 – 0.94 (m, 2H), 0.91 (d, *J* = 6.5 Hz, 3H), 0.86 (dd, *J* = 6.6, 1.9 Hz, 6H), 0.67 (s, 3H).

¹³C NMR (100 MHz, CDCl₃, δ in ppm) 173.25, 139.69, 122.59, 73.68, 56.67, 56.12, 50.01, 42.29, 39.72, 39.50, 38.15, 36.99, 36.58, 36.17, 35.78, 34.67, 33.98, 32.79, 31.89, 31.85, 29.21, 29.12, 29.03, 28.67, 28.21, 28.12, 28.00, 27.80, 25.00, 24.27, 23.81, 22.81, 22.55, 21.02, 19.31, 18.70, 11.84.

FTIR (cm⁻¹) 2928, 2849, 1733, 1470, 1377, 1214, 1175.

3b: Yield = 78 %, ¹H NMR (400 MHz, CDCl₃, δ in ppm) 5.37 (d, *J* = 5.0 Hz, 1H), 4.65 – 4.57 (m, 1H), 3.40 (t, *J* = 6.9, 2H), 2.34 – 2.23 (m, 4H), 1.98 (tt, *J* = 20.1, 16.7, 4.3 Hz, 2H), 1.89 – 1.80 (m, 5H), 1.62 – 1.53 (m, 5H), 1.52 – 1.47 (m, 2H), 1.47 – 1.40 (m, 4H), 1.30 (d, *J* = 16.0 Hz, 14H), 1.18 – 1.04 (m, 7H), 1.02 (s, 4H), 0.99 – 0.93 (m, 2H), 0.91 (d, *J* = 6.4 Hz, 3H), 0.86 (dd, *J* = 6.6, 1.9 Hz, 6H), 0.67 (s, 3H).

¹³C NMR (101 MHz, CDCl₃, δ in ppm) 173.30, 139.71, 122.63, 73.69, 56.69, 56.13, 50.02, 42.32, 39.74, 39.53, 38.18, 37.01, 36.61, 36.19, 35.81, 34.71, 34.05, 32.84, 31.92, 31.87, 29.37,

29.34, 29.22, 29.10, 28.75, 28.25, 28.18, 28.03, 27.83, 25.05, 24.30, 23.84, 22.85, 22.59, 21.04, 19.35, 18.73, 11.87.

FTIR (cm^{-1}) 2940, 2866, 1736, 1598, 1464, 1380, 1169.

3.4.4 General procedure for the synthesis of compound TAP-n (n = 9, 10):

TAP-n was synthesized by a simple phase transfer catalysis reaction. Compound 2 (0.35 mmol, 1 equiv.) was added to the aqueous solution of KOH (10 M, 50 mL) in a round bottom flask, and the mixture was stirred for 15 min at 85 °C. After that, compound 3 (2 mmol, 6 equiv.) added to the mixture, followed by TOAB (catalytic amount), and the mixture was refluxed under continuous stirring for 12 h. The crude product was extracted with DCM. The organic phase dried over Na_2SO_4 was concentrated in a vacuum. The crude product obtained was purified by column chromatography using silica gel with a mixture of hexane/ethyl acetate (v/v 100/4) as eluent. Yield range = 37 – 39 %. The ^1H (Figure A8, A11), ^{13}C NMR (Figure A9, A12) and HRMS (Figure A10, A13), spectra are given in Appendix II.

Characterization details of compound TAP-n (n = 9, 10):

TAP-9: Yield = 39 %, ^1H NMR (400 MHz, CD_2Cl_2 , δ in ppm) 8.06 (d, J = 8.6 Hz, 4H), 7.90 (d, J = 8.5 Hz, 4H), 7.32 (dd, J = 18.2, 8.6 Hz, 8H), 6.61 (s, 2H), 5.36 (d, J = 4 Hz, 4H), 4.58 – 4.52 (m, 4H), 4.32 – 4.25 (m, 8H), 2.30 – 2.22 (m, 16H), 2.03 – 1.94 (m, 8H), 1.87 – 1.83 (m, 8H), 1.82 – 1.78 (m, 6H), 1.74 (t, J = 7.7 Hz, 8H), 1.59 – 1.55 (m, 20H), 1.53 (d, J = 6.6 Hz, 6H), 1.51 – 1.49 (m, 8H), 1.47 – 1.43 (m, 16H), 1.36 – 1.29 (m, 36H), 1.26 (d, J = 8.2 Hz, 8H), 1.20 – 1.15 (m, 8H), 1.13 (d, J = 3.6 Hz, 12H), 1.09 (s, 4H), 1.05 (d, J = 6.3 Hz, 4H), 1.01 (s, 16H), 0.96 (d, J = 5.6 Hz, 4H), 0.92 (d, J = 6.5 Hz, 12H), 0.87 (dd, J = 6.6, 1.7 Hz, 24H), 0.68 (s, 12H).

^{13}C NMR (100 MHz, CD_2Cl_2 , δ in ppm) 173.01, 166.16, 165.78, 143.35, 139.94, 137.25, 135.73, 130.76, 129.57, 128.45, 128.10, 127.69, 124.65, 122.46, 97.35, 73.62, 65.30, 56.19, 54.04, 53.77, 53.50, 53.23, 52.96, 42.31, 39.80, 39.53, 38.20, 37.04, 36.61, 35.86, 31.94, 31.88, 29.35, 29.21, 29.07, 28.74, 28.24, 28.07, 27.83, 26.03, 25.06, 24.28, 23.85, 22.61, 22.35, 21.05, 19.15, 18.53, 11.65.

HRMS (MALDI) for $\text{C}_{182}\text{H}_{271}\text{N}_2\text{O}_{16}(\text{M} + \text{H})$: calculated – 2741.0454; found - 2741.0378.

FTIR (cm^{-1}) 2932, 2872, 2855, 1723, 1606, 1509, 1468, 1378, 1274, 1177, 1102, 1016.

TAP-10: Yield = 37 %, $^1\text{H NMR}$ (400 MHz, CD_2Cl_2 , δ in ppm) 8.06 (d, $J = 8.6$ Hz, 4H), 7.91 (d, $J = 8.4$ Hz, 4H), 7.33 (dd, $J = 18.4, 8.5$ Hz, 8H), 6.61 (s, 2H), 5.37 (d, $J = 8$ Hz, 4H), 4.59 – 4.52 (m, 4H), 4.33 – 4.25 (m, 8H), 2.30 – 2.23 (m, 16H), 2.03 – 1.94 (m, 8H), 1.88 – 1.73 (m, 24H), 1.57 (d, $J = 10.1$ Hz, 20H), 1.53 (d, $J = 2.5$ Hz, 4H), 1.51 – 1.49 (m, 8H), 1.47 (s, 4H), 1.44 (d, $J = 4.5$ Hz, 8H), 1.36 (d, $J = 8$ Hz, 12H), 1.32 – 1.29 (m, 34H), 1.18 (s, 4H), 1.16 (d, $J = 5.9$ Hz, 8H), 1.12 (t, $J = 4.8$ Hz, 12H), 1.09 (d, $J = 2.6$ Hz, 4H), 1.06 (s, 2H), 1.02 (s, 20H), 0.99 – 0.96 (m, 8H), 0.92 (d, $J = 6.1$ Hz, 12H), 0.87 (dd, $J = 6.6, 1.7$ Hz, 24H), 0.68 (s, 12H).

$^{13}\text{C NMR}$ (100 MHz, CD_2Cl_2 , δ in ppm) 173.01, 166.16, 165.78, 143.36, 139.94, 137.25, 135.74, 132.69, 130.76, 129.57, 128.46, 128.11, 127.69, 124.65, 122.45, 97.38, 73.61, 65.31, 56.76, 56.19, 54.04, 53.77, 53.50, 53.23, 52.96, 50.12, 42.31, 39.80, 39.53, 38.20, 37.05, 36.62, 36.22, 35.87, 34.62, 31.94, 29.49, 29.43, 29.29, 29.12, 28.76, 28.25, 28.07, 27.84, 26.08, 25.08, 24.28, 23.85, 22.62, 22.37, 21.06, 19.16, 18.54, 11.66.

HRMS (MALDI) for $\text{C}_{186}\text{H}_{279}\text{N}_2\text{O}_{16}$ (M + H): calculated – 2797.1080; found – 2797.1162.

FTIR (cm^{-1}) 2938, 2882, 2852, 1733, 1719, 1606, 1506, 1456, 1374, 1273, 1177, 1014.

3.5 Quantum Yield Measurement

A direct method of measuring photoluminescence quantum yield (PL-QY) was employed, whereby a reference sample of known quantum efficiency was used as a comparison;^{46,47} the dye Rhodamine 6G was chosen as the reference as it absorbs in a similar region. With the optical spectra of both the reference and compound 1 solution in a given solvent, the following equation was applied:

$$\Phi = \Phi_R \frac{X(1-10^{-A_R})n^2}{X_R(1-10^{-A})n_R^2}$$

Where ' Φ ' is the quantum yield, ' X ' is the integrated area under the emission peak, ' A ' is the absorbance at the excitation wavelength, and ' n ' is the refractive index of the solvent. Each subscript ' R ' refers to the respective values of the reference standard.⁴⁸

3.6 Author Contributions

SR conceptualized the project, designed and performed the experiments, analyzed the data and wrote the chapter. SPG analyzed the SAXS/WAXS data. SKP did the overall project

administration, managed funding, reviewed, edited and finalized the chapter. All authors have given approval to the final version of the chapter.

3.7 Acknowledgements

SR thank CSIR for fellowship with file no (09/947(0091)/2017-EMR-I). SKP acknowledges project file no. CRG/2019/000901/OC from DST-SERB project. We are thankful to IISER Mohali for central and departmental facilities.

References

1. Sang, Y.; Han, J.; Zhao, T.; Duan, P.; Liu, M. Circularly Polarized Luminescence in Nanoassemblies: Generation, Amplification, and Application. *Adv. Mater.* **2020**, *32*, 1900110-1900143.
2. Riehl, J. P.; Richardson, F. S. Circularly Polarized Luminescence. *Chem. Rev.* **1986**, *86*, 1–16.
3. Lunkley, J. L.; Shirotani, D.; Yamanari, K.; Kaizaki, S.; Muller, G. Extraordinary Circularly Polarized Luminescence Activity Exhibited by Cesium Tetrakis(3-heptafluorobutylryl-(+)-camphorato) Eu(III) Complexes in EtOH and CHCl₃ Solutions. *J. Am. Chem. Soc.* **2008**, *130*, 13814–13815.
4. Sánchez-Carnerero, E. M.; Moreno, F.; Maroto, B. L.; A. R. Agarrabeitia, Ortiz, M. J.; Vo, B. G.; Muller, G.; de la Moya, S. Circularly Polarized Luminescence by Visible-Light Absorption in a Chiral O-BODIPY Dye: Unprecedented Design of CPL Organic Molecules from Achiral Chromophores. *J. Am. Chem. Soc.* **2014**, *136*, 3346–3349.
5. Bisoyi, H. K.; Li, Q. Light-Directing Chiral Liquid Crystal Nanostructures: From 1D to 3D. *Acc. Chem. Res.* **2014**, *47*, 3184-3195.
6. Ye, Q.; Zheng, F.; Zhang, E.; Bisoyi, H. K.; Zheng, S.; Zhu, D.; Lu, Q.; Zhang, H.; Li, Q. Solvent polarity driven helicity inversion and circularly polarized luminescence in chiral aggregation induced emission fluorophores. *Chem. Sci.* **2020**, *11*, 9989-9993.
7. Riehl, J. P.; Richardson, F. S. General theory of circularly polarized emission and magnetic circularly polarized emission from molecular systems. *J. Chem. Phys.* **1976**, *65*, 1011–1021.
8. Zinna, F.; Giovanella, U.; Bari, L. D. Highly Circularly Polarized Electroluminescence from a Chiral Europium Complex. *Adv. Mater.* **2015**, *27*, 1791–1795.

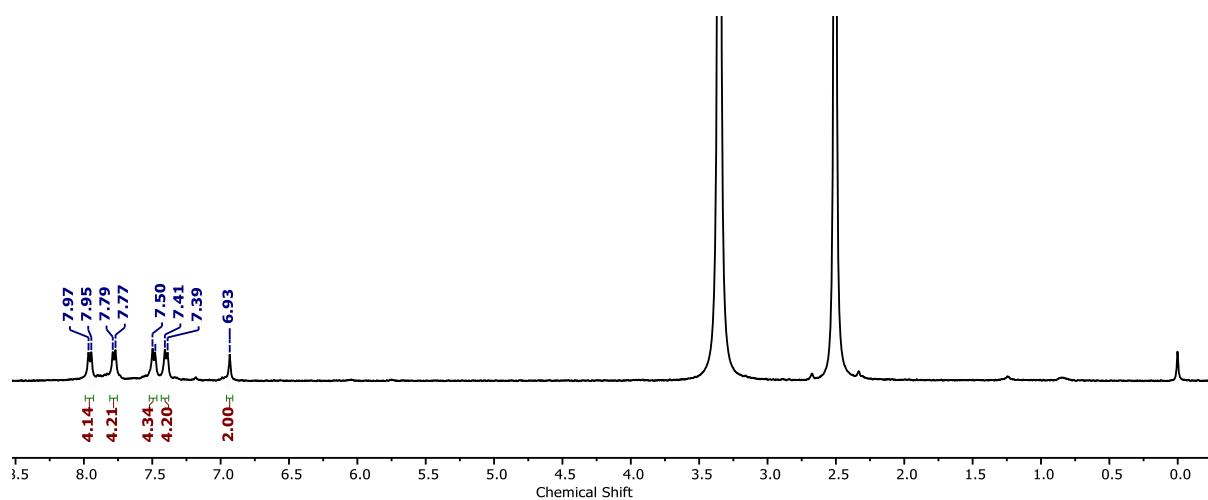
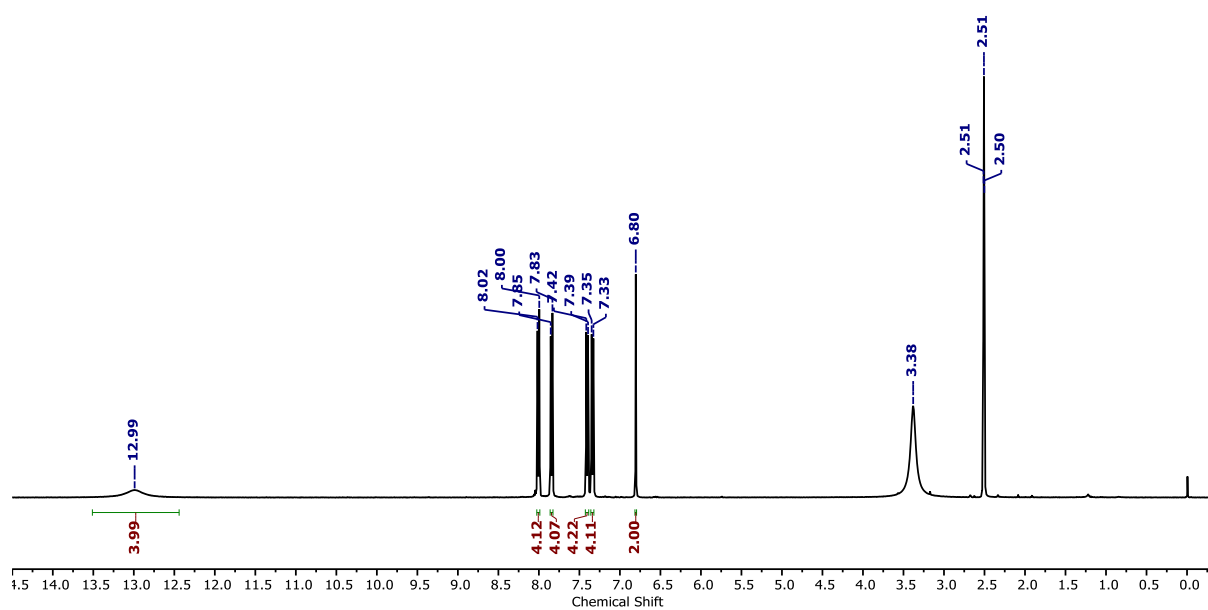
9. Ruangsupapichat, N.; Pollard, M. M.; Harutyunyan, S. R.; Feringa, B. L. Reversing the direction in a light-driven rotary molecular motor. *Nature Chemistry* **2011**, *3*, 53-60.
10. Han, J.; Duan, P.; Li, X.; Liu, M. Amplification of Circularly Polarized Luminescence through Triplet–Triplet Annihilation-Based Photon Upconversion. *J. Am. Chem. Soc.* **2017**, *139*, 9783–9786.
11. Yang, X.; Han, J.; Wang, Y.; Duan, P. Photon-upconverting chiral liquid crystal: significantly amplified upconverted circularly polarized luminescence. *Chem. Sci.* **2019**, *10*, 172–178.
12. Peeters, E.; Christiaans, M. P. T.; Janssen, R. A. J.; Schoo, H. F. M.; Dekkers, H. P. J. M.; Meijer, E. W. Circularly Polarized Electroluminescence from a Polymer Light-Emitting Diode. *J. Am. Chem. Soc.* **1997**, *119*, 9909–9910.
13. Oda, M.; Nothofer, H. G.; Lieser, G.; Scherf, U.; Meskers, S. C. J.; Neher, D. Circularly Polarized Electroluminescence from Liquid-Crystalline Chiral Polyfluorenes. *Adv. Mater.* **2000**, *12*, 362–365.
14. Geelhaar, T.; Griesar, K.; Reckmann, B. 125 Years of Liquid Crystals—A Scientific Revolution in the Home. *Angew. Chem. Int. Ed.* **2013**, *52*, 8798–8809.
15. Ma, J.; Xuan, L. Towards nanoscale molecular switch-based liquid crystal displays. *Displays* **2013**, *34*, 293–300.
16. Chen, S. H.; Katsis, D.; Schmid, A. W.; Mastrangelo, J. C.; Tsutsui, T.; Blanton, T. N. Circularly polarized light generated by photoexcitation of luminophores in glassy liquid-crystal films. *Nature* **1999**, *397*, 506–508.
17. Zheng, H.; Li, W.; Li, W.; Wang, X.; Tang, Z.; Zhang, S. X. A.; Xu, Y. Uncovering the Circular Polarization Potential of Chiral Photonic Cellulose Films for Photonic Applications. *Adv. Mater.* **2018**, *30*, 1705948-1705955.
18. Brandt, J. R.; Salerno, F.; Fuchter, M. J. The added value of small-molecule chirality in technological applications. *Nat. Rev. Chem.* **2017**, *1*, 2397-3358.
19. Han, J.; Guo, S.; Lu, H.; Liu, S.; Zhao, Q.; Huang, W. Recent Progress on Circularly Polarized Luminescent Materials for Organic Optoelectronic Devices. *Adv. Opt. Mater.* **2018**, *6*, 1800538-1800570.

20. Kumar, J.; Nakashima, T.; Kawai, T. Circularly Polarized Luminescence in Chiral Molecules and Supramolecular Assemblies. *J. Phys. Chem. Lett.* **2015**, *6*, 3445–3452.
21. Chen, S.; Jiang, S.; Qiu, J.; Guo, H.; Yang, F. Dual-responding circularly polarized luminescence based on mechanically and thermally induced assemblies of cyano-distyrylbenzene hydrogen bonding liquid crystals. *Chem. Commun.* **2020**, *56*, 7745–7748.
22. Gao, X. H.; Qin, X. J.; Yang, X. F.; Li, Y. G.; Duan, P. F. (R)-Binaphthyl derivatives as chiral dopants: substituent position controlled circularly polarized luminescence in liquid crystals. *Chem. Commun.* **2019**, *55*, 5914–5917.
23. Zhao, D. Y.; He, X. H.; Gu, X. G.; Guo, L.; Wong, K. S.; Lam, J. W. Y.; Tang, B. Z. Circularly Polarized Luminescence and a Reflective Photoluminescent Chiral Nematic Liquid Crystal Display Based on an Aggregation-Induced Emission Luminogen. *Adv. Opt. Mater.* **2016**, *4*, 534–539.
24. Ma, K.; Chen, W.; Jiao, T.; Jin, X.; Sang, Y.; Yang, D.; Zhou, J.; Liu, M.; Duan, P. Boosting the circularly polarized luminescence of small organic molecules via multi-dimensional morphology control. *Chem. Sci.* **2019**, *10*, 6821–6827.
25. Jose, B. A. S.; Matsushita, S.; Akagi, K. Lyotropic Chiral Nematic Liquid Crystalline Aliphatic Conjugated Polymers Based on Disubstituted Polyacetylene Derivatives That Exhibit High Dissymmetry Factors in Circularly Polarized Luminescence. *J. Am. Chem. Soc.* **2012**, *134*, 19795–19807.
26. Qian, X.; Yang, X.; Wang, J. D.; Herod, D. W.; Bruce, S.; Wang, W.; Zhu, P. Duan and Y. Wang, Chiral platinum-based metallomesogens with highly efficient circularly polarized electroluminescence in solution-processed organic lightemitting diodes. *Adv. Opt. Mater.* **2020**, *8*, 202000775–202000783.
27. Li, X.; Hu, W.; Wang, Y.; Quan, Y.; Cheng, Y. Strong CPL of achiral AIE-active dyes induced by supramolecular self-assembly in chiral nematic liquid crystals (AIE-N*-LCs). *Chem. Commun.* **2019**, *55*, 5179–5182.
28. Yao, K.; Shen, Y.; Li, Y.; Li, X.; Quan, Y.; Cheng, Y. Ultrastrong Red Circularly Polarized Luminescence Promoted from Chiral Transfer and Intermolecular Förster Resonance Energy Transfer in Ternary Chiral Emissive Nematic Liquid Crystals. *J. Phys. Chem. Lett.* **2021**, *12*, 598–603.

29. Li, X.; Li, Q.; Wang, Y.; Quan, Y.; Chen, D.; Cheng, Y. Strong Aggregation-Induced CPL Response Promoted by Chiral Emissive Nematic Liquid Crystals (N*-LCs). *Chem. – Eur. J.* **2018**, *24*, 12607–12612.
30. Qiao, J.; Lin, S.; Li, J.; Tian, J.; Guo, J. Reversible chirality inversion of circularly polarized luminescence in a photo-invertible helical cholesteric superstructure. *Chem. Commun.* **2019**, *55*, 14590–14593.
31. He, J.; Bian, K.; Li, N.; Piao, G. Generation of full-color and switchable circularly polarized luminescence from nonchiral dyes assembled in cholesteric cellulose films. *J. Mater. Chem. C* **2019**, *7*, 9278–9283.
32. Wu, Y.; You, L. H.; Yu, Z. Q.; Wang, J. H.; Meng, Z.; Liu, Y.; Li, X. S.; Fu, K.; Ren, X. K.; Tang, B. Z. Rational Design of Circularly Polarized Luminescent Aggregation-Induced Emission Luminogens (AIEgens): Promoting the Dissymmetry Factor and Emission Efficiency Synchronously. *ACS Mater. Lett.* **2020**, *2*, 505–510.
33. Watanabe, K.; Osaka, I.; Yorozuya, S.; Akagi, K. Helically π -Stacked Thiophene-Based Copolymers with Circularly Polarized Fluorescence: High Dissymmetry Factors Enhanced by Self-Ordering in Chiral Nematic Liquid Crystal Phase. *Chem. Mater.* **2012**, *24*, 1011–1024.
34. Song, F.; Cheng, Y.; Liu, Q.; Qiu, Z.; Lam, J. W.; Lin, L.; Yang, F.; Tang, B. Z. Tunable circularly polarized luminescence from molecular assemblies of chiral AIEgens. *Mater. Chem. Front.* **2019**, *3*, 1768–1778.
35. Roose, J.; Tang, B.; Wong, K. Circularly-Polarized Luminescence (CPL) from Chiral AIE Molecules and Macrostructures. *Small* **2016**, *12*, 6495–6512.
36. Li, H.; Li, B.; Tang, B. Molecular Design, Circularly Polarized Luminescence, and Helical Self-Assembly of Chiral Aggregation-Induced Emission Molecules. *Chem.–Asian J.* **2019**, *14*, 674–688.
37. Hu, M.; Feng, H.; Yuan, Y.; Zheng, Y.; Tang, B. Chiral AIEgens – Chiral recognition, CPL materials and other chiral applications. *Coord. Chem. Rev.* **2020**, *416*, 213329–213364.
38. Song, F.; Zhao, Z.; Liu, Z.; Lam, J. W. Y.; Tang, B. Circularly polarized luminescence from AIEgens. *J. Mater. Chem. C* **2020**, *8*, 3284–3301.

-
39. Wang, H.; Huo, J.; Tong, H.; Wei, X.; Zhang, Y.; Li, Y.; Chen, S.; Shi, H.; Tang, B. Z. Synthesis, crystal structure, aggregation-induced emission (AIE) and electroluminescence properties of a novel emitting material based on pyrrolo[3,2-b]pyrrole. *J. Mater. Chem. C* **2020**, *8*, 14208-14218.
40. Krzeszewski, M.; Thorsted, B.; Brewer, J.; Gryko, D. T. Tetraaryl-, Pentaaryl-, and Hexaaryl-1,4-dihydropyrrolo[3,2-b]pyrroles: Synthesis and Optical Properties. *J. Org. Chem.* **2014**, *79*, 3119–3128.
41. Rani, S.; Punjani, V.; Gupta, S. P.; Kanakala, M. B.; Yelamaggad C. V.; Pal, S. K. Observation of helical self-assembly in cyclic triphosphazene-based columnar liquid crystals bearing chiral mesogenic units. *J. Mater. Chem. C* **2023**, *11*, 1067-1075.
42. Dai, S.; Cai, Z.; Peng, Z.; Wang, Z.; Tong, B.; Shi, J.; Gan, S.; He, Q.; Chen, W.; Dong, Y. A stabilized lamellar liquid crystalline phase with aggregation-induced emission features based on pyrrolopyrrole derivatives. *Mater. Chem. Front.* **2019**, *3*, 1105-1112.
43. Dai, S.; Zhou, Y.; Zhang, H.; Cai, Z.; Tong, B.; Shi, J.; Dong, Y. Turn-on and color-switchable red luminescent liquid crystals based on pyrrolopyrrole derivatives. *J. Mater. Chem. C* **2020**, *8*, 11177 -11184.
44. Li, K.; Liu, Y.; Li, Y.; Feng, Q.; Hongwei Hou and Ben Zhong Tang, 2,5-bis(4-alkoxycarbonylphenyl)-1,4-diaryl-1,4-dihydropyrrolo[3,2-b]pyrrole (AAPP) AIEgens: tunable RIR and TICT characteristics and their multifunctional applications. *Chem. Sci.* **2017**, *8*, 7258–7267.
45. Garain, S.; Sarkar, S.; Garain, B. C.; Pati, S. K.; George, S. J. Chiral Arylene Diimide Phosphors: Circularly Polarized Ambient Phosphorescence from Bischromophoric Pyromellitic Diimides. *Angew. Chem.* **2022**, *134*, e202115773.
46. J. R. Lakowicz, Principles of Fluorescence Spectroscopy, *Springer, USA, 3rd edn*, 2006, 55–56.
47. C. E. Finlayson, A. Amezcua, P. J. A. Sazio, P. S. Walker, M. C. Grossel, R. J. Curry, D. C. Smith and J. J. Baumberg, *J. Mod. Opt.*, 2005, **52**, 955–964.
48. A. Brouwer, *Pure Appl. Chem.*, 2011, **83**, 2213–2228.

Appendix II

Figure A1 ¹H NMR spectrum of compound 1 in DMSO-d₆.Figure A2 ¹H NMR spectrum of compound 2 DMSO-d₆.

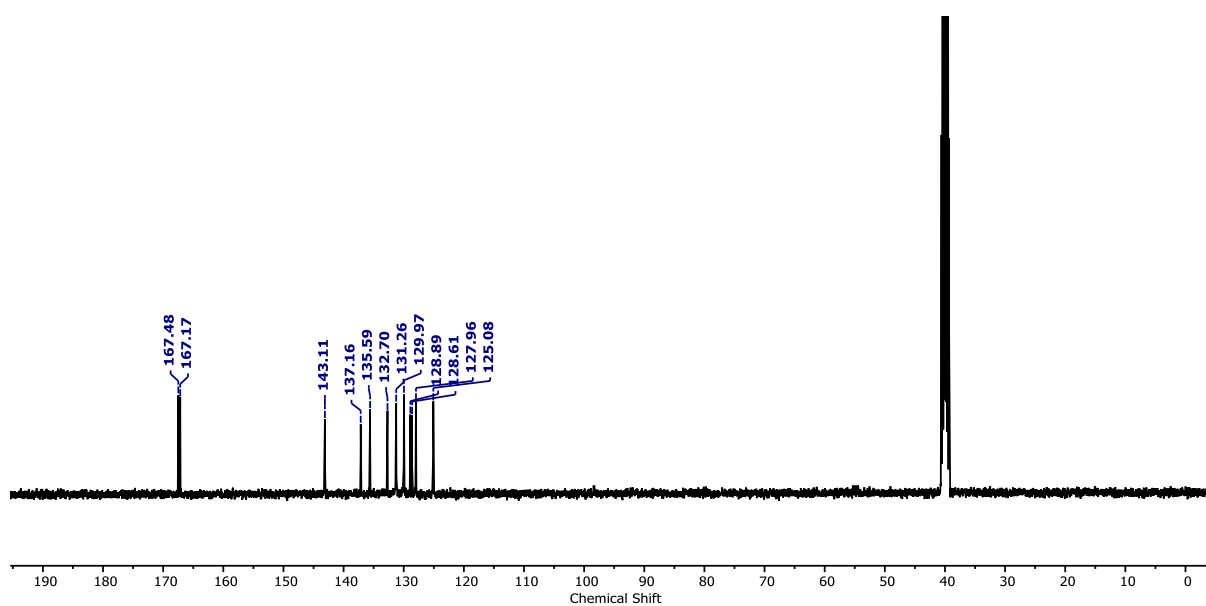


Figure A3 ^{13}C NMR spectrum of compound **2** in DMSO-d_6 .

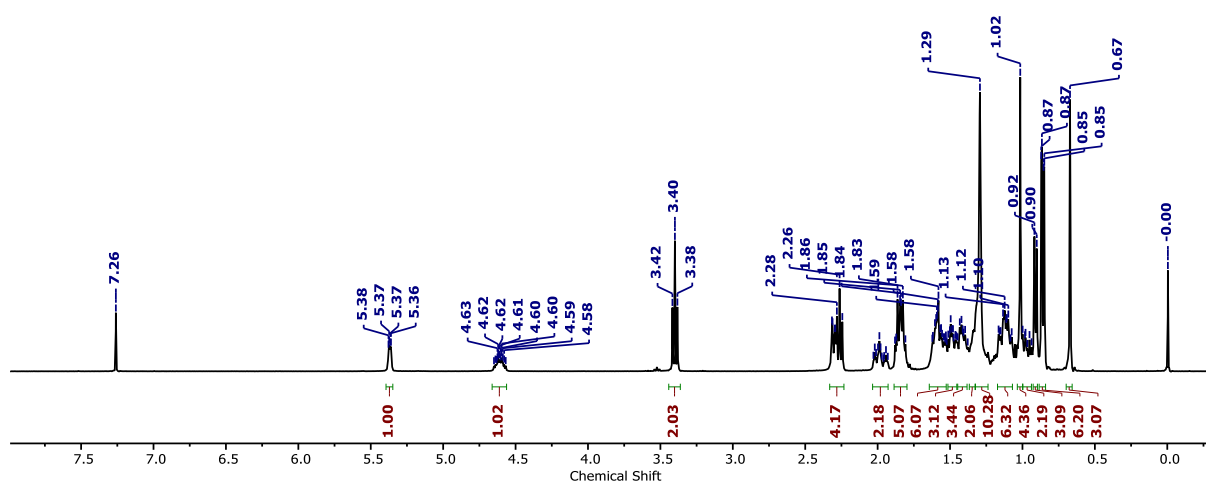


Figure A4 ^1H NMR spectrum of compound **3a** in CDCl_3 .

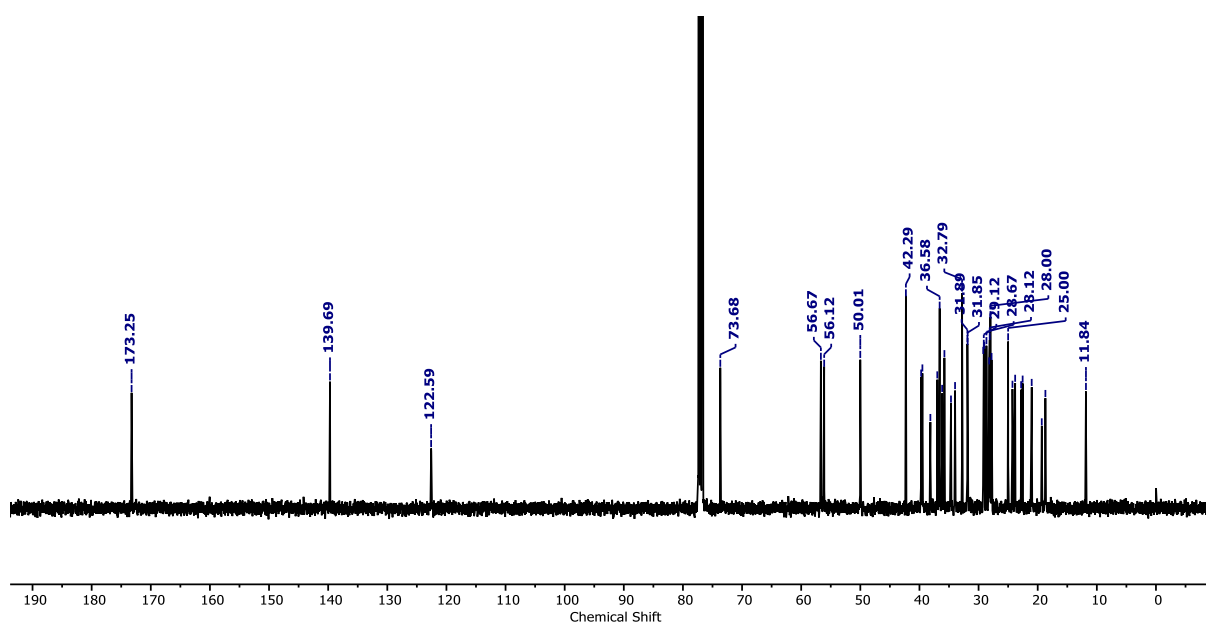


Figure A5 ^{13}C NMR spectrum of compound **3a** in CDCl_3 .

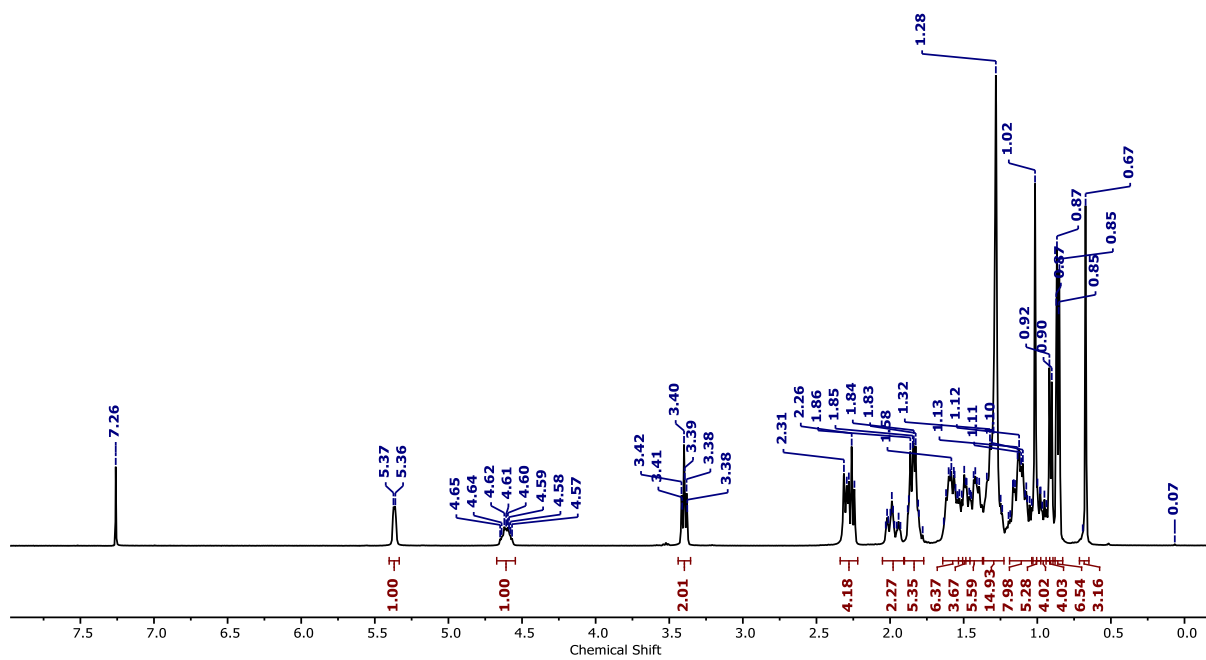


Figure A6 ^1H NMR spectrum of compound **3b** in CDCl_3 .

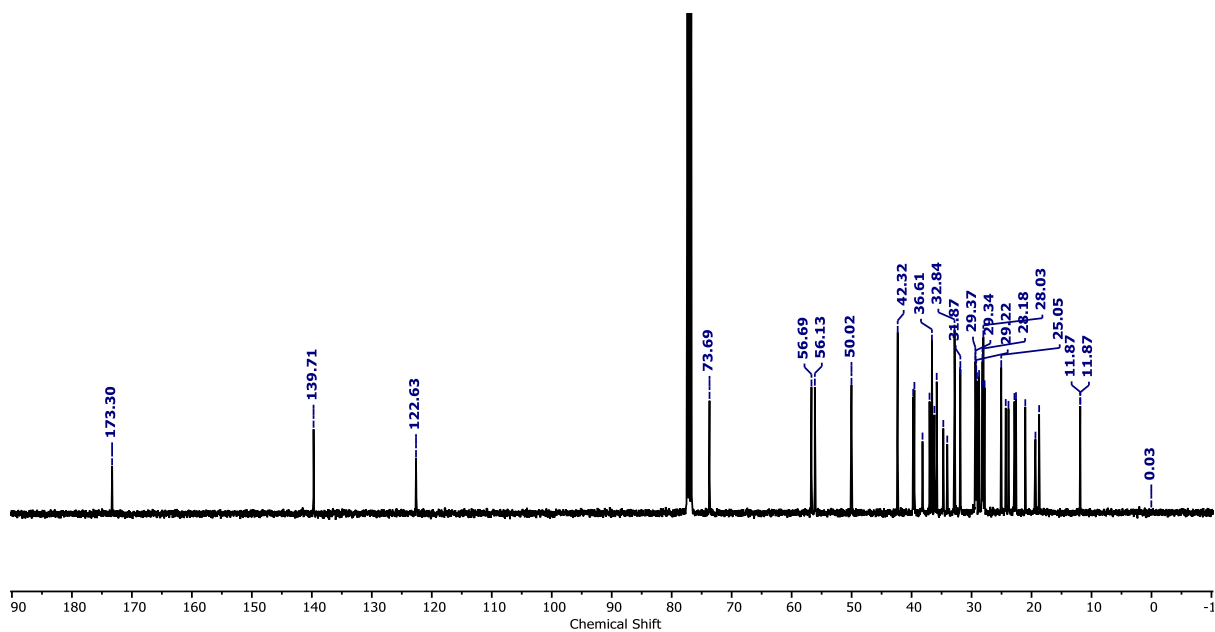


Figure A7 ^{13}C NMR spectrum of compound **3b** in CDCl_3 .

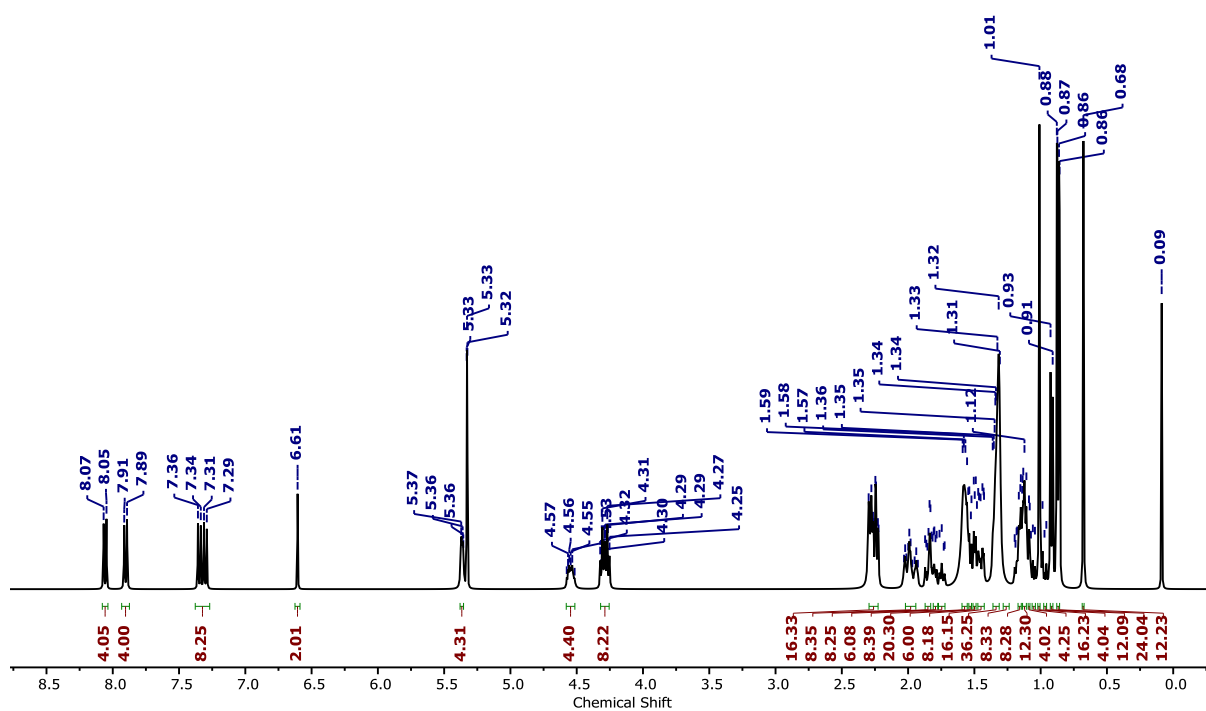


Figure A8 ^1H NMR spectrum of compound **TAP-9** in CD_2Cl_2 .

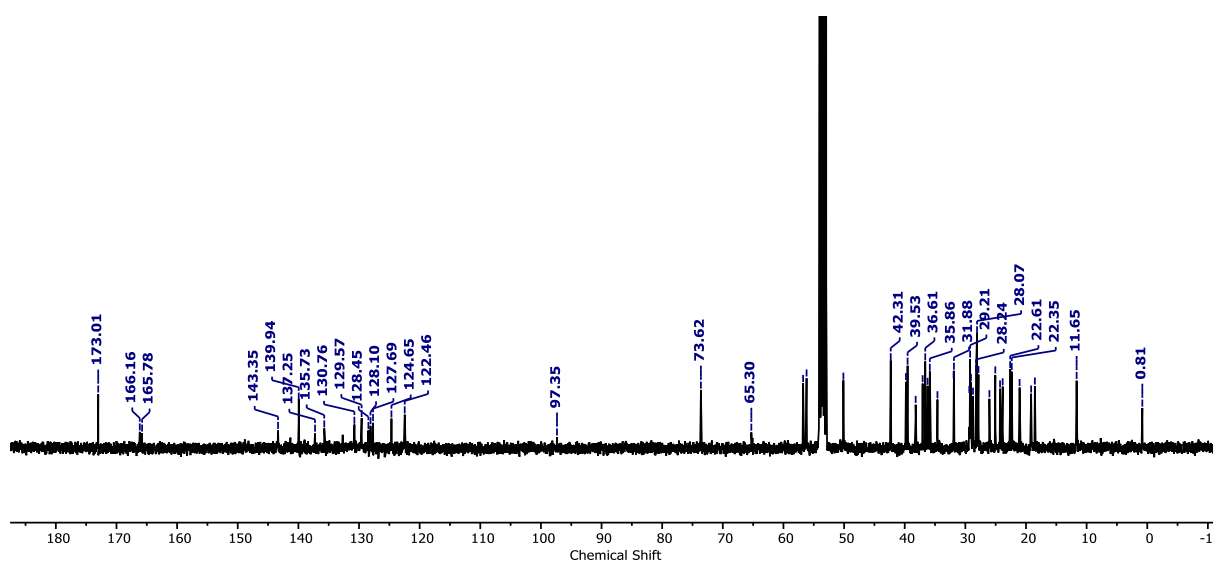


Figure A9 ^{13}C NMR spectrum of compound TAP-9 in CD_2Cl_2 .

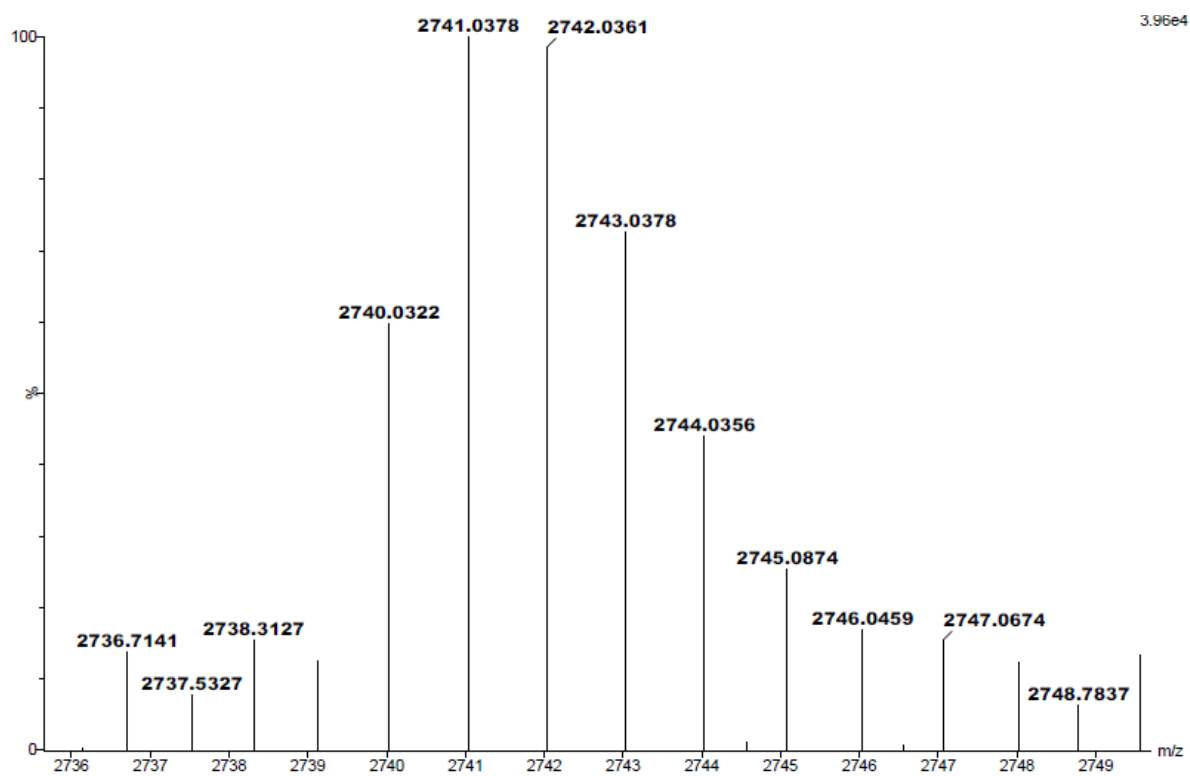


Figure A10 HRMS spectrum of compound TAP-9.

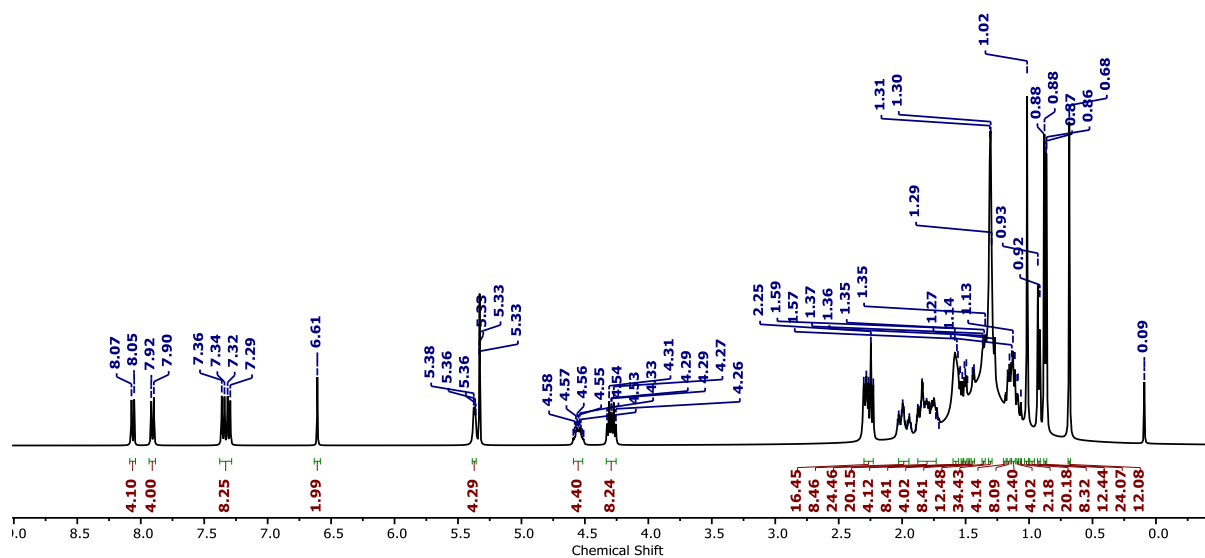


Figure A11 ^1H NMR spectrum of compound TAP-10 in CD_2Cl_2 .

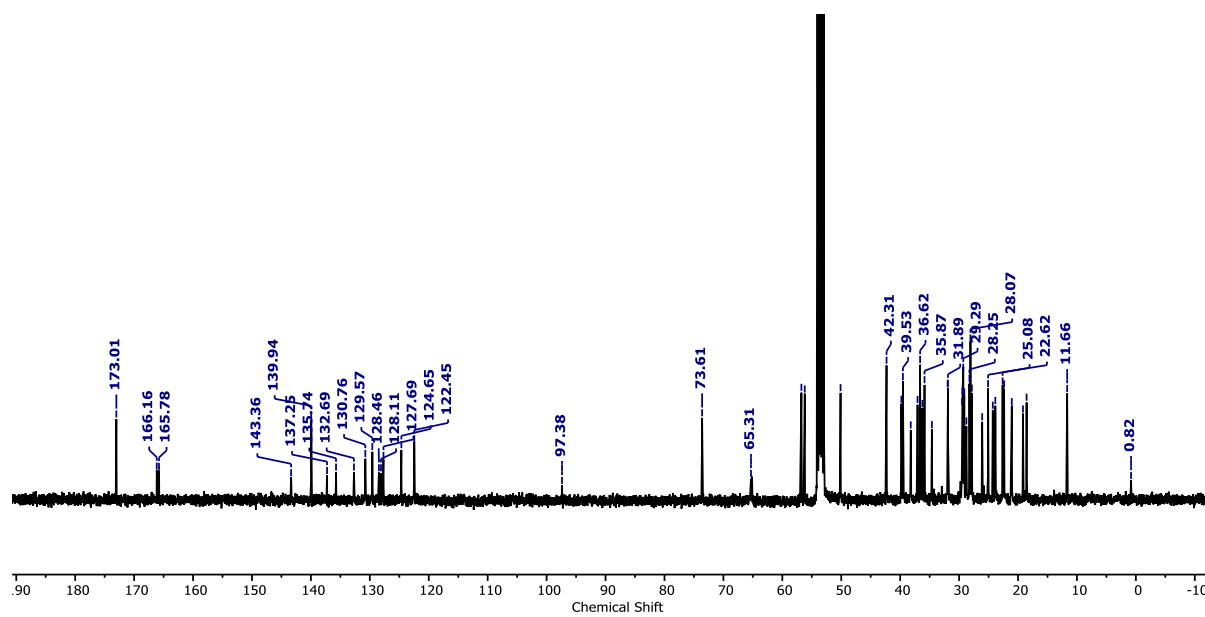


Figure A12 ^{13}C NMR spectrum of compound TAP-10 in CD_2Cl_2 .

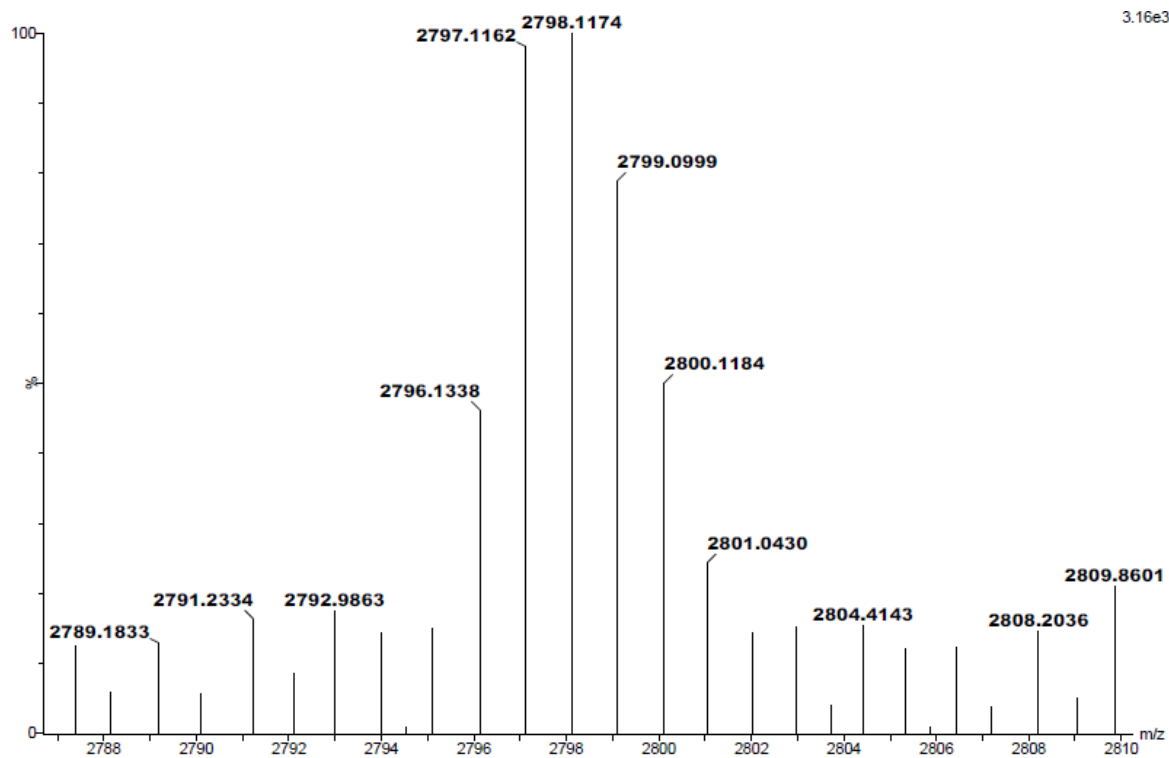


Figure A13 HRMS spectrum of compound TAP-10.

TGA Curves:

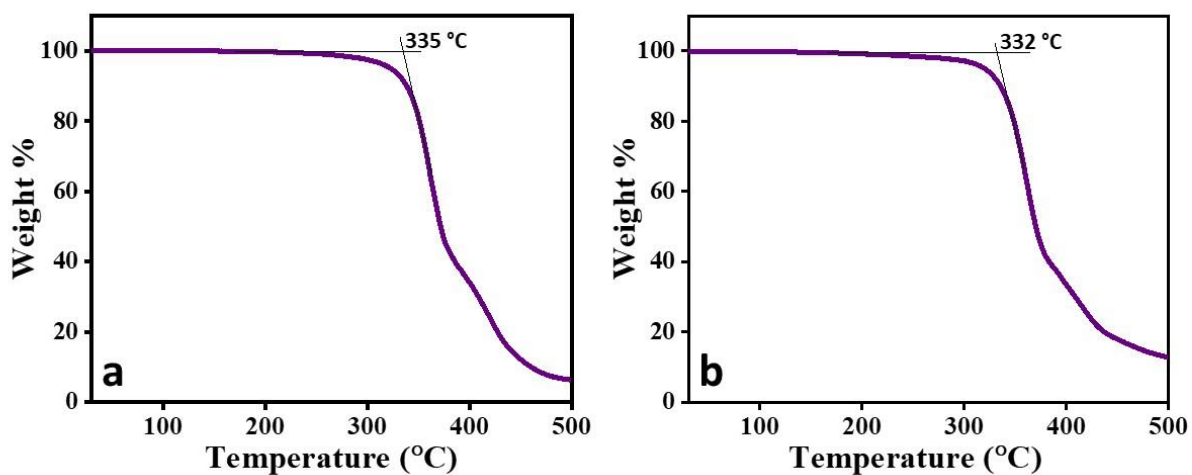


Figure A14 TGA thermographs of compounds (a) TAP-9, (b) TAP-10, obtained at a rate of 5 °C/min.

X-Ray Diffraction Studies:

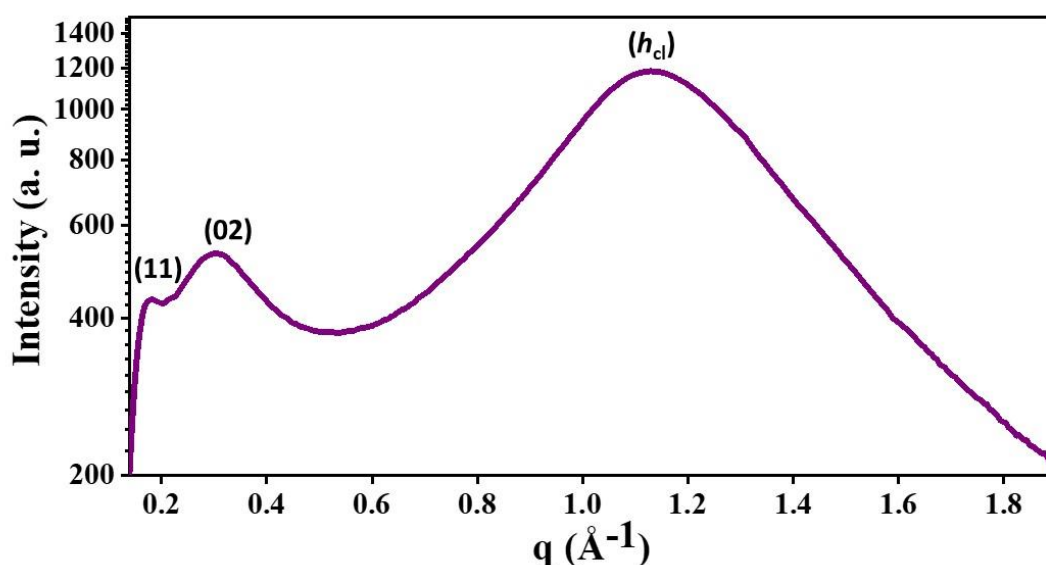


Figure A15 Wide angle X-ray diffraction of **TAP-10**, representing the Col_r phase at 85°C , h_{cl} – due to cholesterol - cholesterol chain correlations.

Table A1 The observed and calculated d-spacings and corresponding reflecting planes for the diffraction peaks indexed on the Col_r lattice at 85°C for the compound **TAP-9** and at 80°C for the compound **TAP-10**. The d-spacing is calculated by using the relation: $d_{cal} = \frac{1}{\sqrt{\frac{h^2}{a^2} + \frac{k^2}{b^2}}}$, where

h, k are the Miller indices and a and b are the lattice parameters.

(hkl)	<i>d-spacing</i> <i>Experimental</i> d_{obs} (Å)	<i>d-spacing</i> <i>Calculated</i> d_{cal} (Å)	<i>Lattice parameters</i>
TAP-9			
11	32.36	32.36	$a = 46.65 \text{ \AA}$ and $b = 44.92 \text{ \AA}$
02	22.46	22.46	
04	11.42	11.23	
h_{cl}	5.82	Fluid cholesterol – cholesterol chain correlations	
84	5.09	5.18	
68	4.30	4.55	
h_c	3.51	Disc – disc separations	
TAP-10			
11	35.19	35.19	$a = 64.51 \text{ \AA}$ and $b = 41.98 \text{ \AA}$
02	20.99	20.99	
h_{cl}	5.53	Fluid cholesterol – cholesterol chain correlations	

Thin film photophysical studies:

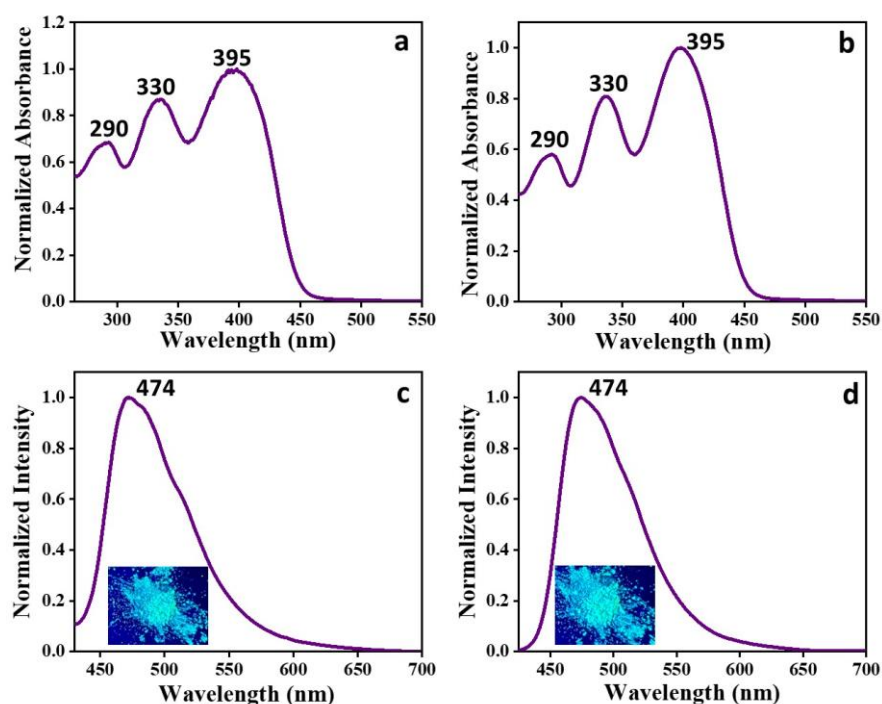


Figure A16 Absorption spectra (a, b) and emission spectrum (c, d) of compounds **TAP-9** and **TAP-10**, respectively, in thin-film state (inset showing the optical photograph of compound under UV-light exhibiting the solid-state fluorescent behavior).

DFT analysis:

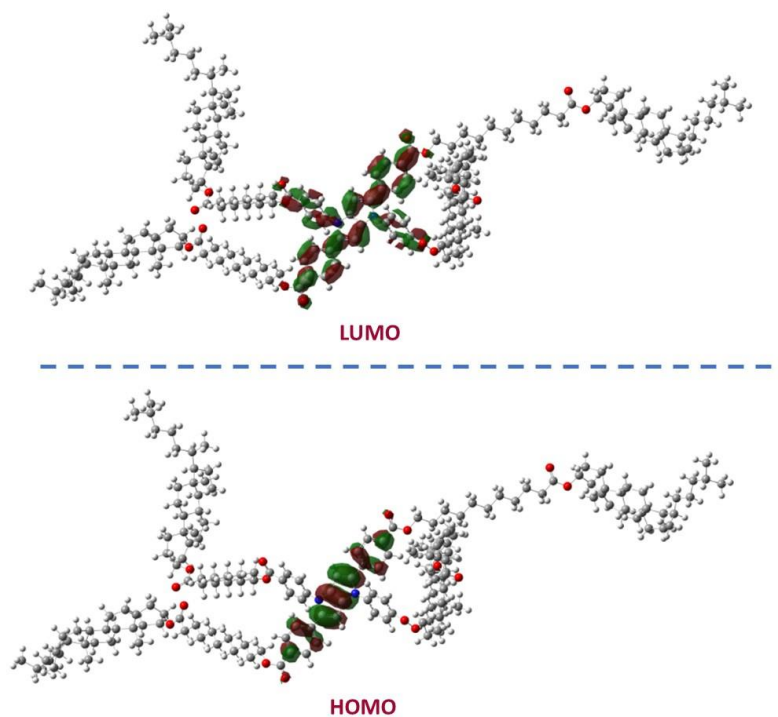
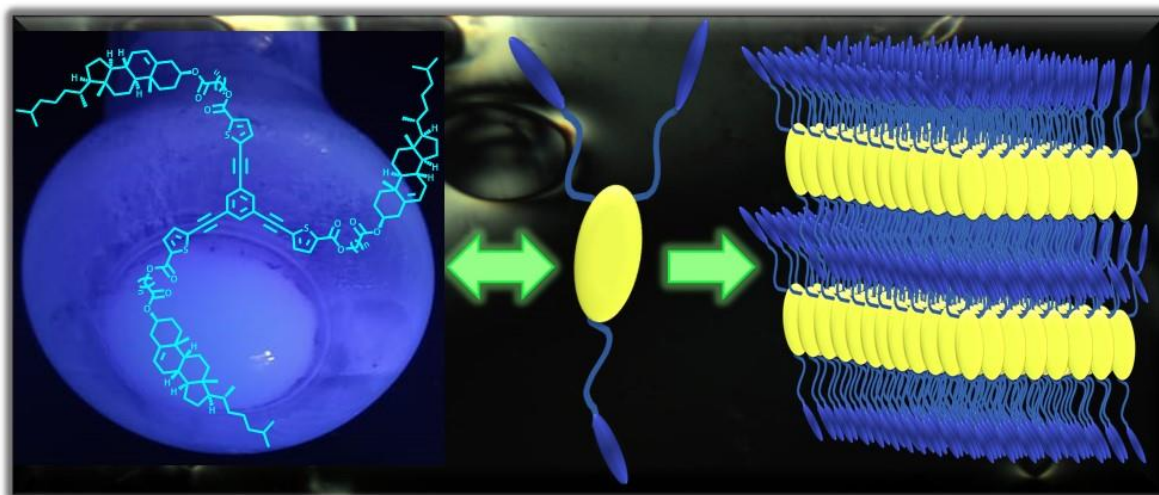


Figure A17 HOMO – LUMO frontier orbitals of compound **TAP-9**.

Chapter 4

Synthesis of new fluorescent star-shaped liquid crystals derived from thiophene and cholesterol unit

The development of microscopic ordering in supramolecular assemblies has piqued the great interest of material chemists because molecular architecture plays an important role in the optoelectronic properties of the material. The molecular engineering of liquid crystals (LCs) has gained expedient space in the field of supramolecular self-assembled systems. Here, we have successfully designed and synthesized the thiophene-induced cholesterol-decorated LCs, with varying spacer alkyl chain lengths. All the derivatives are thermally stable and exhibit a lamellar organization with a significant mesophase thermal range. Additionally, lamellar mesophase is readily frozen into a glassy state at room temperature. Detailed electron density mapping and small-angle/wide-angle X-ray scattering (SAXS/WAXS) studies further confirmed the lamellar assemblies. Besides that, these novel materials showed blue luminescence in solution and thin-film state. A significant value of fluorescence quantum yield and lifetime is obtained for all the compounds.



4.1 Introduction

Over recent years, a great interest of scientist efforts has been dedicated to developing microscopic ordering in supramolecular assemblies because the molecular architecture of a system plays an important role in the properties, such as optical, electrical, enantioselective heterogeneous catalysis, of molecular materials.^{1,2} In this aspect, liquid crystalline systems are of great interest because of their outstanding self-assembly abilities to form mesophase and increasing scope in organic electronics.³⁻¹² Supramolecular assemblies generate by the profound balance between molecule-substrate and intramolecular interactions.¹³ Molecular shapes, terminal groups and flexible alkyl chains are the fundamental variables and strategies for designing new liquid crystals (LCs) with a particular type of molecular organization in a specific temperature range.¹⁴⁻¹⁶

Discotic liquid crystals (DLCs) with fluorescence properties in the solid state are paid much attention due to their effective amalgamation of inherent luminescent ability and molecular self-assembly in a molecule.^{17,18} Therefore, DLCs are prominent materials for various applications such as thin film transistors, organic light-emitting diodes, organic solar cells, photovoltaic cells, etc.^{3,19-21} Furthermore, the inclusion of chiral mesogenic units into the DLCs leads to the highly ordered helical organization.²²⁻²⁴ The helicoidal arrangement of molecules plays a significant role in designing responsive materials, chirality sensors, and chiroptical devices.^{23,24} The design of a new luminescent LC molecule is important for understanding the supramolecular architecture and its influence on the material properties. Consequently, the system's optical and electronic properties can be adjusted at the molecular level by using different organic chromophores.^{25,26}

Incorporating the heterocycle units into the design of LCs can manifest very exciting properties in the system. Heterocycle, in principle, influence the polarization and polarizability as well as the shape of the molecule, which in turn changes the type of the mesophase, geometry, mesophase transition temperature, luminescence and many other properties.²⁷ Many heterocycles, such as thiophene, pyrazole, isoxazole, coumarin, 1,3,4-oxadiazole and 2,1,3-benzothiadiazole, gained enormous attention from the LC community over the last few years.²⁷⁻³⁵ Many reports in the literature show that thiophene-based LC materials played an important role in organic semiconducting materials because of their resourceful/unique chemistry and excellent electronic properties.^{7,36-41} Thiophene, a five-membered heterocycle ring used as the molecular core in LCs, can effectively increase the optical anisotropy, fast switching time, viscosity and provide molecules with relatively low melting point.⁴²⁻⁴⁶

In this chapter, we have explored the thiophene-constituted LCs, as thiophene derivatives were attractive materials for various advanced applications. In this text, a new series of lamellar discotic mesogens consisting of a central 1,3,5-triethynylbenzene directly linked to thiophene and decorated by side mesogenic cholesterol unit linked via different alkyl spacers. Thiophene-based DLCs reported from our group suggest that the incorporation of thiophene moieties at the central part plays an important role by stabilizing the mesophase in wide thermal range through intermolecular S...S interactions. Furthermore, the π - π stacking is also required for efficient charge transport.^{7,47} Also, the cholesterol is incorporated into the molecule with the prime objective of inducing chirality in the system. Hence the molecular chirality enables LCs to self-organize into the helicoidal arrangement. Furthermore, the insertion of double and triple bonds in organic molecules supports the formation of a highly conjugated system. As a result, it can enhance or induce these materials' luminescent properties, which is important for their use in organic devices.

In one previous chapter, we describe the synthesis and organization of cyclictriphosphazene-based DLCs where molecular chirality successfully transfers to the supramolecular chirality and leads to the helicoidal organization of the mesogens.²² These cyclictriphosphazene-based materials show very high clearing temperatures and are also non-fluorescent. Therefore, with this motivation of decreasing clearing temperature and inducing luminescent behaviour in chiral LCs, we successfully synthesized thiophene-induced chiral LCs with a significant mesophase temperature range and showing interesting luminescent behaviour in solution and solid state. The structure deduction of newly synthesized LCs and their intermediates were performed systematically using standard characterization techniques. The mesophase and structure-property relationship of all the target materials was investigated using polarising optical microscopy (POM), differential scanning calorimetry (DSC), and small-angle/wide-angle X-ray scattering (SAXS/WAXS) measurements.

4.2 Results and discussions

4.2.1 Synthesis, Structural Characterization and Thermal stability

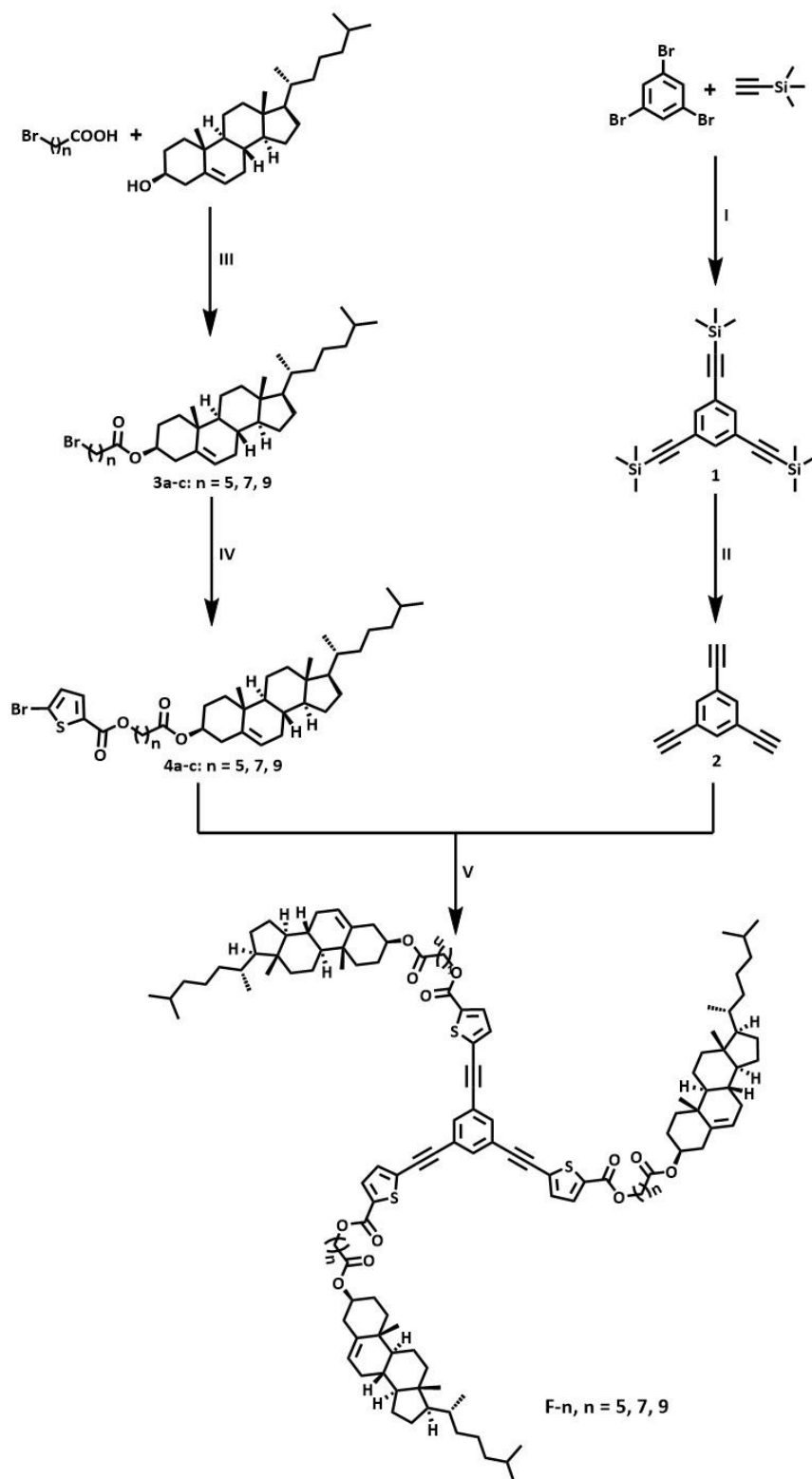
The synthesis of star-shaped thiophene-induced cholesterol-decorated LCs (**F-n**, n = 5, 7, 9) are illustrated in Scheme 5.1 and detailed synthetic procedure in the experimental section of this chapter. The synthetic process started with the esterification reaction between cholesterol and bromoalkanoic acid, yielding the ester derivatives compound **3(a-c)**. The ester derivative was then subjected to the phase transfer catalysis reaction with 5-bromo-2-thiophenecarboxylic

acid in refluxing aq. KOH in the presence of TOAB to give the corresponding thiophene-induced intermediate compounds **4(a-c)**. On the other hand, 1,3,5-triethynylbenzene were synthesized by sonogashira coupling between 1,3,5-tribromobenzene and trimethylsilylacetylene, which subsequently yielded a protected alkyne intermediate compound **1**, which further underwent a deprotection reaction in the presence of methanol and potassium carbonate. The thiophene intermediate compound **4(a-c)** underwent sonogashira coupling reaction with 1,3,5-tribromobenzene, to give the desired targeted compound **F-n** (yield: 35 %, 33 % and 32 % for **F-5**, **F-7** and **F-9**, respectively).

The purity and identity of all the derivatives and intermediate compounds have been analyzed by standard analytical techniques such as ^1H NMR, ^{13}C NMR, IR and mass spectroscopy (Figure A1-A23). All characterization results were well in accordance with the proposed molecular structure of the final synthesized compounds. The thermal stability of all the targeted compounds was determined using thermogravimetric analysis (TGA) (Figure A24 and Table 4.1); apparently, all the compounds presented good thermal stability, with a decomposition temperature above 300 °C.

4.2.2 Mesomorphic behaviour

The mesomorphic behaviour of all the final compounds was first observed under POM during heating/cooling cycles and found to be enantiotropic liquid crystalline materials. The fluidity of the LC phase was determined by the shearing test of the compounds during heating and cooling cycles, which showed fluidic behaviour and birefringent textures, representing their anisotropic nature. The optical photomicrographs recorded during the cooling cycle are depicted in Figure 4.1 as the representative illustration. The fluidic nature and textures showed the characteristics of the lamellar phase. All the compounds displayed the highly ordered lamellar phase during the heating cycle. However, during the cooling cycle, compounds **F-5** and **F-7** first arrange themselves into disordered mesophase, which changes to an ordered phase at a lower temperature and then stabilizes in a glassy state at room temperature. The LC phase transitions and corresponding enthalpy changes of all the compounds were determined using DSC (Figure 4.2 and Table 4.1). Even so, the transition from a glassy state to mesophase for all the derivatives was not perceived in DSC, possibly due to insignificant enthalpy changes.



Scheme 4.1 (I) $\text{Pd(PPh}_3\text{)}_4$, CuI, dry NEt_3 , 60°C , 24 h, Yield = 65 % (II) K_2CO_3 , Methanol, 75°C , 12 h, Yield = 90 % (III) DCC, DMAP, dry DCM, 60°C , 12 h, Yield = 67 % (IV) aq. KOH, TOAB, 100°C , 12 h, Yield = 95 % (V) $\text{Pd(PPh}_3\text{)}_4$, CuI, dry NEt_3 , dry THF, 90°C , 36 h, Yield = 32 % .

In DSC, compounds **F-5** and **F-7** showed an endothermic peak at 106 °C ($\Delta H = 50.83 \text{ kJ mol}^{-1}$) and 89 °C ($\Delta H = 52.25 \text{ kJ mol}^{-1}$), which corresponds to the mesophase to isotropic transitions, respectively. Although, on cooling, the peak referred to isotropic to disordered phase did not appear in the DSC for both the compounds, POM observation revealed the appearance of the mesophase. While the transition perceived at 67.79 °C ($\Delta H = 0.30 \text{ kJ mol}^{-1}$) and 61.27 °C ($\Delta H = 1.42 \text{ kJ mol}^{-1}$), for compound **F-5** and **F-7**, respectively, corresponds to disordered to ordered lamellar mesophase.



Figure 4.1 POM microphotographs of the optical texture of lamellar phases formed by (a) **F-5** at 66 °C, (b) **F-7** at 53 °C, (c) **F-9** at 60 °C, observed on cooling with a rate of 5 °C min⁻¹.

On the other hand, **F-9** directly transformed from isotropic to ordered lamellar mesophase, and the corresponding exothermic transition appeared at 71.63 °C ($\Delta H = 1.78 \text{ kJ mol}^{-1}$). Also, the phase transition observed from POM and DSC data was reproducible across several heating and cooling cycles, which supports the sustainable nature and thermal stability of the lamellar organization of the mesophase. The Figure 4.1 illustrates the first cooling data recorded under POM, while the Figure 4.2 illustrates the 2nd heating and 2nd cooling data via DSC.

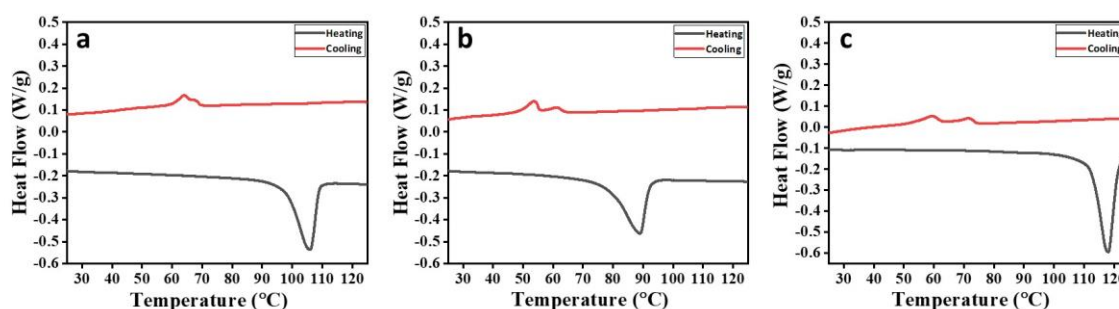


Figure 4.2 DSC thermograms of compounds (a) **F-5**, (b) **F-7**, (c) **F-9**, recorded at a rate of 5 °C/min.

In order to further explore the lamellar organization of the compounds, the temperature-dependent SAXS/WAXS experiments of all the derivatives were performed. The SAXS/WAXS experiments were recorded during cooling from an isotropic state. The X-ray

diffraction pattern of compound **F-5** exhibits three narrow Bragg's peaks in small angle region with d-spacings 58.62 Å, 29.43 Å and 19.62 Å (Figure 4.3a). These peaks could be indexed on

Table 4.1 Thermal behaviour of **F-n** derivatives.^a

C	Heating cycle	Cooling cycle	T _d ^d (°C)
F-5	G 68 ^b lam _o 106 ^c [50.83] Iso	Iso 76 ^b lam _d 67.79 ^c [0.30] lam _o 63.73 ^c [1.98] G	335
F-7	G 63 ^b lam _o 89 ^c [52.25] Iso	Iso 68 ^b lam _d 61.27 ^c [1.42] lam _o 53.51 ^c [4.04] G	325
F-9	G 60 ^b lam _o 118 ^c [72.02] Iso	Iso 71.63 ^c [1.78] lam _o 59.31 ^c [4.27] G	332
^a Enthalpy values in parentheses in kJ mol ⁻¹ and temperature in °C. ^b Phase transition temperatures determined by POM. ^c Phase transition temperatures observed by the DSC technique. ^d Decomposition temperature corresponding to 5 % weight loss. Abbreviation: C = compound; G = glassy; lam _o = ordered lamellar; lam _d = disordered lamellar; Iso = isotropic.			

a one-dimensional lamellar lattice structure and correspond to the reflections from (100), (200) and (300) planes of the lamellar structure, respectively. The calculated lamellar periodicity, a , is found to be 58.85 Å. Further, the X-ray diffraction pattern of the compound showed one non-Bragg's reflection namely, h_{cl} in the wide-angle regime with d-spacing 5.74 Å (Figure 4.3a, Table A1). The h_{cl} peak appears due to the fluid cholesterol - cholesterol chain correlations. The lamellar mesophase organization was exhibited by compound **F-5**, and the observed lattice parameter and miller indices are mentioned in Table A1. The calculated value of the correlation length is 907.75 Å which corresponds to about 15 correlated layers, indicating that the phase is ordered very well. Moreover, the X-ray diffraction pattern of compound **F-7** exhibits two broad Bragg's peaks in small angle region with d-spacings 55.12 Å, and 18.42 Å (Figure A25a) correspond to reflections from (100) and (300) planes of the lamellar structure, respectively. And there is one non-Bragg's peak in the wide-angle regime with d-spacing 5.60 Å, corresponding to h_{cl} (Figure A25a, Table A1). The calculated value of lamellar periodicity, a , is found to be 55.12 Å. Whereas the calculated value of the correlation length is found to be 88.34 Å which corresponds to about 2 correlated layers, indicating that the phase is disordered and corresponds to a molten lamellar phase.

Furthermore, the X-ray diffraction pattern of compound **F-9** is very similar to compound **F-7** and analyzed similarly (Figure A25b, Table A1). The calculated value of lamellar periodicity, a , is found to be 54.63 Å at 65 °C, whereas the calculated value of the correlation length is found to be 70.89 Å which corresponds to about 1 number of correlated layers, indicating that the phase is a molten lamellar phase. Thus, the detailed XRD analysis indicates that compound

F-5, **F-7**, and **F-9** display lamellar organization in their mesophase temperature range. However, the correlation length suggests a high degree of orderliness in **F-5**, compared to compounds **F-7** and **F-9**, possibly due to increasing spacer chain length; the randomness is also increasing in the system.

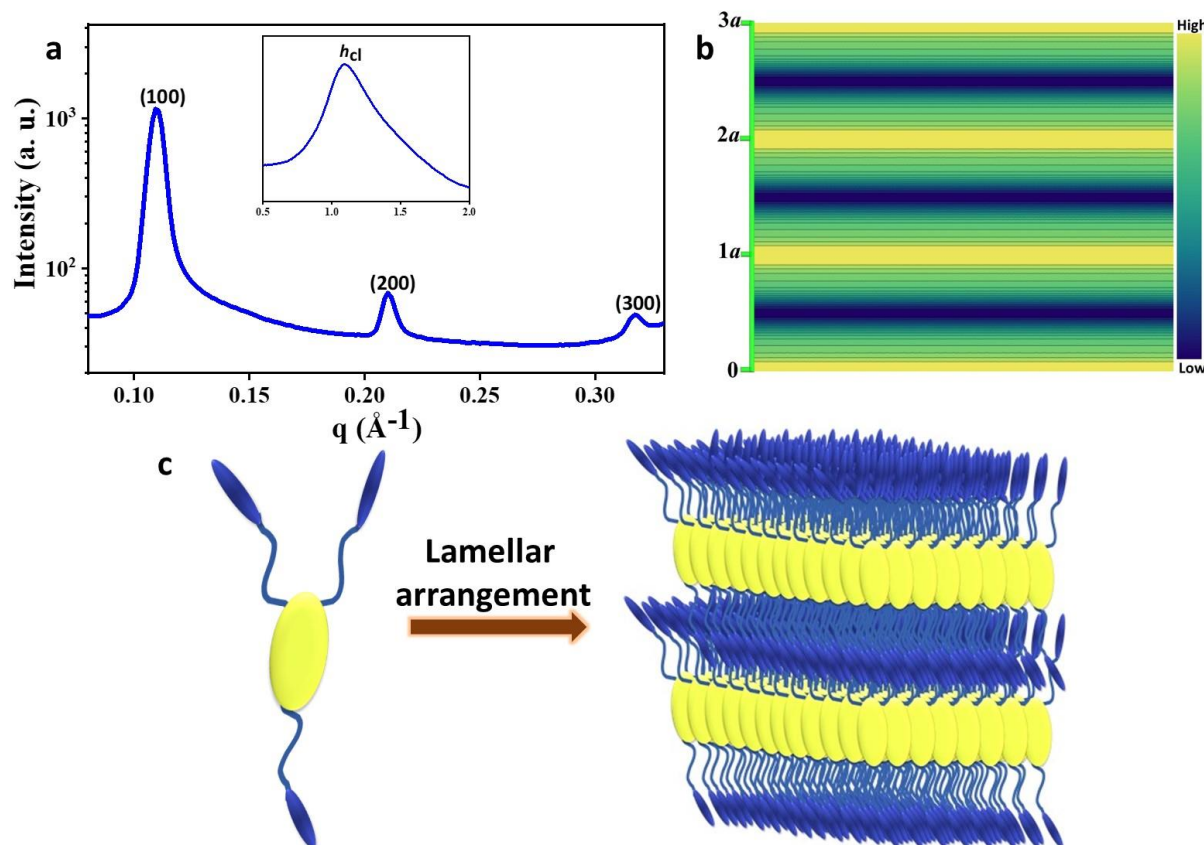


Figure 4.3 (a) Small and wide-angle (inset) X-ray diffraction patterns of the ordered lamellar phase formed by compound **F-5** at 65 °C (lam_o), h_{cl} - fluid cholesterol - cholesterol chain correlations; (b) Reconstructed electron density map corresponding to the lamellar phase of the compound **F-5** at temperature 65 °C. The lamellar periodicity, a , has the value 58.85 Å. Deep yellow represents the highest electron density and deep navy blue is the lowest. (c) Schematic representation of lamellar organization.

4.2.3 Electron density map

Further, to better understand the arrangement of molecules in the lamellar mesophase, electron density maps⁴⁸ have been constructed by using the information of peak Miller planes and their intensities. The electron density map for the compound is shown in Figure 4.3b. All the compound exhibits a lamellar phase, but only compound **F-5** shows a high correlating length; thus, electron density map has been reconstructed only for compound **F-5** (Figure 4.3b). Deep yellow represents the highest electron density, and deep navy blue is the lowest. The map shows

the one-dimensional regular periodic structure. Figure 4.3c demonstrated the lamellar organization of molecules.

4.2.4 Photophysical behavior

In order to explore the photophysical behavior of all the derivatives **F-n**, the absorption and emission experiments in solution as well as in the solid state were performed. The solution state experiments were carried out in 10^{-5} M THF solutions. All three derivatives showed similar peaks in absorption (Figure 4.4a-c) and emission (Figure 4.5a-c) spectra regardless of the chain length. From the Figure 4.4, it is visible that two peaks appeared in the solution absorption state spectra of all the compounds; the peak at 326 nm arises due to the π - π^* transition and the other at 347 nm is due to the n - π^* transition.²² The absorption peaks in the thin-film state were observed to be around the same as those in the solution state in the 300-400 nm range. All the derivatives show blue fluorescence in the solution state, where emission maxima appeared at 372 nm. In addition, in comparison to the solution state, the absorption bands in the solid state are broad and structureless (Figure A26a-c), while the emission peak become broader and red shifted (Figure A27a-c); due to the increased intermolecular interactions.⁴⁹ Relative quantum yield measurements were performed in THF for all the derivatives to get more insights into the luminescence efficacy. Quinine sulphate in 0.1 M sulphuric acid was chosen as a standard as it absorbs around the same wavelength ($\lambda_{\max} = 340$ nm) as that of **F-n** ($\lambda_{\max} = 326$ nm) compounds. The quantum yield value with respect to quinine sulphate (0.54 in 0.1 M H_2SO_4) for compounds **F-5**, **F-7**, and **F-9** is found to be 0.71, 0.78 and 0.48, respectively (Table 4.2).

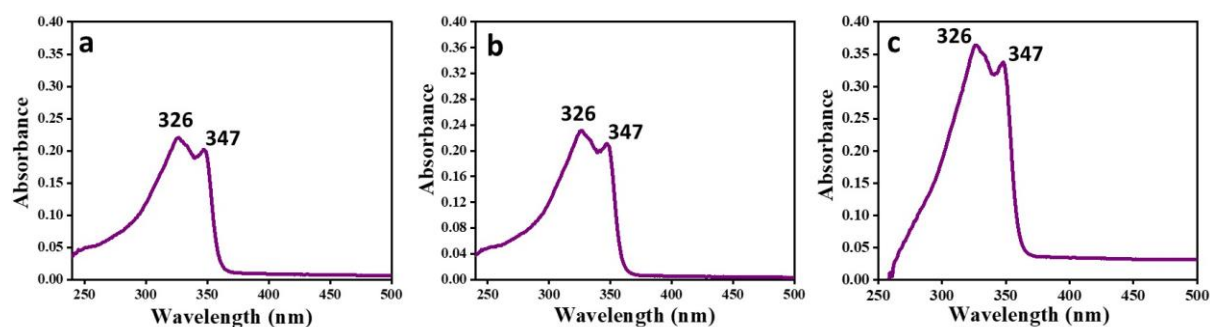


Figure 4.4 Absorption spectra of compounds (a) **F-5**, (b) **F-7**, (c) **F-9**, in 10^{-5} M THF solution.

Besides this, fluorescence decay and lifetime measurement studies were carried out in THF solutions using a time-correlated single photon counting technique. The excitation wavelength is 326 nm, corresponding to absorption maxima and a band-pass filter at 447 nm is used to measure the fluorescence decay profiles shown in Figure A28. The decay curve (red coloured) was fitted with the instrument response function (IRF) (black coloured). The fitted (blue-

coloured) curve overlaps with the decay curve (red). In all the cases, the curves were better fitted by using a mono-exponential function. The average lifetime for all the derivatives comes to around 1.20 ns (Table 4.2).

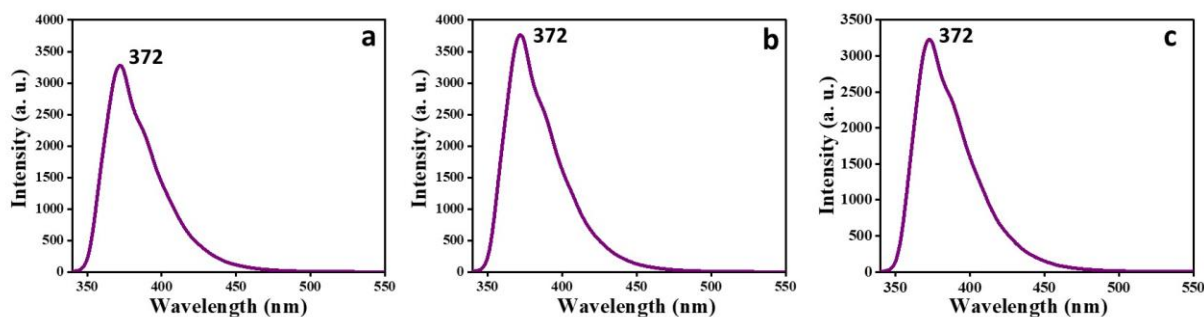


Figure 4.5 Emission spectra of compounds (a) **F-5**, (b) **F-7**, (c) **F-9**, in 10^{-5} M THF solution, where the excitation wavelength is 326 nm.

In addition, as shown in Figure 4.6a, material exhibit considerable solid-state luminescence behaviour, piqued our interest in the aggregation-induced emission (AIE) phenomena. As an illustrative case, THF- H_2O water experiments were carried out to examine the ability of derivative **F-7** as AIE moiety (Figure 4.6b), and we discovered that the luminescence intensity steadily decreases with increasing water ratio. However, the compounds show significant blue emission in the solid state but do not exhibit AIE behaviour. Additionally, we carried out the solvent-dependent fluorescence experiment with various solvents of different polarity (Figure 4.6c); aside from the change in luminescence intensity, no significant shifting was seen with increasing polarity of the solvents.

4.3 Conclusion

In conclusion, we reported a new series of star-shaped LCs (**F-n**, $n = 5, 7, 9$) with varying spacer alkyl chain lengths based on the thiophene-induced cholesterol system. Their synthesis and mesomorphic, photophysical properties were thoroughly explained. All the highly stable derivatives acquire lamellar mesophase self-assembly, as confirmed by POM and XRD, over a significant thermal range. Photophysical studies showed that all three derivatives display blue-emission in solution and thin-film states, exhibiting notable fluorescence quantum yield. Furthermore, these compounds stabilized in a glassy state at room temperature, which revealed their potential application for many exciting applications. Also, the bulky cholesterol broadens the material range for chiroptical characteristics.

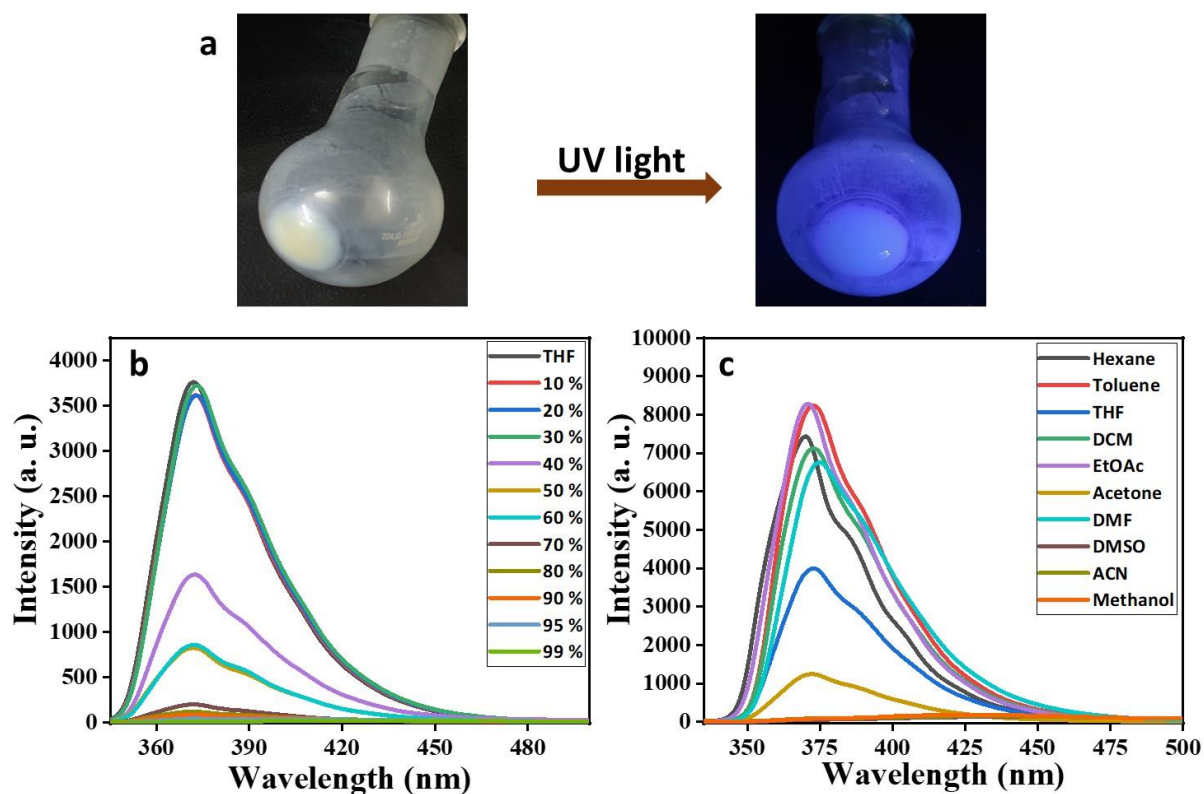


Figure 4.6 (a) Optical photographs of compound **F-8** in solid state under 365 nm light; (b) Emission spectra of compound **F-8** in different THF-H₂O ratio; and (c) Emission spectra of compound **F-8** in solvents of different polarities (10⁻⁵ M).

Table 4.2 Photophysical data of **F-n** derivatives.

C	A_{solution}^a peaks (nm)	$E_{\text{solution}}^{a,c}$ peaks (nm)	A_{solid} peaks (nm)	E_{solid}^c peaks (nm)	τ (α) (ns)	τ_{av}^d (ns)	Φ_{F}^e
F-5	326, ^b 347	372	300-400	416	1.22 (1.00)	1.22	0.71
F-7	326, ^b 347	372	300-400	430	1.21 (1.00)	1.21	0.78
F-9	326, ^b 347	372	300-400	445	1.20 (1.00)	1.20	0.48

^a In micro molar THF solution. ^b λ_{max} . ^c Obtained after exciting at their corresponding λ_{max} . A_{solution} : absorbance in the solution state, E_{solution} : emission in the solution state. A_{solid} : absorbance in thin film, E_{solid} : emission in thin film. ^d τ_{av} = average lifetime. ^e Φ_{F} = fluorescence quantum yield.

4.4 Experimental section

4.4.1 General procedure for the synthesis of compound 1:

Compound 1 was synthesized following the previously reported procedure.⁵⁰ In a clean, dry 100 mL, double neck round bottom flask, 60 mL of dry triethylamine was taken under an inert atmosphere and was purged for approximately 30 min. After this, 1,3,5-tribromobenzene (1 equiv.), was added to the flask and again purged for 15 min, followed by the addition of Pd(PPh₃)₄ (0.06 equiv.) and CuI (0.06 equiv.), while carefully maintaining the inert atmosphere. Trimethylsilylacetylene (5 equiv.) was then added to the reaction mixture. The reaction mixture refluxed for 24 h. The reaction mixture was then cooled to room temperature and neutralized by HCl (5 N). The crude product was extracted using DCM. The organic phase dried over Na₂SO₄ was concentrated in a vacuum. The crude product was then purified by flash column chromatography using silica gel with a mixture of hexane/ethyl acetate (v/v, 100/0.1) as an eluent. This compound was directly used for the next step without any further purification.

4.4.2 General procedure for the synthesis of compound 2:

Compound 1 (1 equiv.) was dissolved in methanol (40 mL) in a 100 mL round bottom flask. To this reaction mixture, anhyd. K₂CO₃ (6 equiv.) was added. The reaction mixture was refluxed for 12 h. After this, the mixture was cooled down to room temperature, and the organic layer was extracted using DCM. The organic phase dried over Na₂SO₄ was concentrated in a vacuum. The crude product was purified via crystallization using hexane. Yield = 90 %. The ¹H NMR (Figure A1) and ¹³C NMR (Figure A2), spectra are given in Appendix III.

Characterization details of compound 2:

¹H NMR (400 MHz, CDCl₃, δ in ppm) 7.57 (s, 3H), 3.10 (s, 3H).

¹³C NMR (100 MHz, CDCl₃, δ in ppm) 135.79, 123.09, 81.76, 78.82.

FTIR (cm⁻¹) 3277, 1580, 887.

4.4.3 General procedure for the synthesis of compound 3a-c:

This reaction follows the previously reported procedure.²² Cholesterol (1.2 equiv.) was added to the stirred solution of bromoalkanoic acid (2 g, 1 equiv.) in dry DCM (40 mL). The resulting mixture was stirred under a nitrogen atmosphere, and DMAP (catalytic amount) was added to

the solution. A solution of DCC (1.25 equiv.) in DCM was further added to the reaction mixture, and the mixture was stirred at 60 °C for 12 h. The reaction mixture was filtered, and the filtrate obtained was concentrated in a vacuum. The crude product was then purified by column chromatography using silica gel with a mixture of hexane/ethyl acetate (v/v, 100/1) as an eluent. The white solid obtained was air-dried and stored in a clean sample vial. Yield = 75 – 78 %. The ^1H NMR and ^{13}C NMR (Figure A3-A8), spectra are given in Appendix III.

Characterization details of 3(a-c):

3a: Yield = 76 %, ^1H NMR (400 MHz, CDCl_3 , δ in ppm) 5.37 (d, $J = 5.5$ Hz, 1H), 4.66 – 4.57 (m, 1H), 3.41 (t, $J = 6.8$ Hz, 2H), 2.29 (t, $J = 7.5$ Hz, 4H), 2.03 – 1.93 (m, 2H), 1.91 – 1.82 (m, 5H), 1.68 – 1.62 (m, 2H), 1.57 – 1.53 (m, 2H), 1.51 – 1.42 (m, 6H), 1.40 – 1.31 (m, 3H), 1.28 – 1.23 (m, 1H), 1.19 – 1.05 (m, 8H), 1.01 (s, 4H), 0.96 (dd, $J = 11.4, 5.3$ Hz, 2H), 0.91 (d, $J = 6.5$ Hz, 3H), 0.86 (dd, $J = 6.6, 1.9$ Hz, 6H), 0.67 (s, 3H).

^{13}C NMR (100 MHz, CDCl_3 , δ in ppm) 173.01, 139.79, 122.79, 122.79, 74.02, 56.82, 56.27, 50.16, 42.45, 39.86, 39.66, 38.29, 37.13, 36.32, 35.93, 34.56, 33.65, 32.55, 32.04, 32.00, 28.37, 28.15, 27.95, 27.76, 24.42, 24.31, 23.97, 22.96, 22.71, 21.17, 19.46, 18.86, 12.00.

FTIR (cm^{-1}) 2948, 2886, 2866, 1733, 1466, 1373, 1257, 1990, 1176.

3b: Yield = 78 %, ^1H NMR (400 MHz, CDCl_3 , δ in ppm) 5.37 (d, $J = 4.9$ Hz, 1H), 4.65 – 4.58 (m, 1H), 3.39 (t, $J = 6.7$ Hz, 2H), 2.34 – 2.22 (m, 4H), 2.04 – 1.92 (m, 2H), 1.89 – 1.77 (m, 5H), 1.65 – 1.52 (m, 6H), 1.51 – 1.40 (m, 6H), 1.36 – 1.30 (m, 6H), 1.25 (s, 2H), 1.16 – 1.05 (m, 7H), 1.01 (s, 4H), 0.96 (d, $J = 11.1$ Hz, 1H), 0.91 (d, $J = 6.3$ Hz, 3H), 0.86 (d, $J = 6.7$ Hz, 6H), 0.67 (s, 3H).

^{13}C NMR (100 MHz, CDCl_3 , δ in ppm) 173.30, 139.80, 122.75, 73.88, 56.81, 56.25, 50.14, 42.43, 39.85, 39.64, 38.28, 37.12, 36.72, 36.31, 35.92, 34.73, 34.00, 32.84, 32.03, 31.98, 29.01, 28.53, 28.36, 28.14, 28.10, 27.94, 25.03, 24.41, 23.96, 22.96, 22.70, 21.16, 19.46, 18.84, 11.98.

FTIR (cm^{-1}) 2944, 2888, 2868, 1732, 1469, 1368, 1245, 1184, 1172.

3c: Yield = 75 %, ^1H NMR (400 MHz, CDCl_3 , δ in ppm) 5.37 (d, $J = 4.0$ Hz, 1H), 4.66 – 4.55 (m, 1H), 3.40 (t, $J = 6.9$ Hz, 2H), 2.33 – 2.24 (m, 4H), 2.03 – 1.93 (m, 2H), 1.89 – 1.80 (m, 5H), 1.64 – 1.52 (m, 6H), 1.52 – 1.45 (m, 3H), 1.43 – 1.38 (m, 3H), 1.34 – 1.27 (m, 10H), 1.21

– 1.05 (m, 8H), 1.02 (s, 4H), 0.96 (dd, $J = 11.4, 5.3$ Hz, 2H), 0.91 (d, $J = 6.5$ Hz, 3H), 0.86 (dd, $J = 6.6, 1.8$ Hz, 6H), 0.67 (s, 3H).

^{13}C NMR (100 MHz, CDCl_3 , δ in ppm) 173.41, 139.5, 122.75, 73.84, 56.83, 56.28, 50.17, 42.45, 39.88, 39.66, 38.31, 37.15, 36.74, 36.33, 35.94, 34.83, 34.14, 32.95, 32.05, 32.01, 29.37, 29.28, 29.19, 28.83, 28.37, 28.28, 28.16, 27.96, 25.16, 24.43, 23.97, 22.97, 22.71, 21.18, 19.47, 18.86, 12.00.

FTIR (cm^{-1}) 2930, 2900, 2952, 1730, 1465, 1376, 1225, 1173.

4.4.4 General procedure for the synthesis of compound 4a-c:

5-Bromo-2-thiophene carboxylic acid (1.5 equiv.) was added to the aq. solution of KOH (50 mL), and the system was continuously stirred for 10-15 min at 85 °C. After that, compound 3 (1 equiv.) was added to the reaction mixture, followed by the catalytic amount of TOAB. The reaction mixture was refluxed for about 12 h. The reaction mixture was then cooled to room temperature and extracted using DCM. The organic phase dried over Na_2SO_4 was concentrated in a vacuum. The crude product was then purified by column chromatography using silica gel with a mixture of hexane/ethyl acetate (v/v, 100/5) as an eluent. The white solid obtained was air-dried and stored in a clean sample vial. Yield = 88 – 90 %. The ^1H NMR and ^{13}C NMR (Figure A9-A14), spectra are given in Appendix III.

Characterization details of 4(a-c):

4a: Yield = 89 %, ^1H NMR (400 MHz, CDCl_3 , δ in ppm) 7.54 (d, $J = 4.0$ Hz, 1H), 7.06 (d, $J = 4.0$ Hz, 1H), 5.36 (d, $J = 5.0$ Hz, 1H), 4.66 – 4.56 (m, 1H), 4.27 (t, $J = 6.5$ Hz, 2H), 2.30 (t, $J = 7.4$ Hz, 4H), 2.03 – 1.94 (m, 2H), 1.86 – 1.80 (m, 3H), 1.78 – 1.65 (m, 5H), 1.57 – 1.51 (m, 3H), 1.51 – 1.42 (m, 6H), 1.38 – 1.30 (m, 3H), 1.28 – 1.24 (m, 1H), 1.16 – 1.05 (m, 7H), 1.01 (s, 3H), 0.98 – 0.93 (m, 2H), 0.91 (d, $J = 6.5$ Hz, 3H), 0.86 (dd, $J = 6.6, 1.8$ Hz, 6H), 0.67 (s, 3H).

^{13}C NMR (100 MHz, CDCl_3 , δ in ppm) 172.98, 161.22, 139.74, 135.13, 133.65, 131.00, 122.76, 120.21, 73.96, 65.31, 56.80, 56.26, 50.15, 42.43, 39.86, 39.64, 38.27, 37.11, 36.71, 36.31, 35.91, 34.62, 32.03, 31.98, 28.48, 28.35, 28.13, 27.94, 25.62, 24.79, 24.41, 23.96, 22.94, 22.69, 21.16, 19.43, 18.84, 11.98.

FTIR (cm^{-1}) 2944, 2898, 1717, 1418, 1279, 1249, 1089.

4b: Yield = 90 %, ^1H NMR (400 MHz, CDCl_3 , δ in ppm) 7.53 (d, $J = 4.0$ Hz, 1H), 7.06 (d, $J = 4.0$ Hz, 1H), 5.36 (d, $J = 4.3$ Hz, 1H), 4.65 – 4.56 (m, 1H), 4.25 (t, $J = 6.7$ Hz, 2H), 2.31 – 2.24 (m, 4H), 2.02 – 1.93 (m, 2H), 1.87 – 1.81 (m, 3H), 1.75 – 1.68 (m, 3H), 1.62 – 1.58 (m, 3H), 1.56 (t, $J = 2.4$ Hz, 1H), 1.52 (dd, $J = 6.8, 3.4$ Hz, 2H), 1.50 – 1.47 (m, 2H), 1.38 – 1.31 (m, 6H), 1.28 – 1.24 (m, 3H), 1.16 – 1.05 (m, 9H), 1.01 (s, 3H), 0.96 (d, $J = 6.6$ Hz, 2H), 0.91 (d, $J = 6.5$ Hz, 3H), 0.86 (dd, $J = 6.6, 1.8$ Hz, 6H), 0.67 (s, 3H).

^{13}C NMR (100 MHz, CDCl_3 , δ in ppm) 173.14, 161.15, 139.71, 135.18, 133.52, 130.91, 122.66, 120.09, 73.76, 65.47, 56.74, 56.21, 50.08, 42.36, 39.80, 39.59, 38.23, 37.07, 36.64, 36.26, 35.86, 34.65, 31.97, 31.91, 28.99, 28.92, 28.63, 28.31, 28.07, 27.88, 25.80, 24.98, 24.35, 23.92, 22.91, 22.66, 21.10, 19.39, 18.80, 11.92.

FTIR (cm^{-1}) 2942, 2867, 1720, 1416, 1282, 1248, 1088.

4c: Yield = 88 %, ^1H NMR (400 MHz, CDCl_3 , δ in ppm) 7.53 (d, $J = 4.0$ Hz, 1H), 7.06 (d, $J = 4.0$ Hz, 1H), 5.36 (d, $J = 5.0$ Hz, 1H), 4.65 – 4.57 (m, 1H), 4.26 (t, $J = 6.7$ Hz, 2H), 2.32 – 2.23 (m, 4H), 2.03 – 1.92 (m, 2H), 1.87 – 1.81 (m, 3H), 1.71 (p, $J = 7.0$ Hz, 2H), 1.62 – 1.45 (m, 9H), 1.40 – 1.28 (m, 14H), 1.17 – 1.05 (m, 7H), 1.01 (s, 4H), 0.98 – 0.93 (m, 2H), 0.91 (d, $J = 6.5$ Hz, 3H), 0.86 (dd, $J = 6.7, 1.8$ Hz, 6H), 0.67 (s, 3H).

^{13}C NMR (100 MHz, CDCl_3 , δ in ppm) 173.39, 161.32, 139.83, 135.28, 133.59, 130.98, 122.72, 120.15, 73.82, 65.65, 56.81, 56.26, 50.15, 42.44, 39.86, 39.65, 38.30, 37.13, 36.72, 36.31, 35.93, 34.82, 32.03, 31.99, 29.41, 29.28, 29.18, 28.74, 28.36, 28.14, 27.95, 26.01, 25.15, 24.42, 23.96, 22.96, 22.70, 21.16, 19.45, 18.85, 11.99.

FTIR (cm^{-1}) 2933, 2860, 1722, 1419, 1281, 1251, 1092.

4.4.5 General procedure for the synthesis of compound F-n (n = 5, 7, 9):

In a 100 mL double neck round bottom flask, dry NEt_3 (30 mL) was taken under inert conditions and purged for approximately 30 min; then, an equal amount of dry THF was added to the flask, and the mixture was purged for another 20 min. Compound 4 (5 equiv.) was added to the mixture of solvents while maintaining the inert atmosphere. Compound 2 (1 equiv.) was added to the reaction mixture, followed by the addition of $\text{Pd}(\text{PPh}_3)_4$ (0.06 equiv). After 5 min, CuI (0.06 equiv.) was added to the reaction mixture. The system was refluxed at 80 °C for 36-40 h. The mixture was then cooled down to room temperature, and the triethylamine was

quenched by HCl (5N). The organic layer was extracted using DCM. The organic phase dried over Na₂SO₄ was concentrated in a vacuum. The crude product was purified by column chromatography using silica gel with a mixture of hexane/ethyl acetate (v/v, 100/7) as an eluent, followed by recrystallization using a hexane/ethanol mixture. Yield = 32-35 %. The ¹H, ¹³C (Figure A15-A20), and HRMS spectra (Figure A21-A23) are given in Appendix III.

Characterization details of F-n (n = 5, 7, 9)

F-5: Yield = 35 %, UV-vis (absorbance in nm): 326, 347, Fluorescence: 372. ¹H NMR (400 MHz, CDCl₃, δ in ppm) 7.69 (d, *J* = 3.9 Hz, 3H), 7.66 (s, 3H), 7.23 (d, *J* = 3.9 Hz, 3H), 5.35 (d, *J* = 5.1 Hz, 3H), 4.65 – 4.57 (m, 3H), 4.31 (t, *J* = 6.4 Hz, 6H), 2.34 – 2.28 (m, 12H), 1.98 – 1.91 (m, 6H), 1.85 – 1.84 (m, 2H), 1.82 – 1.81 (m, 3H), 1.79 – 1.75 (m, 6H), 1.74 – 1.66 (m, 8H), 1.58 – 1.53 (m, 7H), 1.52 – 1.45 (m, 16H), 1.44 – 1.39 (m, 6H), 1.33 – 1.29 (m, 9H), 1.25 (s, 8H), 1.23 – 1.18 (m, 3H), 1.15 (d, *J* = 3.1 Hz, 2H), 1.12 – 1.07 (m, 12H), 1.04 (d, *J* = 7.0 Hz, 2H), 1.00 (s, 10H), 0.96 – 0.92 (m, 5H), 0.89 (d, *J* = 6.5 Hz, 9H), 0.85 (dd, *J* = 6.6, 1.9 Hz, 18H), 0.65 (s, 9H).

¹³C NMR (100 MHz, CDCl₃, δ in ppm) 173.08, 161.56, 139.72, 135.07, 134.41, 133.29, 132.92, 128.99, 123.60, 122.80, 93.38, 83.86, 73.99, 65.41, 56.77, 56.24, 50.12, 42.40, 39.81, 39.63, 38.27, 37.10, 36.69, 36.30, 35.92, 34.66, 32.02, 31.94, 29.83, 28.49, 28.36, 28.14, 27.95, 25.65, 24.83, 24.40, 23.97, 22.96, 22.83, 22.70, 21.14, 19.44, 18.83, 14.27, 11.96.

HRMS (MALDI) for C₁₂₆H₁₇₄S₃NaO₁₂ (M + Na): calculated – 1998.2065; found- 1998.2014.

FTIR (cm⁻¹) 2935, 2866, 1730, 1711, 1452, 1281, 1263, 1089.

F-7: Yield = 33 %, UV-vis (absorbance in nm): 326, 347, Fluorescence: 372. ¹H NMR (400 MHz, CDCl₃, δ in ppm) 7.68 (d, *J* = 3.9 Hz, 3H), 7.65 (s, 3H), 7.23 (d, *J* = 3.9 Hz, 3H), 5.35 (d, *J* = 5.4 Hz, 3H), 4.65 – 4.56 (m, 3H), 4.29 (t, *J* = 6.6 Hz, 6H), 2.31 – 2.25 (m, 12H), 2.00 – 1.92 (m, 8H), 1.85 (d, *J* = 2.9 Hz, 3H), 1.83 – 1.80 (m, 5H), 1.77 – 1.71 (m, 9H), 1.64 – 1.61 (m, 7H), 1.56 – 1.52 (m, 8H), 1.49 – 1.43 (m, 15H), 1.41 – 1.31 (m, 28H), 1.25 (s, 4H), 1.14 – 1.10 (m, 8H), 1.08 – 1.05 (m, 6H), 1.00 (s, 10H), 0.96 – 0.93 (m, 6H), 0.89 (d, *J* = 6.5 Hz, 9H), 0.85 (dd, *J* = 6.6, 1.8 Hz, 18H), 0.65 (s, 9H).

¹³C NMR (100 MHz, CDCl₃, δ in ppm) 173.32, 161.59, 139.76, 135.18, 134.39, 133.21, 132.89, 128.93, 123.57, 122.75, 122.72, 93.35, 83.83, 73.85, 65.63, 56.77, 56.23, 50.10, 42.40,

39.82, 39.62, 38.27, 37.09, 36.69, 36.29, 35.91, 34.73, 32.01, 31.95, 29.83, 29.04, 28.95, 28.67, 28.35, 28.13, 27.93, 25.86, 25.03, 24.40, 23.96, 22.95, 22.69, 21.13, 19.43, 18.82, 11.96.

HRMS (MALDI) for $C_{132}H_{186}S_3NaO_{12}$ ($M + Na$): calculated – 2082.3004; found - 2082.2013.

FTIR (cm^{-1}) 2941, 2870, 1733, 1714, 1452, 1280, 1255, 1094.

F-9: Yield = 32 %, UV-vis (absorbance in nm): 326, 347, Fluorescence: 372. 1H NMR (400 MHz, $CDCl_3$, δ in ppm) 7.69 (d, $J = 3.9$ Hz, 3H), 7.66 (s, 3H), 7.24 (d, $J = 3.9$ Hz, 3H), 5.36 (d, $J = 5.0$ Hz, 3H), 4.65 – 4.57 (m, 3H), 4.29 (t, $J = 6.7$ Hz, 6H), 2.32 – 2.24 (m, 12H), 2.02 – 1.92 (m, 6H), 1.87 – 1.80 (m, 9H), 1.72 (p, $J = 7.0$ Hz, 7H), 1.64 – 1.57 (m, 12H), 1.56 – 1.51 (m, 8H), 1.50 – 1.40 (m, 18H), 1.32 (s, 32H), 1.24 (d, $J = 8.2$ Hz, 5H), 1.15 – 1.06 (m, 18H), 1.01 (s, 10H), 0.97 – 0.94 (m, 4H), 0.90 (d, $J = 6.5$ Hz, 9H), 0.86 (dd, $J = 6.6, 1.8$ Hz, 18H), 0.66 (s, 9H).

^{13}C NMR (100 MHz, $CDCl_3$, δ in ppm) 173.29, 161.51, 139.70, 135.15, 134.30, 133.06, 132.78, 128.81, 123.46, 122.61, 93.22, 83.72, 73.70, 65.62, 56.68, 56.13, 50.01, 42.30, 39.73, 39.52, 38.17, 37.00, 36.59, 36.19, 35.81, 34.70, 31.91, 31.85, 29.30, 29.15, 29.06, 28.64, 28.24, 28.03, 27.83, 25.90, 25.04, 24.29, 23.84, 22.84, 22.58, 21.03, 19.33, 18.72, 11.86.

HRMS (MALDI) for $C_{138}H_{198}S_3NaO_{12}$ ($M + Na$): calculated – 2166.3943; found- 2166.3967.

FTIR (cm^{-1}) 2929, 2853, 1734, 1717, 1455, 1282, 1260, 1092.

4.5 Electron density map

The procedure for reconstructing the electron density map has been adopted from our previous chapter 2. Briefly, we reproduced here for the reader's convenience.

“The electron density $\rho(x,y,z)$ of a liquid crystalline phase is linked to its structure factor $F(hkl)$ by inverse Fourier transformation as follows:

$$\rho(x,y,z) = \sum_{hk} F(hkl) e^{2\pi i(hx+ky+lz)}$$

In this formula (hkl) are the Miller Indices and x, y, z are the fractional coordinates in the unit cell. To calculate the electron density, the complex structure factor $F(hkl)$ has to be written as the product of the phase, $\Phi(hkl)$ and the modulus $|F(hkl)|$ which is proportional to the square root of the intensity $I(hkl)$ of the observed reflection as shown below:

$$F(hkl) = |F(hkl)|e^{i\Phi(hkl)} = \sqrt{I(hkl)}e^{i\Phi(hkl)}$$

The intensities of the different peaks in the diffraction pattern can be estimated from the areas under each peak after subtracting the background and then applying the relevant geometric and multiplicity corrections. The only information that cannot be obtained directly from experiment is the phase, $\Phi(hkl)$, for each diffraction peaks. However, this problem becomes easily tractable when the structure under study is centrosymmetric, i.e., if $\rho(x, y, z) = \rho(-x, -y, -z)$. In that case $F(hkl)$ can only be real and hence $\Phi(hkl)$ can be either 0 or π . For non-centrosymmetric groups, the phase may take every value between 0 and 2π . As the liquid crystalline phases observed are generally centrosymmetric, it is easy to reconstruct the electron density maps by taking the value of $\Phi(hkl)$ as 0 or π . The “correct” map is subsequently chosen on the merit of the reconstructed maps along with other physical and chemical knowledge of the system, such as chemical constituents and their sizes.”

4.6 Quantum Yield Measurement

A direct method of measuring photoluminescence quantum yield (PL-QY) was employed, whereby a reference sample of known quantum efficiency was used as a comparison;^{51,52} the dye Rhodamine 6G was chosen as the reference as it absorbs in a similar region. With the optical spectra of both the reference and compound 1 solution in a given solvent, the following equation was applied:

$$\Phi = \Phi_R \frac{X(1-10^{-A_R})n^2}{X_R(1-10^{-A})n_R^2}$$

Where ‘ Φ ’ is the quantum yield, ‘ X ’ is the integrated area under the emission peak, ‘ A ’ is the absorbance at the excitation wavelength, and ‘ n ’ is the refractive index of the solvent. Each subscript ‘ R ’ refers to the respective values of the reference standard.⁵³

4.7 Author Contributions

SR conceptualized the project, designed and performed the experiments, analysed the data and wrote the chapter. SPG analyzed the SAXS/WAXS data. PR performed some of the initial experiments which have been included in her MS thesis at IISER Mohali. SKP did the overall project administration, managed funding, reviewed, edited and finalized the chapter. All authors have given approval to the final version of the chapter.

4.8 Acknowledgements

SR thank CSIR for fellowship with file no (09/947(0091)/2017-EMR-I). SKP acknowledges project file no. CRG/2019/000901/OC from DST-SERB project. We are thankful to IISER Mohali for central and departmental facilities.

References

1. Verbiest, T.; Elshocht, S. V.; Kauranen, M.; Hellemans, L.; Snauwaert, J.; Nuckolls, C.; Katz, T. J.; Persoons, A. Strong Enhancement of Nonlinear Optical Properties Through Supramolecular Chirality. *Science* **1998**, *282*, 913-915.
2. Ray, K.; Ananthavel, S. P.; Waldeck, D. H.; Naaman, R. Asymmetric Scattering of Polarized Electrons by Organized Organic Films of Chiral Molecules. *Science* **1999**, *283*, 814-816.
3. Gupta, R. K.; Achalkumar, A. S. Perylene-Based Liquid Crystals as Materials for Organic Electronics Applications. *Langmuir* **2019**, *35*, 2455–2479.
4. Bala, I.; Joydip De, J.; Gupta, S. P.; Pandey, U. K.; Pal, S. K.; Enabling efficient ambipolar charge carrier mobility in a H-bonded heptazine–triphenylene system forming segregated donor–acceptor columnar assemblies. *J. Mater. Chem. C* **2021**, *9*, 8552-8561.
5. De, J.; Devi, M.; Shah, A.; Gupta, S. P.; Bala, I.; Singh, D. P.; Douali, R.; Pal, S. K. Luminescent Conductive Columnar π -Gelators for Fe(II) Sensing and Bio-Imaging Applications. *J. Phys. Chem. B* **2020**, *45*, 10257–10265.
6. De, J.; Abdul, H. M. M.; Yadav, R. A. K.; Gupta, S. P.; Bala, I.; Chawla, P.; Kesavan, K. K.; Jou, J. H.; Pal, S. K. AIE-active mechanoluminescent discotic liquid crystals for applications in OLEDs and bio-imaging. *Chem. Commun.* **2020**, *56*, 14279-14282.
7. Bala, I.; De, J.; Gupta, S. P.; Singh, H.; Pandey, U. K.; Pal, S. K. High hole mobility in room temperature discotic liquid crystalline tetrathienoanthracenes. *Chem. Commun.* **2020**, *56*, 5629-5632.
8. De, J.; Bala, I.; Gupta, S. P.; Pandey, U. K.; Pal, S. K. High Hole Mobility and Efficient Ambipolar Charge Transport in Heterocoronene-Based Ordered Columnar Discotics. *J. Am. Chem. Soc.* **2019**, *47*, 18799–18805.

9. De, R.; De, J.; Gupta, S. P.; Bala, I.; Ankita; Tarun; Pandey, U. K.; Pal, S. K. Oxadiazole-integrated heterocoronene discotics as ambipolar organic semiconductors. *J. Mater. Chem. C* **2023**, *11*, 980-985.
10. Bala, I.; Kaur, H.; Maity, M.; Yadav, R. A. K.; De, J.; Gupta, S. P.; Jou, J. H.; Pandey, U. K.; Pal, S. K. Electroluminescent Aggregation-Induced Emission-Active Discotic Liquid Crystals Based on Alkoxy Cyanostilbene-Functionalized Benzenetricarboxamide with Ambipolar Charge Transport. *ACS Appl. Electron. Mater.* **2022**, *3*, 1163–1174.
11. Vishwakarma, V. K.; Nagar, M. R.; Lhouvum, N.; Jou, J. H.; Achalkumar, A. S. A New Class of Solution Processable Pyrazino[2,3-g]quinoxaline Carbazole Derivative Based on D–A–D Architecture for Achieving High EQE in Yellow and White OLEDs. *Adv. Optical Mater.* **2022**, *10*, 2200241.
12. Gupta, R. K.; Anamika Dey, A.; Singh, A.; Iyer, P. K.; Achalkumar, A. S. Heteroatom Bay-Annulated Perylene Bisimides: New Materials for Organic Field Effect Transistors. *ACS Appl. Electron. Mater.* **2019**, *8*, 1378–1386.
13. Li, C.; Zeng, Q.; Wu, P.; Xu, S.; Wang, C.; Qiao, Y.; Wan, L.; Bai, C. Molecular Symmetry Breaking and Chiral Expression of Discotic Liquid Crystals in Two-Dimensional Systems. *J. Phys. Chem. B* **2002**, *106*, 13262-13267.
14. Collings, P. J.; Goodby, J. W. *Introduction to Liquid crystals: Physics and Chemistry*, 2nd ed.; CRC Press: Boca Raton, 2020.
15. H. K. Bisoyi, H. K.; Li, Q. *Liquid Crystals. Kirk-Othmer Encyclopedia of Chemical Technology* **2014**, 1–52.
16. Chandrasekhar, S. *Liquid Crystals*, Cambridge University Press: Cambridge, U.K., 1992.
17. Li, X. Q.; Zhang, X.; Ghosh, S.; Würthner, F. Highly Fluorescent Lyotropic Mesophases and Organogels Based on J-Aggregates of Core-Twisted Perylene Bisimide Dyes. *Chem. Eur J.* **2008**, *14*, 8074–8078.
18. Yasuda, T.; Ooi, H.; Morita, J.; Akama, Y.; Minoura, K.; Funahashi, M.; Shimomura, T.; Kato, T. π -Conjugated Oligothiophene-Based Polycatenar Liquid Crystals: Self-Organization and Photoconductive, Luminescent, and Redox Properties. *Adv. Funct. Mater.* **2009**, *19*, 411–419.

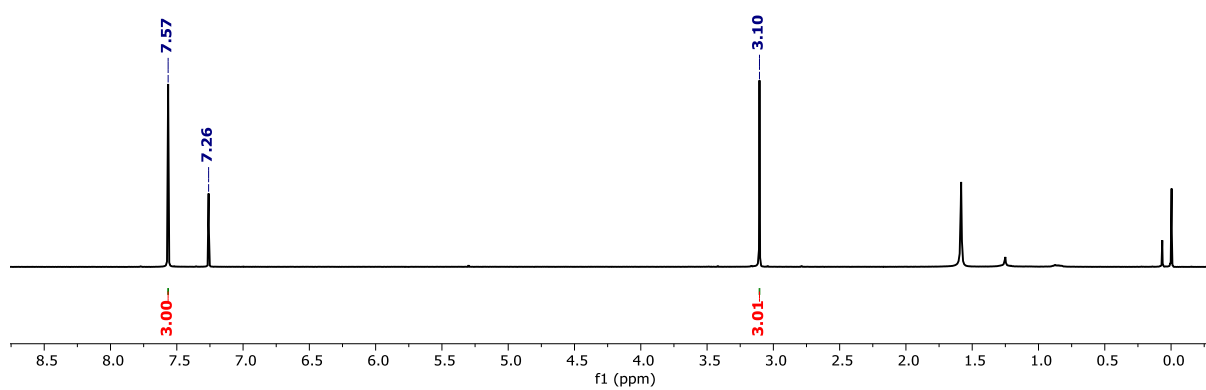
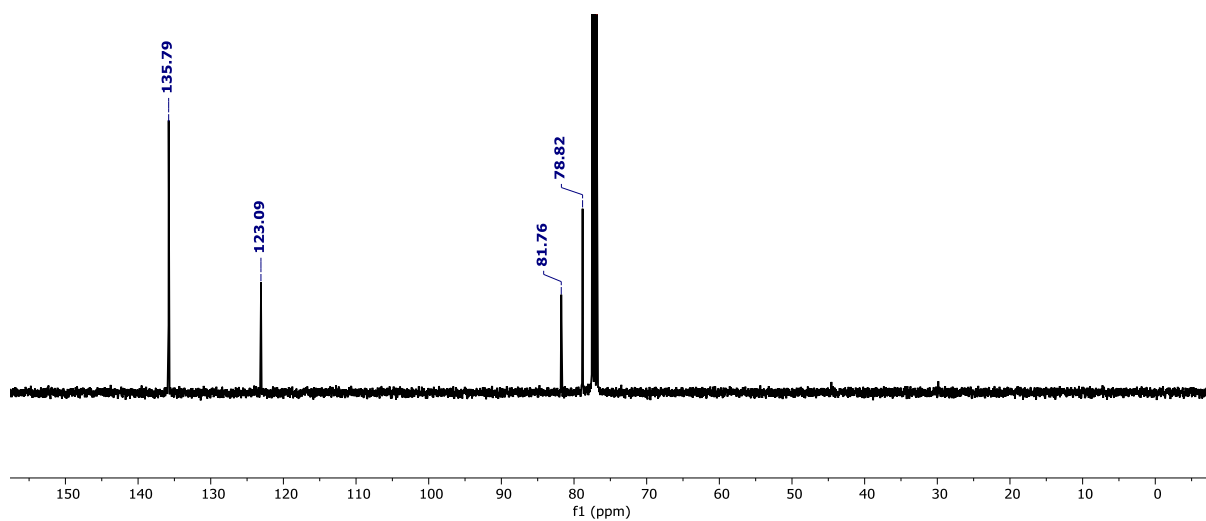
19. Kumar, S. *Chemistry of Discotic Liquid Crystals*, CRC Press, Taylor and Francis Group, 2011.
20. Bisoyi, H. K.; Kumar, S. Discotic nematic liquid crystals: science and technology. *Chem. Soc. Rev.* **2010**, *39*, 264-285.
21. Kumar, S.; Self-organization of disc-like molecules: chemical aspects. *Chem. Soc. Rev.* **2006**, *35*, 83-109.
22. Rani, S.; Punjani, V.; Gupta, S. P.; Kanakala, M. B.; Yelamaggad, C. V.; Pal, S. K. Observation of helical self-assembly in cyclic triphosphazene-based columnar liquid crystals bearing chiral mesogenic units. *J. Mater. Chem. C* **2023**, *11*, 1067-1075.
23. Malthete, J.; Jacques, J.; Tinh, N. H.; Destrade, C. Macroscopic Evidence of Molecular Chirality in Columnar Mesophases. *Nature* **1982**, *298*, 46-48.
24. Fontes, E.; Heiney, P. A.; de Jeu, W. H. Liquid-Crystalline and Helical Order in a Discotic Mesophase. *Phys. Rev. Lett.* **1988**, *61*, 1202-1205.
25. Aldred, M. P.; Vlachos, P.; Dong, D.; Kitney, S. P.; Tsoi, W. C.; O'Neill, M.; Kelly, S. M. Heterocyclic reactive mesogens: synthesis, characterisation and mesomorphic behaviour. *Liq Cryst.* **2005**, *32*, 951-965.
26. Merlo, A. A.; Braun, J. E.; Vasconcelos, U.; Ely, F.; Gallardo, H. Chiral liquid crystalline m-nitrotolans and tolans: synthesis and mesomorphic properties. *Liq Cryst.* **2000**, *27*, 657-663.
27. Seed, A. Synthesis of self-organizing mesogenic materials containing a sulfur-based five-membered heterocyclic core. *Chem Soc Rev.* **2007**, *36*, 2046-2069.
28. Hariprasad, S.; Srinivasa, H. T. Symmetric 3,5-pyrazole and isoxazole heterocycles comprising a bent core unit: synthesis and mesomorphic characterization. *Liq Cryst.* **2015**, *42*, 1612-1620.
29. Roy, B.; De, N.; Majumdar, K. C. *Chem. – Eur. J.* **2012**, *18*, 14560-14588.
30. Aldred, M. P.; Hudson, R.; Kitney, S. P.; Vlachos, P.; Liedtke, A.; Woon, K. L.; O'Neill, M.; Kelly, S. M. *Liq. Cryst.* **2008**, *35*, 413-427.
31. Lehmann, M.; Kestemont, G.; Aspe, R. G.; Herman, C. B.; Koch, M. H. J.; Debije, M. G.; Piris, J.; de Haas, M. P.; Warman, J. M.; Watson, M. D.; Lemaur, V.; Cornil, J.; Geerts, Y.

- H.; Gearba, R.; Ivanov, D. A. High Charge-Carrier Mobility in π -Deficient Discotic Mesogens: Design and Structure–Property Relationship. *Chem. – Eur. J.* **2005**, *11*, 3349–3362.
32. Takase, M.; Enkelmann, V.; Sebastiani, D.; Baumgarten, M.; Müllen, K. Annularly Fused Hexapyrrolohexaazacoronenes: An Extended p System with Multiple Interior Nitrogen Atoms Displays Stable Oxidation States. *Angew. Chem., Int. Ed.* **2007**, *46*, 5524–5527.
33. Górski, K.; Noworyta, K.; J. Mech-Piskorz, J. Influence of the heteroatom introduction on the physicochemical properties of 5-heterotruxenes containing nitrogen, oxygen and sulfur atom. *RSC Adv.* **2020**, *10*, 42363–42377.
34. (a) Tsai, H. H. G.; Chou, L. C.; Lin, S. C.; Sheu, H. S.; Lai, C. K. Heterocyclic columnar hexacatenar bisthiazoles. *Tetrahedron Lett.* **2009**, *50*, 1906–1910. (b) Han, J. 1,3,4-Oxadiazole based liquid crystals. *J. Mater. Chem. C* **2013**, *1*, 7779–7797.
35. Schulz, B.; Bruma, M.; Brehmer, L. Aromatic Poly(1, 3, 4-Oxadiazole)s as Advanced materials. *Adv. Mater.* **1997**, *9*, 601–613.
36. Tian, D.; Zhou, Y.; Li, Z.; Liu, S.; Shao, J.; Yang, X.; Shao, J.; Huang, W.; Zhao, B. Thieno[3,2-b]thiophene-Based Discotic Liquid Crystal Mesogens: Rational Synthesis, Physical Properties and Self-Assembly. *Chemistry Select* **2017**, *2*, 8137–8145.
37. Bag, S.; Maingi, V.; Maiti, P. K.; Yelk, J.; Glaser, M. A.; Walba, D. M.; Clark, N. A. Molecular structure of the discotic liquid crystalline phase of hexa-peri-hexabenzocoronene/oligothiophene hybrid and their charge transport properties. *J. Chem. Phys.* **2015**, *143*, 144505-144514.
38. Bag, S.; Maingi, V.; Maiti, P. K.; Yelk, J.; Glaser, M. A.; Walba, D. M.; Clark, N. A.; Luo, J.; Zhao, B.; Shao, J.; Lim, K. A.; Chan, H. S. O.; Chi, C. Room-temperature discotic liquid crystals based on oligothiophenes—attached and fused triazatruxenes. *J. Mater. Chem.* **2009**, *19*, 8327-8334.
39. Li, Y.; Concellón, A.; Lin, C. J.; Romero, N. A.; Lin, S.; Swager, T. M. Thiophene-fused polyaromatics: synthesis, columnar liquid crystal, fluorescence and electrochemical properties. *Chem. Sci.* **2020**, *11*, 4695-4701.

40. Tober, N.; Winter, J.; Jochem, M.; Lehmann, M.; Detert, H. Tris(5-aryl-1,3,4-oxadiazolyl)benzotrithiophenes – Discotic Liquid Crystals with Enormous Mesophase Ranges. *Eur. J. Org. Chem.* **2021**, 798–809.
41. Lambov, M.; Hensiek, N.; Pöppler, A. C.; Lehmann, M. Columnar Liquid Crystals from Star-Shaped Conjugated Mesogens as Nano-Reservoirs for Small Acceptors. *Chem Plus Chem* **2020**, *85*, 2219–2229.
42. Han J.; Wang Y.M.; Wang X.G. Synthesis, Mesogenic and Spectroscopic Properties of 2,5-Disubstituted Thiophene Derivatives. *Chin. J. Chem.* **2006**, *24*, 1594–1598.
43. Kimura, M.; Yasuda, T.; Kishimoto, K.; Götz, G.; Bäuerle, P.; Kato, T. Oligothiophene-based Liquid Crystals Exhibiting Smectic-A Phases in Wider Temperature Ranges. *Chem. Lett.* **2006**, *35*, 1150–1151.
44. Paraskos, A. J.; Swager, T. M. Effects of Desymmetrization on Thiophene-Based Bent-Rod Mesogens. *Chem. Mater.* **2002**, *14*, 4543–4549.
45. Seed, A. J., Toyne, K. J., & Goodby, J. W. Synthesis of some 2,4- and 2,5-disubstituted thiophene systems and the effect of the pattern of substitution on the refractive indices, optical anisotropies, polarisabilities and order parameters in comparison with those of the parent biphenyl and dithienyl systems. *J. Mater. Chem.* **1995**, *5*, 653-661.
46. Seed, A. J.; Toyne, K. J.; Goodby, J. W.; Hird, M. Synthesis, transition temperatures, and optical properties of various 2,6-disubstituted naphthalenes and related 1-benzothiophenes with butylsulfanyl and cyano or isothiocyanato terminal groups. *J. Mater. Chem.* **2000**, *10*, 2069-2080.
47. De, J.; Sarkar, I.; Yadav, R. A. K.; Bala, I.; Gupta, S. P.; Siddiqui, I.; Jou, J. H.; Pal, S. K. Luminescent columnar discotics as highly efficient emitters in pure deep-blue OLEDs with an external quantum efficiency of 4.7%. *Soft Matter*, **2022**, *18*, 4214-4219.
48. Gupta, S. P.; Gupta, M.; Pal, S. K. Highly Resolved Morphology of Room-Temperature Columnar Liquid Crystals Derived from Triphenylene and Multialkynylbenzene Using Reconstructed Electron Density Maps. *Chemistry Select* **2017**, *21*, 6070–6077.
49. Bala, I.; Singh, N.; Yadav, R. A. K.; De, J.; Gupta, S. P.; Singh, D. P.; Dubey, D. K.; Jou, J. H.; Doualid, R.; Pal, S. K. Room temperature perylene based columnar liquid crystals as

-
- solid-state fluorescent emitters in solution-processable organic light-emitting diodes. *J. Mater. Chem. C* **2020**, *8*, 12485-12494.
50. Kotha, S.; Meshram, M.; Panguluri, N. R.; Shah, V. R.; Todeti, S.; Shirbhate, M. E. Synthetic Approaches to Star-Shaped Molecules with 1,3,5-Trisubstituted Aromatic Cores. *Chemistry – An Asian Journal* **2019**, *14*, 1356–1403.
51. Lakowicz, J. R. *Principles of Fluorescence Spectroscopy*, Springer, USA, 3rd edn, **2006**, 55–56.
52. Finlayson, C. E.; Amezcua, A.; Sazio, P. J. A.; Walker, P. S.; Grossel, M. C.; Curry, R. J.; Smith, D. C.; Baumberg, J. J. Infrared emitting PbSe nanocrystals for telecommunications window applications. *J. Mod. Opt.* **2005**, *52*, 955–964.
53. Brouwer, A. Standards for photoluminescence quantum yield measurements in solution (IUPAC Technical Report). *Pure Appl. Chem.* **2011**, *83*, 2213–2228.

Appendix III

Figure A1 ^1H NMR spectrum of compound **2** in CDCl_3 .Figure A2 ^{13}C NMR spectrum of compound **2** in CDCl_3 .

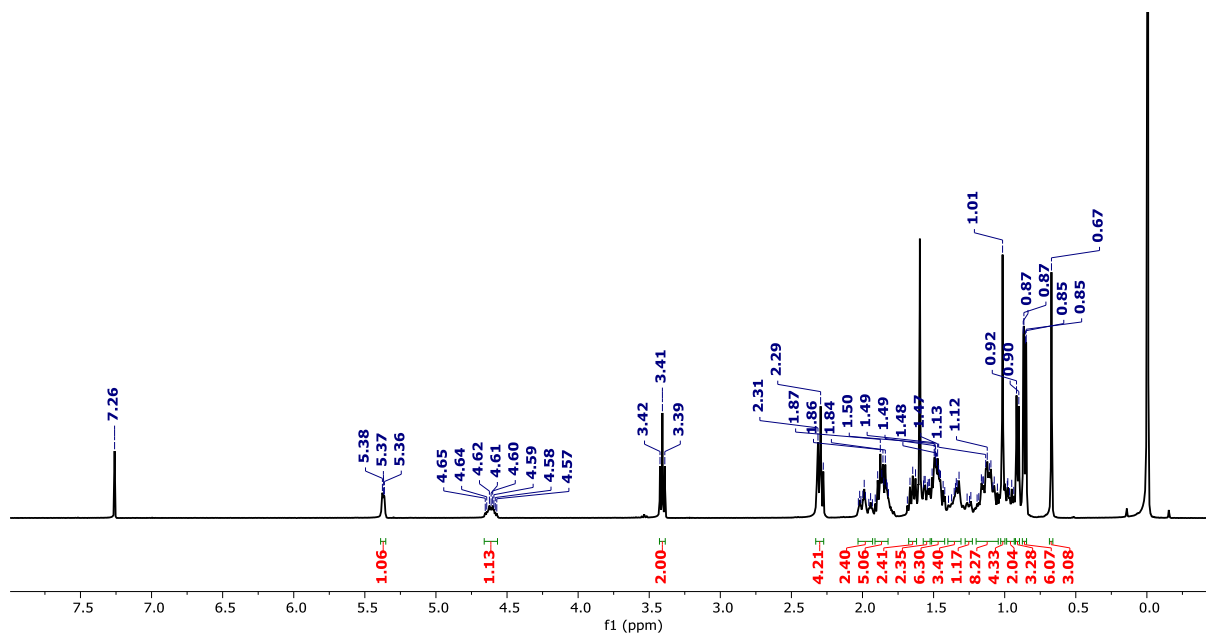


Figure A3 ^1H NMR spectrum of compound **3a** in CDCl_3 .

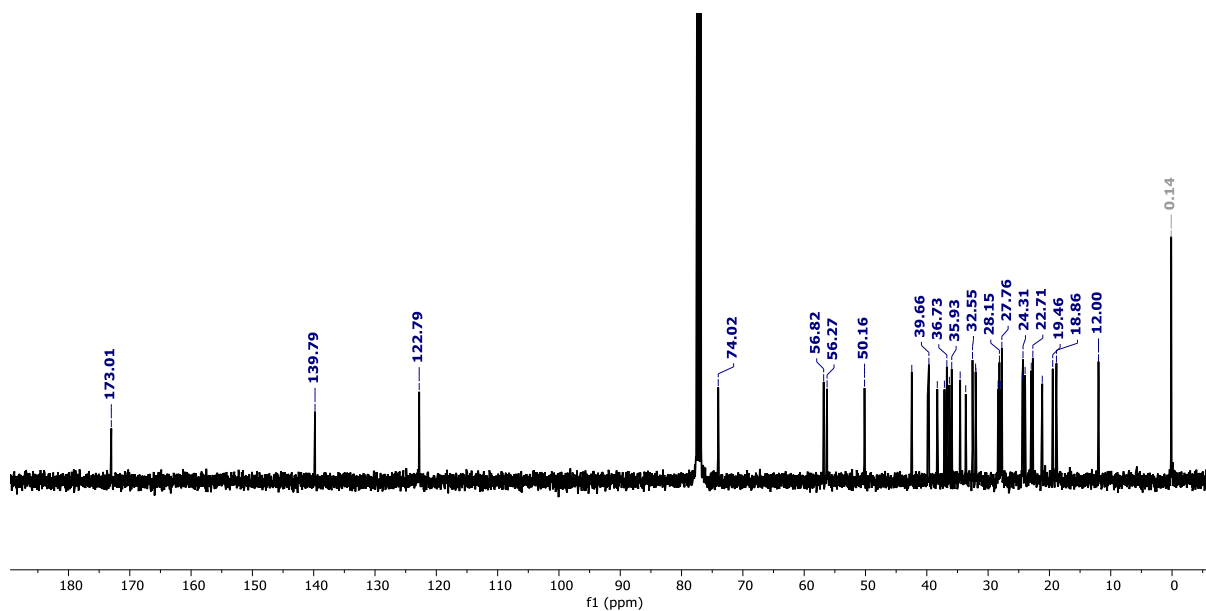


Figure A4 ^{13}C NMR spectrum of compound **3a** in CDCl_3 .

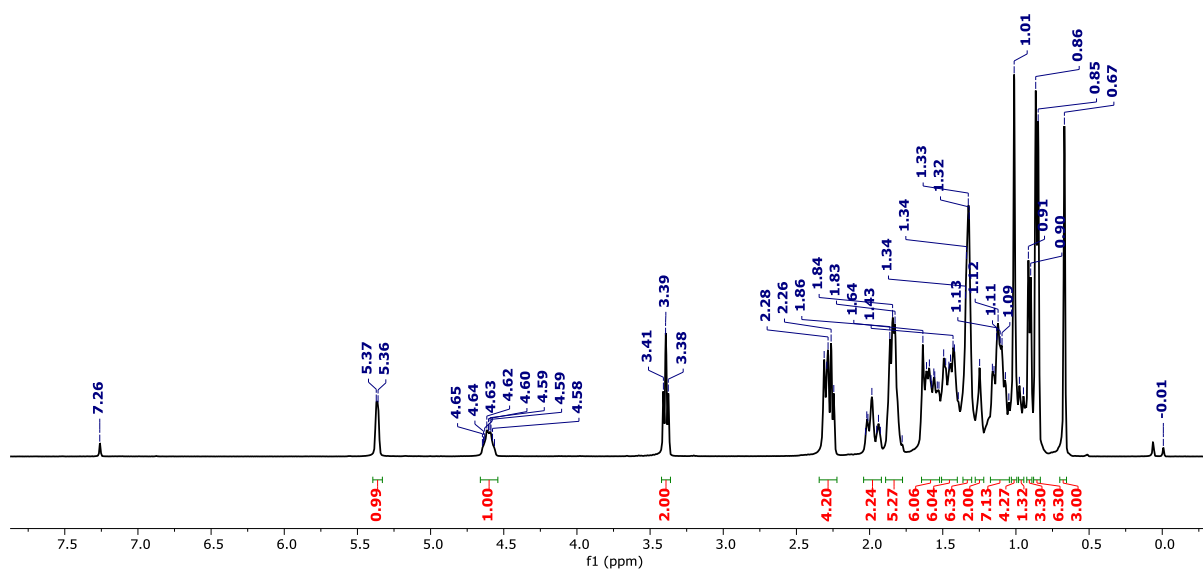


Figure A5 ^1H NMR spectrum of compound **3b** in CDCl_3 .

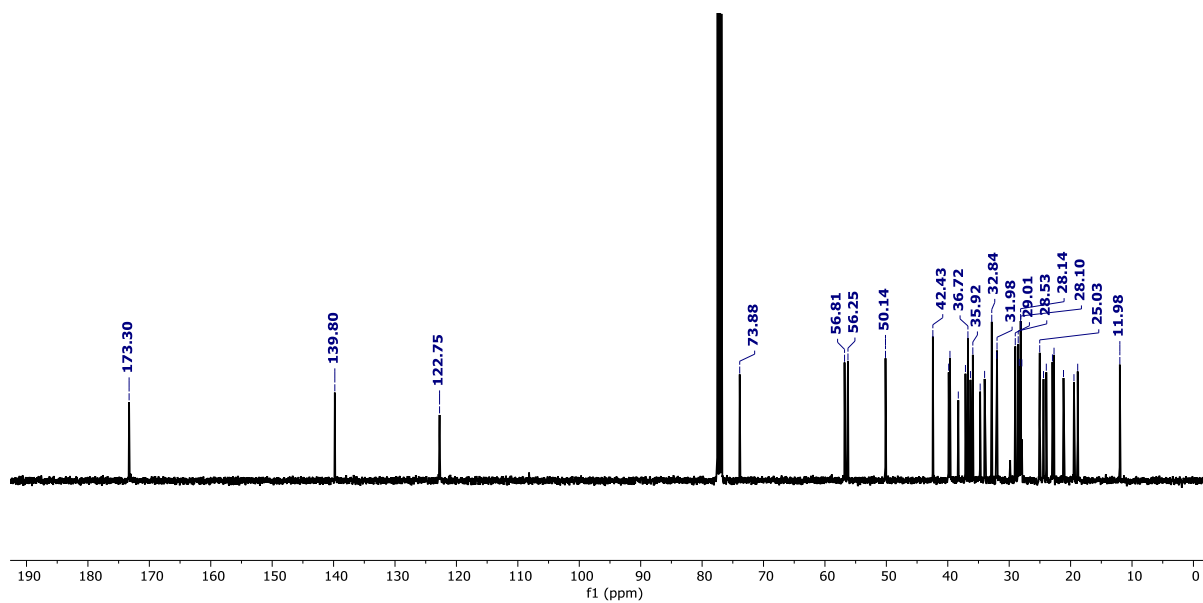


Figure A6 ^{13}C NMR spectrum of compound **3b** in CDCl_3 .

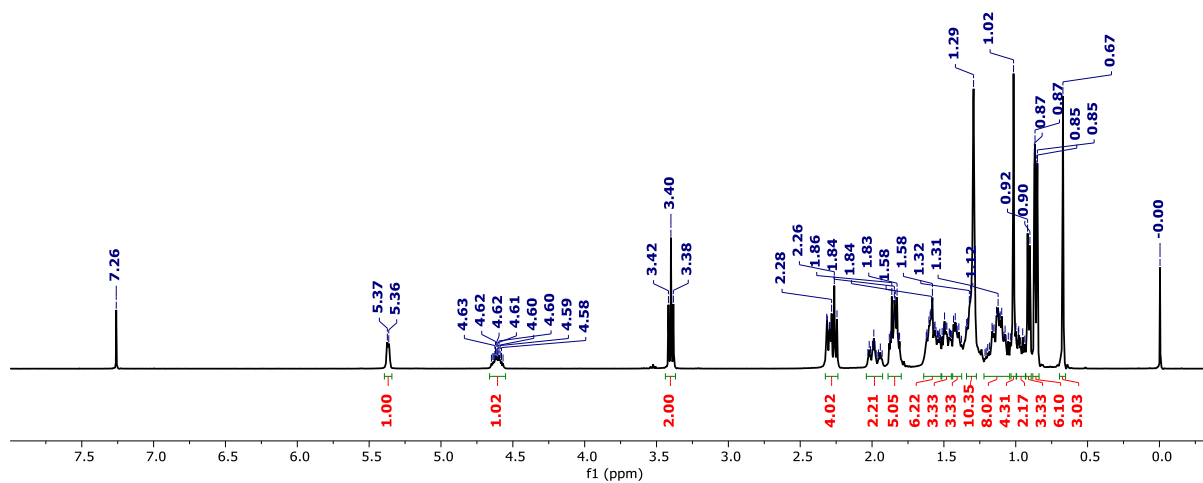


Figure A7 ^1H NMR spectrum of compound **3c** in CDCl_3 .

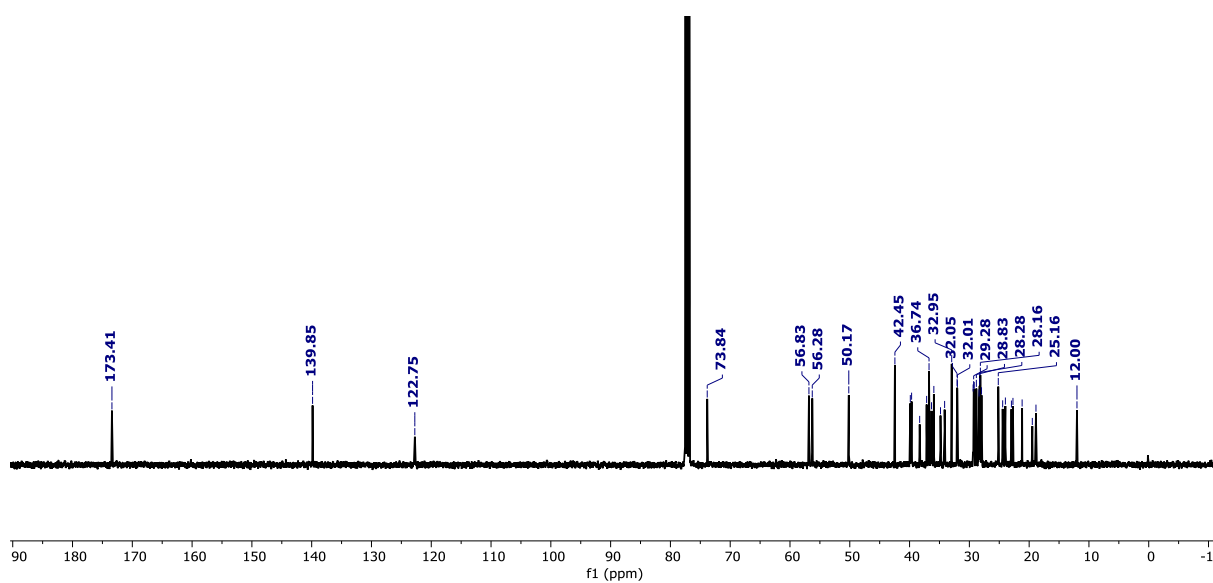


Figure A8 ^{13}C NMR spectrum of compound **3c** in CDCl_3 .

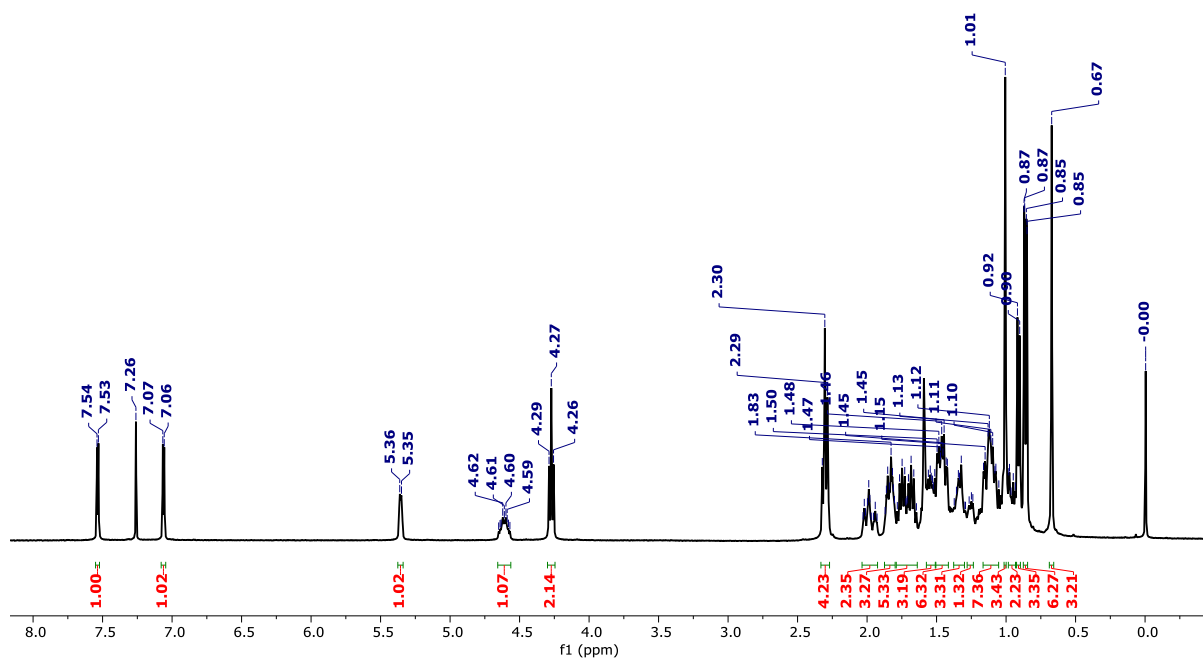


Figure A9 ¹H NMR spectrum of compound **4a** in CDCl₃.

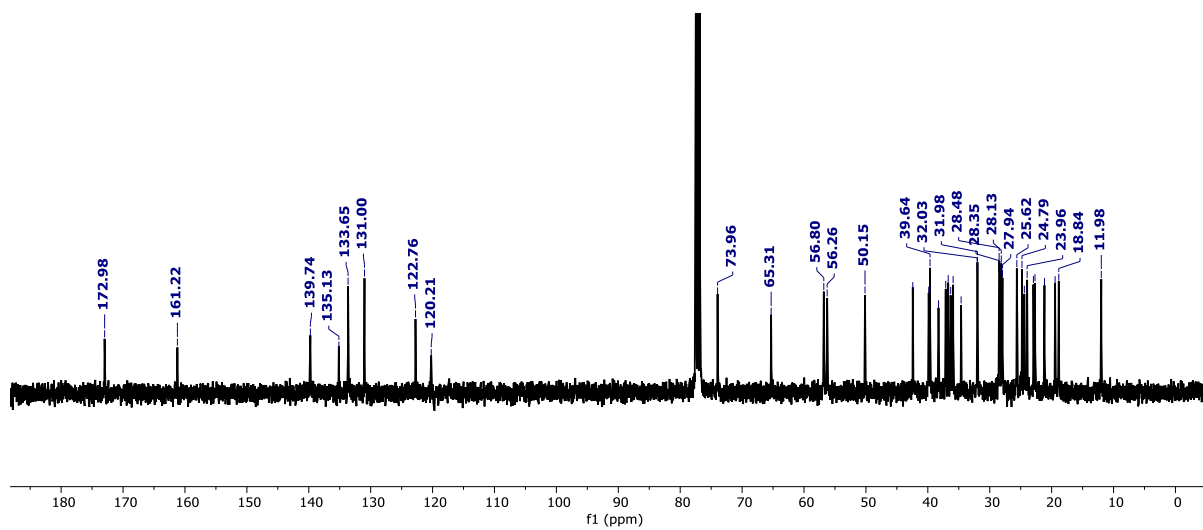


Figure A10 ¹³C NMR spectrum of compound **4a** in CDCl₃.

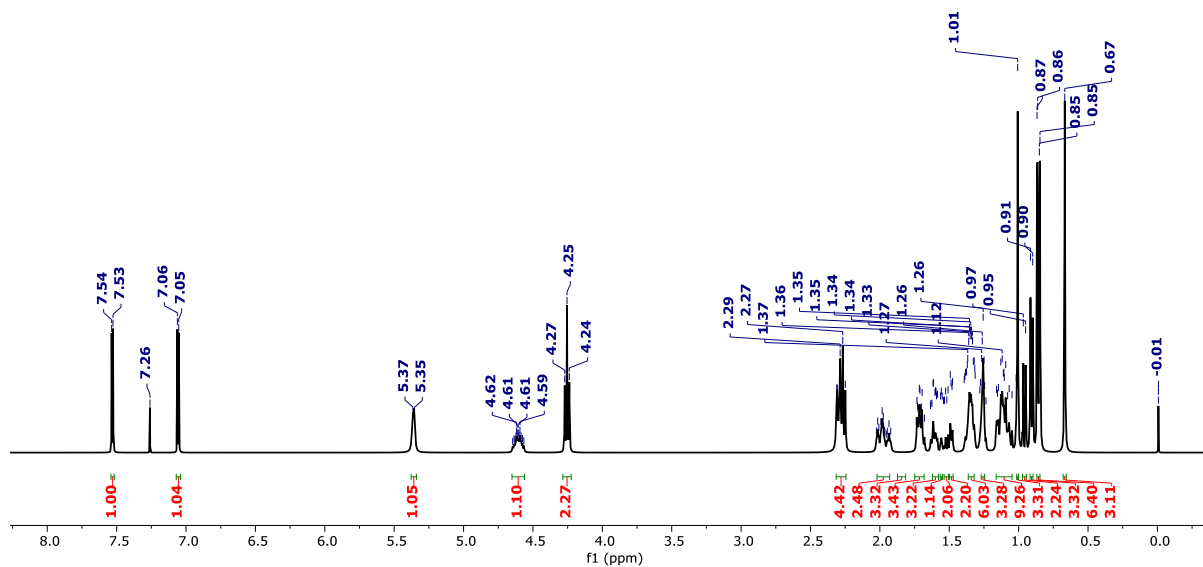


Figure A11 ^1H NMR spectrum of compound **4b** in CDCl_3 .

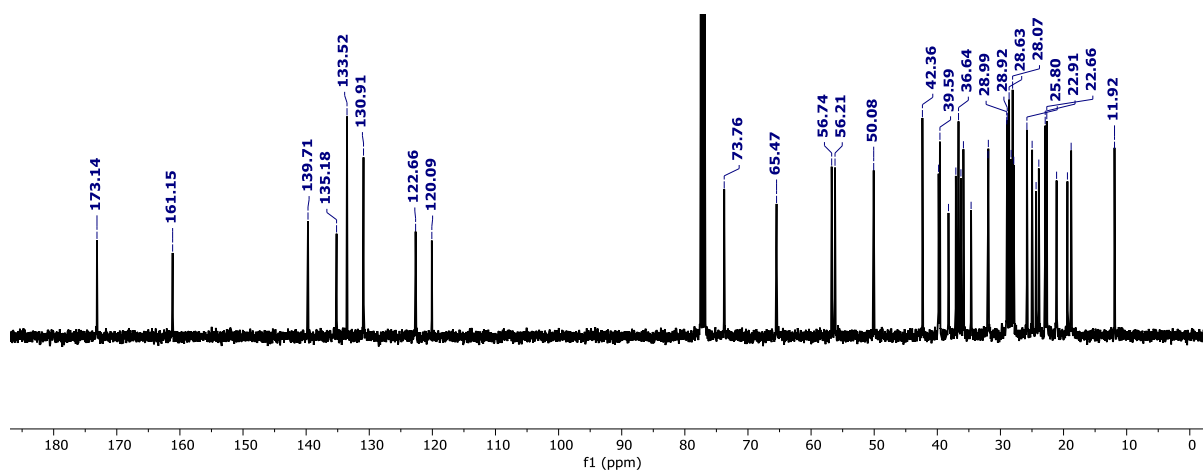
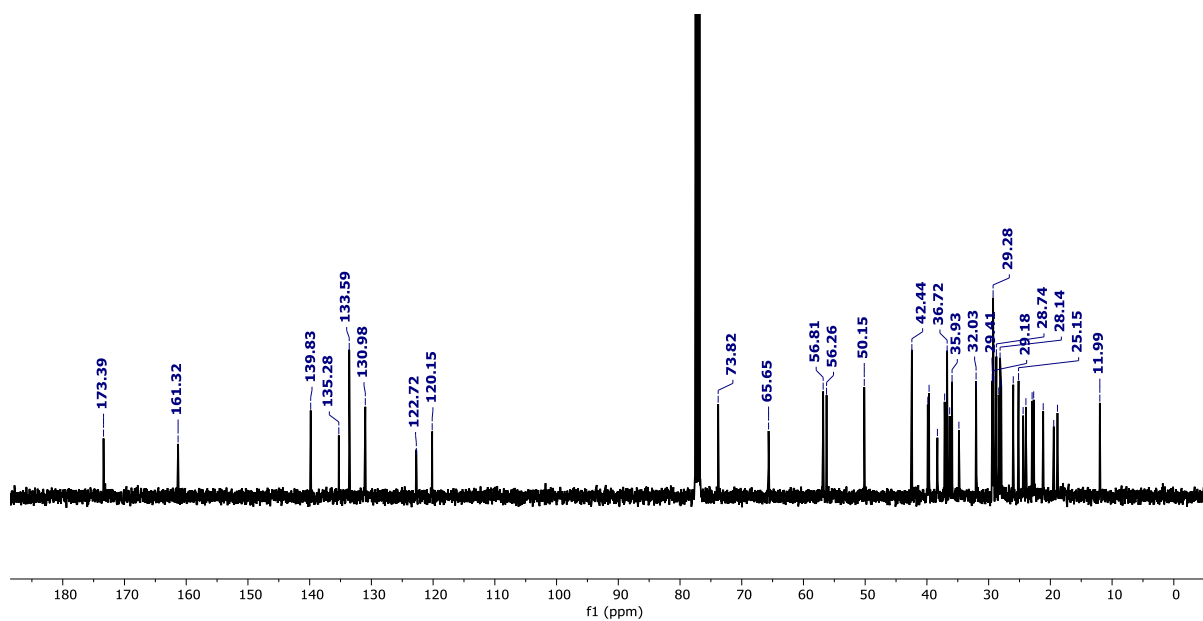
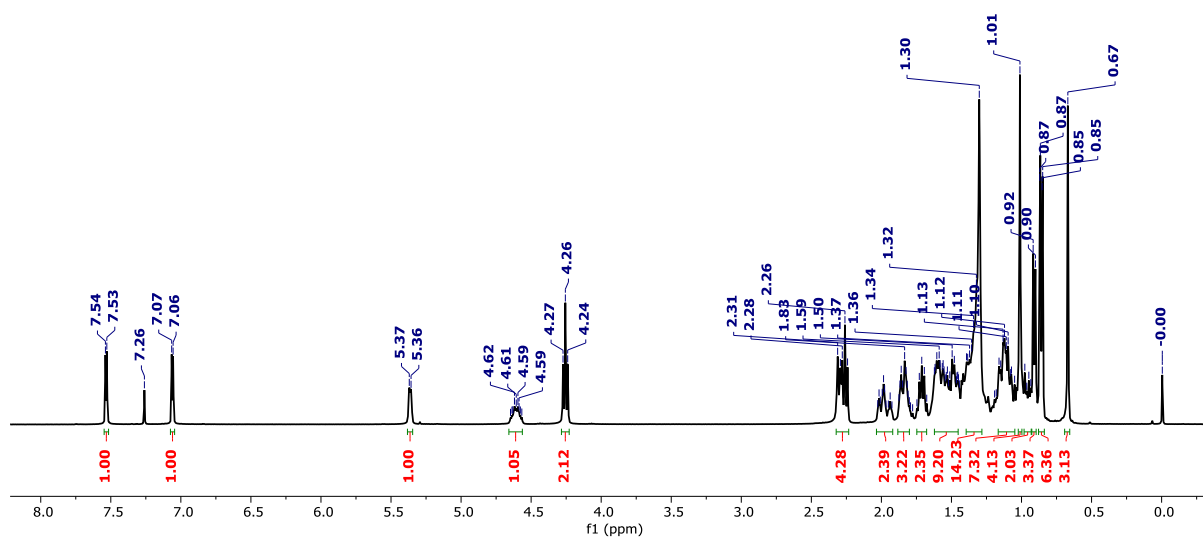


Figure A12 ^{13}C NMR spectrum of compound **4b** in CDCl_3 .



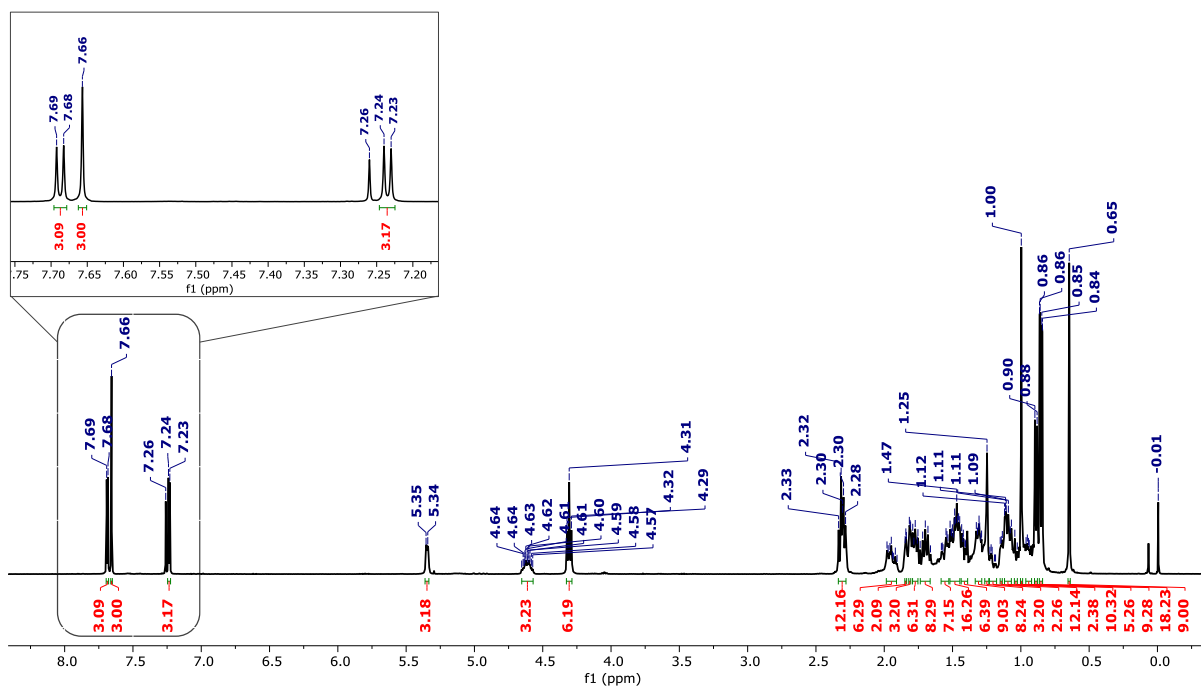


Figure A15 ^1H NMR spectrum of compound F-5 in CDCl_3 .

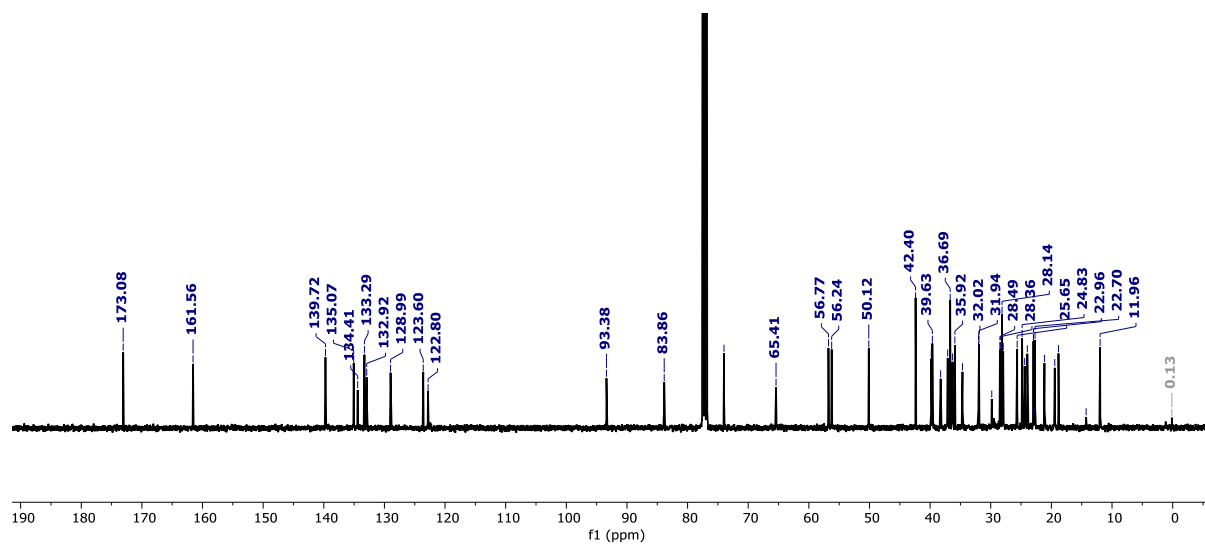


Figure A16 ^{13}C NMR spectrum of compound F-5 in CDCl_3 .

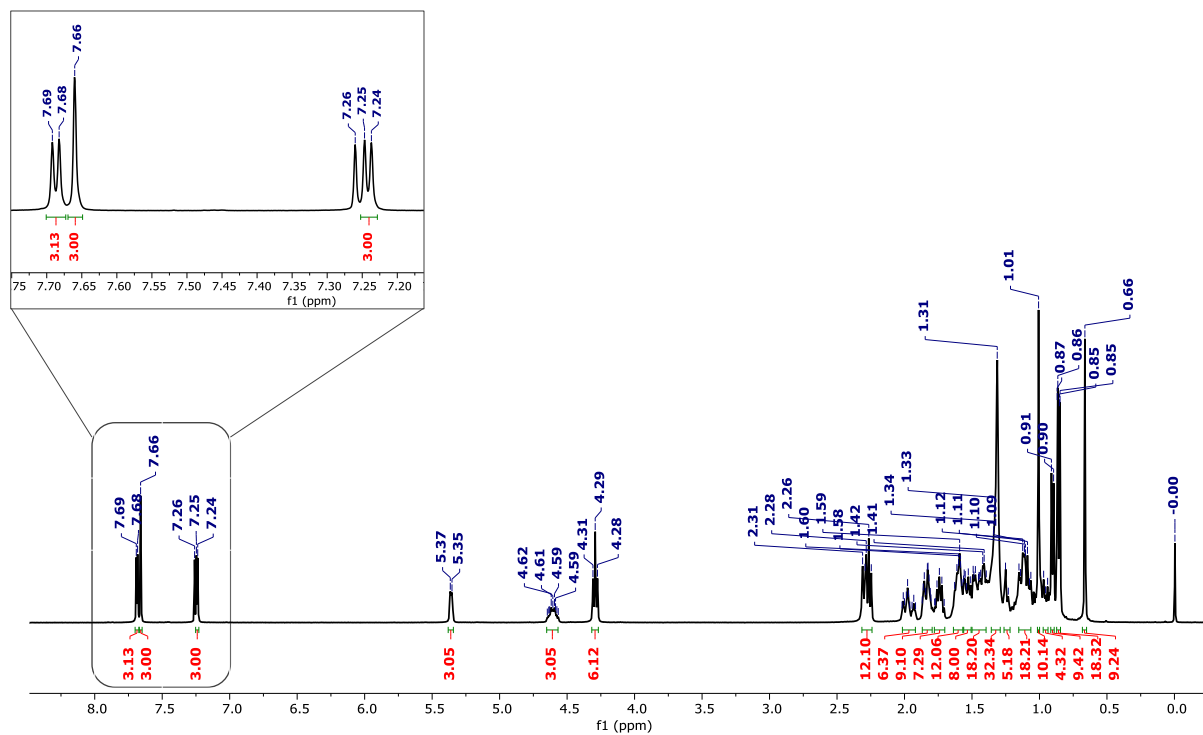


Figure A19 ^1H NMR spectrum of compound F-9 in CDCl_3 .

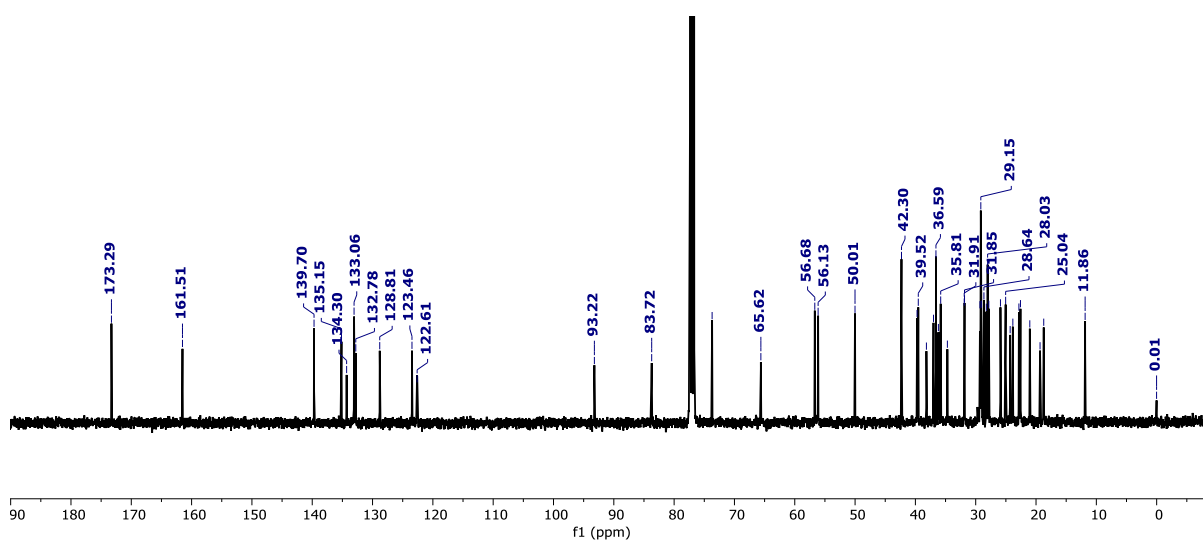


Figure A20 ^{13}C NMR spectrum of compound F-9 in CDCl_3 .

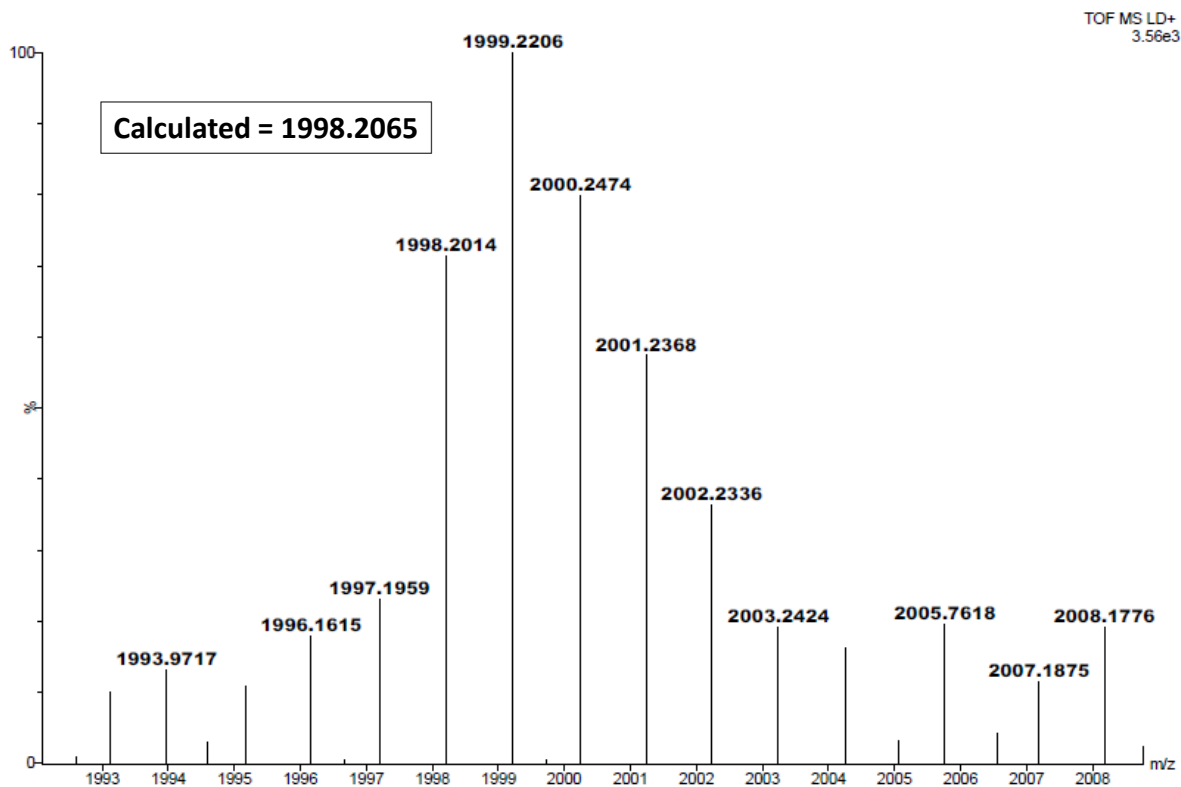


Figure A21 HRMS spectrum of compound F-5.

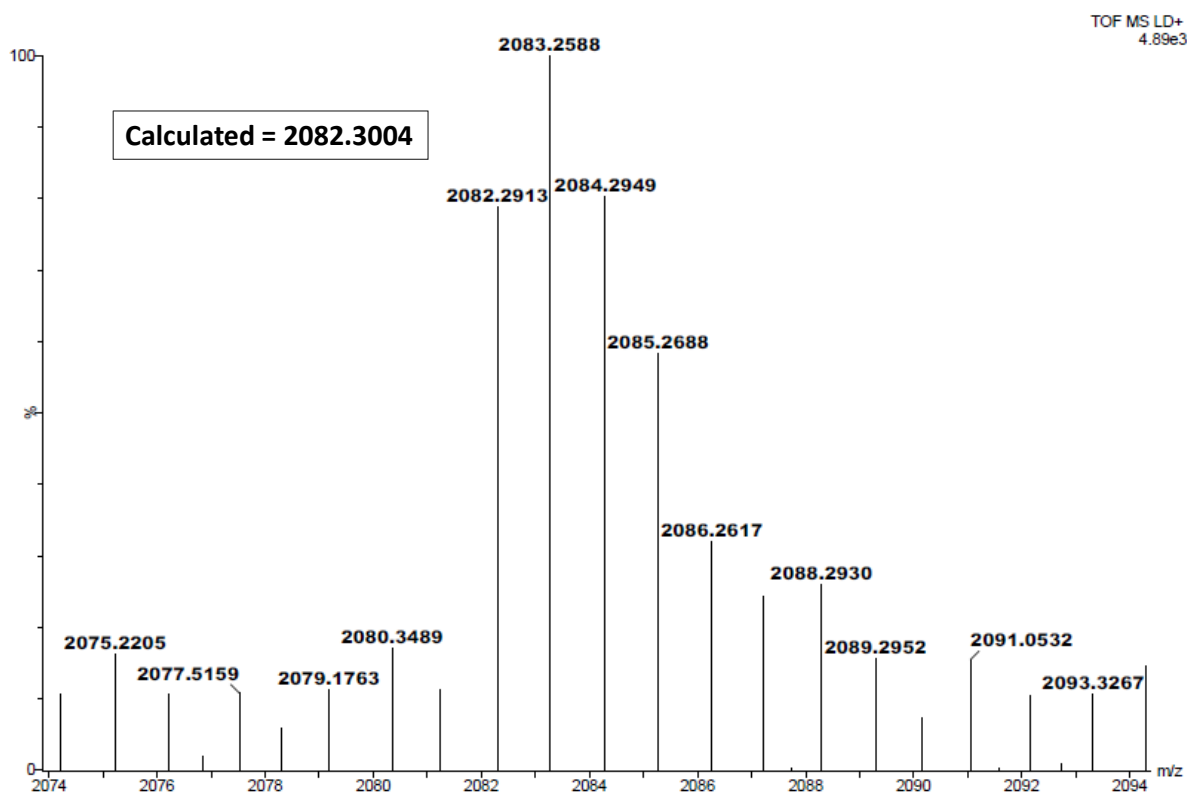


Figure A22 HRMS spectrum of compound F-7.

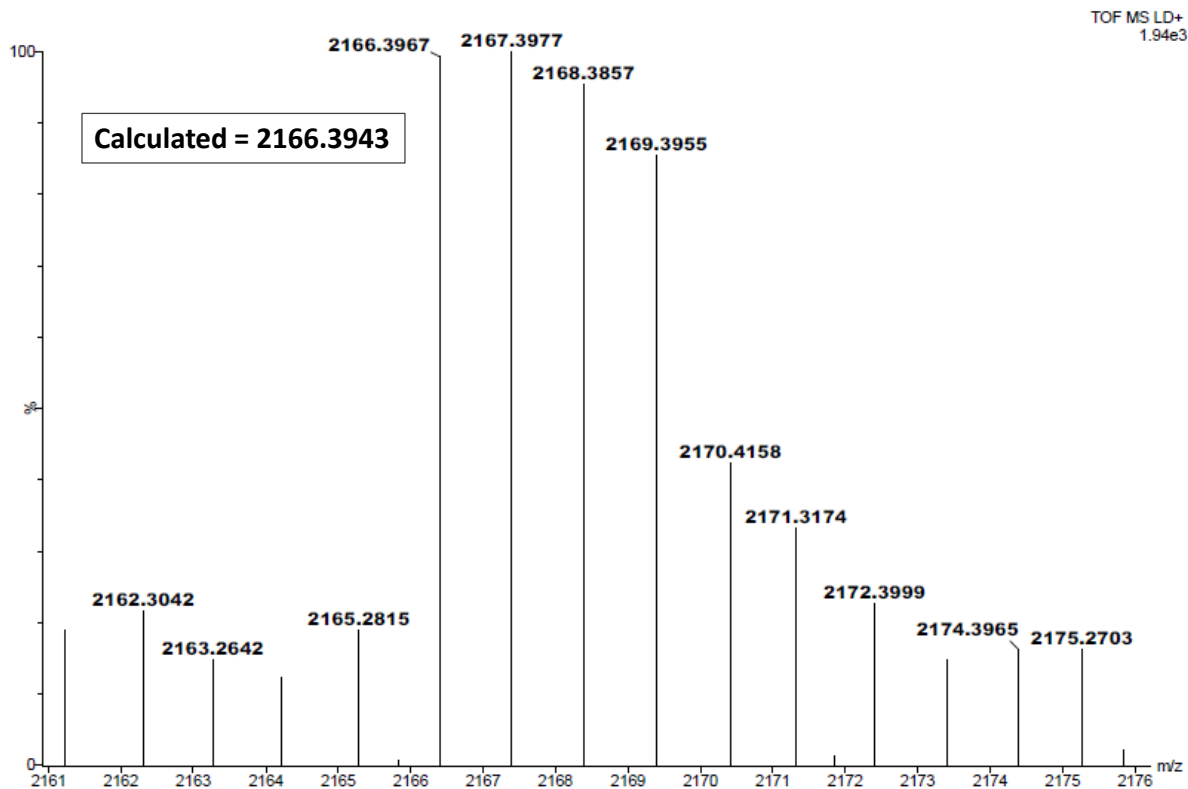


Figure A23 HRMS spectrum of compound F-9.

TGA Curves:

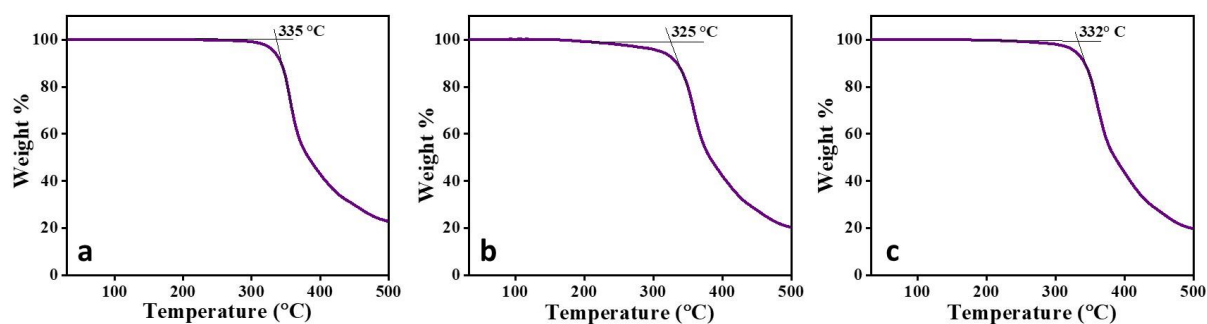


Figure A24 TGA thermographs of compounds (a) F-5, (b) P-7, (c) F-9, obtained at a rate of 5 °C/min.

X-Ray Diffraction Studies:

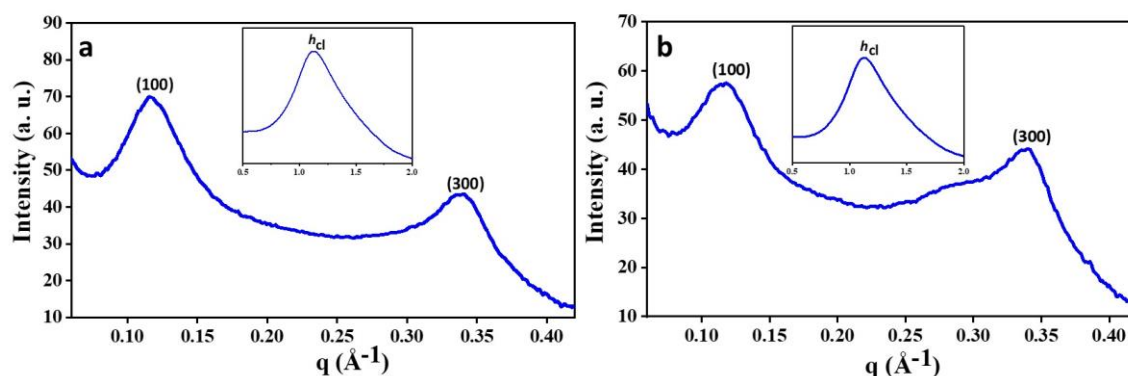


Figure A25 Small and wide-angle (inset) X-ray diffraction patterns of the ordered lamellar phase formed by compound (a) **F-7** at 60 °C (lam_o), (a) **F-9** at 65 °C (lam_o), h_{cl} - fluid cholesterol - cholesterol chain correlations.

Table A1 The observed and calculated d-spacings and corresponding reflecting planes for the diffraction peaks indexed on the lamellar structure observed at 65°C for the compound F-5, at 60°C for the compound F-7 and at 65°C for the compound F-9. The d-spacing is calculated by using the relation: $d_{cal} = \frac{a}{h}$, where h, k, l are the Miller indices and a is the lamellar periodicity.

(hkl)	d-spacing Experimental d_{obs} (Å)	d-spacing Calculated d_{cal} (Å)	Relative Intensity $I(hk)$	Multiplicity	Phase $\Phi(hkl)$
Compound F-5 , calculated value of $a = 58.85$ Å					
100	58.85	58.85	100.00	2	0
200	29.64	29.42	5.89	2	π
300	19.72	19.62	4.25	2	0
h_{cl}	5.74	fluid cholesterol – cholesterol chains			//
Compound F-7 , calculated value of $a = 55.12$ Å					
100	55.12	55.12	100.00	2	
300	18.42	18.37	61.43	2	
h_{cl}	5.60	fluid cholesterol – cholesterol chains			
Compound F-9 , calculated value of $a = 54.63$ Å					
100	54.63	54.63	100.00	2	
300	18.24	18.21	74.14	2	
h_{cl}	5.54	fluid cholesterol – cholesterol chains			

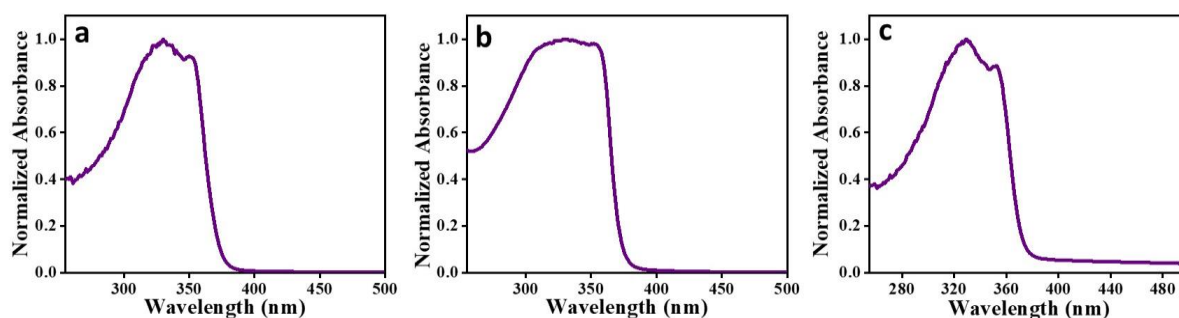
Thin-film UV-vis spectroscopy:

Figure A26 Absorption spectra of compounds (a) F-5, (b) F-7, (c) F-9, in thin-film state.

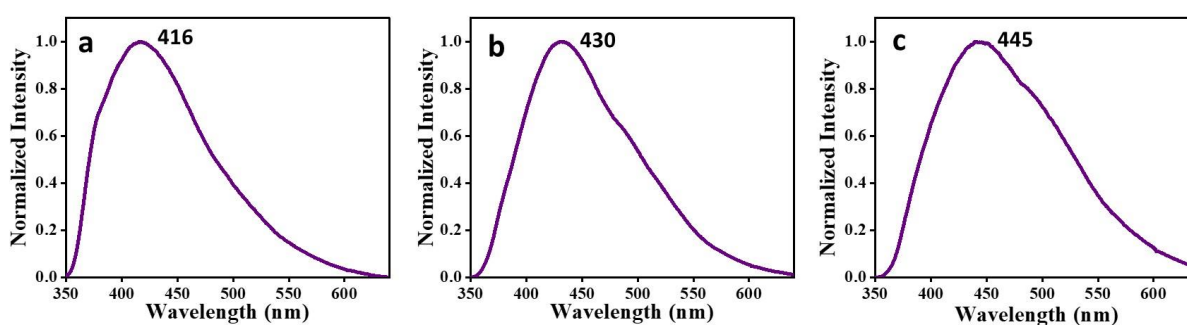
Thin-film emission spectroscopy:

Figure A27 Emission spectra of compounds (a) F-5, (b) F-7, (c) F-9, in thin-film state.

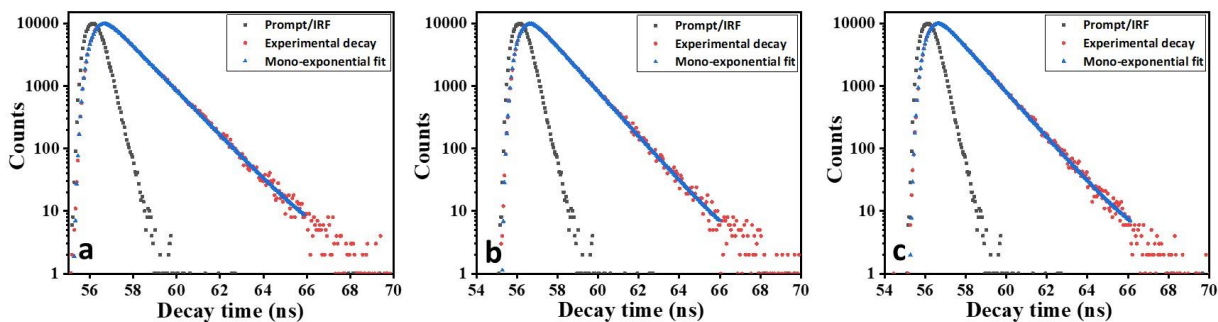
Fluorescence decay measurements:

Figure A28 Fluorescence decay curve of compounds (a) F-5, (b) F-7, (c) F-9, in THF solution fitted by mono-exponential fitting.

Chapter 5

Color-tunable photoluminescent discotic liquid crystal based on Perylene - Pentaalkynylbenzene triad

This chapter describes the design and development of a discotic triad, where perylene is sandwiched between two pentaalkynyl benzene units, linked via a flexible alkyl spacer. The thermotropic liquid crystalline properties of the compound were analyzed by differential scanning calorimetry (DSC), polarising optical microscopy (POM), and wide-angle X-ray diffraction (WXR) techniques. The compound exhibits columnar oblique (Col_{ob}) mesophase that sustains over a significant temperature range. The corresponding electron density map was derived from the intensities observed in the diffraction pattern. The photophysical behaviour of the compound in various solvents of varying polarity has been studied. The compound shows positive solvatochromism with a significant increase in the Stoke's shift of around 91 nm between toluene and ethanol. The compound shows high fluorescence quantum yield in non-polar solvents and lowest in polar solvents. The presented luminescent material with positive solvatochromism will reveal its potential application in fluorescence imaging and the field of optoelectronic organic materials.



5.1 Introduction

Liquid crystalline materials (LCs) consisting of self-organized molecules have attracted growing interest owing to their significant importance as new anisotropic functional soft materials in many device applications by employing a combination of self-healing, processability, and aligned directional conduction of either energy or charge.¹ The organization and self-assembly of π conjugated discotic materials constructing highly ordered supramolecular architecture have been explored due to their promising application in various devices such as photoconductors, one-dimensional conductors, photovoltaic devices, organic light-emitting diodes, field-effect transistors and so on.²⁻¹¹ Mesophase built by discotic molecules is mainly of two types: columnar and nematic discotics. Self-organized columnar arrangements are obtained if the discotic mesogens are assemble on top of one another due to effective π - π interaction between the polyaromatic core with cogent overlap of p orbitals, which encourage the 1D charge transfer. In general, depending on the degree of organization in the molecular orientation along the columnar axis, molecular stacking, dynamics/modeling of the molecules within the columns, and the 2-D lattice symmetry of the columnar arrangement, they assemble themselves into a different kind of lattice symmetry.¹² A large number of the discotic mesogens, such as substituted benzenes,¹³⁻¹⁷ triphenylenes,¹⁸⁻²⁰ pentaalkynylbenzene,²¹⁻²³ perylene,²⁴⁻³⁰ porphyrins,³¹⁻³³ and phthalocyanines,³⁴⁻³⁸ tetrathienoanthracene,³⁹ heterocoronene,⁴⁰ heptazine,⁴¹ anthraquinone⁴² have been synthesized to probe their mesophase arrangement as well as the physical properties. Other materials having a non-disc organization are also used as the constructing unit for the discotic columnar and nematic liquid crystals.

Among the various discotic mesogens, perylene derivatives have evolved as one of the most thoroughly explored class of discotic liquid crystal molecules because of their easy functionalization, π -conjugation, extended rigid planar backbones, high chemical and thermal stability, extreme luminescence, large band gap, and n-type semiconductor properties. The confined strong π - π interactions of the perylene chromophores, which accelerates the molecule aggregation, are responsible for the optical and electrical properties of these molecules. These aggregations also provide a way for efficient electron conduction within the aggregates.²¹ Highly efficient π - π transition within perylene molecules exhibit strong visible light absorption and fluorescence, which is very important for optical sensors based on colorimetric modulation or fluorescence.²⁴ Perylene cores can have their structural properties changed easily through

chemical synthesis by substituting different elements in the ortho, bay, and imide positions. This addition of substituents at different positions can induce various effects on packing structures, solubility, spectroscopic and redox properties.^{24,43} Modifications at imide positions directly affect the solubility and aggregation of perylene molecules; as a result, this will lead to different solvation behaviour and accompanying photophysical patterns.⁴³

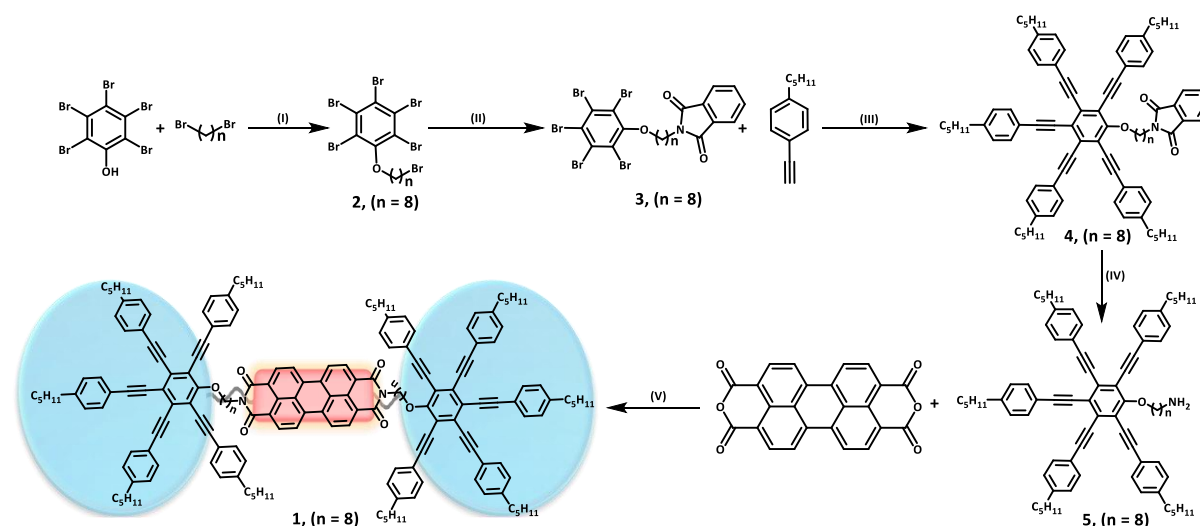
In general, various soft groups easily produced perylene-based liquid crystals by decorating imide and bay positions.²⁵⁻²⁹ A literature survey reveals a wide range of perylene-based dyads and triads exhibiting liquid crystalline behaviour, which could be effectively mediated by the numbers and structures of soft chains at the different positions.^{21,44,45} Non-symmetric liquid crystalline materials made up of two independent mesogenic units have piqued the interest of researchers because they can combine the both discrete mesogenic units into one component. Therefore, one can combine two mesogenic units according to their interests to create a new liquid crystalline material. Perylene derivatives mainly favour the columnar organization due to strong π - π interacting rigid core. Pentaalkynyl benzenes, on the other hand, are the highly studied discotic nematic columnar unit in the literature.¹⁹⁻²³ The discotic nematic mesophase in pentaalkynylbenzene results from the ethynyl linkers' rotational freedom, which restricts the powerful columnar stacking of pentaalkynylbenzene.

Herein, we have reported a new molecular design of discotic liquid crystal triad based on perylene core, in which perylene is sandwiched between two multialkynyl units at the imide position to construct the functional smart material. This strategy of combining two mesogenic units with different structural organizations inspired us to gain complete structural understanding of the packing of the molecule in the phase arrangement. As a result, this strategy accelerates the supramolecular self-assembly of the hybrid triad in a columnar arrangement. In addition, this triad exhibited high fluorescence quantum yield and a quantifying fluorescence response with different solvents according to the polarity of the different solvents, i.e., positive solvatochromic behaviour. Furthermore, we carried out systematic photophysical studies of the molecule to get deep insights of the solvatochromic behaviour. We believe that such solvatochromic behaviour of discotic liquid crystals can potentially be used for fluorescence imaging, display applications and various optoelectronic applications.

5.2 Result and discussions

5.2.1 Synthesis, Structural Characterization and Thermal stability

The target compound **1** was prepared using the synthetic route depicted in Scheme 5.1. The synthesis of intermediate compounds **2** and **3** have been reported earlier.^{1,19,21} The final compound **1** was synthesized by reacting amine substituted pentaalkynyl unit with perylene-3,4,9,10-tetracarboxylic dianhydride in dry DMF with a catalytic amount of acetic acid. The mixture was maintained at 90 °C for 48 h, resulting in the final material in a 30% yield (after chromatographic purification). It was then structurally and analytically characterized by ¹H NMR, ¹³C NMR, FT-IR, HRMS (Figure A1 - A11) and absorption/emission spectroscopy. The thermal stability of synthesized compound **1** was determined using thermogravimetric analysis (TGA) (Figure A12); apparently compound **1** is stable up to 250 °C.



Scheme 5.1 (I) K₂CO₃, Acetone, 48 h, 80 °C, 82 % (II) Potassium phthalimide, Butanone, 48 h, 80 °C, 86 % (III) Pd(PPh₃)₂Cl₂, CuI, PPh₃, NEt₃, 48 h, 90 °C, 60 %, (IV) NH₂NH₂·H₂O, Ethanol, 24 h, 70 °C, 74 % (V) Acetic Acid, DMF, 48 h, 90 °C, 30 %.

5.2.2 Mesomorphic behaviour

To determine the phase behaviour of the synthesized compound **1**, polarizing optical microscopy (POM), differential scanning calorimetry (DSC), and wide-angle X-ray diffraction (WAXRD) studies by the variation of temperature, were performed. Under POM, compound **1** displayed a highly fluidic birefringent texture with the growth of smaller domains,⁴⁰ mesophases appeared at 56 °C during heating and cleared at 114 °C (Figure 5.1a). Upon cooling, the reappearance of textures was not observed. The birefringence was observed when the compound **1** was kept at ambient temperature for almost 24 hours, and this can be explained

possibly due to the impotence of the mesogens to overcome the rotational freedom that the molecules have acquired in their isotropic form and consequently take one day to reassemble. Similar behaviour was also observed in the DSC study (Figure 5.1b, Table 5.1); the thermogram was recorded in the temperature range of 30 °C to 130 °C. In the first heating cycle, one endothermic peak was observed at 54 °C ($\Delta H = 14.61$ kJ/mol), which denotes the crystalline to mesophase transition and second endothermic peak at 116 °C ($\Delta H = 31.48$ kJ/mol), which corresponds to the mesophase to isotropic transition. The transition temperature and respective enthalpy transition are listed in Table 5.1. Previously, there was a report from our lab based on multialkynyl and triphenylene units, where these two moieties were connected via a triazole unit. In this report, the pure compound display Col_r structure, but on cooling, these materials took time to reassemble and show a less ordered smectic phase. But after doping with trinitrofluorenone (TNF), these materials exhibit the enantiotropic Col_h phase.²⁰

Table 5.1 Thermal behaviour of compound **1**.^a

C	Heating Scan	Cooling Scan
1	Cr 54 [14.61] Col_{ob} 116 [31.48] Iso	Iso
^a Enthalpy values in parentheses in kJ/mol and temperatures in °C. Abbreviations: C = compound; Cr = crystalline solid; Col_{ob} = columnar oblique; Iso = isotropic liquid.		

Based on a thorough microscopic examination, it was observed that, once the compounds were heated to an isotropic temperature, it took almost 24 hours for them to get back together effectively into the discotic columnar mesophase. The detailed study of the supramolecular organization of compound **1** in the columnar mesophase was studied by the wide-angle X-ray diffraction technique (Figure 5.1c). The compound exhibits a columnar oblique (Col_{ob}) phase in the mesophase temperature range. The X-ray diffraction pattern of the compound shows many narrow Bragg's peaks in the wide-angle regime. These peaks could be indexed on the oblique lattice, and d-spacing could be calculated by using the relation: $d_{cal} = \frac{\sin(\alpha)}{\sqrt{\frac{h^2}{a^2} + \frac{k^2}{b^2} - \frac{2hk \cos(\alpha)}{ab}}}$; where (hk) is the Miller indices of the reflections corresponding to the oblique lattice; a , and b & α are the unit cell parameters, α is the angle between a and b . The calculated lattice parameters at 70 °C temperature is found to be $a = 27.46$ Å, $b = 51.92$ Å & $\alpha = 115.65^\circ$. Further, the X-ray diffraction pattern of the compound shows two non-Bragg's reflections, namely, h_a and h_c , in the wide-angle regime with d-spacing 4.97 Å and 3.95 Å, respectively (Figure 5.1c, Table 5.2). The h_a peak denotes the fluid chain-chain correlations,

whereas h_c peak refers the π - π interaction between the discotic cores and confirms the occurrence of columnar structure. Therefore, the observed phase is columnar oblique (Col_{ob}).

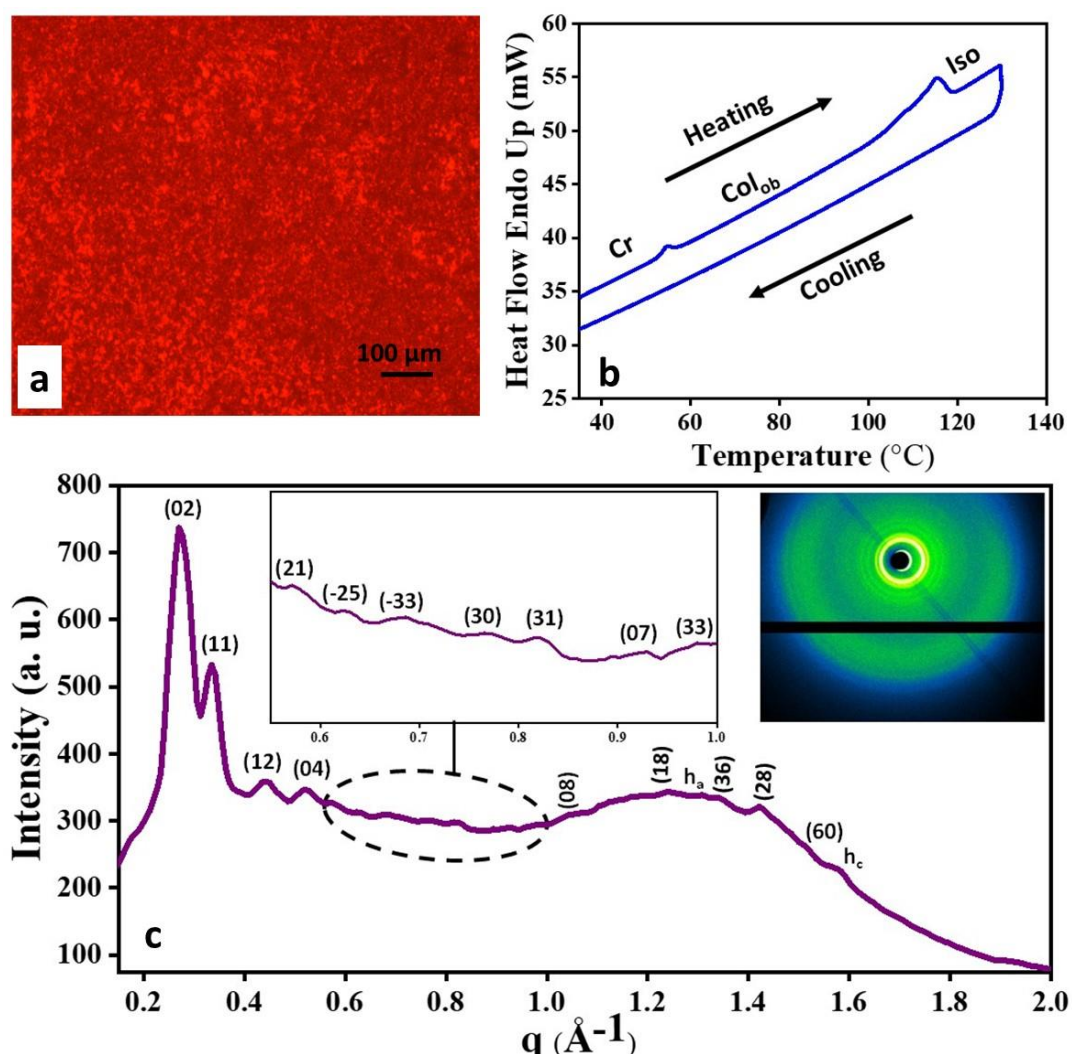


Figure 5.1 (a) POM microphotograph of the optical texture of Col_{ob} phase formed by compound **1** at 70 °C, (b) DSC thermogram of compound **1**, and (c) Wide angle X-ray diffraction and 2-D diffraction pattern (inset) of Col_{ob} phase at 70 °C, h_a – due to alkyl chain-chain correlation and h_c – due to disc-disc correlation.

5.2.3 Electron density maps

Further, to have a better understanding of the arrangement of molecules in the columnar oblique phase, electron density maps¹² have been designed by using the information of peak Miller planes and their intensities. The electron density map for the compound is shown in Figure 5.2a. Deep red represents the high electron density, and deep blue represents the low-density part. Following the information of the reconstructed electron density map, a two-dimensional projection of the arrangement of the compound corresponding to Col_{ob} phase is also shown in

Figure 5.2b. The compound consists of two pentaalkynylbenzene groups connected through perylene. The perylene group is keen to form the column and exhibit columnar structure, whereas pentaalkynylbenzene group does not like to form a columnar phase and shows the discotic nematic arrangement.

Table 5.2 The Indices observed and calculated d -spacings and planes of the diffraction peaks of the oblique lattice observed at 70 °C for compound **1**. The lattice parameters are $a = 27.46$ Å, $b = 51.92$ Å and $\alpha = 115.65^\circ$. h_a - alkyl chain-chain correlation, h_c – disc-disc correlation.

Calculated d -spacing by using the relation: $d_{cal} = \frac{\sin(\alpha)}{\sqrt{\frac{h^2}{a^2} + \frac{k^2}{b^2} - \frac{2hk \cos(\alpha)}{ab}}}$.

(hk)	d-spacing Experimental d_{obs} (Å)	d-spacing Calculated d_{cal} (Å)	Relative Intensity $I(hk)$	Multiplicity	Phase $\Phi(hkl)$
02	23.40	23.40	100.00	2	0
11	18.78	18.78	72.18	2	0
12	14.21	14.21	48.57	2	π
04	11.89	11.70	47.08	2	0
21	10.99	10.86	44.36	2	π
-25	9.98	9.77	//	//	//
-33	9.15	9.10	//	//	//
30	8.13	8.25	//	//	//
31	7.63	7.58	//	//	//
07	6.75	6.69	//	//	//
33	6.41	6.26			
08	5.98	5.85			
18	5.08	5.21			
h_a	4.97	Fluid alkyl chain-chain correlation			
36	4.68	4.74			
28	4.21	4.58			
60	4.16	4.12			
h_c	3.95	π - π interaction between disc core			

However, pentaalkynylbenzene group connected with perylene is found to display a variety of columnar phases. In the present case, as observed, the columnar forming nature of the perylene

group led to the formation of columnar oblique phase. The two-dimensional projection of the phase can be better understood by the schematic as shown in Figure 5.2c.

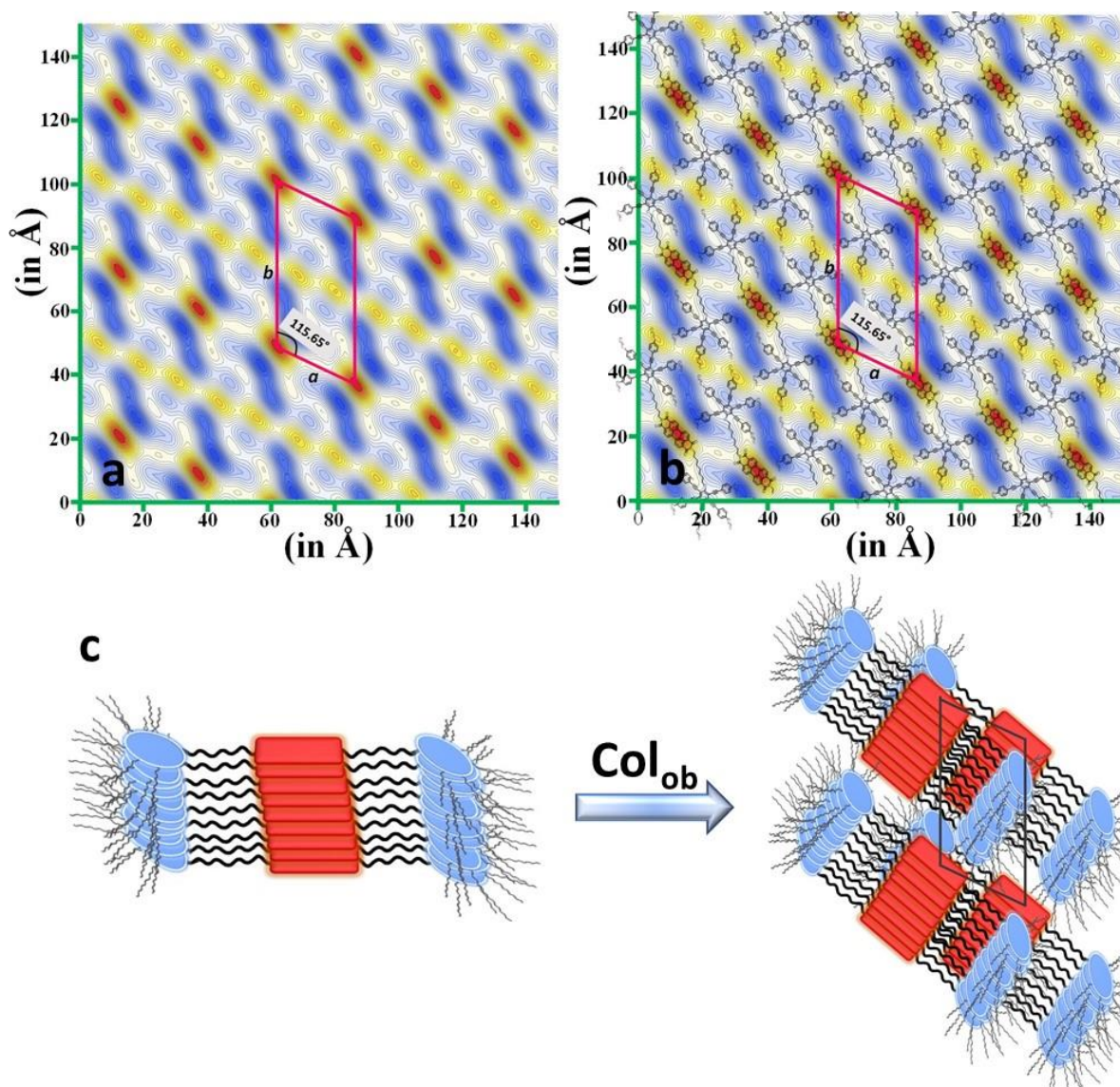


Figure 5.2 (a) Electron density map of compound **1** in Col_{ob} phase, red colour represents the high electron density region and blue is the lowest. The rectangle (pink colour) represents the unit cell of the Col_{ob} phase with lattice parameters *a* and *b*, (b) Arrangements of molecules in Col_{ob} phase, and (c) Schematic showing the self-assembly behaviour of compound **1** in columnar arrangement.

5.2.4 Photophysical behaviour

Compound **1** exhibits good absorption and emission properties. Figure 5.3 shows the UV absorption (Figure 5.3a) and fluorescence emission (Figure 5.3b) spectra of compound **1** in different solvents (10^{-5} M) with increasing polarity. Both spectra show a bathochromic shift with increasing polarity of the solvent. As shown in Figure 5.3b, compound **1** shows a sharp

and structured emission in nonpolar solvents, whereas, in high polarity, it shows a broad and structureless emission because of agglomerate formation. The agglomeration can be proved by a temperature-dependent UV experiment in ethanol (Figure 5.4a) and DMF (Figure 5.4b); with increasing the temperature, the peaks are more structured. Also, it is very clear from Figure 5.3b that the solvent induces a shift in the emission spectra that is larger than the shift in the absorption spectrum.

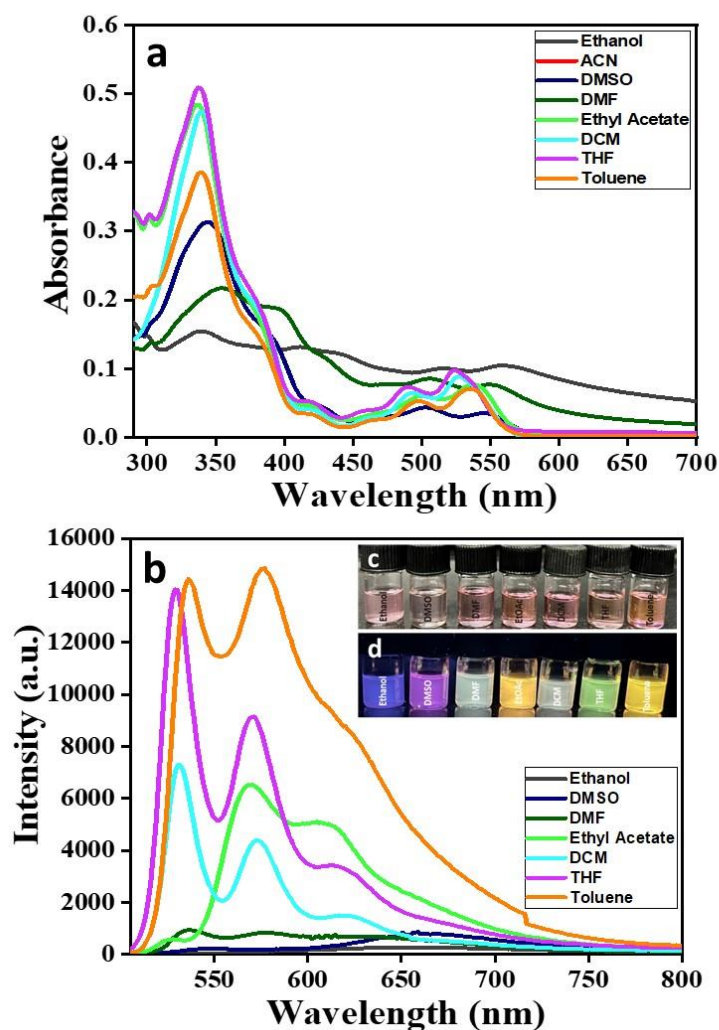


Figure 5.3 (a) Absorption and (b) Emission spectra of compound **1** in solvents of different polarities (10^{-5} M). Optical photographs of compound **1** in different solvents (c) in daylight, and (d) under UV light.

The observed shifts are dependent on the dielectric constant and nature of the solvent (polar and non-polar)⁴⁶, and here we observed an impressive increase in the Stokes' shift of almost 91 nm between toluene and ethanol. The Stokes shift value increased notably with increasing the solvent polarity, indicating the presence of a different charge distribution in the excited

state (S_1), than in the ground state (S_0).^{47,48} The shift observed in the spectral band with various solvents appeared from the high reaction field that a solute molecule experiences due to the polarization of the surroundings solvent molecules.⁴⁶ The solvent-induced Stoke's shift is visible in the photograph (Figure 5.3c and 5.3d), where Figure 5.3c is under normal light, and Figure 5.3d is captured under UV light. Table 5.3 summarises the emission maxima, absorption maxima, Stokes' shift and fluorescence quantum yield values of the compound in the different solvents (10^{-5} M). In the same solvents, the quantum yield was also calculated to assess the solvent effect. In the calculated quantum yield summarized in Table 5.3, compound **1** exhibited the very high quantum yield value of 0.72 in toluene, whereas it is found to be the lowest value of 0.04 and 0.07 in ethanol and DMF, respectively. These results indicated that the solute and solvents led to a change in the transition state accountable for the shifts in the emission maxima.⁴⁹

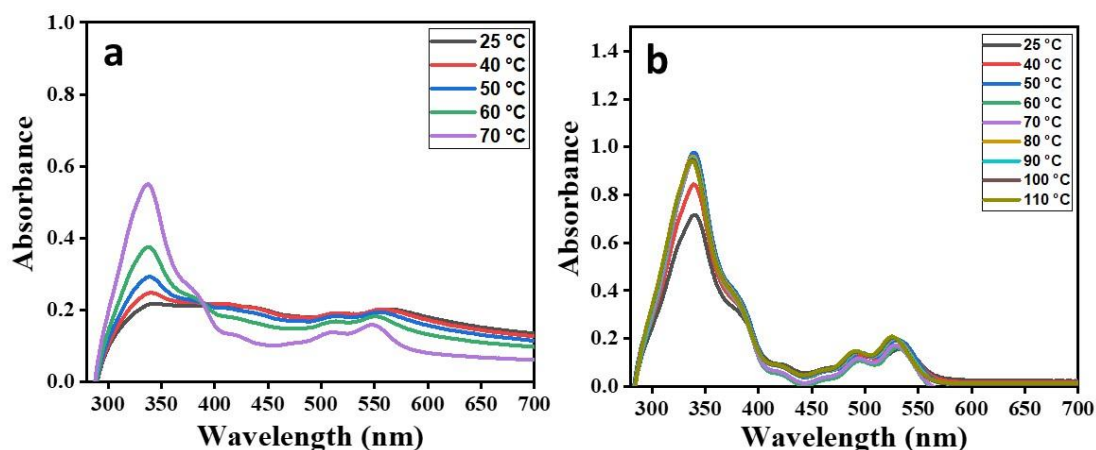


Figure 5.4 Temperature-dependent UV-vis spectrum of compound **1** in (a) Ethanol and (b) DMF solvent.

Further, the solvent-dependent spectral shifts are described by the Lippert Mataga Plot, which defines a plot of Stokes' shift versus orientation polarizability (Δf) of the solvent. This explained Stokes' shift in terms of changes in the dipole moment of fluorophore upon excitation and the dependence of energy of the dipole on the refractive index and dielectric constant of the solvent. For compound **1**, the plot of Stokes' shift versus orientation polarizability (Figure A13) shows a weak correlation, and this generally explains that the best correlation of the Lippert mataga plot is observed for the stronger electron donor-acceptor system. In contrast, for the weak electron donor-acceptor, the correlation is not as good.^{49,50}

Table 5.3 Photophysical properties of compound **1**.

Solvents	λ_{abs} (max)/nm	λ_{em} (max)/nm	Stokes Shift/cm ⁻¹	η^a	ϵ^b	Δf^c	Φ_F^d
Ethanol	560	667	2864.6	1.36	24.5	0.29	0.04
DMSO	546	664	3254.8	1.48	46.7	0.26	0.14
DMF	550	578	880.8	1.43	36.7	0.27	0.07
EtOAc	537	611	2255.4	1.37	6.0	0.28	0.22
DCM	527	578	1674.3	1.42	8.9	0.20	0.14
THF	524	570	1540.1	1.41	7.6	0.22	0.26
Toluene	535	576	1330.5	1.50	2.4	0.21	0.72

^aRefractive Index; ^bDielectric Constant; ^cSolvent Polarity; ^dFluorescence Quantum Yield. Quantum yield was measured by using Rhodamine (10⁻⁵ M) in ethanol as a standard.

5.2.5 Electrochemical properties and DFT calculations

To investigate the electronic energy states and oxidation/reduction potential, cyclic voltammetry (CV) was carried out. The CV experiment was performed by using a millimolar solution of the compound in oxygen-free DCM at a scan rate of 50 mVs⁻¹. A 0.1 M solution of TBAH was used as a supporting electrolyte. The experimental condition for CV, and electrochemical data for compound **1** (Figure 5.5a) and ferrocene (Figure A14) are listed in Table 5.4. The compound shows reversible oxidation and reduction potentials (Figure 5.5a). The HOMO and LUMO energy levels are found to be -5.83 eV and 3.46 eV, respectively. The electrochemical band gap was calculated as $\Delta E_{g, CV} = E_{LUMO} - E_{HOMO}$ and found to be 2.37 eV. The optical band gap was calculated from the absorption data and estimated to be 2.18 eV (Table 5.4). Further, the density functional theory (DFT) calculations using Gaussian 09 software with B3LYP/ 631G (d,p), were performed to calculate the energy minimized structures. The frontier molecular orbitals of compound **1** are shown in Figure 5.5b.

5.3 Conclusions

We have systematically presented the synthesis and characterization of perylene – pentaalkynyl benzene-based triad, where perylene is connected to two pentaalkynylbenzene units via flexible alkyl chain. Detailed characterization using POM, DSC and WXRd established that compound **1** exhibited the columnar oblique arrangement in the mesophase temperature range. As clearly revealed from the studies that, by combining discotic nematic (pentaalkynylbenzene) and discotic columnar moiety (perylene) in the same molecule, give

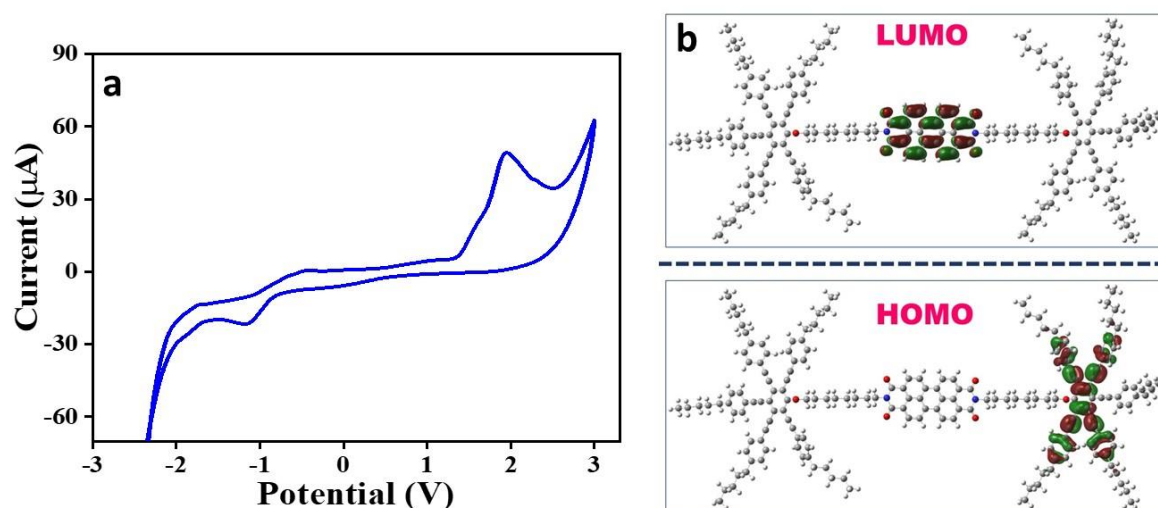


Figure 5.5 (a) Cyclic voltammogram and (b) HOMO – LUMO frontier orbitals of compound **1**.

rise to the formation of discotic columnar mesophase. Hence, the strong π - π interaction ability of perylene is dominated in the final columnar mesophase organization. The luminescent behaviour of perylene is also preserved. In addition, the effect of various solvents of different polarity on the photophysical properties of compound **1** was studied. We observed a positive solvatochromism with a significant increase in the Stoke's shift of around 91 nm from non-polar (toluene) to polar (ethanol) solvents. Compound **1** displays good fluorescent quantum yield in non-polar solvents. These findings imply that this molecule has potential application in fluorescence imaging as well as optoelectronics.

Table 5.4 Electrochemical properties of compound **1**.^a

C	$\lambda_{\text{onset,UV}}$ (nm)	$\Delta E_{\text{g,UV}}^b$ (eV)	$E_{\text{ox,onset}}$ (V)	$E_{\text{red,onset}}$ (V)	E_{HOMO}^c (eV)	E_{LUMO}^d (eV)	$\Delta E_{\text{g,CV}}^e$ (eV)
1	568	2.18	1.54	-0.82	-5.83	-3.46	2.37

^aRecorded in DCM solution (mM). Experimental conditions: reference electrode used was Ag/AgNO₃, counter electrode used was platinum wire, glassy carbon used as working electrode, tetrabutylammonium perchlorate (TBAP) (0.1 M) acts as supporting electrolyte. ^bOptical Band gap obtained from the red edge of the longest wavelength in the UV – vis absorption spectrum. Calculated as: $\Delta E_{\text{g,UV}}$ (optical band gap) = $1240/\lambda_{\text{onset,UV}}$. ^cEstimated from the formula $E_{\text{HOMO}} = -(4.8 - E_{1/2,\text{Fe,Fe}^+} + E_{\text{oxd,onset}})$ eV, where $E_{1/2,\text{Fe,Fe}^+} = 0.52$ V. ^dObtained from the formula $E_{\text{LUMO}} = -(4.8 - E_{1/2,\text{Fe,Fe}^+} + E_{\text{red,onset}})$ eV. ^eElectrochemical band gap: $\Delta E_{\text{g,CV}} = E_{\text{LUMO}} - E_{\text{HOMO}}$. Abbreviation: C – compound.

5.4 Experimental section

5.4.1 General procedure for the synthesis of compound 2:

In a round bottom flask (R.B), pentabromophenol (1 equiv.), potassium carbonate (5 equiv.) and alkyl bromide (5 equiv.) were dissolved in 30 mL acetone and refluxed at 80 °C for 48 h. After completion of the reaction, the acetone was evaporated and extracted with DCM. The reaction mixture was purified by column chromatography in 60-120 silica gel by using hexane as eluent. Yield = 82 %. The ¹H (Figure A1) and ¹³C NMR (Figure A2) spectrum are given in Appendix IV.

Characterization details of compound 2:

¹H NMR (400 MHz, CDCl₃, δ in ppm) 3.99 (t, J = 6.6 Hz, 2H), 3.42 (t, J = 8 Hz, 2H), 1.87 (p, J = 7.0 Hz, 4H), 1.54 – 1.43 (m, 4H), 1.43 – 1.36 (m, 4H).

¹³C NMR (100 MHz, CDCl₃, δ in ppm) 171.24, 154.47, 135.53, 132.50, 128.38, 124.56, 121.88, 73.32, 64.48, 29.76, 28.56, 25.79, 25.51, 21.07.

FTIR (cm⁻¹) 2945.3, 1463.6, 1419.3, 1341.8, 1238.9, 1036.4, 983.8, 892.8.

5.4.2 General procedure for the synthesis of compound 3:

A mixture of compound 2 (1 equiv.), potassium phthalimide (3 equiv.) in 50 mL of butanone was heated under reflux for 48 h. After completion of the reaction, butanone was evaporated and extracted with DCM. The organic solution was washed with water (50 mL) twice and brine (20 mL) and dried over sodium sulphate. After the solvent was removed under reduced pressure, the resulting residue was purified by column chromatography (60-120 silica gel, hexane/EtOAc as eluent) to give 3. Yield = 86 %. The ¹H (Figure A3) and ¹³C NMR (Figure A4) spectrum are given in Appendix IV.

Characterization details of compound 3:

¹H NMR (400 MHz, CDCl₃, δ in ppm) 7.84 (dd, J = 5.4, 3.1 Hz, 2H), 7.70 (dd, J = 5.4, 3.1 Hz, 2H), 3.97 (t, J = 6.5 Hz, 2H), 3.68 (t, J = 7.3 Hz, 2H), 1.84 (h, J = 6.8 Hz, 2H), 1.68 (p, J = 7.1 Hz, 2H), 1.50 (p, J = 6.9, 6.3 Hz, 2H), 1.39 – 1.33 (m, 6H).

^{13}C NMR (100 MHz, CDCl_3 , δ in ppm) 171.24, 154.47, 128.38, 124.56, 121.88, 73.32, 64.48, 29.76, 28.56, 25.79, 25.51, 21.07.

FTIR (cm^{-1}) 2943.1, 2859.4, 1735.6, 1523.3, 1467, 1418.3, 1341.7, 1236.6, 1037.2, 983.3, 891.4.

5.4.3 General procedure for the synthesis of compound 4:

The sonogashira of compound **3** (1 equiv.) was done by taking 50 mL of dry triethylamine in a round bottom flask which was degassed for 30 min, and then compound **3** was added, followed by the addition of $\text{Pd}(\text{PPh}_3)_2\text{Cl}_2$ (0.1 equiv.), CuI (0.1 equiv.) & PPh_3 (0.2 equiv.). The mixture was stirred for 15 min, followed by the gradual addition of 4-pentylphenylacetylene. The reaction mixture was stirred at 90 °C for 48 h under a nitrogen atmosphere & after cooling to room temperature, it was poured into 50 mL of 5 M HCl. After extracting the reaction mixture with DCM, the compound was purified in 100-200 silica gel by using hexane/EtOAc as an eluent. Yield = 60 %. The ^1H (Figure A5) and ^{13}C NMR (Figure A6) spectrum are given in Appendix IV.

Characterization details of compound 4:

^1H NMR (400 MHz, CDCl_3 , δ in ppm) 7.83 (dd, $J = 5.4, 3.1$ Hz, 2H), 7.69 (dd, $J = 5.5, 3.0$ Hz, 2H), 7.56 – 7.47 (m, 10H), 7.20 – 7.14 (m, 10H), 4.34 (t, $J = 6.4$ Hz, 2H), 3.65 (t, $J = 8$ Hz, 2H), 2.63 (t, $J = 7.8$ Hz, 10H), 1.91 (p, $J = 6.5$ Hz, 2H), 1.68 – 1.59 (m, 16H), 1.37 – 1.30 (m, 24H), 0.93 – 0.88 (m, 15H).

^{13}C NMR (100 MHz, CDCl_3 , δ in ppm) 168.45, 144.02, 143.95, 133.84, 132.20, 131.80, 131.60, 128.57, 123.15, 120.50, 120.14, 84.06, 38.05, 35.99, 31.50, 30.98, 29.73, 29.50, 28.60, 22.56, 14.07.

FTIR (cm^{-1}) 3027.2, 2925.7, 2855.5, 2207.1, 1772.4, 1713.3, 1606.5, 1510.8, 1395.5, 1367.3, 1180.7, 1020.2, 969.4, 838.2.

5.4.4 General procedure for the synthesis of compound 5:

Compound **4** (1 equiv.) was dissolved in hot ethanol (50 mL), and aqueous hydrazine hydrate (3 mL, 85 %) was added. The reaction mixture was heated under reflux for 24 h. After the mixture was cooled, water and DCM were added. The organic layer was washed with water

and brine, dried (Na_2SO_4) and concentrated. The crude material was purified by column chromatography (silica gel, DCM/Methanol 15:1). Yield = 74 %. The ^1H (Figure A7) and ^{13}C NMR (Figure A8) spectrum are given in Appendix IV.

Characterization details of compound 5:

^1H NMR (400 MHz, CDCl_3 , δ in ppm) 7.53 – 7.47 (m, 10H), 7.17 – 7.13 (m, 10H), 4.32 (t, $J = 6.3$ Hz, 2H), 2.92 (t, $J = 7.7$ Hz, 2H), 2.61 (t, $J = 8$ Hz, 10H), 1.92 – 1.85 (m, 2H), 1.66 – 1.57 (m, 16H), 1.35 – 1.30 (m, 24H), 1.28 (s, 2H), 0.92 – 0.86 (m, 15H).

^{13}C NMR (100 MHz, CDCl_3 , δ in ppm) 170.00, 160.11, 144.10, 131.79, 131.58, 128.58, 120.48, 120.02, 99.66, 87.04, 84.10, 39.60, 35.99, 31.96, 31.50, 31.00, 30.97, 30.34, 29.73, 29.45, 29.40, 26.78, 26.05, 23.35, 22.73, 22.56, 14.07.

FTIR (cm^{-1}) 3291.9, 3027.4, 2925.3, 2855.2, 2207.9, 1653.6, 1554.2, 1511.9, 1461.6, 1425, 1374, 1347.8, 1180.8, 1113.9, 1082.6, 1019.7, 973, 837.7.

5.4.5 General procedure for the synthesis of compound 1:

Compound **5** (1 equiv.) was dissolved in DMF (10 mL). 3,4:9,10-Perylenetetracarboxylic dianhydride (0.6 equiv.) and acetic acid (0.3 equiv.) were added to the solution, and the mixture was heated to 85 °C for two hours under Argon. Then 0.4 equivalent of 3,4:9,10-Perylenetetracarboxylic dianhydride was added, and the reaction was maintained at 90 °C for 48 h. The mixture was cooled to room temperature and extracted with diethyl ether. The crude product was purified by repeated column chromatography in 100-200 silica gel by using hexane/EtOAc as an eluent. Yield = 30 %. The HRMS (Figure A9), ^1H (Figure A10) and ^{13}C NMR (Figure A11) spectrum are given in Appendix IV.

Characterization details of compound 1:

^1H NMR (400 MHz, CD_2Cl_2 , δ in ppm) 8.19 (d, $J = 7.8$ Hz, 4H), 7.97 (d, $J = 8.3$ Hz, 4H), 7.45 – 7.35 (m, 20H), 7.23 – 7.15 (m, 20H), 4.13 (t, $J = 6.1$ Hz, 4H), 3.91 (t, $J = 7.2$ Hz, 4H), 2.66 (t, $J = 7.8$ Hz, 20H), 1.81 – 1.73 (m, 6H), 1.69 – 1.64 (m, 22H), 1.55 (s, 6H), 1.41 – 1.33 (m, 50H), 0.92 (q, $J = 6.9$ Hz, 30H).

^{13}C NMR (100 MHz, CD_2Cl_2 , δ in ppm) 159.97, 144.42, 144.28, 144.07, 131.48, 130.53, 128.60, 128.52, 128.14, 122.73, 120.18, 120.03, 119.75, 99.30, 86.69, 83.76, 35.91, 31.52, 30.94, 22.55, 13.83.

HRMS (MALDI) for $\text{C}_{182}\text{H}_{190}\text{N}_2\text{KO}_6$ (M + K): calculated – 2538.4261; found- 2538.5713.

FTIR (cm^{-1}) 3030, 2926.8, 2856, 2208, 1694.2, 1657.8, 1595, 1512.2, 1425.8, 1404.1, 1347.2, 1257.4, 1179.2, 1088.2, 968.6, 838.9, 811.

5.5 Electron density map

The procedure for reconstructing the electron density map has been adopted from our previous reports.^{20,51} Briefly, we reproduced here for the reader's convenience.

“The electron density $\rho(x,y,z)$ of a liquid crystalline phase is linked to its structure factor $F(hkl)$ by inverse Fourier transformation as follows:

$$\rho(x,y,z) = \sum_{hk} F(hkl) e^{2\pi i(hx+ky+lz)}$$

In this formula (hkl) are the Miller Indices and x, y, z are the fractional coordinates in the unit cell. To calculate the electron density, the complex structure factor $F(hkl)$ has to be written as the product of the phase, $\Phi(hkl)$ and the modulus $|F(hkl)|$ which is proportional to the square root of the intensity $I(hkl)$ of the observed reflection as shown below:

$$F(hkl) = |F(hkl)|e^{i\Phi(hkl)} = \sqrt{I(hkl)}e^{i\Phi(hkl)}$$

The intensities of the different peaks in the diffraction pattern can be estimated from the areas under each peak after subtracting the background and then applying the relevant geometric and multiplicity corrections. The only information that cannot be obtained directly from experiment is the phase, $\Phi(hkl)$, for each diffraction peaks. However, this problem becomes easily tractable when the structure under study is centrosymmetric, i.e., if $\rho(x, y,z) = \rho(-x, -y,-z)$. In that case $F(hkl)$ can only be real and hence $\Phi(hkl)$ can be either 0 or π . For non-centrosymmetric groups, the phase may take every value between 0 and 2π . As the liquid crystalline phases observed are generally centrosymmetric, it is easy to reconstruct the electron density maps by taking the value of $\Phi(hkl)$ as 0 or π . The “correct” map is subsequently chosen on the merit of the reconstructed maps along with other physical and chemical knowledge of the system, such as chemical constituents and their sizes.”

5.6 Quantum Yield Measurement

A direct method of measuring photoluminescence quantum yield (PL-QY) was employed, whereby a reference sample of known quantum efficiency was used as a comparison;^{52,53} the dye Rhodamine 6G was chosen as the reference as it absorbs in a similar region. With the optical spectra of both the reference and compound 1 solution in a given solvent, the following equation was applied:

$$\Phi = \Phi_R \frac{X(1-10^{-A_R})n^2}{X_R(1-10^{-A})n_R^2}$$

Where ‘ Φ ’ is the quantum yield, ‘ X ’ is the integrated area under the emission peak, ‘ A ’ is the absorbance at the excitation wavelength, and ‘ n ’ is the refractive index of the solvent. Each subscript ‘ R ’ refers to the respective values of the reference standard.⁵⁴

5.7 The Lippert-Mataga Plot

The expression for $\Delta f(\epsilon, n)$, given as,

$$\Delta f(\epsilon, n) = \frac{\epsilon - 1}{2\epsilon + 1} - \frac{n^2 - 1}{2n^2 + 1}$$

Where ϵ and n are the dielectric constant and refractive index of the solvents, respectively.

5.8 Author Contributions

SR, MG and SKP conceptualised the project. SR performed all the experiments and analysed the data. SPG analysed the SAXS/WAXS data. All authors have given approval to the final version of the chapter.

5.9 Acknowledgements

Dr. S. K. Pal is grateful to the CRG-SERB project no CRG/2019/000901/OC for financial support. SR thank CSIR for fellowship with file no (09/947(0091)/2017-EMR-I). We are thankful to IISER Mohali for central and departmental facilities.

References

1. Gupta, M.; Bala, I.; Pal, S. K. A room temperature discotic mesogenic dyad based-on triphenylene and pentaalkynylbenzene. *Tetrahedron Letters* **2014**, *55*, 5836-5840.
2. Eccher, J.; Faria, G. C.; Bock, H.; von Seggern, H.; Bechtold, I. H. Order Induced Charge Carrier Mobility Enhancement in Columnar Liquid Crystal Diodes. *ACS Appl. Mater. Interfaces* **2013**, *5*, 11935-11943.
3. Leng, S.; Chan, L. H.; Jing, J.; Hu, J.; Moustafa, R. M.; Van Horn, R. M.; Graham, M. J.; Sun, B.; Jeong, K.-U.; Kaafarani, B. R.; Zhang, W.; Harris, F. W.; Cheng, S. Z. D. From crystals to columnar liquid crystal phases: molecular design, synthesis and phase structure characterization of a series of novel phenazines potentially useful in photovoltaic applications. *Soft Matter* **2010**, *6*, 100-112.
4. Kaafarani, B. R. Discotic Liquid Crystals for Opto-Electronic Applications. *Chem. Mater.* **2011**, *23*, 378-396.
5. Haverkate, L. A.; Zbiri, M.; Johnson, M. R.; Deme, B.; de Groot, H. J. M.; Lefeber, F.; Kotlewski, A.; Picken, S. J.; Mulder, F. M.; Kearleys, G. J. On the Morphology of a Discotic Liquid Crystalline Charge Transfer Complex. *J. Phys. Chem. B* **2012**, *116*, 13098-13105.
6. Iino, H.; Hanna, J. Ambipolar charge carrier transport in liquid crystals. *Opto-Electron. Rev.* **2005**, *13*, 295.
7. Kasdorf, O.; Vollbrecht, J.; Ohms, B.; Hilleringmann, U.; Bock, H.; Kitzerow, H. S. Enhanced organic light-emitting diode based on a columnar liquid crystal by integration in a microresonator. *Int. J. Energy Res.* **2014**, *38*, 452-458.
8. Demus, D.; Goodby, J.; Gray, G. W.; Spiess, H.-W.; Vill, V. *Wiley-VCH* **1998**, 2B, Chapter IX.
9. Van de Craats, A. M.; Warman, J. M.; Haas, M. P. D.; Adam, D.; Simmerer, J.; Haarer, D.; Schuhmacher, P. The mobility of charge carriers in all four phases of the columnar discotic material hexakis(hexylthio)triphenylene: Combined TOF and PR-TRMC results. *Adv. Mater.* **1996**, *8*, 823-826.
10. Van de Craats, A. M.; Warman, J. M. The Core-Size Effect on the Mobility of Charge in Discotic Liquid Crystalline Materials. *Adv. Mater.* **2001**, *13*, 130-133.

11. Markovitsi, D.; Marguet, S.; Bondkowski, J.; Kumar, S. Triplet Excitation Transfer in Triphenylene Columnar Phases. *J. Phys. Chem. B* **2001**, *105*, 1299-1306.
12. Gupta, S. P.; Gupta, M.; Pal, S. K. Highly Resolved Morphology of Room-Temperature Columnar Liquid Crystals Derived from Triphenylene and Multialkynylbenzene Using Reconstructed Electron Density Maps. *Chemistry Select* **2017**, *2*, 6070-6077.
13. Chandrasekhar, S.; Sadashiva, B. K.; Suresh, K. A. Liquid crystals of disc-like molecules. *Pramana* **1977**, *9*, 471-480.
14. Tabushi, I.; Yamamura, K.; Okuda, Y. Liquid Crystals. 1. β -Oxygen Effect on Stabilization of Hexakis(acyloxy)benzene Mesophase. *J. Org. Chem.* **1987**, *52*, 2502-2505.
15. Collard, D. M.; Lillya, C. P. Control of Thermal Phase Behavior of Disklike Molecules by Modification of Side-Chain Structure. *J. Am. Chem. Soc.* **1989**, *111*, 1829-1830.
16. (a) Pugh, C.; Percec, V. Columnar mesophases of cyclic trimers of disubstituted acetylenes. *J. Mater. Chem.* **1991**, *1*, 765-773; (b) Chang, J. Y.; Yeon, J. R.; Shin, Y. S.; Han, M. J.; Hong, S. K. Synthesis and Characterization of Mesogenic Disklike Benzenetricarboxylates Containing Diacetylenic Groups and Their Polymerization. *Chem. Mater.* **2000**, *12*, 1076-1082.
17. Ito, S.; Ando, M.; Nomura, A.; Morita, N.; Kabutom, C.; Mukai, H.; Ohta, K.; Kawakami, J.; Yoshizawa, A.; Tajiri, A. Synthesis and Properties of Hexakis(6-octyl-2-azulenyl)benzene as a Multielectron Redox System with Liquid Crystalline Behavior. *J. Org. Chem.* **2005**, *70*, 3939-3949.
18. Kong, X.; He, Z.; Zhang, Y.; Mu, L.; Liang, C.; Chen, B.; Jing, X.; Cammidge, A. N. A Mesogenic Triphenylene-Perylene-Triphenylene Triad. *Org. Lett.* **2011**, *13*, 4.
19. Gupta, M.; Gupta, S. P.; Rasna, M. V.; Adhikari, D.; Dhara, S.; Pal, S. K. A new strategy towards the synthesis of a room-temperature discotic nematic liquid crystal employing triphenylene and pentaalkynylbenzene units. *Chem. Commun.* **2017**, *53*, 3014-3017.
20. Bala, I.; Yang, W. Y.; Gupta, S. P.; De, J.; Yadav, R. A. K.; Singh, D. P.; Dubey, D. K.; Jou, J. H.; Doualid, R.; Pal, S. K. Room temperature discotic liquid crystalline triphenylene-pentaalkynylbenzene dyads as an emitter in blue OLEDs and their charge transfer complexes with ambipolar charge transport behaviour. *J. Mater. Chem. C* **2019**, *7*, 5724-5738.

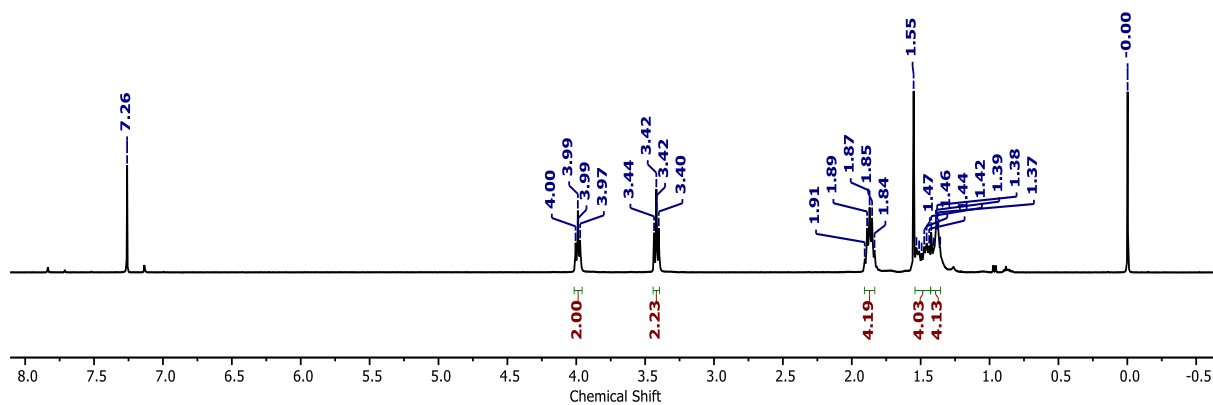
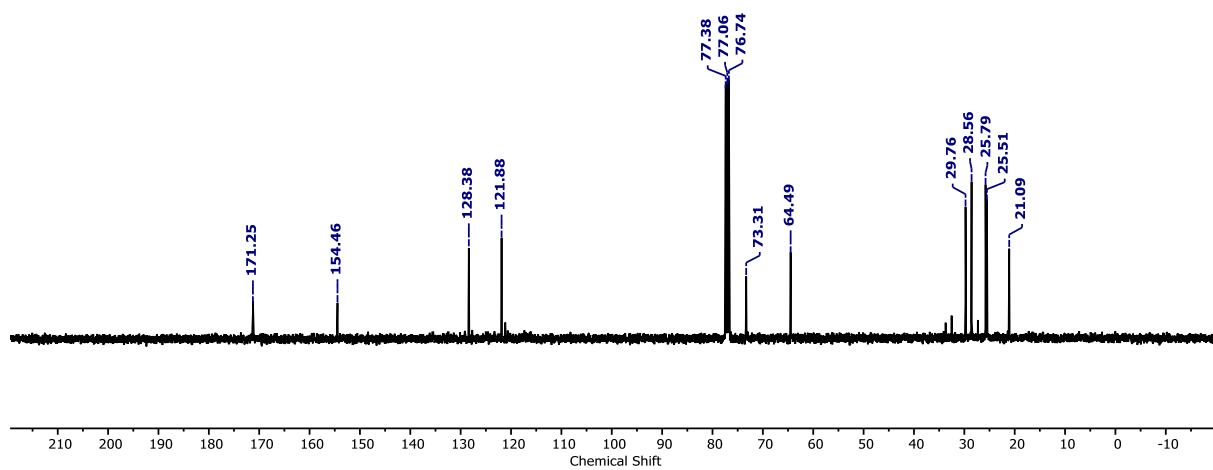
21. Bala, I.; Gupta, S. P.; De, J.; Pal, S. K. Room-Temperature Columnar Nematic and Soft Crystalline Columnar Assemblies of a New Series of Perylene-Centred Disc Tetramers. *Chem.Eur.J.* **2017**, *23*, 12767-12778.
22. Gupta, M.; Pal, S. K. The first examples of room temperature liquid crystal dimers based on cholesterol and pentaalkynylbenzene. *Liquid Crystals* **2015**, *42*, 1250-1256.
23. Gupta, M.; Mohapatra, S. S.; Dhara, S.; Pal, S. K. Supramolecular self-assembly of thiol functionalized pentaalkynylbenzene-decorated gold nanoparticles exhibiting a room temperature discotic nematic liquid crystal phase. *J.Mater. Chem. C* **2018**, *6*, 2303-2310.
24. Chen, S.; Xue, Z.; Gao, N.; Yang, X.; Zang, L. Perylene Diimide-Based Fluorescent and Colorimetric Sensors for Environmental Detection. *Sensors* **2020**, *20*, 917.
25. Zhu, M.; Chen, Y.; Guo, H.; Yang, F.; Songa, X. Perylene liquid crystals with multiple alkyl chains: investigation of the influence of peripheral alkyl chain number on mesomorphic and photophysical properties. *New J. Chem.* **2018**, *42*, 8998-9005.
26. Gupta, R. K.; Das, D.; Gupta, M.; Pal, S. K.; Iyer, P. K.; Achalkumar, A. S. Electroluminescent room temperature columnar liquid crystals based on bay-annulated perylene tetraesters. *J. Mater. Chem. C* **2017**, *5*, 1767-1781.
27. Gupta, S. K.; Setia, S.; Sidiq, S.; Gupta, M.; Kumar, S.; Pal, S. K. New perylene-based non-conventional discotic liquid crystals. *RSC Advances* **2013**, *3*, 12060-12065.
28. Gupta, R. K.; Pathak, S. K.; Pradhan, B.; Gupta, M.; Pal, S. K.; Achalkumar, A. S. Bay-Annulated Perylene Tetraesters: A New Class of Discotic Liquid Crystals. *ChemPhysChem* **2016**, *17*, 859-872.
29. Pathak, S. K.; Gupta, M.; Pal, S. K.; Achalkumar, A. S. Hexacatenars Exhibiting π - π Driven Supergelation, Aggregation Induced Blue Light Emission and Thermochromism. *Chemistry Select* **2016**, *1*, 5107-5120.
30. Schwartz, P. O.; Biniek, L.; Zaborova, E.; Heinrich, B.; Brinkmann, M.; Leclerc, N.; Méry, S. Perylenediimide-Based Donor–Acceptor Dyads and Triads: Impact of Molecular Architecture on Self-Assembling Properties. *J. Am. Chem. Soc.* **2014**, *136*, 5981-5992.
31. Schouten, P. G.; Warman, J. M.; de Haas, M. P.; Fox, M. A.; Pan, H. L. Charge migration in supramolecular stacks of peripherally substituted porphyrins. *Nature*, **1991**, *353*, 736-737.

-
32. Godquin, A. M. G.; Maitlis, P. M. Metallomesogens: Metal Complexes in Organized Fluid Phases. *Angew. Chem. Int. Ed.* **1991**, *30*, 375-402.
33. (a) Ohta, K.; Yamaguchi, N.; Yamamoto, I. Discotic liquid crystals of transition metal complexes. Part 24 Synthesis and mesomorphism of porphyrin derivatives substituted with two or four bulky groups. *J. Mater. Chem.* **1998**, *8*, 2637-2650; (b) Liu, C.-Y.; Fechtenkotter, A.; Watson, M. D.; Müllen, K.; Bard, A. J. Room Temperature Discotic Liquid Crystalline Thin Films of Hexa-*peri*-hexabenzocoronene: Synthesis and Optoelectronic Properties. *Chem. Mater.* **2003**, *15*, 124-130.
34. Markovitsi, D.; Lecuyer, I.; Simon, J. One-Dimensional Triplet Energy Migration In Columnar Liquid Crystals of Octasubstituted Phthalocyanines *J. Phys. Chem.* **1991**, *95*, 3620-3626.
35. Schouten, P. G.; Warman, J. M.; de Haas, M. P.; van Nostrum, C. F.; Gelinck, G. H.; Nolte, R. J. M.; Copyn, M. J.; Zwikker, J. W.; Engel, M. K.; Hanack, M.; Chang, Y. H.; Ford, W. T. The Effect of Structural Modifications on Charge Migration in Mesomorphic Phthalocyanines. *J. Am. Chem. Soc.* **1994**, *116*, 6880-6894.
36. Nostrum, C. F. V.; Nolte, R. J. M. *Chem. Commun.* **1996**, *66*, 2385-2392.
37. Duro, J. A.; Torre, G. D.; Barbera, J.; Serrano, J. L.; Torres, T. Synthesis and Liquid-Crystal Behavior of Metal-Free and Metal-Containing Phthalocyanines Substituted with Long-Chain Amide Groups. *Chem. Mater.* **1996**, *8*, 1061-1066.
38. Kimura, M.; Muto, T.; Takimoto, H.; Wada, K.; Ohta, K.; Hanabusa, K.; Shirai, H.; Kobayashi, N. Fibrous Assemblies Made of Amphiphilic Metallophthalocyanines. *Langmuir* **2000**, *16*, 2078-2082.
39. Bala, I.; De, J.; Gupta, S. P.; Singh, H.; Pandey, U. K.; Pal, S. K. High hole mobility in room temperature discotic liquid crystalline tetrathienoanthracenes. *Chem. Commun.* **2020**, *56*, 5629.
40. De, J.; Bala, I.; Gupta, S. P.; Pandey, U. K.; Pal, S. K. High Hole Mobility and Efficient Ambipolar Charge Transport in Heterocoronene-Based Ordered Columnar Discotics. *J. Am. Chem. Soc.*, 2019, **141**, 18799-18805.

41. Bala, I.; Gupta, S. P.; Kumar, S.; Singh, H.; De, J.; Sharma, N.; Kamalakannan, K.; Pal, S. K. Hydrogen-bond mediated columnar liquid crystalline assemblies of C_3 -symmetric heptazine derivatives at ambient temperature. *Soft Matter* **2018**, *14*, 6342-6352.
42. De, J.; Gupta, S. P.; Bala, I.; Kumar, S.; Pal, S. K. Phase Behaviour of a New Class of Anthraquinone-Based Discotic Liquid Crystals. *Langmuir* **2017**, *33*, 13849-13860.
43. Fuller, C. A.; Finlayson, C. E. Solvatochromism in perylene diimides; experiment and theory. *Phys. Chem. Chem. Phys.* **2017**, *19*, 31781-31787.
44. Bala, I.; Singh, N.; Yadav, R. A. K.; De, J.; Gupta, S. P.; Singh, D. P.; Dubey, D. K.; Jou, J. H.; Doualid, R.; Pal, S. K. Room temperature perylene based columnar liquid crystals as solid-state fluorescent emitters in solution-processable organic light-emitting diodes. *J. Mater. Chem. C* **2020**, *8*, 12485-12494.
45. Lee, K. J.; Woo, J. H.; Xiao, Y.; Kim, E.; Mazur, L. M.; Kreher, D.; Attias, A. -J.; Matczyszyn, K.; Samoc, M.; Heinrich, B.; Fages, S. M. F.; Mager, L.; Wu, A. D. J. W.; Mathevet, F.; André P.; Ribierre, J. C. Structure–charge transfer property relationship in self-assembled discotic liquid-crystalline donor–acceptor dyad and triad thin films. *RSC Adv.* **2016**, *6*, 57811-57819.
46. Karthik, C.; Manjuladevi, V.; Gupta, R. K.; Kumar, S. Solvatochromism of a tricycloquinazoline based disk-shaped liquid crystal: a potential molecular probe for fluorescence imaging. *RSC Adv.* **2015**, *5*, 84592-84600.
47. Mitani, M.; Yoshio, M.; Kato, T. Tuning of luminescence color of π -conjugated liquid crystals through co-assembly with ionic liquids. *J. Mater. Chem. C* **2017**, *5*, 9972-9978.
48. Subuddhi, U.; Haldar, S.; Sankararaman S.; Mishra, A. K. Photophysical behaviour of 1-(4-*N,N*-dimethylaminophenylethynyl)pyrene (DMAPEPy) in homogeneous media. *Photochem. Photobiol. Sci.* **2006**, *5*, 459-466.
49. Ceñon, M.; Perumal, V.; Anandhan, K.; Ceballos, P.; Guerra, P. G.; Gutiérrez, E. P.; Castillo, A. E.; Thamotharanb, S.; Percino, M. J. Solvatochromism and pH effect on the emission of a triphenylimidazole-phenylacrylonitrile derivative: experimental and DFT studies. *RSC Adv.* **2019**, *9*, 12085-12096.
50. Yang, S. -W.; Elangovan, A.; Hwang, K. -C.; Ho, T. -I. Electronic Polarization Reversal and Excited State Intramolecular Charge Transfer in Donor/Acceptor Ethynylpyrenes. *J. Phys. Chem. B* **2005**, *109*, 16628-16635.

51. Bala, I.; Singh, H.; Battula, V. R.; Gupta, S. P.; De, J.; Kumar, S.; Kailasam, K.; Pal, S. K. Heptazine: an Electron-Deficient Fluorescent Core for Discotic Liquid Crystals. *Chem. Eur. J.* **2017**, *23*, 14718-14722.
52. Lakowicz, J. R.; Principles of Fluorescence Spectroscopy, *Springer, USA, 3rd edn, 2006*, 55–56.
53. Finlayson, C. E.; Amezcua, A.; Sazio, P. J. A.; Walker, P. S.; Grossel, M. C.; Curry, R. J.; Smith, D. C.; Baumberg, J. J. Infrared emitting PbSe nanocrystals for telecommunications window applications. *J. Mod. Opt.* **2005**, *52*, 955–964.
54. Brouwer, A. M. Standards for photoluminescence quantum yield measurements in solution (IUPAC Technical Report). *Pure Appl. Chem.* **2011**, *83*, 2213–2228.

Appendix IV

Figure A1 ¹H NMR spectrum of compound 2 in CDCl₃.Figure A2 ¹³C NMR spectrum of compound 2 in CDCl₃.

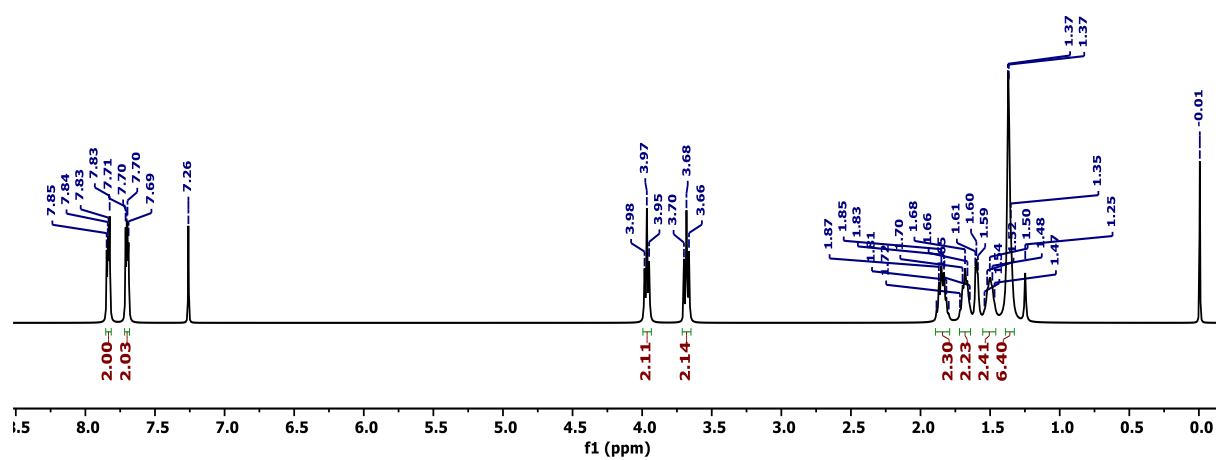


Figure A3 ^1H NMR spectrum of compound **3** in CDCl_3 .

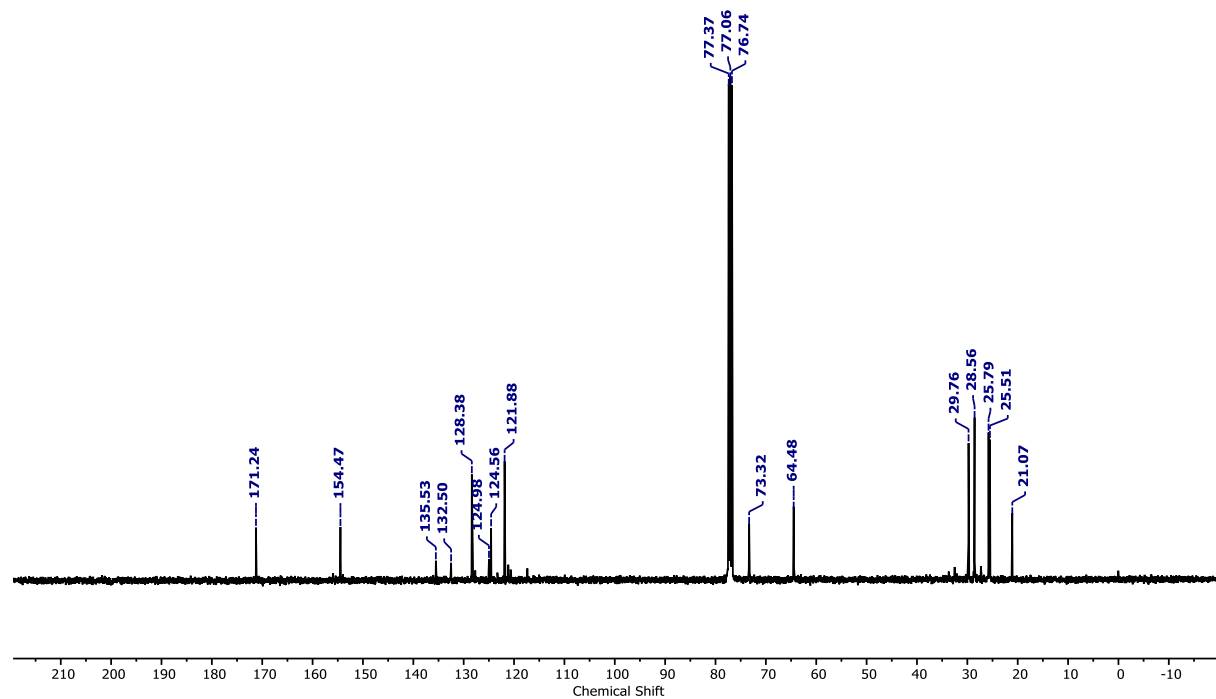


Figure A4 ^{13}C NMR spectrum of compound **3** in CDCl_3 .

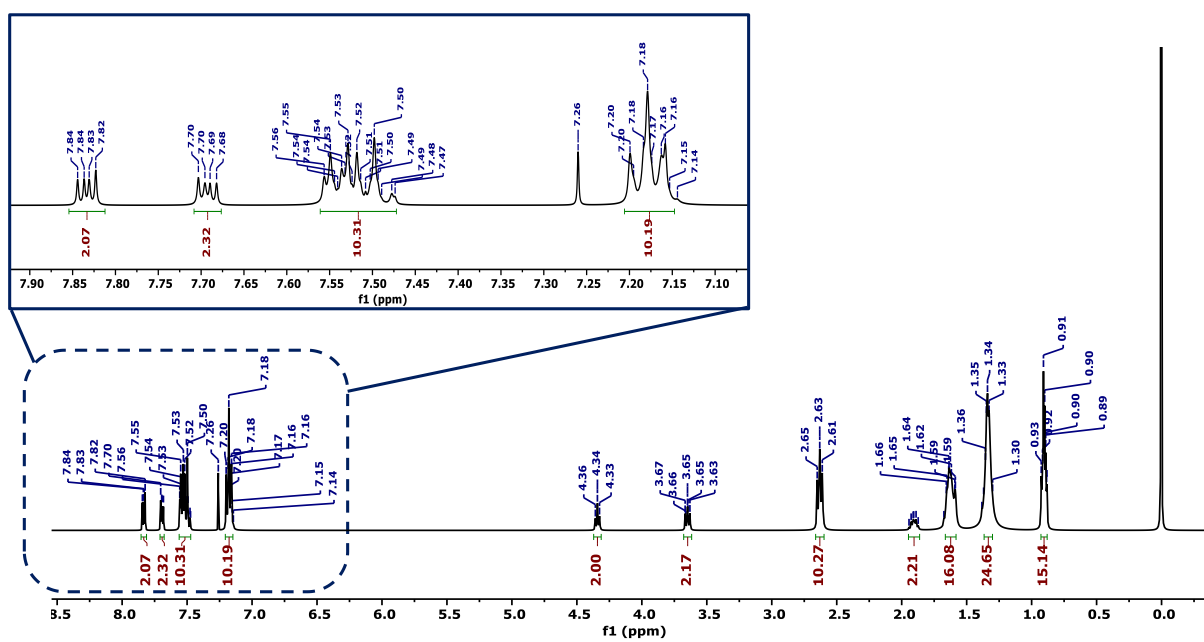


Figure A5 ^1H NMR spectrum of compound **4** in CDCl_3 .

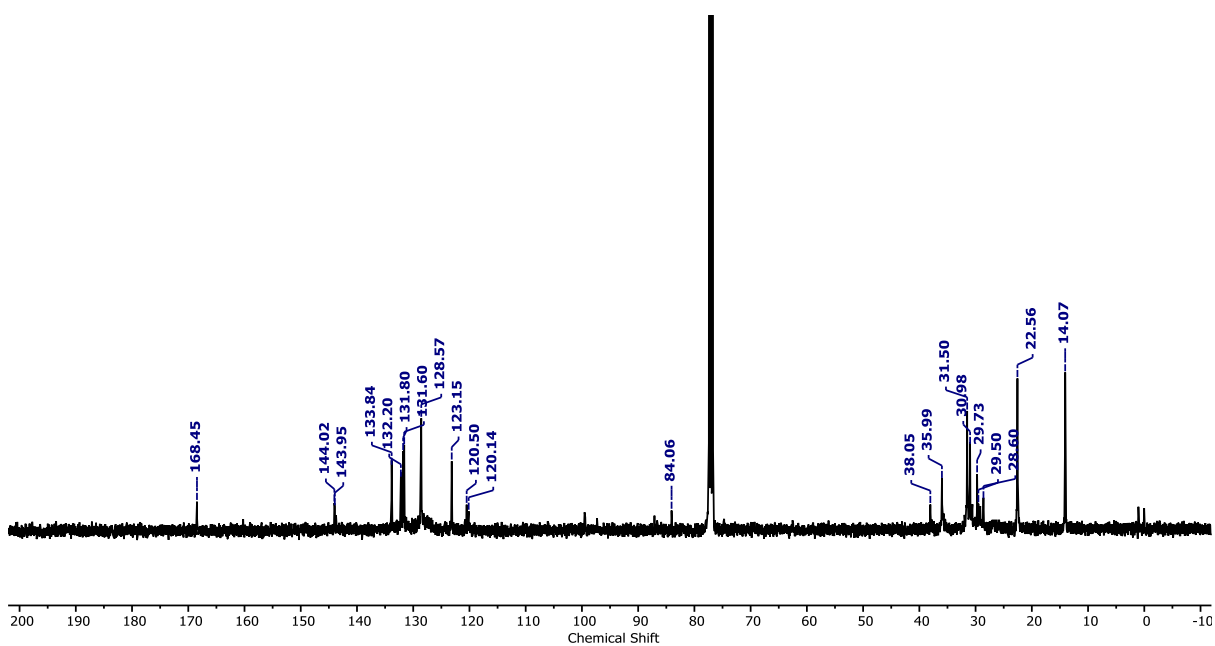


Figure A6 ^{13}C NMR spectrum of compound **4** in CDCl_3 .

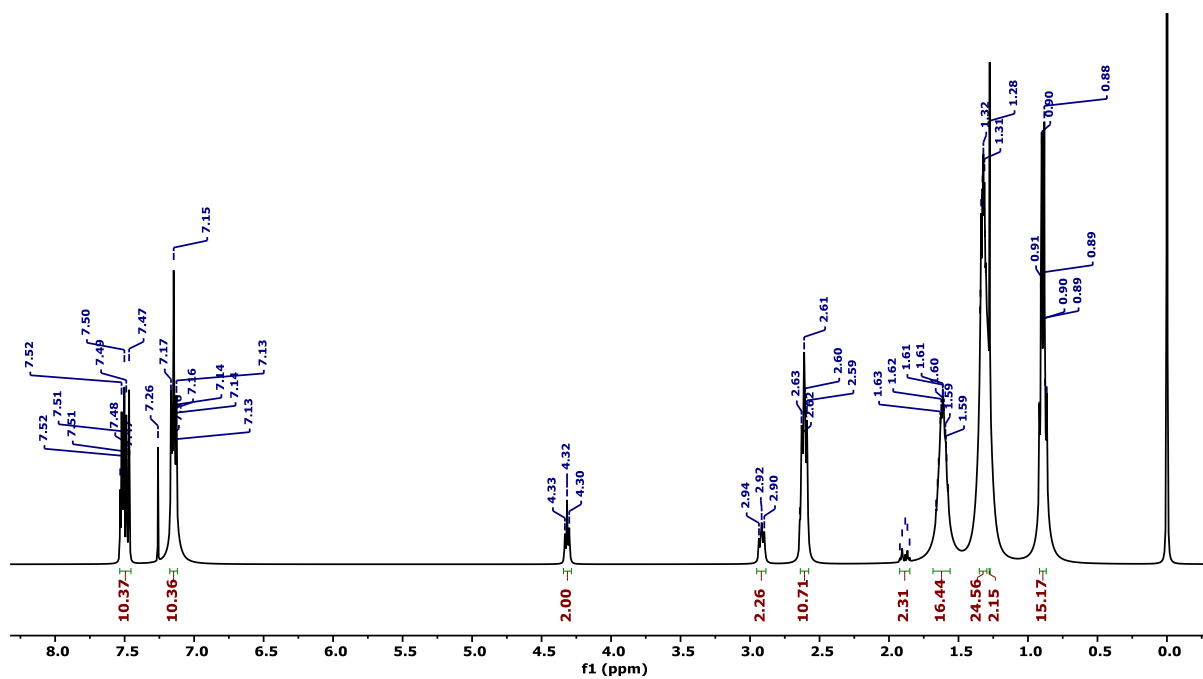


Figure A7 ^1H NMR spectrum of compound **5** in CDCl_3 .

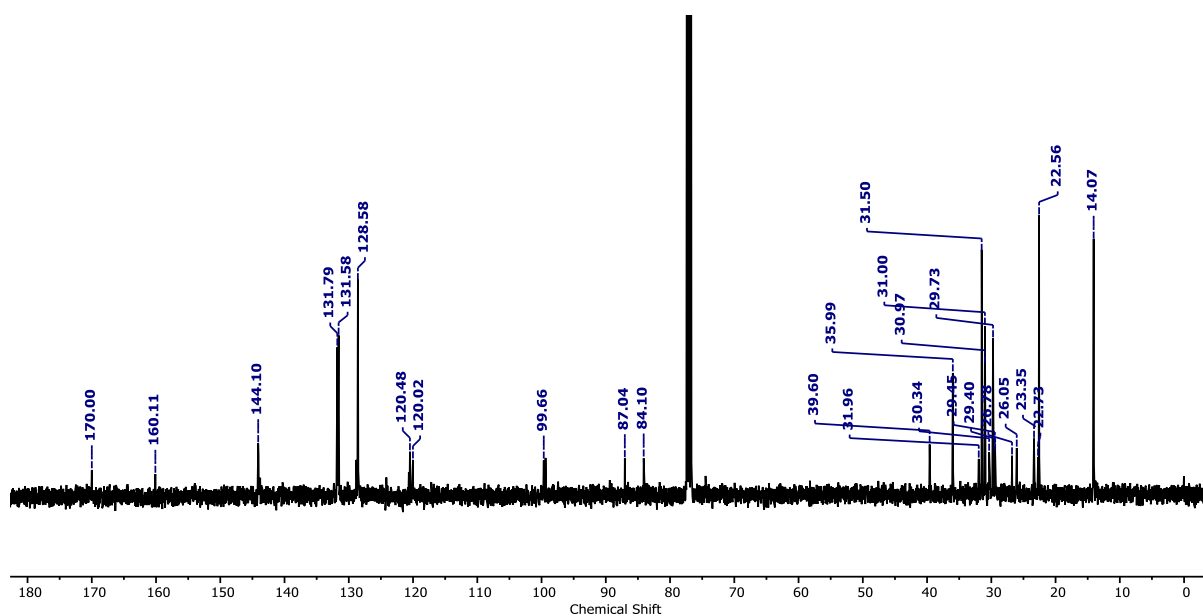


Figure A8 ^{13}C NMR spectrum of compound **5** in CDCl_3 .

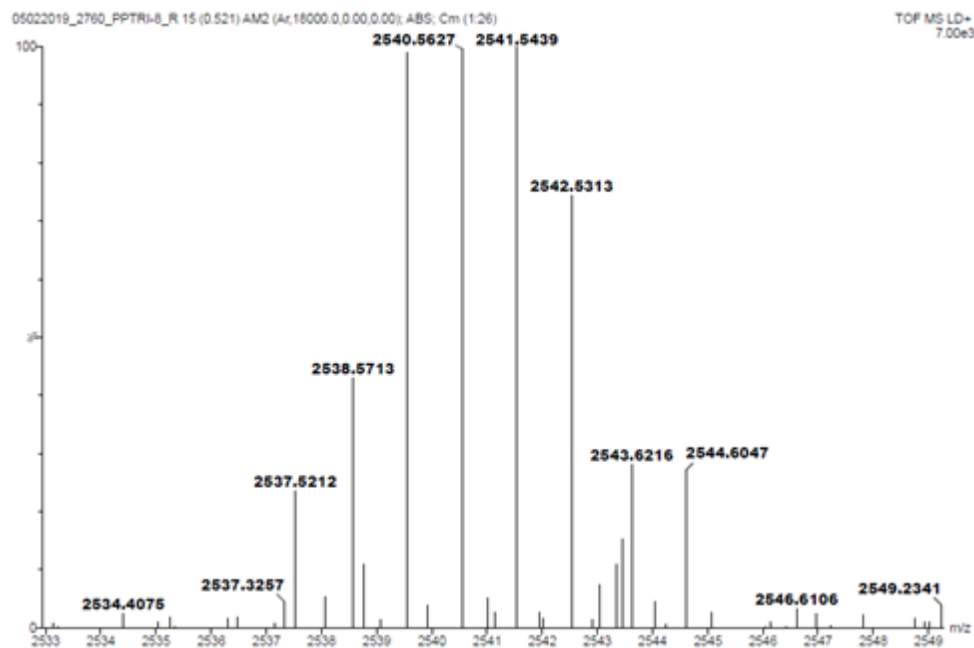
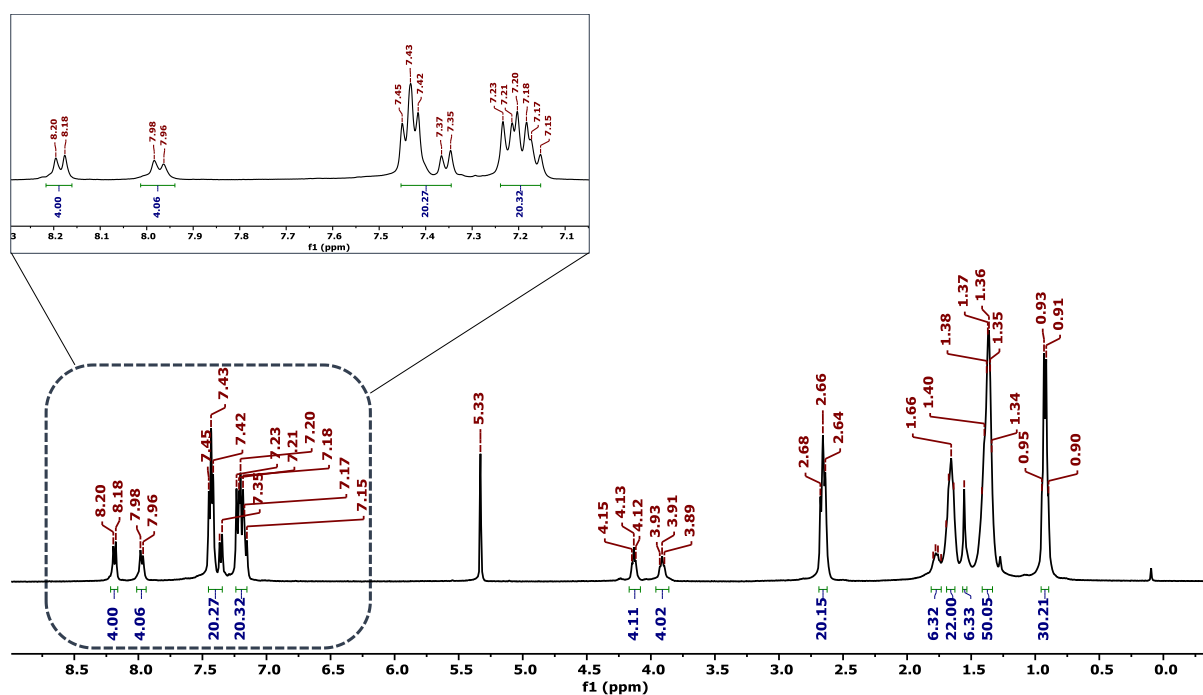


figure A9 HRMS spectrum of compound 1.

Figure A10 ^1H NMR spectrum of compound 1 in CD_2Cl_2 .

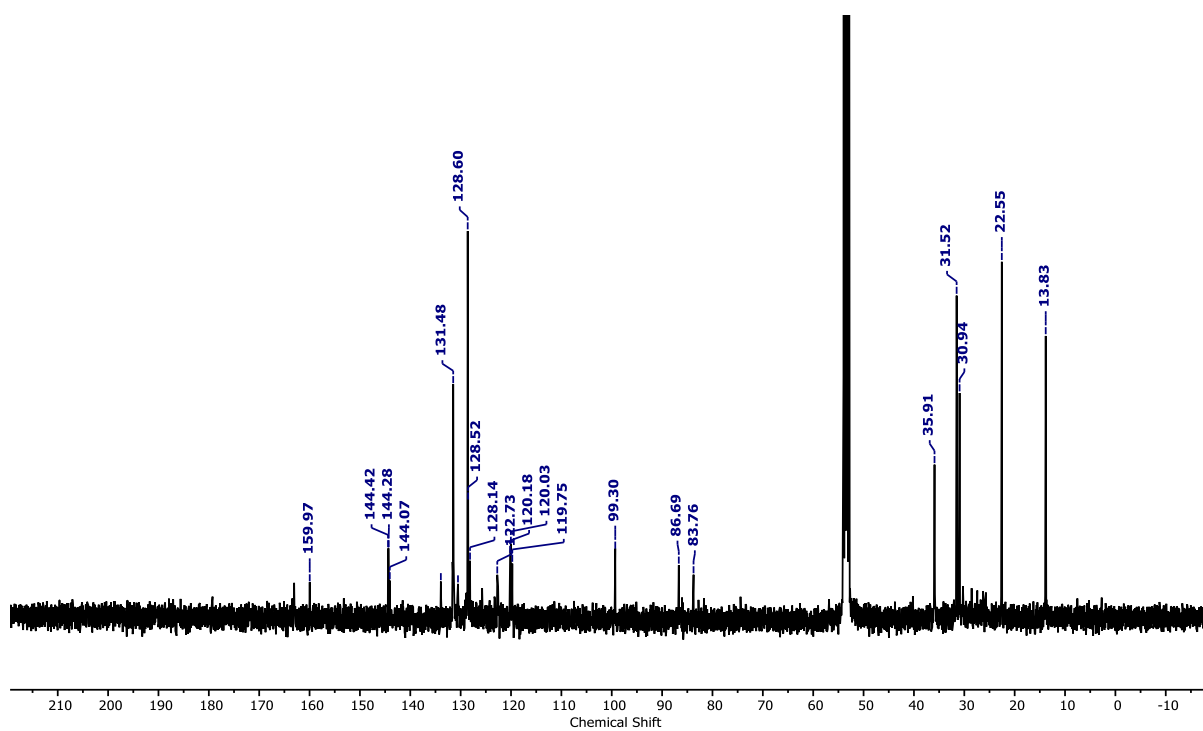


Figure A11 ^{13}C NMR spectrum of compound 1 in CD_2Cl_2 .

Thermogravimetric Analysis:

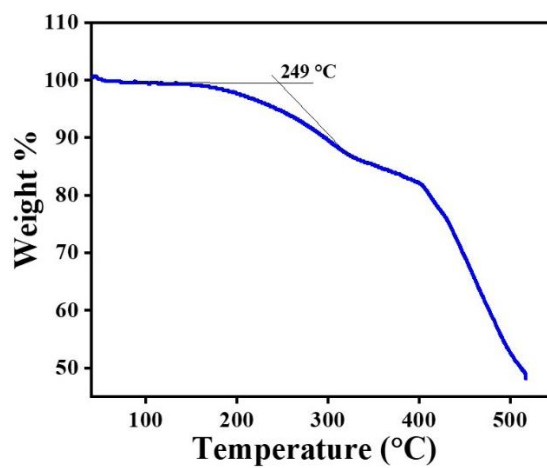


Figure A12 TGA thermographs of compound 1, recorded at rate of 10 $^{\circ}\text{C}/\text{min}$.

The Lippert-Mataga Plot:

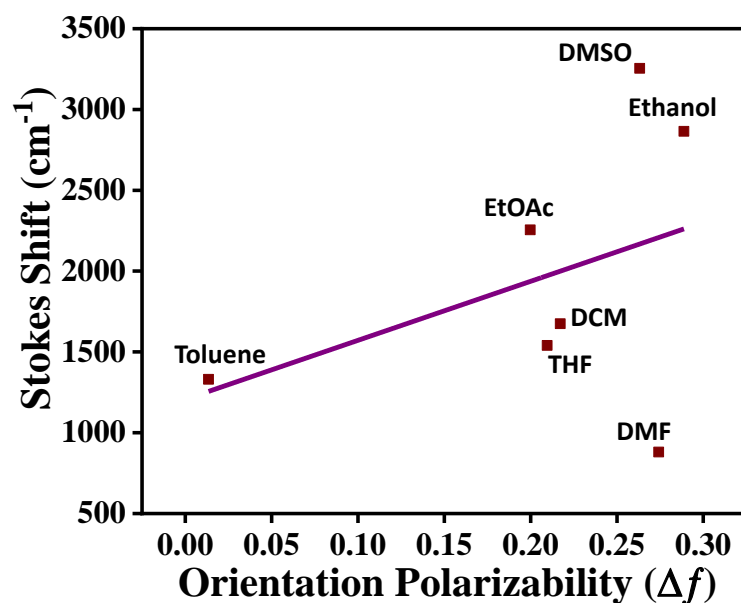


Figure A13 The relationship between Stokes shift (cm⁻¹) and the orientation polarizability parameter for compound **1** in a different solvent.

Cyclic Voltammetry studies:

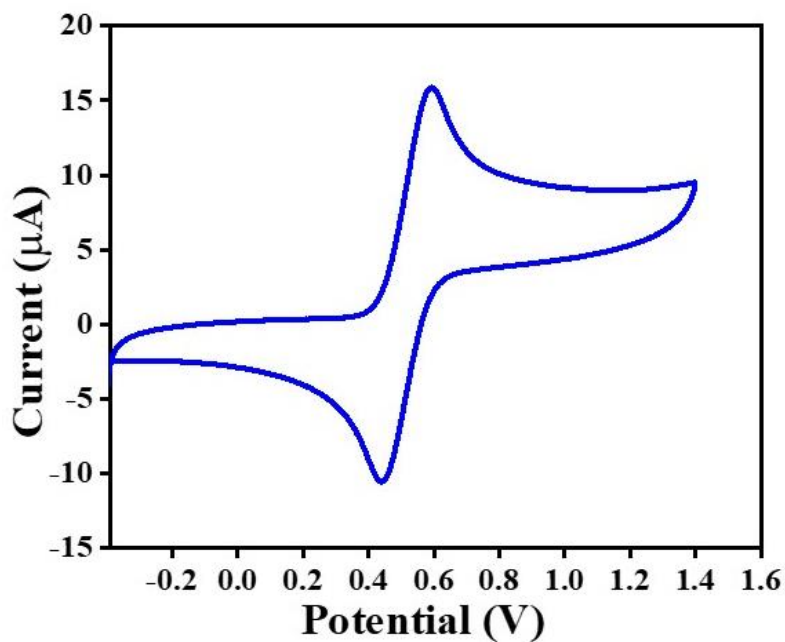


Figure A14 Cyclic Voltammogram of ferrocene in DCM (50 mVs⁻¹ scan rate).

Chapter 6

6.1 Conclusions

The use of molecular self-assembly has become a novel approach to developing soft functional materials with broad implications in both material science and biology. The creation of microscopic order within supramolecular assemblies is particularly important as it can greatly impact the optoelectronic properties of the resulting material. Supramolecular assemblies are formed through a delicate balance between molecule-substrate and intramolecular interactions. The molecular engineering of liquid crystals, especially DLCs, has become a significant area of focus within the realm of supramolecular self-assembled systems. Developing novel DLCs and their application as functional smart materials is of great interest to the scientific community, leading to extensive research in their design, synthesis, and characterization.

Herein, this thesis describes new approaches to designing chiral discotic liquid crystals and shows how the molecular engineering of liquid crystals leads to the formation of new helical self-organized functional materials. We have adopted different methodologies to obtain helically organized chiral DLCs and chiroptical properties, which are useful for many optoelectronic devices. The work described in this thesis can be concluded as follows:

Chapter 2, demonstrates the new synthetic approach to design and synthesize a series of non-conventional chiral columnar liquid crystals, where the cyclotriphosphazene core is surrounded by cholesterol-based Schiff base dimeric units. Cholesterol covalently bound to the two-ring Schiff base core via a flexible spacer of varying length and parity has been premeditatedly incorporated to induce handedness in columnar fluid macrostructure. The mesogenic Schiff base units have been inserted purposely as they possess various properties, including chemical sensing. To understand the structure-property correlation, the length and parity of the spacer of the cholesterol-based dimeric units have been varied, and detailed investigations reveal the influence of the spacer's length on the packing of the columns on a 2D lattice. For example, mesogens **P-6**, **P-7**, and **P-11** show the columnar-centred rectangular (Col_r) phase, whereas the LCs **P-8** and **P-10** exhibit the columnar oblique (Col_{ob}) phase. On the other hand, compound **P-5** display a columnar hexagonal (Col_h) phase, which is notably fascinating in terms of its structure.

Furthermore, the induction of molecular chirality enables the discotic LCs to self-organize into a highly ordered macroscopic structure. The helicity of the Col LCs has been confirmed by

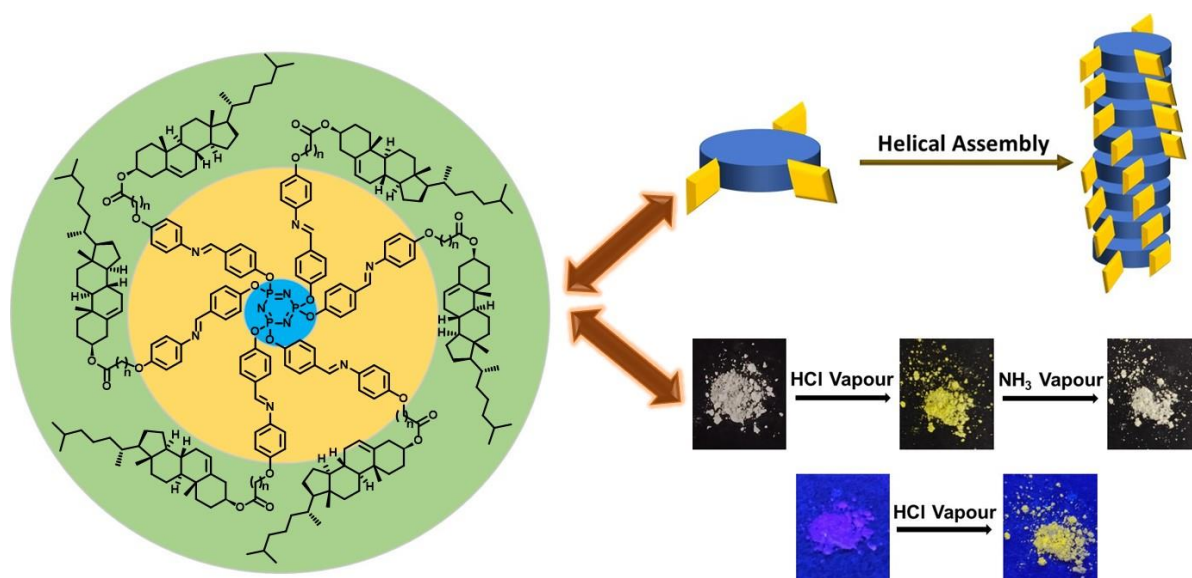


Figure 6.1 Formation of columnar helical mesophase in cyclotriphosphazene and cholesterol based DLCs, showing excellent HCl sensing behaviour.

temperature-dependent chiroptical measurements where the intensity of peak in circular dichroism (CD) spectra increase with a decrease in temperature, implying the core-core correlation within the columns and, thus, the proximity of the chromophores varies with the temperature. The helicity of the mesophases was also supported by the transmission electron microscopy (TEM) technique. Notably, these novel materials exhibit fluorescent "turn-on" characteristics in their solid state upon exposure to hydrochloric acid (HCl) that can be visualized by the naked eye instantly, where the colour change occurs with a low detection limit of $5.6 \mu\text{M}$.

Inspired by the previous study, in **chapter 3**, we designed and synthesized a new series of fluorescent chiral discotic liquid crystals based on tetrapyrrolopyrole and cholesterol. These derivatives were self-assembled in Col_h mesophase and froze to a glassy state at room temperature. Photophysical studies show the highly fluorescent nature of compounds in solution and solid state. To study the donor-acceptor charge transfer, solvent-dependent fluorescence experiments have been performed, and with high polar solvents, there is red shift with decreased emission intensity. Furthermore, the effect of the alkyl spacer was also observed in the THF-H₂O experiment. Additionally, the chiral DLCs with interesting luminescent properties inspired us to investigate the CPL activity of compound **TAP-9**. The effectiveness was assessed using the luminescence dissymmetry factor (g_{lum}), with a $|g_{\text{lum}}|$ value of around 6.39×10^{-3} . This work provides an exciting application in the field of optoelectronics and photonics.

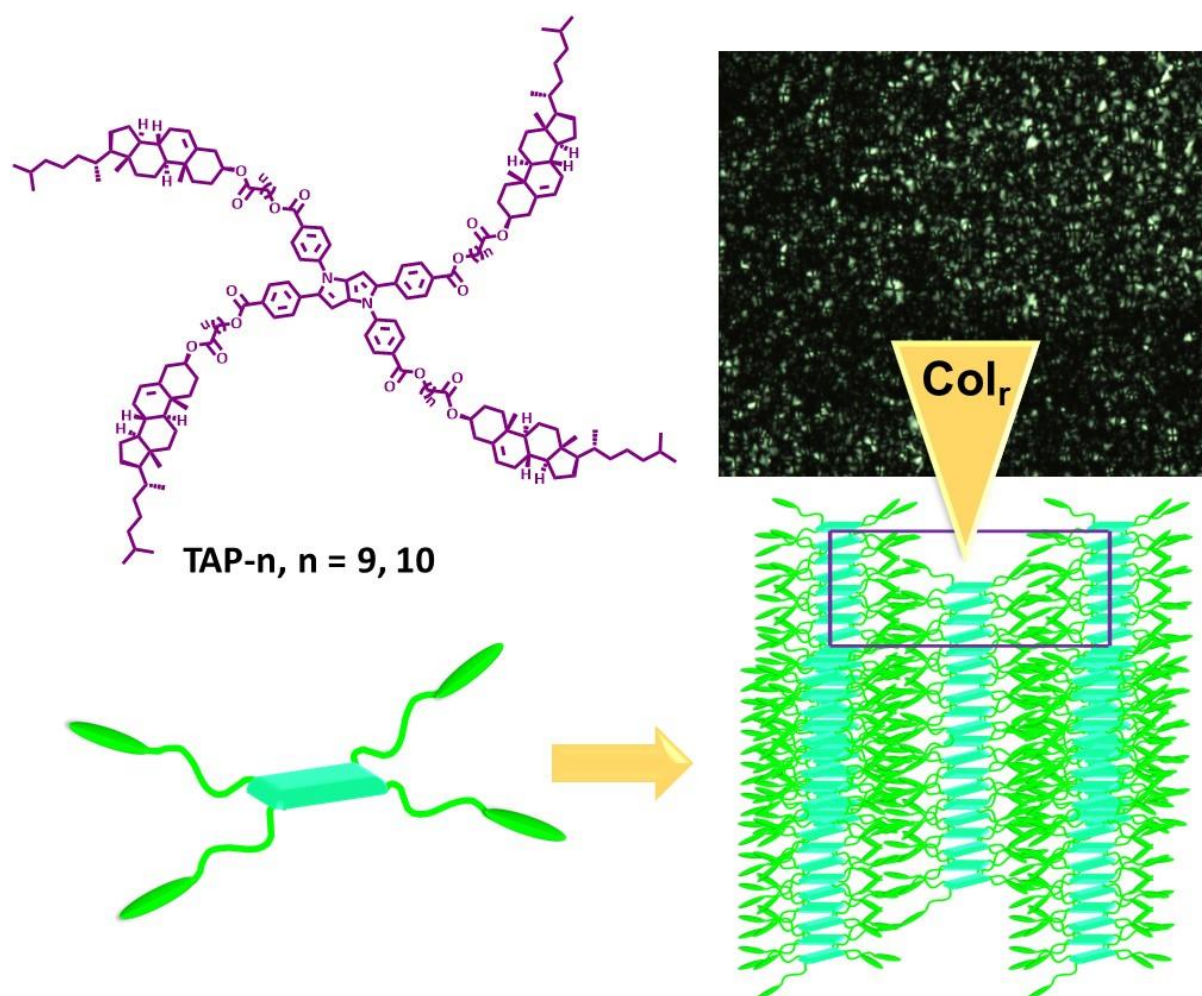


Figure 6.2 Formation of luminescent DLCs where the four side of tetrarylpyrrolopyrrole decorated with cholesterol unit.

The molecular engineering of liquid crystals has a very important space in the field of supramolecular self-assembled systems. **Chapter 4** of this thesis describes the supramolecular self-assembly of thiophene-induced cholesterol-decorated liquid crystal derivatives by varying the spacer alkyl chain lengths. All the synthesized derivatives are thermally stable and show a significant mesophase thermal range. The mesophase and structure-property relationship of all the target materials was investigated using POM, DSC and SAXS/WAXS measurements. The supramolecular self-assembly of all the derivatives stabilized the lamellar arrangement that sustains over a significant temperature range and freezes to a glassy state at room temperature. Here, the motivation is to lower the isotropic temperature and solid-state luminescence behaviour by minimizing the core-core interactions. Photophysical studies showed that all three derivatives display blue-emission in solution and thin-film states, exhibiting notable fluorescence quantum yield. Furthermore, these compounds stabilized in a glassy state at room temperature, which revealed their potential application for

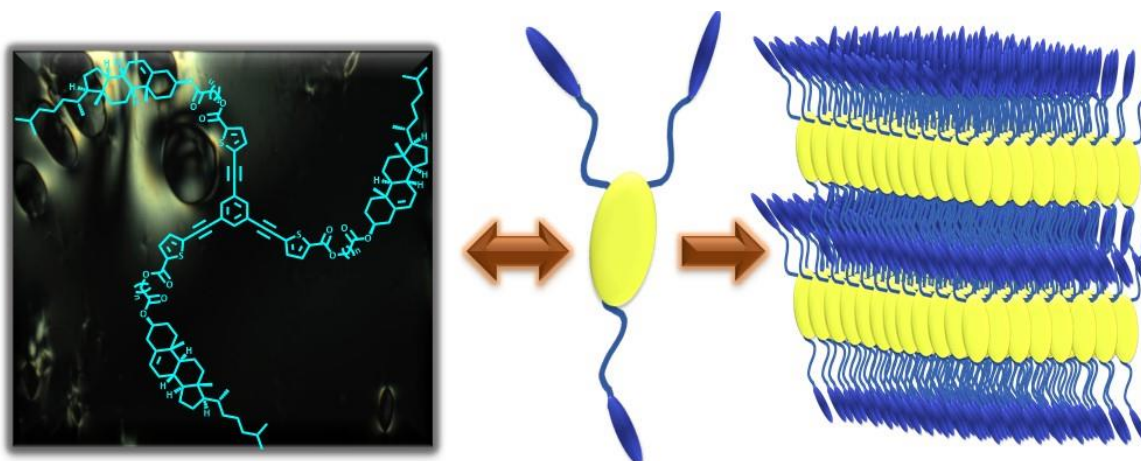


Figure 6.3 Cholesterol as a side mesogenic unit in LC molecular architecture demonstrates a lamellar structure.

many exciting applications. Also, the bulky cholesterol broadens the material range for chiroptical characteristics.

The last **chapter 5** of this thesis describes the new molecular design of a discotic liquid crystal triad based on a perylene core, in which perylene is sandwiched between two multialkynyl units at the imide position to construct the functional smart material. This strategy of combining two mesogenic units with different structural organizations inspired us to gain a complete structural understanding of the packing of the molecule in the phase arrangement. As a result, this strategy accelerates the supramolecular self-assembly of the hybrid triad in an oblique columnar arrangement that sustains over a significant temperature range. The formation of these organizations is well supported by polarising optical microscopy (POM) and X-ray diffraction (XRD). In addition, this triad exhibited high fluorescence quantum yield and a quantifying fluorescence response with different solvents according to the polarity of the different solvents, i.e., positive solvatochromic behaviour. A detailed experiment of the photophysical behaviour of the compound in various solvents of varying polarity has been performed. The compound shows positive solvatochromism with a significant increase in the Stoke's shift of around 91 nm between toluene and ethanol. The compound shows high fluorescence quantum yield in non-polar solvents and the lowest in polar solvents. This luminescent triad with positive solvatochromism will reveal its potential application in fluorescence imaging and optoelectronic organic materials.

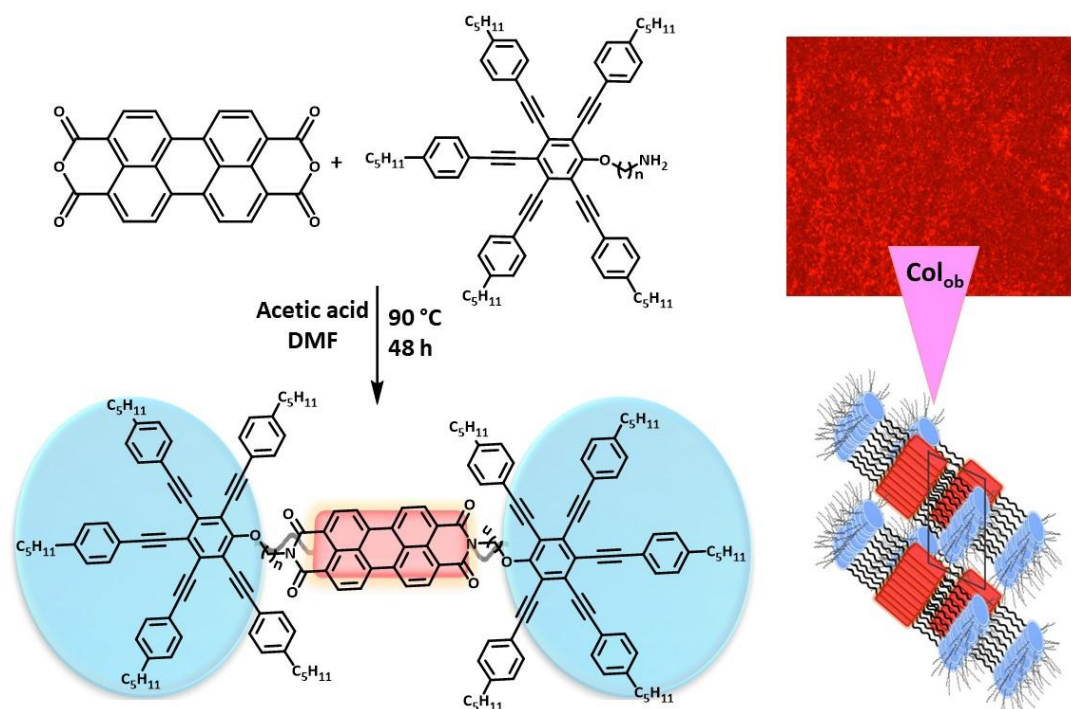


Figure 6.4 Pentalkynylbenzene unit connected to perylene at imide position to form columnar oblique mesophase.

Overall, **chapter 6** concludes this thesis, which highlights the importance of molecular design in obtaining helically organized luminescent chiral LCs. The work done in this thesis shows the way to highly ordered supramolecular self-assembled systems. The formation of the helical phase is influenced by various factors, such as molecular chirality, the shape of the mesogens, and intermolecular interactions. The helical structure of the columns gives rise to unique physical and optical properties, making it a promising area of research. These works advance the understanding of the design of the fluorescent chiral LCs for potential applications in various fields, including chiral sensing, chiral memory devices, enantioselective catalysis, optoelectronic devices etc.

List of Publications

1. **Rani, S.**; Punjani, V.; Gupta, S. P.; Kanakala, M. B.; Yelamaggad C. V.; Pal, S. K. Observation of helical self-assembly in cyclic triphosphazene-based columnar liquid crystals bearing chiral mesogenic units. *J. Mater. Chem. C* **2023**, *11*, 1067-1075.
2. **Rani, S.**; Gupta, S. P.; Gupta, M.; Pal, S. K. Color-tunable photoluminescent discotic liquid crystal based on Perylene-Pentaalkynylbenzene triad. *Journal of Molecular Liquids* **2023**, *385*, 122202.
3. **Rani, S.**; Gupta, S. P.; Pal, S. K. Circularly polarized luminescence from pyrrolopyrrole-based discotic columnar liquid crystals (*Manuscript to be communicated*)
4. **Rani, S.**; Kumar, P.; Gupta, S. P.; Pal, S. K. Synthesis of new fluorescent star-shaped liquid crystals derived from thiophene and cholesterol unit. (*Manuscript to be communicated*)

Conferences, Awards and Workshops

1. International travel support awarded by Department of Science and Technology, Government of India to attend and give Oral presentation at *16th European Conference on Liquid Crystals (ECLC - 2023)* organized by University of Calabria, Rende, Italy in July 2023.
2. Oral presentation at *29th National Conference on Liquid Crystals (29th NCLC - 2022)* organized by Christ University, Bangalore.
3. Best poster presentation award at International Conference on *Emerging Materials for Sustainable Development (EMSD - 2022)* organized by CSIR-CSIO Chandigarh.
4. Poster presentation at *International Conference on Emerging Trends in Science and Technology (ICETST - 2022)* organized by PEC Chandigarh.
5. Poster presentation at *29th Chemical Research Society of India- National Chemistry Symposium (CRSI-NSC) 2022* organized by IISER Mohali.
6. Participated in *National Intellectual Property Awareness Mission* on 2 February, 2022 organized by Intellectual Property Office, India.
7. Poster presentation at *26th National Conference on Liquid Crystals (26th NCLC - 2019)*.
8. Poster presentation at *Frontiers in Chemical Sciences (FICS 2018)* organized by IIT Guwahati.
9. Participated at the *Royal Society of Chemistry Roadshows 2017* held at IISER Mohali.
10. Participated in the ACS ON CAMPUS, 2018 held at IISER Mohali.
11. Participated in *24th National Conference on Liquid Crystals (26th NCLC - 2017)*.

Originality Reports and Copyrights

Plagiarism Checked using “Turnitin” software.

Chapter 1: Introduction to discotic liquid crystal and supramolecular chirality

ORIGINALITY REPORT

10 %	3 %	9 %	0 %
SIMILARITY INDEX	INTERNET SOURCES	PUBLICATIONS	STUDENT PAPERS

Chapter 3: Circularly polarized luminescence from pyrrolopyrrole-based discotic columnar liquid crystals

ORIGINALITY REPORT

6 %	1 %	6 %	0 %
SIMILARITY INDEX	INTERNET SOURCES	PUBLICATIONS	STUDENT PAPERS

Chapter 4: Synthesis of new fluorescent star-shaped liquid crystals derived from thiophene and cholesterol unit

ORIGINALITY REPORT

5 %	1 %	4 %	0 %
SIMILARITY INDEX	INTERNET SOURCES	PUBLICATIONS	STUDENT PAPERS

Chapter 6: Conclusions

ORIGINALITY REPORT

4%

SIMILARITY INDEX

4%

INTERNET SOURCES

0%

PUBLICATIONS

0%

STUDENT PAPERS



From the journal:
Journal of Materials Chemistry C

Observation of helical self-assembly in cyclic triphosphazene-based columnar liquid crystals bearing chiral mesogenic units†

Check for updates

Shruti Rani, ^a Vidhika Punjani, ^a Santosh Prasad Gupta,^b Madhu Babu Kanakala,^c C. V. Yelamaggad ^{*c} and Santanu Kumar Pal ^{*a}

Author affiliations

Abstract

Nowadays, intensive research has focused on the design and synthesis of function-integrated smart materials resulting from the spontaneous self-assembly of appropriately chosen functional molecules. Working in this direction, we have synthesized a new series of non-conventional, chiral columnar liquid crystals (Col LCs), where the cyclotriphosphazene core is surrounded by cholesterol-based Schiff base dimeric units. Cholesterol, which is covalently bound to the two ring Schiff base core via a flexible spacer of varying length and parity, has



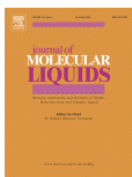
Observation of helical self-assembly in cyclic triphosphazene-based columnar liquid crystals bearing chiral mesogenic units

S. Rani, V. Punjani, S. P. Gupta, M. B. Kanakala, C. V. Yelamaggad and S. K. Pal, *J. Mater. Chem. C*, 2023, **11**, 1067
DOI: 10.1039/D2TC03847A

To request permission to reproduce material from this article, please go to the [Copyright Clearance Center request page](#).

If you are **an author contributing to an RSC publication, you do not need to request permission** provided correct acknowledgement is given.

If you are **the author of this article, you do not need to request permission to reproduce figures and diagrams** provided correct acknowledgement is given. If you want to reproduce the whole article in a third-party publication (excluding your thesis/dissertation for which permission is not required) please go to the [Copyright Clearance Center request page](#).



Color-tunable photoluminescent discotic liquid crystal based on perylene – Pentaalkynylbenzene triad

Author: Shruti Rani, Santosh Prasad Gupta, Monika Gupta, Santanu Kumar Pal

Publication: Journal of Molecular Liquids

Publisher: Elsevier

Date: 1 September 2023

© 2023 Elsevier B.V. All rights reserved.

Journal Author Rights

Please note that, as the author of this Elsevier article, you retain the right to include it in a thesis or dissertation, provided it is not published commercially. Permission is not required, but please ensure that you reference the journal as the original source. For more information on this and on your other retained rights, please visit: <https://www.elsevier.com/about/our-business/policies/copyright#Author-rights>

BACK

CLOSE WINDOW

Please note that if the material specified below or any part of it appears with credit or acknowledgement to a third party then you must also secure permission from that third party before reproducing that material.

Please ensure that the thesis includes the correct acknowledgement (see <http://rsc.li/permissions> for details) and a link is included to the paper on the Royal Society of Chemistry's website.

Please also ensure that your co-authors are aware that you are including the paper in your thesis.

You can take this email as permission to reuse your full article in your thesis, as per the above.

With thanks

Best wishes

Becky

Becky Roberts

Contracts & Copyright Executive, Sales Operations

Royal Society of Chemistry

T: +44 (0) 1223 432304 | www.rsc.org



[Quoted text hidden]

This communication is from The Royal Society of Chemistry, a company incorporated in England by Royal Charter (registered number RC000524) and a charity registered in England and Wales (charity number 207890). Registered office: Burlington House, Piccadilly, London W1J 0BA. Telephone: +44 (0) 20 7437 8656.

The content of this communication (including any attachments) is confidential, and may be privileged or contain copyright material. It may not be relied upon or disclosed to any person other than the intended recipient(s) without the consent of The Royal Society of Chemistry. If you are not the intended recipient(s), please (1) notify us immediately by replying to this email, (2) delete all copies from your system, and (3) note that disclosure, distribution, copying or use of this communication is strictly prohibited.

Any advice given by The Royal Society of Chemistry has been carefully formulated but is based on the information available to it. The Royal Society of Chemistry cannot be held responsible for accuracy or completeness of this communication or any attachment. Any views or opinions presented in this email are solely those of the author and do not represent those of The Royal Society of Chemistry. The views expressed in this communication are personal to the sender and unless specifically stated, this e-mail does not constitute any part of an offer or contract. The Royal Society of Chemistry shall not be liable for any resulting damage or loss as a result of the use of this email and/or attachments, or for the consequences of any actions taken on the basis of the information provided. The Royal Society of Chemistry does not warrant that its emails or attachments are Virus-free; The Royal Society of Chemistry has taken reasonable precautions to ensure that no viruses are contained in this email, but does not accept any responsibility once this email has been transmitted. Please rely on your own screening of electronic communication.

More information on The Royal Society of Chemistry can be found on our website: www.rsc.org



Shruti Suthar <105shruti@gmail.com>

Requesting publisher's permission to reuse full article in the author's dissertation

2 messages

Shruti Suthar <105shruti@gmail.com>
To: customercare@copyright.com

Tue, Sep 5, 2023 at 10:51 AM

Dear sir/ma'am,

I am Shruti Rani, a graduate student at IISER Mohali. I am requesting the rights and permission to reuse the full article (<https://doi.org/10.1016/j.molliq.2023.122202>) in my PhD dissertation.

I have attached a print of the permission page which states that "Please note that, as the author of this Elsevier article, you retain the rights to include it in a thesis or dissertation, provided it is not published commercially. permission is not required, but please ensure that you reference the journal as the original source."

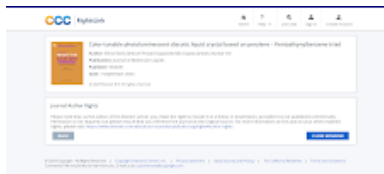
Is it sufficient to attach the following permission? Since I have to keep a copy of the copyright permission in my dissertation, I request you to help me with this. If anything else needs to be done, kindly let me know.

Thanks and Regards

Shruti Rani

PhD Scholar

Dr Santanu K Pal's Lab, IISER Mohali
Knowlegde City, SAS nagar, 140306
Contact No. - 8708217045, 9887686337



Screenshot (31).png
101K

customercare@copyright.com <customercare@copyright.com>
To: "105shruti@gmail.com" <105shruti@gmail.com>

Wed, Sep 6, 2023 at 4:13 AM

Hello Shruti Rani,

Thank you for your email to Copyright Clearance Center (CCC). My name is Christine with CCC Customer Service and I am happy to assist you today. Congratulation on your thesis completion.

To your question: **"Is it sufficient to attach the following permission? Since I have to keep a copy of the copyright permission in my dissertation, I request you to help me with this. If anything else needs to be done, kindly let me know."**

As you are also the author of the paper, you do retain rights. I would also recommend reviewing the agreement you signed with Elsevier to see what rights you retained to use your paper in support of your thesis. Using RightsLink will indicate no 'official' permission is required, as you also encountered. If you need something 'official' from Elsevier you can email them the Permissions Helpdesk please go to: <https://service.elsevier.com/app/contact/supporthub/permissions-helpdesk/>

*Here are the steps again that illustrate no permission as the author using the material in support of their thesis is needed:

Getting Started:

Step 1: Please visit the article abstract:

<https://www.sciencedirect.com/science/article/pii/S016773222301005X>

Step 2: Please click "Get Rights and Content" to open up the RightsLink permission form.

Step 3: Please choose your type of use, reuse in a thesis/dissertation, as well as the rest of the selections such as portion. Also, for the statement, 'I am the author of this Elsevier article...' please select 'yes'.

Step 4: You may obtain a price quote in advance by using the "Quick Price" button. When you do that you will see this message:

Journal Author Rights

Please note that, as the author of this Elsevier article, you retain the right to include it in a thesis or dissertation, provided it is not published commercially. Permission is not required, but please ensure that you reference the journal as the original source. For more information on this and on your other retained rights, please visit: <https://www.elsevier.com/about/our-business/policies/copyright#Author-rights>



Color-tunable photoluminescent discotic liquid crystal based on perylene - Pentaalkynylbenzene triad

Author: Shruti Rani,Santosh Prasad Gupta,Monika Gupta,Santanu Kumar Pal

Publication: Journal of Molecular Liquids

Publisher: Elsevier

Date: 1 September 2023

© 2023 Elsevier B.V. All rights reserved.

Journal Author Rights

Please note that, as the author of this Elsevier article, you retain the right to include it in a thesis or dissertation, provided it is not published commercially. Permission is not required, but please ensure that you reference the journal as the original source. For more information on this and on your other retained rights, please visit: <https://www.elsevier.com/about/our-business/policies/copyright#Author-rights>

BACK

CLOSE WINDOW

If you have any questions, our services are available 24 hours a day, Monday through Friday. To call a Customer Service Representative toll-free, the number is 855.239.3415 or send an e-mail to customercare@copyright.com anytime.

Sincerely,
Christine

Christine Z.
Customer Account Specialist
Copyright Clearance Center
[222 Rosewood Drive](https://www.copyright.com)
Danvers, MA 01923
www.copyright.com
Toll Free US +1.855.239.3415
International +1.978-646-2600

[Quoted text hidden]

This message (including attachments) is confidential, unless marked otherwise. It is intended for the addressee(s) only. If you are not an intended recipient, please delete it without further distribution and reply to the sender that you have received the message in error.

VITA

Shruti Rani was born and raised in the small village of Sirsa, Haryana, India, where she did her primary schooling. She did her bachelor's degree in Science from Kurukshetra University, Kurukshetra, Haryana. After that, she did her master's degree in chemistry from Banasthali University, Jaipur. She qualified for CSIR-JRF 2016 with AIR 51 and GATE 2017 with AIR 257.



Thereafter, she joined IISER Mohali in 2017 for the Department of Chemical Sciences PhD program. She joined the lab of Prof. Santanu Kumar Pal for her thesis work in September 2017. Her research mainly focuses on the design and synthesis of non-conventional chiral discotic liquid crystals and their different chiroptical properties. During her PhD, she has presented oral and poster presentations at many national and international conferences. She received the Best Poster Award in Chemistry for her presentation at International Conference on Emerging Materials for Sustainable Development (EMSD - 2022). She has authored and co-authored four publications in reputed peer-reviewed international journals.